THE JOURNAL
OF
CHEMICAL PHYSICS

VOLUME 19, NUMBER 4 APRIL, 1951

The Dielectric Constant of Water and the Saturation Effect

F. BOOTH
Department of Theoretical Physics, King's College, London, England
(Received October 23, 1950)

The Onsager and Kirkwood theories of polar dielectrics are extended to give expressions for the dielectric constant at high field strengths. The theory is applied in detail to water and simple formulas for the dielectric constant in terms of well-known quantities are obtained. The results of the calculation are embodied in the formula

$$\epsilon=n^2+\frac{\alpha\pi N_0(n^2+2)\mu_v}{E}L\left(\frac{\beta\mu_v(n^2+2)E}{kT}\right),$$

where n is the optical refractive index, N_0 the number of molecules per unit volume, μ_v the dipole moment of the water molecule, E is the field strength, and T the absolute temperature. $L(x)$ is the usual Langevin function, and α and β are numerical factors which have the following values

(a) Onsager method $\alpha=4/3$, $\beta=1/2$.
(b) Kirkwood method $\alpha=28/3\sqrt{73}$, $\beta=\sqrt{73}/6$.

From these formulas it is shown that the reduction of the dielectric constant due to the saturation effect is of importance for fields greater than 10^6 volts per cm.

I. INTRODUCTION

THE first attempt to furnish a theory of the dielectric constant of polar liquids at high field strengths was made by Debye.[1] He pointed out that in electrolytes, owing to the small size of the ions, very intense fields would be set up in their neighborhood; at these field strengths the water would probably become saturated so that its effective dielectric constant would be less than the ordinary value. To estimate the effect, Debye merely replaced the applied field $\mathbf{E}$ in the usual Langevin formula by the Lorentz field, that is by $\mathbf{E}+4\pi\mathbf{P}/3$ where $\mathbf{P}$ is the polarization. It is now known that this procedure is not valid, since it assumes that there is no field at the center of the "Lorentz sphere" due to its own polarization. Moreover the experimental results for polar liquids do not agree with the predictions of the above theory; in particular the Clausius-Mossotti law is not followed. More recently Onsager[2] has given a much better theory. The model he adopts is oversimplified however and gives values for strongly polar liquids like water, which are far too small. Later Kirkwood[3] gave a more general analysis from which, using the known dipole moment of the H_2O molecule, he was able to obtain a very good value for the dielectric constant of water.

Unfortunately both the Onsager and Kirkwood treatments confine attention to the case of *small* field strengths. For the purpose of studying the electrical properties of electrolytes it is desirable to have a fairly reliable estimate of the dielectric constant of water at high field strengths, when the saturation effect is of importance. In the following paper we shall accordingly generalize the Onsager and Kirkwood theories so as to give the desired expressions. In later publications the theory will be applied to concrete problems—for example the determination of the field near a charged surface in an electrolyte.

The problem we are to examine has also been treated by Anselm[4] but his result is more restricted than the one we shall obtain and cannot be used in the region of very strong fields.

[1] P. Debye, *Polar Molecules* (Chemical Catalogue Company, Reinhold, New York, 1929).
[2] L. Onsager, J. Am. Chem. Soc. **58**, 1486 (1936).
[3] J. Kirkwood, J. Chem. Phys. **7**, 911 (1939); H. Fröhlich, *Theory of Dielectrics* (Oxford University Press, New York, 1949), Chapter II.
[4] A. Anselm, J. Exp. Theoret. Phys. Acad. Sci. U.R.S.S. **14**, 364 (1945).

UNIVERSITY OF MICHIGAN LIBRARIES

II. ONSAGER METHOD

Although the calculation of Onsager has largely been superseded by that of Kirkwood, it is of interest to deal with this case first owing to its simplicity. Moreover the Onsager method is valid for small dipole moments and high temperatures. We shall assume spherical molecules with negligible short range interaction. The polarization of the molecule is the sum of its permanent dipole moment and the electronic polarization, which will be assumed to be proportional to the field strength. To take account of the electronic polarization, we shall ignore its effect on the moment, but assume that the permanent dipoles are embedded in a medium of dielectric constant n^2, where n is the optical refractive index. If $\bar{M}_E$ is the mean moment of a volume V due to the dipoles and induced by the external field E, the dielectric constant ϵ is given by

$$\epsilon - n^2 = 4\pi \bar{M}_E / VE. \tag{2.1}$$

To find $\bar{M}_E$ isolate a single molecule; then if $\boldsymbol{\mu}_v$ is the *external* moment, then its moment in the medium of dielectric constant n^2 is

$$\boldsymbol{\mu} = (n^2+2)\boldsymbol{\mu}_v/3. \tag{2.2}$$

If $\mathbf{F}$ is the local field acting on the molecule, we have, if the dielectric constant has the same value ϵ everywhere

$$\mathbf{F} = \frac{3\epsilon}{2\epsilon+n^2}\mathbf{E} + \frac{2(\epsilon-n^2)}{n^2a^3(2\epsilon+n^2)}\boldsymbol{\mu}, \tag{2.3}$$

where a is the radius of the molecules. In (2.3) the material outside the molecule is replaced by a continuous medium; the first term represents the cavity field, the second the reaction field. The expressions in (2.3) are only strictly valid provided ϵ is constant. In our case ϵ is a function of the field strength. But if $\epsilon \gg n^2$, which is true for water at ordinary field strengths, we may write

$$\mathbf{F} = \tfrac{3}{2}\mathbf{E} + (\boldsymbol{\mu}/n^2a^3), \tag{2.4}$$

and we see that the precise value of ϵ is not involved. Hence it seems reasonable to suppose that (2.4) is very nearly correct even though ϵ is a function of the field strength, provided $\epsilon \gg n^2$ always. Of course as E increases ϵ will decrease owing to saturation and consequently the approximation embodied in Eq. (2.4) becomes steadily worse as E becomes larger and larger. Unfortunately there is no simple way of finding the cavity and reaction fields when ϵ is variable. The only feasible method seems to be, first to find ϵ using Eq. (2.4) and then from the result to obtain a more correct expression for $\mathbf{F}$ than given in Eq. (2.4). This question will be examined in a later paper.

For the mean value of $\cos\theta$, where θ is the angle between $\boldsymbol{\mu}$ and $\mathbf{E}$, we have

$$\langle\cos\theta\rangle = \frac{\int_0^\pi \sin\theta\cos\theta \exp(\boldsymbol{\mu}\cdot\mathbf{F})/kTd\theta}{\int_0^\pi \sin\theta \exp(\boldsymbol{\mu}\cdot\mathbf{F})/kTd\theta} = L\left(\frac{3E\mu}{2kT}\right), \tag{2.5}$$

where $L(x)$ is the usual Langevin function.

$$L(x) = \coth x - \frac{1}{x}. \tag{2.6}$$

Hence

$$\bar{M}_E = N\mu L\left(\frac{3\mu E}{2kT}\right), \tag{2.7}$$

where N is the number of molecules in a volume V. Using (2.1) for ϵ and (2.2) for μ, we have

$$\epsilon = n^2 + \frac{4\pi N_0\mu_v(n^2+2)}{3E} L\left(\frac{[n^2+2]\mu_v E}{2kT}\right), \tag{2.8}$$

where N_0 is the number of molecules per unit volume. For *small* E

$$\epsilon = n^2 + \frac{2\pi\mu_v^2 N_0}{kT}\left(\frac{n^2+2}{3}\right)^2 \tag{2.9}$$

which is Onsager's formula. In the accompanying figure ϵ is plotted as a function of E with $\mu_v = 1.9$ Debye units (corresponding to the H_2O molecule), $T = 25°C$, $n = 1.33$. It will be seen that the saturation effect becomes important for $E > 5\times10^6$ volts per cm; but the small value of ϵ for small fields indicates that the theory is hardly adequate, for water at any rate.

III. KIRKWOOD METHOD

Instead of using the original form of the Kirkwood method, it will be more convenient to employ a slightly modified version suggested by a paper due to Fröhlich.[5] From an infinite specimen of the dielectric, uniformly polarized by a field E, a macroscopic spherical region of volume V is selected. As in the Onsager method, the effect of electronic polarization will be taken into account by regarding the permanent dipoles as rigid dipoles embedded in a medium of dielectric constant n^2. If we assume as before that $\epsilon \gg n^2$, then the cavity field in V is

$$\mathbf{G} = \tfrac{3}{2}\mathbf{E}. \tag{3.1}$$

The average component of the permanent dipole moment of any molecule, for example a molecule labelled

[5] H. Fröhlich, Trans. Faraday Soc. 44, 238 (1948).

"i," in the direction of the field $\mathbf{E}$ is

$$\bar{\boldsymbol{\mu}}_i=\frac{\int_N\cdots\int(\boldsymbol{\mu}_i\cdot\mathbf{e})\exp\{-[U_N-(\mathbf{M}\cdot\mathbf{G})]/kT\}dx_1\cdots dx_N}{\int_N\cdots\int\exp\{-[U_N-(\mathbf{M}\cdot\mathbf{G})]/kT\}dx_1\cdots dx_N}, \tag{3.2}$$

where $\mathbf{e}$ is a unit vector in the direction of $\mathbf{E}$, N is the total number of dipoles in the volume V, U_N is the potential of the intermolecular forces for the whole assembly, and $\mathbf{M}$ is the total electric moment,

$$\mathbf{M}=\sum_{i=1}^{N}\boldsymbol{\mu}_i. \tag{3.3}$$

The integrations are over-all allowed values of the coordinates, abbreviated by the symbols $(x_1, x_2\cdots x_N)$ or collectively by the symbol x. Expanding the integrands and using (3.1), (3.2) may be written in the form

$$\bar{\boldsymbol{\mu}}_i=\frac{\sum_{n=0}^{\infty}(3E/2kT)^n(n!)^{-1}I\{x;[(\boldsymbol{\mu}_i\cdot\mathbf{e})(\mathbf{M}\cdot\mathbf{e})^n]\}}{\sum_{n=0}^{\infty}(3E/2kT)^n(n!)^{-1}I[x;(\mathbf{M}\cdot\mathbf{e})^n]}, \tag{3.4}$$

where $I[\cdots]$ denotes the following integral over the N coordinates

$$I[x;f]=\int_N\cdots\int f\exp(-U_N/kT)dx. \tag{3.5}$$

Averaging over the field direction $\mathbf{e}$ we have

$$\bar{\boldsymbol{\mu}}_i=\frac{\sum_{n=0}^{\infty}(3E/2kT)^{2n+1}[(2n+1)!]^{-1}(2n+3)^{-1}I[x;(\boldsymbol{\mu}\cdot\mathbf{M})\mathbf{M}^{2n}]}{\sum_{n=0}^{\infty}(3E/2kT)^{2n}[(2n+1)!]^{-1}I[x;\mathbf{M}^{2n}]}. \tag{3.6}$$

Following Kirkwood, the integrations are carried out in two stages, first over all configurations of the coordinates except those of the ith dipole and then over all x_i. Expression (3.6) now gives

$$\bar{\boldsymbol{\mu}}_i=\frac{\sum_{n=0}^{\infty}(3E/2kT)^{2n+1}[(2n+1)!]^{-1}(2n+3)^{-1}(\boldsymbol{\mu}_i\cdot A_i[\mathbf{M}^{2n+1}])}{\sum_{n=0}^{\infty}(3E/2kT)^{2n}[(2n+1)!]^{-1}A_i[\mathbf{M}^{2n}]} \tag{3.7}$$

where

$$A_i[f]=\frac{\int_{(N-1)}\cdots\int f\exp(-U_N/kT)dX_i}{\int_{(N-1)}\cdots\int\exp(-U_N/kT)dX_i} \tag{3.8}$$

and dX_i is given by

$$dX_i=dx_1dx_2\cdots dx_{i-1}dx_{i+1}\cdots dx_N. \tag{3.9}$$

From Eq. (3.8) it follows that $A_i[f]$ is the average over all coordinates X_i of the quantity f for given values of the x_i. In a liquid the quantities $A_i[f]$ will be independent of the coordinates of the dipole i except in a thin region near the boundary of the region V in which the N dipoles lie. By taking V sufficiently large the ratio of the volume of this

region to the total volume V can be made very small. Hence the suffix i in Eq. (3.7) may be dropped everywhere and using (2.1), we find for ϵ the general formula

$$\epsilon=n^2+\frac{4\pi N\sum_{n=0}^{\infty}(3E/2kT)^{2n+1}[(2n+1)!]^{-1}(2n+3)^{-1}(\mathfrak{y}\cdot A[\mathbf{M}^{2n+1}])}{EV\sum_{n=0}^{\infty}(3E/2kT)^{2n}[(2n+1)!]^{-1}A[\mathbf{M}^{2n}]}. \tag{3.10}$$

To make further progress it is now necessary to take into account the structure of the liquid, since this determines the mean moments $A[\mathbf{M}^{2n+1}]$ and $A[\mathbf{M}^{2n}]$. If all short-range interaction is ignored, then

$$A[\mathbf{M}^{2n}]=\mu^{2n}, \qquad A[\mathbf{M}^{2n+1}]=\mathfrak{y}\mu^{2n}, \tag{3.11}$$

and (3.10) reduces to the formula which we derived in the second paragraph. To get a better approximation Kirkwood's method may be used. In a liquid like water, there is a fairly high degree of order round any given molecule but the order is very localized and falls away rapidly with the distance. To find the averages we assume that the ordering is complete for nearest neighbors, but vanishes outside the range of nearest neighbors. The generally accepted tetrahedral model for water now gives

$$\langle\cos\gamma\rangle=\tfrac{1}{3}; \quad \langle\cos\gamma'\rangle=1/27, \tag{3.12}$$

where γ is the angle between the axes of nearest neighbor moments, and γ' the angle between the axes of the four nearest neighbors of a given molecule. From the condition that the connections between nearest neighbors must be of the form O···H—O and not —O—H···H—O— it follows that

$$(\mathfrak{y}\cdot A[\mathbf{M}])=\mu^2(1+4\langle\cos\gamma\rangle);$$
$$A[\mathbf{M}^2]=\mu^2(5+8\langle\cos\gamma\rangle+12\langle\cos\gamma'\rangle). \tag{3.13}$$

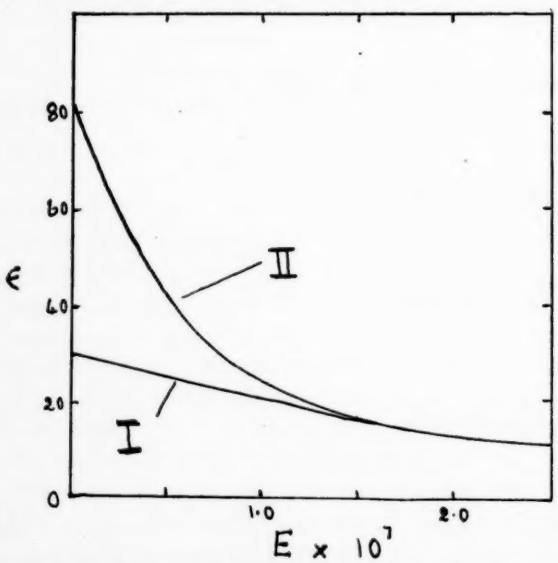

FIG. 1. The dielectric constant ϵ of water as a function of field strength E (in volts per cm). *Curve I*, Eq. (2.8). *Curve II*, Eq. (3.15).

Also for the particular model we have chosen, we have the relations

$$A[\mathbf{M}^{2n}]=A^n[\mathbf{M}^2];$$
$$(\mathfrak{y}\cdot A[\mathbf{M}^{2n+1}])=A[(\mathfrak{y}\mathbf{M})]A^n[\mathbf{M}^2]. \tag{3.14}$$

Using (3.13) and (3.14) in (3.10) the final result for the dielectric constant is

$$\epsilon=n^2+\frac{28N_0\pi(n^2+2)\mu_v}{3\sqrt{(73)E}}L\left[\frac{\sqrt{(73)}E\mu_v(n^2+2)}{6kT}\right]. \tag{3.15}$$

In Fig. 1 ϵ has been plotted as a function of E for $T=300°$K and $\mu_v=2.1$ Debye units; this is a little greater than the usual figure, but we have adjusted the value of μ_v slightly so that (3.15) gives the experimental value of ϵ at low field strengths. As to be expected the onset of saturation occurs at lower field strengths than with the generalized Onsager formula. From the curve II it is seen that the dielectric constant has fallen to a half of its usual figure when the field is 5.0×10^6 volts per cm. The corresponding field for expression (2.8) is 2.0×10^7 volts per cm. When the field is not sufficiently strong for the dielectric constant to differ very much from its low field value (3.15) gives

$$\epsilon=n^2+\frac{14N_0\pi(n^2+2)^2\mu_v}{27kT}\left[1-\frac{73E^2\mu_v^2(n^2+2)^2}{180k^2T^2}\right]. \tag{3.16}$$

From this formula it is found that a field of 2.5×10^5 volts per cm is required to reduce the dielectric constant by one percent.

In conclusion it must be noted that the whole method depends on the validity of several simplifying assumptions. The success of the Kirkwood analysis suggests that these approximations are fairly reliable at low field strengths. For strong fields they may not be so satisfactory. For this reason experimental investigation with fields sufficiently strong to show some dependence of ϵ on E would be very useful. If the results agreed fairly well with (3.16) it would indicate that (3.15) is probably reliable at values of E which are much higher than are feasible in experimental determinations of ϵ.

Note added in proof.—Some confirmation of the theory developed above, is provided by some experimental results due to Malsch.[6] He found, using fields up to 2.5×10^5 volts per cm, that the dependence of dielectric constant on field strength followed closely formula (3.16), the reduction being about 0.7 percent for the maximum field strength.

[6] J. Malsch, Physik Z. **29**, 770 (1928).

The Stereochemistry of the Imidazolidine Ring

ERNST FISCHER
The Weizmann Institute of Science, Rehovoth, Israel

(Received November 13, 1950)

The electric moments of several imidazolidine derivatives in *p*-xylene solution have been measured at various temperatures. It is suggested that the substances are mixtures of geometrical isomers which are in thermal equilibrium, the isomerism being due to the pyramidal arrangement of the valencies of the tervalent nitrogen.

From the temperature dependence of the moments, the energy difference between the two postulated isomers is calculated to be about 1.6 kcal/mole.

IN a recent investigation,[1] the electric moment of 2-pentamethyleno-imidazolidine (I) and the related substances (II), (III) have been determined in benzene solution at 30°. It was suggested that the values found (1.4–1.5D) were due to the existence of thermal equilibrium between two possible geometrical isomers, in which the NH-bonds were either on the same side (*cis*) or on different sides (*trans*) of the plane of the ring.

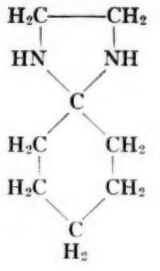

I

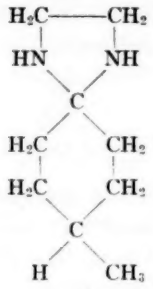

II

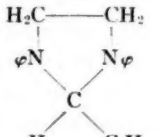

III

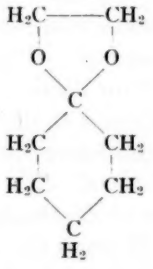

IV

Assuming, as a first approximation, that the five-membered ring is regular and that the N−H bonds form an angle of about 120° with the plane of the ring, the moments (m_1, m_2) of the *trans* and *cis* forms should be 0.6 and 2.4D, respectively (**C−H**=0.4, **N−C**=0.4, **N−H**=1.3D). Additional support for these calculations is provided by the fact that the moment (1.07) found[1] for 2-pentamethyleno-1,3-dioxolane (IV), a compound geometrically similar to (I), agrees well with the calculated value (**C−O**=0.7D).

From the above values for m_1 and m_2, and the experimental moment m of the assumed mixture of isomers, the position of the equilibrium can be estimated:

$$m^2 = m_1^2 x_1 + m_2^2(1-x_1), \qquad (1)$$

where x_1 is the weight fraction of the first isomer.

From the stereochemistry of tervalent nitrogen, one should expect the potential barrier between isomers of the previously postulated type to be low.[2] It can, therefore, be expected that equilibrium between them exists even at room temperature, provided their energy difference is sufficiently small. This energy difference could be estimated from the temperature dependence of the equilibrium, which should express itself in a rise of the measured moment with temperature. As the vapor pressure of the substances involved is too low to make possible accurate determination of the moment in the gaseous state, the measurements were carried out in *p*-xylene solution.*

The results summarized in the last column of Table I show, indeed, a significant rise of the moments of (I) and (II) with temperature. That this effect is not due to a parallel change in the solute-solvent interaction follows from the observation that piperidine, which contains the same polar grouping C−NH−C as the imidazolidines, has a virtually temperature-independent dipole moment in *p*-xylene solution.[3]

TABLE I. Empirical constants, molar polarizations and refractions, and dipole moments.

Substance	Temperature	$C\alpha_0$	$1-\beta$	P_∞	R_D	$P_\infty - 1.05R_D$	μ
I	30°C	0.290	0.860	82.5	42.2	38.0	1.37±0.02
I	80	0.302	0.852	83.9	42.2	39.4	1.52±0.03
I	100	0.306	(0.849)	84.6	42.2	40.1	1.57±0.03
II	30	0.274	0.885	89.5	46.8	40.3	1.41±0.02
II	70	0.278	0.877	90.0	46.8	40.8	1.51±0.03
II	90	0.285	(0.875)	91.0	46.8	41.8	1.58±0.03
III	30	0.141	0.805	130.0	100.0	25.0	1.11±0.03
III	80	0.140	0.790	128.5	100.0	23.5	1.17±0.04
Piperidine	30	0.258	1.008	51.7	26.8	23.5	1.08±0.02
Piperidine	80	0.210	1.015	48.0	26.8	19.8	1.07±0.03

[1] Bergmann, Fischer, Zimkin, and Pinchas, Rec. trav. chim. Pays-Bas, to be published (1951).

[2] Only in specific cases, such as that of Troeger's base, the pyramidal structure is "frozen" and molecular asymmetry results. Prelog and Wieland, Helv. Chim. Acta **27**, 1127 (1944). Havinga, Chem. Abstracts **43**, 9072 (1949).

* Note: In view of the approximate nature of the various quantitative assumptions on which the calculations are based, all numerical results should be regarded as first approximations only.

[3] Rau and Narayanaswamy, Z. physik. Chem. **B26**, 23 (1934), report a value of 1.17D for the moment of piperidine in benzene solution.

TABLE II. Temperature dependence of the dipole moments and isomeric composition of (I) and (II).

Substance	Temperature (°C)	Dipole moment (D)	% *cis* form	Ratio Q of *cis*/*trans*	ΔE kcal/mole
I	30	1.37	28	0.39	
I	80	1.52	36	0.57	1.6
I	100	1.57	39	0.64	
II	30	1.41	30	0.43	
II	70	1.51	35.5	0.55	1.5
II	90	1.58	39.5	0.65	

In Table II, the weight fraction of the *cis* form and the ratio Q between the two isomers has been calculated from the measured moments of (I) and (II) according to Eq. (1). From these figures, the energy difference ΔE between the isomers follows thus:

$$Q_T = \text{const}\ e^{-\Delta E/RT}. \qquad (2)$$

ΔE values of about 1.6 kcal/mole were found by this method.

The case studied here somewhat resembles the thermal equilibrium between rotational isomers, such as *s-cis* and *s-trans* butadiene[4–7] and *trans* and *gauche* 1,2-dichloroethane.[8] In the latter case, the energy difference between the rotational isomers has been calculated from the variation with temperature of both the electric moment and the relative intensities of certain infrared absorption lines to be 1.2 and 1.0 kcal/mole, respectively.

For the sake of comparison, the moment of N,N′-diphenyl-2-hexyl-imidazolidine (III) has also been measured at two temperatures. As expected, the influence of temperature is less pronounced in this case, since for steric and other reasons, the angle formed between the N-phenyl bonds and the plane of the ring should *a priori* be much smaller.[1]

EXPERIMENTAL

The substances (I), (II), (III) have been described before.[1] The *p*-xylene used as solvent had a freezing point of 13.2°C. Its dielectric constant ϵ_0 and density d_0 were as follows:

	30°	80°	100°
ϵ_0	2.255	2.170	2.136
d_0	0.8523	0.8073	0.7891

The methods of measurement and computation have also been described elsewhere[9] in detail and will only be outlined here. The dielectric constants of the solutions were determined in a Sayce-Briscoe cell of about 50 $\mu\mu$F air capacity, the densities in a bicapillary pycnometer of about 7 ml capacity. The molar polarizations at infinite dilution P_∞ were calculated from the slopes $\alpha\epsilon_0$ and βd_0 of the straight lines describing the variation of the dielectric constant ϵ and the density d of the solutions with the weight fraction of the solute ω. The relevant figures are given in Table III, where $\Delta\epsilon = \epsilon - \epsilon_0$, $\Delta d = d - d_0$.

The sum of electronic and atomic polarization was taken as 1.05 times the molar refraction R_D for sodium light, as calculated from the bond refractions.[10]

TABLE III. Dielectric constants and densities of solutions in *p*-xylene.

$\omega\times10^5$	$\Delta\epsilon\times10^4$	$\Delta d\times10^5$	$\omega\times10^5$	$\Delta\epsilon\times10^4$	$\Delta d\times10^5$	$\omega\times10^5$	$\Delta\epsilon\times10^4$	$\Delta d\times10^5$
(I) at 30°			(II) at 30°			(III) at 30°		
330	47	—	360	47		245	15	
845	121	—	660	87		625	44	
1215	179	—	915	125		1010	71	
1730	259	206	1320	181	129	1350	99	225
3655	—	435	3165	—	310	2505	—	415
(I) at 80°			(II) at 70°			(III) at 80°		
1275	183	—	690	93		485	33	
2185	309	261	1035	136		710	46	
3060	434	—	1380	182		1010	63	
			1655	220	172	1210	80	216
			3060	—	323	2505	—	455
(I) at 100°			(II) at 90°			Piperidine at 30°		
545	68		710	95		490	62	
1000	129		1070	140		895	117	
1390	184		1425	186		1240	164	
1720	236		1710	220		1790	236	minus 12
						5150	—	minus 33
Piperidine at 80°								
465	42							
1180	112							
1685	163							
5150	—	minus 65						

[4] Mulliken, J. Chem. Phys. **7**, 121 (1939); Revs. Modern Phys. **14**, 269 (1942).
[5] Carr, Pickett, and Stuecklen, Revs. Modern Phys. **14**, 260 (1942).
[6] Rasmussen, Tunnicliff, and Brattein, J. Chem. Phys. **11**, 432 (1949).
[7] Pullman and Berthier, Bull. soc. chim. France 81 (1950).
[8] Mizushima *et al.*, J. Chem. Phys. **17**, 591 (1949).
[9] Bergmann, Weizmann, and Fischer, J. Am. Chem. Soc. **72**, 5009 (1950).
[10] Denbigh, Trans. Faraday Soc. **36**, 936 (1940).

Theory of High Polymer Solutions (The Dumbbell Model)

A. ISIHARA
Department of Physics, Faculty of Science, University of Tokyo, Tokyo, Japan
(Received November 6, 1950)

Following the theories of McMillan, Mayer, and Zimm, and extending the previous theories of the author, the second virial coefficient A_2 for high polymer solutions of the dumbbell model is calculated. The results are rigorous within the approximation of rigid-body potential. A_2 varies smoothly with l/R, where R is the radius of spheres of the dumbbell and l is their separation. Based on the present results, comparisons between the gas and the lattice theories are made.

INTRODUCTION

ONE of the main objects of the theories of high polymer solutions is to find the relation between the degree of polymerization of high polymers and their physical properties. The theoretical model which we often use is the so-called pearl-necklace model. For flexible and threadlike polymers, this model surpasses the alternative one—the compact single-body model which fits for compact polymers, such as globular proteins. The simplest case of the pearl-necklace model is the dumbbell model. This model seems rather peculiar for threadlike polymers, but it often gives signposts for finding the true ways of solving the problems of high polymer solutions. Of course, the reason is that it corresponds to the "threadlike polymers" of degree 2—a dimer. We know Kuhn's theory for the intrinsic viscosity of high polymer solutions started with the dumbbell model[1] and is revealed to be on the correct line by the appearance of Debye's theory,[2] although the latter has been refined over again by Kirkwood and Riseman[3] and Debye[4] himself. Also, Simha's result[5] for the same quantity can be deduced as a special case from that of Kirkwood and Riseman.[6] Similarly, the main results of the theories of high polymer solutions based on the lattice model, which has been used by Huggins[7] and Flory,[8] can be obtained by an extrapolation from the theories of Chang[9] and Miller[10] on the solution of dimers.

But as was pointed out by several authors,[11] the uniform distribution of polymer segments, assumed more or less in the above lattice theories, will not be realized at lower concentrations where the regions in the solution occupied by polymers and by solvent are distinguishable with each other.

From this point of view, the "gas theories" developed by McMillan and Mayer[12] and by Zimm[13] are noteworthy in the case of dilute solutions. Thus, following these gas theories, the present author[14] has reported a new method for calculating the second virial coefficient A_2 in the expansion of osmotic pressure π. Although the molecular potential used there was of rigid-body type, A_2 calculated is applicable to general ovaloids; and if we assume the shape and size of solute molecules, we can determine their axial ratios as spheroidal or rod-shaped particles by comparing the theoretical results with the experiments.

Now the next step on this line is to see the effect of polymerization on the second virial coefficient A_2, because polymerized molecules are not ovaloid-shaped in general. Already, Zimm[13] has proposed a trial on this line, but in order to avoid mathematical difficulties, he cut off the "pearl-necklace" separately so that the effect of polymerization on A_2 cannot be seen correctly from his result. Very recently, Flory and Krigbaum[15] have given a new theory for calculating the second and third virial coefficients. The dependence of these virial coefficients on temperature is determined by the intra- or inter-molecular interaction of high polymers in solution, but our knowledge about this is very slight. Taking the average of the free energy obtained from lattice theory by using the spatial distribution[16] of segments of a polymer about the center of gravity, Flory and Krigbaum have made progress against this problem and obtained the "partition function"—the probability—for a pair of molecules with center of gravity separated by a definite distance. But their procedure is phenomenological, because the probability must be determined from the potential of average force and not from the macroscopic free energy. Indeed, Flory and

[1] W. Kuhn, Z. physik. Chem. **A161**, 1, 427 (1932).
[2] P. Debye, J. Chem. Phys. **14**, 636 (1946).
[3] J. G. Kirkwood and J. Riseman, J. Chem. Phys. **14**, 565 (1948)
[4] P. Debye and A. M. Buche, J. Chem. Phys. **16**, 573 (1948).
[5] R. Simha, J. Research Natl. Bur. Standards **42**, 409 (1949).
[6] J. G. Kirkwood and J. Riseman, J. Chem. Phys. **18**, 512 (1950).
[7] M. L. Huggins, J. Chem. Phys. **9**, 660 (1941); J. Phys. Chem. **46**, 151 (1942); Ann. N. Y. Acad. Sci. **43**, 1 (1942).
[8] P. J. Flory, J. Chem. Phys. **9**, 660 (1941); **10**, 51 (1942); **11**, 521 (1943).
[9] T. S. Chang, Proc. Cambridge Phil. Soc. **35**, 265 (1939).
[10] His main results are published, to the point, in book form: A. R. Miller, *The Theory of High Polymer Solutions* (Oxford University Press, London, 1948).
[11] G. Gee and L. R. G. Treloar, Trans. Faraday Soc. **38**, 147 (1942). G. Gee, *Advances in Colloid Science* (Interscience Publishers, Inc., New York, 1946), Vol. II, p. 145.
[12] W. G. McMillan and J. E. Mayer, J. Chem. Phys. **13**, 276 (1945).
[13] B. H. Zimm, J. Chem. Phys. **14**, 164 (1946).
[14] A. Isihara, J. Chem. Phys. **18**, 1446 (1950); A. Isihara and T. Hayashida, J. Phys. Soc. Japan **6**, 40, 46 (1951).
[15] P. J. Flory and W. R. Krigbaum, J. Chem. Phys. **18**, 1086 (1950).
[16] According to Flory and Krigbaum this spatial distribution was deduced by Debye and Krieger. The same result has also been reported by the present author independently: A. Isihara, J. Phys. Soc. Japan **5**, 201 (1950).

Krigbaum used the free energy which is altered in two ways—first, to avoid the theoretical conflict of the application of the results of lattice theory to the dilute solutions, whereas they fit concentrated solutions, and secondly, to change the macroscopic free energy to the local free energy—but apart from this, the entropy of mixing which they used had been derived when the connectivity of segments was not too strong.

Under these circumstances, the author will calculate, in this paper, the second virial coefficient in the case of the dumbbell model, abolishing somewhat obscure assumptions. For the molecular potential in solution, the author was forced to use the rigid-body one, but within this approximation the final results obtained here are rigorous and are given as functions of the dimension of the dumbbell. As the calculated virial coefficient is the same as that of imperfect gases, the results can be applied to these cases also.

FUNDAMENTAL EQUATIONS

Using the generalized grand partition function, McMillan and Mayer[12] derived the rigorous expansion for the osmotic pressure in terms of concentration c:

$$\frac{\pi}{RTC}=\frac{1}{M_2}+A_2c+A_3c^2+\cdots, \tag{1}$$

where M_2 is the molecular weight of the solute, A_n are constants at constant temperature and are related to the molecular distribution functions, and c is measured in mass per unit volume. In this expansion the second virial coefficient A_2 is expressed as

$$A_2=-(N_0/2VM_2^2)\int g_2\{2\}d\{2\}, \tag{2}$$

where N_0 is Avogadro's number, and V is the volume of the system. If we take the rigid-body model, the function g_2 of a pair distribution of solute molecules, the configurations of which are expressed by $\{2\}$, assumes the value -1 when the two solute molecules interpenetrate each other, and zero when they are separated from each other. Thus, A_2 can be obtained by calculating the common volume of two solute molecules.

As has been explained in the previous papers,[14] this is the Haar's measure $m(I)$ of coset I, which is composed by the relative motions in the group of motions G of molecule B in touch with another molecule A:

$$A_2=4N_0v\varphi/M_2^2;\quad \varphi=m(I)/8v, \tag{3}$$

$$m(I)=\int_G f(x)dx;\quad x\epsilon G, \tag{4}$$

where $f(x)$ is the characteristic function of I in G:

$$f(x)=\begin{cases}1 & x\epsilon I\\ 0 & x\bar{\epsilon} I,\end{cases} \tag{5}$$

and v is the volume of a solute molecule. In those papers, we have shown that the above integral can be calculated by integration by parts where the first integration is to be done over each coset of the translation group g which is the normal subgroup of G:

$$f(\bar{x})=\int_g f(x\xi)d\xi;\quad \xi\epsilon g. \tag{6}$$

$\bar{f}(\bar{x})$ thus obtained is the function of the factor group $(G/g)\epsilon\bar{x}$, and it corresponds to the common volume swept by the motions of the molecule B around A while keeping its orientation. Then $m(I)$ is given by the following integral:

$$m(I)=\int_{G/g}\bar{f}(\bar{x})d\bar{x}$$

$$=(1/8\pi^2)\int\bar{f}(\bar{x})\sin\theta d\theta d\varphi d\tau, \tag{7}$$

where θ and φ are the polar coordinates determining the orientation of molecule B, τ is the spin of B around one direction, $1/8\pi^2$ is the normalizing constant, and finally, the elements $\bar{x}$ of the rotation group G/g are expressed by

$$\begin{bmatrix}\sin\varphi\sin\tau+\cos\theta\cos\varphi\cos\tau, & -\cos\varphi\sin\tau+\cos\theta\sin\varphi\cos\tau, & -\cos\tau\sin\theta\\ -\sin\varphi\cos\tau+\cos\theta\cos\varphi\sin\tau, & \cos\varphi\cos\tau+\cos\theta\sin\varphi\sin\tau, & -\sin\theta\sin\tau\\ \sin\theta\cos\varphi, & \sin\theta\sin\varphi, & \cos\theta\end{bmatrix}. \tag{8}$$

On calculating the integral of Eq. (7), we expressed in the previous papers the volume $\bar{f}(\bar{x})$ by an integral over spherical coordinates. This is because we could use the property that the eigenvalues of the matrix $(H_{\alpha\beta})$ are the principal radii of the ovaloid. $(H_{\alpha\beta})$ is the matrix obtained by the second derivatives of the supporting function H of the ovaloid with respect to the direction cosines α, β, and γ.

Now, in the case of the dumbbell model, we can't use such property, but there are two rotation symmetries, and $\bar{f}(\bar{x})$ depends only on θ. Therefore, $m(I)$ assumes the expression:

$$m(I)=\frac{1}{2}\int_0^{\pi}F(\theta)\sin\theta d\theta$$

$$=\int_0^{\pi/2}F(\theta)\sin\theta d\theta, \tag{9}$$

$$\bar{f}(\bar{x})=F(\theta). \tag{10}$$

Thus, it becomes the problem to find the explicit expression for $F(\theta)$. For this aim, we shall name the two spheres of a dumbbell A and B, and that of the second dumbbell a and b. Let four spheres have the same radii R, and the separations of two spheres both be l. At the standard position, the dumbbells A-B and a-b are put so that the vectors **BA** and **ab** are directed to the polar axis of spherical coordinates (Fig. 1). From this position the dumbbell a-b begins its rotation corresponding to $\bar{x}$ given by Eq. (8), and the angle between **BA** and **ab** becomes θ. The above equation (9) corresponds to this configuration.

In this orientation, all the positions of b (or a) in touch with A (or B) are contained in the volume of the concentric sphere of radius $2R$ to sphere A (or B). Accordingly, to calculate $m(I)$, we can replace A and B by two spheres of radii $2R$ and of separation l, and a and b by two points of separation l. Then, if b moves around the magnified A and B, the other endpoint a moves the shaded dumbbell which is magnified similar to A-B. This is illustrated in Fig. 2. The magnified A-B

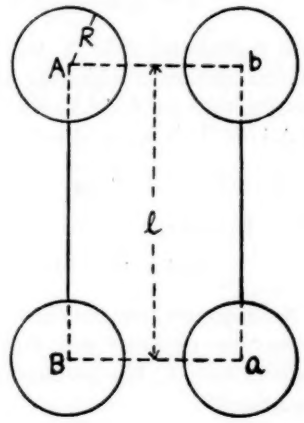

FIG. 1. Two dumbbells at their standard positions.

has not always the ordinary dumbbell shape. If the separation l is less than $4R$, it assumes a cocoon shape.

At any rate, we can now conceive that $F(\theta)$ can be obtained by calculating the common volume, $\Phi(\theta)$, between the enlarged dumbbell A-B and the shaded one which may be called a-b. As is shown in Fig. 3, if we designate by $Q(\theta, h)$ the cross section of this common volume cut by a plane that is laid at a distance h from the plane of centers of four speres, $\Phi(\theta)$ is expressed as

$$\Phi(\theta)=2\int_0^{2R} Q(\theta, h)dh. \tag{11}$$

In order to accomplish the calculation of $\Phi(\theta)$ in an orderly way, we shall transform the variable of integration. Let the radius of circles obtained as the cut ends of spheres by the plane π be r. Then r is given by

$$r=(4R^2-h^2)^{\frac{1}{2}}. \tag{12}$$

Thus, if we write

$$Q(\theta, h)=S(\theta, r), \tag{13}$$

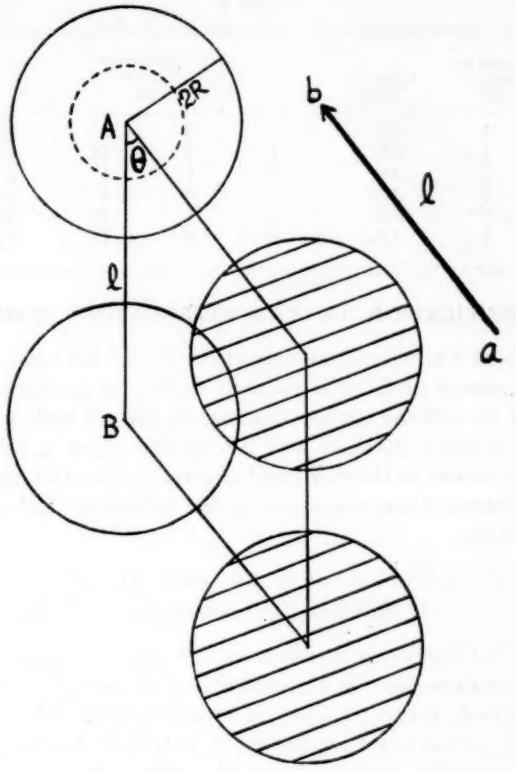

FIG. 2. The "interaction sphere" of two dumbbells A-B and a-b. These are replaced by a dumbbell of radius $2R$ and a line segment, respectively, the angle between them being θ.

Eq. (11) becomes

$$\Phi(\theta)=2\int_0^{2R} S(\theta, r)[r/(4R^2-r^2)^{\frac{1}{2}}]dr. \tag{14}$$

Accordingly, if the volume of A-B, composed of spheres of radius $2R$ and separation l, be $v(2R, l)$, the desired integral given by Eq. (7) becomes:

$$m(I)=2v(2R, l)-\int_0^{\pi/2}\Phi(\theta)\sin\theta d\theta=2v(2R, l)$$

$$-2\int_0^{\pi/2}\int_0^{2R} S(\theta, r)[r/(4R^2-r^2)^{\frac{1}{2}}]\sin\theta d\theta dr. \tag{15}$$

This is the fundamental equation for the calculation of the second virial coefficient of a dumbbell model.

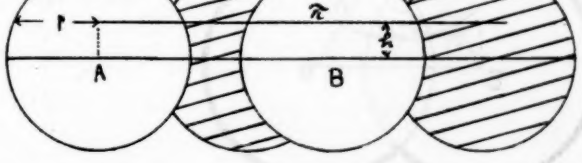

FIG. 3. The cut ends of the four spheres of Fig. 2 by a plane π.

TABLE I.

Factors to obtain $m(I)$	Common area	Classification $2r=$ 0	l	$2^{\frac{1}{2}}l$	$2l$
1	Aa	0	0	I	II
1	Bb	I	I	II	II
2	Ab	0	I	I	I
−2	Aab	0	0	I	II
−2	Bab	0	I	II	II
1	$ABab$	0	0	I	II

CLASSIFICATION OF THE INTEGRATION DOMAIN

From the above consideration it can be seen that the present problem is reduced to the one on the plane π. If we call the circles obtained as the cut ends of the four spheres A, B, a, and b with the plane π, by the same names as their original spheres, we are calculating the intersections expressed by the following algebraical equation:

$$(A+B-AB)(a+b-ab)=Aa+Bb+(Ab+aB)-(ABb+abB)-(ABb+abA)+ABab. \quad (16)$$

The left-hand side members of this equation mean that the intersection of a dumbbell A-B with the other rigid body C can be obtained by subtracting the volume $AB.C$, where the two spheres A and B of the dumbbell intersect the rigid body at the same time, from the volume of intersection of A and B with C obtained when the two spheres move independently with each other. Thus, in the right-hand members, for example, $ABab$ means the common volume of four spheres A, B, a, and b. The two members in parentheses on the right hand side are equal to each other owing to the symmetry relation.

This representation also holds when the members of this equation are considered on the above mentioned plane, π; A and B, etc., correspond to the circles on the plane. In this case the common surfaces aA or bB, and Ab or aB, between these circles, can be easily calculated based on the configurations of four spheres illustrated in Fig. 2. Figure 2 corresponds to the case where $l>4R$, but of course we must calculate the other case. We wish to omit the explanation of the classification arising from these situations and tabulate the final result in Table I.

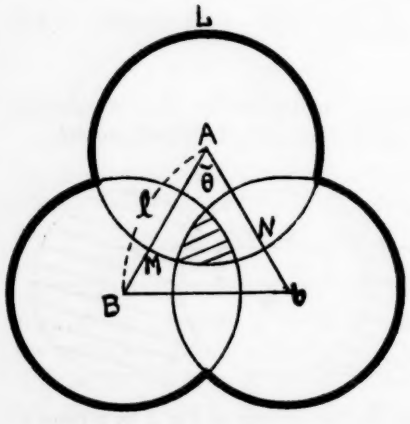

FIG. 4. The calculation of ABb.

In this table, the factors in the first column mean that they are to be multiplied by the corresponding common areas in the second column to obtain $m(I)$. The third column shows the types of equations of common surfaces. 0 means that there is no corresponding area. To calculate $m(I)$, we need not know here the explicit equations classified as I or II in this table. It is only necessary to add here the remark that I or II corresponds to different equations in each case. So, stopping to present the actual equations corresponding to this table, we shall add further remarks which will facilitate the calculation of the common surfaces of three or four circles.

The domain with shade in Fig. 4 illustrates the common area of three circles A, B, and b; that is, ABb in our notation. To obtain this area, let us at first calculate the area in the heavy curve of Fig. 4, expressed in two ways by the following equation:

$$A+B+b-AB-Bb-Ab+ABb=(5/2)\pi r^2+\Delta ABb-\tfrac{1}{2}(AB+Bb+Ab). \quad (17)$$

The right-hand side of this equation corresponds to the calculation in which we at first sum up the areas of sectors, such as $AMLN$, with respect to all the corners of ΔABb. This is equal to

$$(r^2/2)\{(2\pi-\angle A)+(2\pi-\angle B)+(2\pi-\angle C)\}=(5/2)\pi r^2.$$

Thus, from Eq. (17) we obtain:

$$ABb=AB+\tfrac{1}{2}Bb-(\pi/2)r^2+\tfrac{1}{2}l^2\sin\theta. \quad (18)$$

Analogously, we can calculate Aab and $ABab$, but in these cases we must note that there are cases when Aab reduces to Aa. The results are given by the following equations:

$$2r\geqq 2^{\frac{1}{2}}l;\quad (1-r^2/l^2)^{\frac{1}{2}}\leqq\sin\tfrac{1}{2}\theta\leqq l/2r:\quad Aab=Aa=ABab, \quad (19)$$

$$2r\geqq 2^{\frac{1}{2}}l;\quad l/2r\leqq\sin\tfrac{1}{2}\theta\leqq 2^{-\frac{1}{2}}:\quad Aab=AB+\tfrac{1}{2}Aa-\tfrac{1}{2}\pi r^2+\tfrac{1}{2}l^2\sin\theta,\quad ABab=2AB-\pi r^2+l^2\sin\theta. \quad (20)$$

Summarizing these considerations, we illustrate, in Fig. 5, the above classification with respect to common surfaces.

INTEGRAL FORMULAS

Comparing Fig. 5 with Table I we shall proceed to show $S(\theta, r)$ and its integration domain. As is shown in Fig. 6, this domain is divided into four subregions and we are required to integrate the common surfaces Bb, Ab, and $\pi r^2-l^2\sin\theta$ over respective regions illustrated in this figure. Figure 6 resembles Fig. 5, but the latter is more complicated. Thus, we can see that we have avoided using the needless calculation that occurs when we calculate the common areas in Table I from the beginning.

In Fig. 6 the maximum value of the ordinate r must be $2R$ and according to this value three different regions occur for the calculation of $m(I)$:

$$\begin{aligned} &\text{(I)} && 4 \leqq l/R, \\ &\text{(II)} && 2^{\frac{1}{2}} \leqq l/R \leqq 4, \\ &\text{(III)} && 0 \leqq l/R \leqq 2\cdot 2^{\frac{1}{2}}. \end{aligned} \tag{21}$$

Obviously, the first boundary value of R is determined by the condition of whether the two spheres of the dumbbell attach to each other or not. The second boundary value $2R=2^{-\frac{1}{2}}l$ corresponds to the case where the two spheres are orthogonal to each other. The physical origin of this is not obvious. Indeed, from the results in the next section, we can see that this is only the mathematical point of junction. When $l \leqq 2R$, the two spheres of the original dumbbell begin attaching to each other, but this point does not appear in the above domains.

Summarizing the above results, we shall arrange the necessary equations for calculating $m(I)$. From Eq. (15),

$$m(I)=2v(2R, l)-2J,$$

$$J=\int_0^{\pi/2}\int_0^{2R} S(\theta, r)\frac{r}{(4R^2-r^2)^{\frac{1}{2}}}\sin\theta d\theta dr\Big\}, \tag{22}$$

where J is given by the following equations:

(I) $4 \leqq l/R$

$$J_I(2R)=\int_0^{2R}\frac{rdr}{(4R^2-r^2)^{\frac{1}{2}}}\int_0^{2\sin^{-1}r/l}\Big\{2r^2\cos^{-1}\Big(\frac{l}{r}\sin\frac{\theta}{2}\Big) -2l\Big(r^2-l^2\sin^2\frac{\theta}{2}\Big)^{\frac{1}{2}}\sin\frac{\theta}{2}\Big\}\sin\theta d\theta. \tag{23}$$

(II) $2^{\frac{1}{2}} \leqq l/R \leqq 4$

$$I_1(2R)=\int_{l/2}^{2R}\frac{rdr}{(4R^2-r^2)^{\frac{1}{2}}}\int_{2\cos^{-1}l/2r}^{2\sin^{-1}r/l}\Big\{2r^2\cos^{-1}\Big(\frac{l}{r}\sin\frac{\theta}{2}\Big) -2l\Big(r^2-l^2\sin^2\frac{\theta}{2}\Big)^{\frac{1}{2}}\Big\}\sin\theta d\theta, \tag{24}$$

$$I_2(2R)=\int_{l/2}^{2R}\frac{rdr}{(4R^2-r^2)^{\frac{1}{2}}}\int_{2\cos^{-1}l/2r}^{\pi/2}\Big\{2r^2\cos^{-1}\frac{l}{2r} -l\Big(r^2-\frac{l^2}{4}\Big)^{\frac{1}{2}}\Big\}\sin\theta d\theta, \tag{25}$$

$$I_3(2R)=\int_{l/2}^{2R}\frac{rdr}{(4R^2-r^2)^{\frac{1}{2}}}\int_0^{2\cos^{-1}l/2r}(\pi r^2 -l^2\sin\theta)\sin\theta d\theta d\theta, \tag{26}$$

$$J_{II}=J_I(l/2)+I_1(2R)+2I_2(2R)+I_3(2R). \tag{27}$$

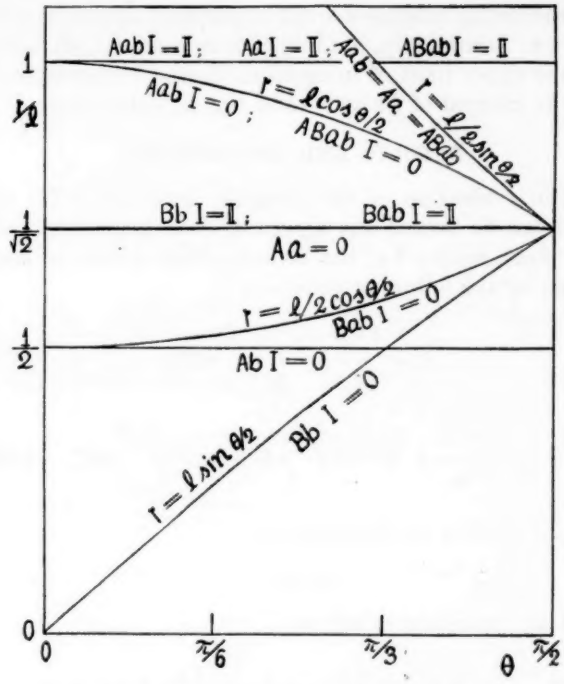

FIG. 5. The classification of common surfaces. Lines or curves represent "equilibrium curves" for different functional forms of the common surfaces. For example, *Bb* $I=0$ attached *under* the curve $r=l\sin\frac{1}{2}\theta$ means that *under* this curve, *Bb* vanishes, whereas it exists over the curve. Also, *Bb* $I=II$ above the line $r=l/2^{\frac{1}{2}}$ expresses that we must use different functional forms for *Bb* over and below the line.

(III) $0 \leqq l/R \leqq 2^{\frac{1}{2}}$

$$I_4(2R)=\int_{2^{-\frac{1}{2}}l}^{2R}\frac{rdr}{(4R^2-r^2)^{\frac{1}{2}}}\int_0^{\pi/2}(\pi r^2-l^2\sin\theta)\sin\theta d\theta, \tag{28}$$

$$J_{III}=J_I(l/2)+I_1(2^{-\frac{1}{2}}l)+2I_2(2^{-\frac{1}{2}}l) +I_3(2^{-\frac{1}{2}}l)+I_4(2R). \tag{29}$$

In these equations $J_I(2R)$ and $I_n(2R)(n=1, 2, 3)$ are

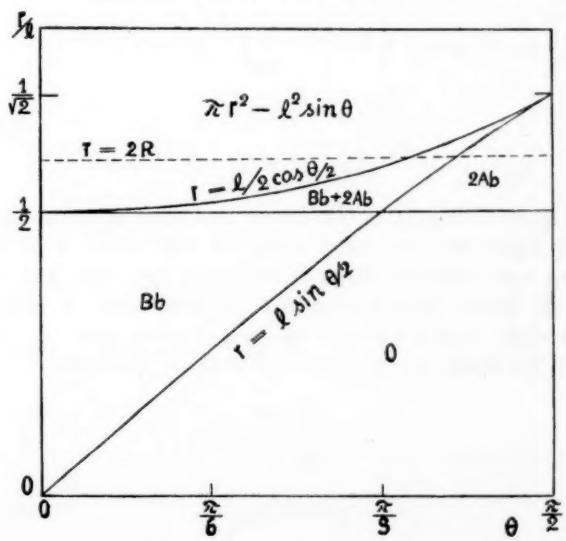

FIG. 6. Integration domain of $S(\theta, r)$.

considered as functions of the upper limit of integration over r. Accordingly, $I_n(2-\frac{1}{2}l)$ differs from $I_n(2R)$ only in the upper limit of integration. I_1 and I_2 correspond to the integral of Bb and Ab of Fig. 6, respectively.

RESULTS AND DISCUSSIONS

The evaluation of the integrals from Eqs. (22) to (28) can be carried out rigorously (see Appendix) and the final results for the second virial coefficient are given by the following equations:

$$A_2=\frac{4N_0v}{M_2^2}\varphi=\frac{N_0}{M_2^2}\frac{32}{3}\pi R^3\psi, \tag{30}$$

$$\varphi=\frac{m(I)}{8v};\quad \psi=v\varphi\Big/\frac{8}{3}\pi R^3=m(I)\Big/\frac{64}{3}\pi R^3, \tag{31}$$

where φ and ψ are functions of

$$x=l/R, \tag{32}$$

and are expressed as follows:

$$\varphi=\begin{cases}\varphi_I=2\left(1-\dfrac{2}{5x^2}\right); & x\geqq 4\\[2ex] \varphi_{II}=\dfrac{4}{5x^2}+\dfrac{x}{2}+\dfrac{3}{32}x^2-\dfrac{x^3}{40}; & 2\tfrac{1}{2}\leqq x\leqq 4\\[2ex] \varphi_{III}=\varphi_{II}(x)-\dfrac{1}{4\pi}\Bigg\{\left(1-\dfrac{x^2}{8}\right)^{\frac{1}{2}}\left(\dfrac{2}{5}+\dfrac{x^2}{20}\right)\\ \quad+\left(\dfrac{64}{5x^2}-8+\dfrac{3}{4}x^2\right)\tan^{-1}\left(1-\dfrac{x^2}{8}\right)^{\frac{1}{2}}\\ \quad+\left(x-\dfrac{11}{80}x^3\right)\tan^{-1}\dfrac{4}{x}\left(1-\dfrac{x^2}{8}\right)^{\frac{1}{2}}\Bigg\}; & 2\leqq x\leqq 2\tfrac{1}{2}\\[2ex] \varphi_{IV}=2\varphi_{III}\Big/\left(1+\dfrac{3}{4}x-\dfrac{x^3}{16}\right); & 0\leqq x\leqq 2\end{cases} \tag{33}$$

$$\psi=\begin{cases}\varphi; & 2\leqq x,\\ \varphi_{III}; & 0\leqq x\leqq 2.\end{cases} \tag{34}$$

Figure 7 illustrates the above functions φ and ψ. At first sight the functional forms of the factor φ or ψ seem very different in each region of Eq. (21), but φ (or ψ) shows no discontinuity or even nick at each boundary, and is a slowly varying function of x.

In the limit, $x\to\infty$; that is, $l\gg R$, A_2 becomes

$$A_2=\frac{N_0}{M_2^2}\frac{64}{3}\pi R^3$$

$$=4(A_2)_s, \tag{35}$$

where $(A_2)_s$ is the second virial coefficient for the spherical particle of radius R. The factor 4 corresponds, of course, to the combinations of two spheres of two ovaloids. This is the case treated by Zimm,[13] and we can infer that the virial coefficient of a polymer of degree n does not depend on its molecular weight in such a limiting case. But this case is very particular and the effect of polymerization does not appear. The coupling of two spheres diminishes A_2 gradually and reduces it, at last, to the value $(A_2)_s$ of a single sphere when l becomes zero. Also, if the polymers are randomly kinked and nearly spherical rigid bodies, A_2 will vary inversely as the square of the degree of polymerization. The logarithmic plot of the results of the recent experiment of Outer, Carr, and Zimm[17] shows this dependence.

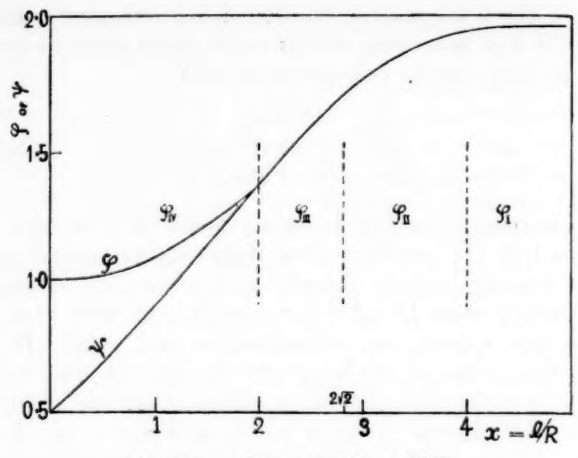

FIG. 7. φ and ψ as functions of l/R.

The best way of finding agreement of theoretical results on dilute high polymer solutions, with experiments, is to plot $\bar{V}_1[(\pi/v_2)-(\pi/v_2)_0]$ against v_2, where $\bar{V}_1$ is the partial molar volume of the solvent, v_2 the volume concentration of polymers, and $(\pi/v_2)_0$ is the limiting value of π/v_2 when v_2 approaches zero. According to the lattice theories of Miller,[11] the osmotic pressure π is given by the following expression:

$$\frac{\pi}{RTc}=\frac{1}{M_2}+\left(\frac{1}{2}-\frac{1}{z}\right)\left(1-\frac{1}{n}\right)^2\frac{c}{\rho_2^2\bar{V}_1}, \tag{36}$$

where z is the coordination number, ρ_2 the density of polymer, and n is the degree of polymerization. From this equation, we can obtain the slope of the above plot:

$$\bar{V}_1[(\pi/v_2)-(\pi/v_2)_0]/v_2=RT(\tfrac{1}{2}-1/z)(1-1/n)^2. \tag{37}$$

If we take $z=6$ and $T=300°$K, this slope becomes 50 in the case of dimers. This is nearly close to the mean value of several experimental values.[18] But in general, n must be very large, and the magnitude of the slope approaches 200 or more. In this case, the theories of Miller coincide with those of Huggins[7] and Flory.[9] Thus, we can say that the deviation of their lattice

[17] Outer, Carr, and Zimm, J. Chem. Phys. **18**, 830 (1950).
[18] P. J. Flory, J. Chem. Phys. **13**, 453 (1945), Fig. 3.

theories from experiments is more serious when n becomes larger.

On the other hand, Eq. (3) gives the slope:

$$RT\bar{V}_1\rho_2^2A_2=4RT\varphi/n. \tag{38}$$

For the dumbbell model, this slope is too large, even if φ assumes its minimum value 1. In the case of gas theory, there is, of course, some ambiguity about n—the ratio of molecular volume of polymer to that of solvent; but the general tendency of Eq. (38) is more suitable to experiments for larger n, because from the result of this paper we can expect that φ does not increase in proportion to n, except in a special case. When polymers are so entangled that they cannot be "drained" freely,[19] the order of magnitude of φ is probably 1. In other words, φ is a function of the screening constant of high polymers,[4] and a further consideration of this will be favorable to the gas theory.

In conclusion, the author wishes to thank Mr. T. Hayashida and Mr. K. Yamazi for their interest and support of this paper.

APPENDIX

The evaluation of the integrals from Eq. (22) to Eq. (28) is somewhat annoying. Therefore, it will be convenient to give a brief account of it. The integrations of J_I, J_{II}, and J_{III} can be obtained by suitable combinations of integrals A_n to E_n in this appendix.

$$J_1(r)=\int_0^r\frac{rdr}{(4R^2-r^2)^{\frac{1}{2}}}\int_0^{2\sin^{-1}r/l}\{2r^2\cos^{-1}\left(\frac{l}{r}\sin\frac{\theta}{2}\right)-2l(r^2-l^2\sin^2\tfrac{1}{2}\theta)^{\frac{1}{2}}\sin\tfrac{1}{2}\theta\}\sin\theta d\theta=\frac{\pi}{2l^2}A_5(r), \tag{A1}$$

$$I_1(r)=\int_{l/2}^r\frac{rdr}{(4R^2-r^2)^{\frac{1}{2}}}\int_{2\cos^{-1}l/2r}^{2\sin^{-1}r/l}\{2r^2\cos^{-1}\left(\frac{l}{r}\sin\frac{\theta}{2}\right)-2l(r^2-l^2\sin^2\tfrac{1}{2}\theta)^{\frac{1}{2}}\sin\tfrac{1}{2}\theta\}\sin\theta d\theta$$
$$=-\frac{l^5}{8}C_{-3}(r)+\tfrac{3}{4}l^3C_{-1}(r)-\tfrac{3}{2}lC_1(r)-\frac{1}{2l}C_3(r)+l^2D_1(r)-4D_3(r)+\frac{1}{l^2}D_5(r), \tag{A2}$$

$$I_2(r)=\int_{l/2}^r\frac{rdr}{(4R^2-r^2)^{\frac{1}{2}}}\int_{2\cos^{-1}l/2r}^{\pi/2}\left\{2r^2\cos^{-1}\frac{l}{2r}-l\left(r^2-\frac{l^2}{4}\right)^{\frac{1}{2}}\right\}\times\sin\theta d\theta=l^2E_1(r)-2E_3(r)-\frac{l^3}{4}C_{-1}(r)+\frac{l}{2}C_1(r), \tag{A3}$$

$$I_3(r)=\int_{l/2}^r\frac{rdr}{(4R^2-r^2)^{\frac{1}{2}}}\int_0^{2\cos^{-1}l/2r}(\pi r^2-l^2\sin\theta)\sin\theta d\theta=2\pi A_3(r)-\frac{\pi}{2}l^2A_1(r)-l^2E_1(r)+\frac{l^5}{8}C_{-3}(r)-\frac{l^3}{4}C_{-1}(r); \tag{A4}$$

$$I_4(2R)=\pi(16R^2-2l^2)^{\frac{1}{2}}[(4/3)R^2-l^2/24]; \tag{A5}$$

$$A_n(r)=\int_0^r\frac{r^n}{(4R^2-r^2)^{\frac{1}{2}}}dr, \tag{A6}$$

$$A_5(r)=\frac{256}{15}R^5-(4R^2-r^2)^{\frac{1}{2}}\left(\frac{r^4}{5}+\frac{16}{15}r^2R^2+\frac{128}{15}R^4\right), \tag{A7}$$

$$A_3(r)=(16R^2-l^2)^{\frac{1}{2}}\left(\frac{4}{3}R^2+\frac{l^2}{24}\right)-(4R^2-r^2)^{\frac{1}{2}}\left(\frac{r^2}{3}+\frac{8}{3}R^2\right), \tag{A8}$$

$$A_1(r)=\tfrac{1}{2}(16R^2-l^2)^{\frac{1}{2}}-(4R^2-r^2)^{\frac{1}{2}}; \tag{A9}$$

$$B_n(r)=\int_{l/2}^r\frac{(4R^2-r^2)^{\frac{1}{2}}}{(4r^2-l^2)^{\frac{1}{2}}}r^ndr, \tag{A10}$$

$$z=\left(\frac{4R^2-r^2}{4r^2-l^2}\right)^{\frac{1}{2}}, \tag{A11}$$

$$B_3(r)=(16R^2-l^2)\left[\pi\left(\frac{R^2}{32}+\frac{3}{512}l^2\right)+\frac{16R^2-l^2}{64}\frac{z}{(1+4z^2)^2}+\left(\frac{5}{128}l^2-\frac{R^2}{8}\right)\frac{z}{(1+4z^2)}-\left(\frac{R^2}{16}+\frac{3}{256}l^2\right)\tan^{-1}2z\right], \tag{A12}$$

$$B_1(r)=(16R^2-l^2)\left[\frac{\pi}{32}+\frac{1}{8}\frac{z}{1+4z^2}-\frac{1}{16}\tan^{-1}2z\right], \tag{A13}$$

$$B_{-1}(r)=-\frac{\pi}{4}+\frac{R}{l}\pi+\tfrac{1}{2}\tan^{-1}2z-\frac{2R}{l}\tan^{-1}\frac{l}{2R}z; \tag{A14}$$

$$C_n(r)=\int_{l/2}^r\frac{(4r^2-l^2)^{\frac{1}{2}}}{(4R^2-r^2)^{\frac{1}{2}}}r^ndr, \tag{A15}$$

$$C_3(r)=(16R^2-l^2)\left[\frac{16R^2-l^2}{16}\frac{z}{(4z^2+1)^2}+(\tfrac{3}{4}R^2+\tfrac{1}{32}l^2)\frac{z}{4z^2+1}+(\tfrac{3}{4}R^2+\tfrac{1}{64}l^2)\tan^{-1}2z\right]_z^\infty, \tag{A16}$$

$$C_1(r)=(16R^2-l^2)\left[\frac{\pi}{8}-\frac{1}{2}\frac{z}{1+4z^2}-\tfrac{1}{4}\tan^{-1}2z\right]; \tag{A17}$$

$$D_n(r)=\int_{l/2}^r\frac{r^n}{(4R^2-r^2)^{\frac{1}{2}}}\cos^{-1}\frac{l(4r^2-l^2)^{\frac{1}{2}}}{2r^2}dr, \tag{A18}$$

$$D_5(2R)=\frac{\pi}{2}\{A_5(2R)-A_5(l/2)\}-\frac{256}{15}lR^4B_{-1}(2R)-\frac{32}{15}lR^2B_1(2R)-\tfrac{3}{2}lB_3(2R), \tag{A19}$$

$$D_5(2^{-\frac{1}{2}}l)=\frac{\pi}{2}\{A_5(2R)-A_5(l/2)\}-\frac{256}{15}lR^4B_{-1}(2^{-\frac{1}{2}}l)-\frac{32}{15}lR^2B_1(2^{-\frac{1}{2}}l)-\tfrac{3}{2}lB_3(2^{-\frac{1}{2}}l), \tag{A20}$$

$$D_3(2R)=\frac{\pi}{2}A_3(2R)-\frac{16}{3}lR^2B_{-1}(2R)-\tfrac{3}{2}lB_1(2R), \tag{A21}$$

$$D_3(2^{-\frac{1}{2}}l)=\frac{\pi}{2}A_3(2R)-\frac{16}{3}lR^2B_{-1}(2^{-\frac{1}{2}}l)-\tfrac{3}{2}lB_1(2^{-\frac{1}{2}}l), \tag{A22}$$

$$D_1(2R)=\frac{\pi}{2}A_1(2R)-2lB_{-1}(2R), \tag{A23}$$

$$D_1(2^{-\frac{1}{2}}l)=\frac{\pi}{2}A_1(2R)-2lB_{-1}(2^{-\frac{1}{2}}l); \tag{A24}$$

$$E_n(r)=\int_{l/2}^r\frac{r^n}{(4R^2-r^2)^{\frac{1}{2}}}\cos^{-1}\frac{l}{2r}dr, \tag{A25}$$

$$E_1(2R)=lB_{-1}(2R), \tag{A26}$$

$$E_1(2^{-\frac{1}{2}}l)=lB_{-1}(2^{-\frac{1}{2}}l)+\frac{\pi}{4}\{A_1(2^{-\frac{1}{2}}l)-A_1(2R)\}, \tag{A27}$$

$$E_3(2R)=\frac{8}{3}lR^2B_{-1}(2R)+\frac{l}{3}B_1(2R), \tag{A28}$$

$$E_3(2^{-\frac{1}{2}}l)=\frac{8}{3}lR^2B_{-1}(2^{-\frac{1}{2}}l)+\frac{l}{3}B_1(2^{-\frac{1}{2}}l)+\frac{\pi}{4}\{A_3(2^{-\frac{1}{2}}l)-A_3(2R)\}. \tag{A27}$$

[19] P. M. Doty and H. Mark, Ind. Eng. Chem. **38**, 682 (1946).

Isotope Effect on Dissociation Probabilities in the Mass Spectra of Chloroform and Chloroform-*d*

VERNON H. DIBELER
National Bureau of Standards, Washington, D. C.

AND

RICHARD B. BERNSTEIN
Illinois Institute of Technology, Chicago, Illinois

(Received October 30, 1950)

The mass spectra of the isotopic molecules $CHCl_3$ and $CDCl_3$ have been determined, using electron energies of 50 v and 70 v. It was found that the probability of dissociation of the C−H bond is approximately three times that for the dissociation of the C−D bond. The relative probability of dissociating H+Cl and D+Cl is the same as the relative probability of obtaining HCl^+ and DCl^+ ions, namely, about 1.6. Equal probability was observed for the dissociation of H+2Cl and D+2Cl. The probability of removing chlorine atoms is only slightly affected by the deuterium substitution.

INTRODUCTION

DIFFERENCES in the probability of dissociating C−H and C−D bonds by electron impact have been observed in a few simple hydrocarbons.[1–3] In general, these studies indicate that, although the sensitivity (ion current per unit of pressure) of the molecule ion is the same for isotopic molecules, the effect of deuterium substitution on the relative probabilities of the various dissociation processes is not predictable from statistical considerations alone. The abnormal ratio of the probabilities of dissociating a C−H bond compared with a C−D bond has been called the "π-effect" by Evans, Bauer, and Beach.[2] The increased probability of dissociating a C−H bond if a D atom is attached to the same carbon atom has been termed by them the "Γ-effect." Although these effects are found to be somewhat different for analogous processes in the various deuteromethanes,[4] they were found to be approximately constant for dissociation processes in the same molecule. It is of considerable interest to test these effects in other types of organic molecules whose bonds exhibit other than covalent properties. A study of the mass spectra of $CHCl_3$ and $CDCl_3$ provides such an opportunity, where the partially ionic C−Cl bonds are involved. An interesting addition is also made to the reference mass spectra of isotopic molecules for analytical applications as well as theoretical use.

EXPERIMENTAL

Chloroform (reagent grade) was purified by fractiona distillation through a vacuum-jacketed column (1.2×90 cm) packed with glass helices. Chloroform-*d* was prepared by the reaction of trichloroacetophenone with sodium deuteroxide.[5] After separation from the aqueous phase the product was distilled through a small Vigreaux column. The constant-boiling center cut was then redistilled in vacuum. The chloroform-*d* contained 0.8 M percent of ordinary chloroform, as determined by examination of the mass spectrum.

The mass spectra were obtained with a Consolidated mass spectrometer, model 21–102, equipped with automatic emission control and temperature control of the ionization chamber. The temperature of the ion source was about 245°C. Data were obtained for ionization by electrons whose nominal energies were 50 and 70 v. Conventional operating procedures were used except that sample pressures in the reservoir bottles were measured with a micromanometer.[6]

RESULTS

Table I gives a portion of the polyisotopic mass spectra of $CHCl_3$ and $CDCl_3$ for 50-v and 70-v electrons. The contributions of 0.8 M percent $CHCl_3$ impurity in the $CDCl_3$ were removed from the spectrum of the latter. The contributions of ions containing C^{13} have also been removed using the isotope ratio $C^{13}/C^{12}=0.0109$ observed with the above instrument. Omitted from the table for the sake of brevity are the peaks due to all doubly charged ions. However, their relative abundances are included in Table II. Two ion peaks of uncertain origin at $m/e=71$ and 73 have also been omitted from the $CHCl_3$ spectrum. Their intensities were 0.03 percent and 0.01 percent, respectively, of the maximum peak. The columns in Table I list, respectively, the mass to charge ratio (m/e) of the ions, and their intensities relative to the maximum peak in each spectrum. Total ionization and the observed sensitivity of the maximum peak are given at the bottom of the table. No ions due to metastable transitions were observed.

In order to compare the relative probability of various dissociation processes for $CHCl_3$ and $CDCl_3$, it is first

[1] J. Delfosse and J. A. Hipple, Phys. Rev. **54**, 1060 (1938).
[2] Evans, Bauer, and Beach, J. Chem. Phys. **14**, 701 (1946).
[3] J. Turkevich, *et al.*, J. Am. Chem. Soc. **70**, 2638 (1948).
[4] V. H. Dibeler and F. L. Mohler, J. Research Natl. Bur. Standards **45**, 441 (1950).
[5] Boyer, Bernstein, Brown, and Dibeler, J. Am. Chem. Soc., to be published.
[6] V. H. Dibeler and F. Cordero, J. Research, Natl. Bur. Standards **46**, 1 (1951).

necessary to compute the spectrum that would be obtained if chlorine were monoisotopic. For $CHCl_3$, this is done by adding the abundances of all ions with the same configuration regardless of isotopic specie and then normalizing on the basis of the maximum peak. Thus, the total abundance of the Cl^+ ions is the sum of the 35 and 37 peaks (Table I), whereas the total abundance of the HCl^+ ions is the sum of the 36 and 38 peaks, and so forth. The normalized, monoisotopic 50-v spectrum is given in Table II, column 2. The 70-v spectrum (column 3) was obtained similarly from the complete polyisotopic mass spectrum.

The calculation for $CDCl_3$ is slightly complicated by the superposition of ions containing Cl^{37} atoms and ions containing D atoms. The normal isotope abundance ratio Cl^{37}/Cl^{35} obtained in this laboratory was found to be 0.319. Thus, the total abundance of Cl^+ ions from $CDCl_3$ (Table I) is expected to be 1.319 times the 35 peak (22.6), or 29.8. The total abundance of DCl^+ ions is the sum of the 35, 37, and 39 peaks (31.85) minus the total Cl^+ ions (29.8), or 2.05. Similarly, the total abundance of the CCl^+ ions is 1.319 times the 47 peak (37.0), or 48.8. The total $CDCl^+$ ion abundance is the sum of the 47, 49, and 51 peaks (69.7) minus the total CCl^+ abundance (48.8), or 20.9. For ions containing two chlorine atoms, the abundances of the ions CCl_2^{35}, $CCl^{35}Cl^{37}$, and CCl_2^{37} are in the statistical ratios of 1:0.638:0.102. The total abundance of CCl_2^+ ions is thus 1.740 times the 82 peak (2.22), or 3.86. The total $CDCl_2^+$ ion abundance is the sum of the 82, 84, 86, and 88 peaks (175.42) minus the total CCl_2^+ ions (3.86), or 171.6. Similarly, the total abundance of the CCl_3^+ ions is $1+0.957+0.305+0.0325=2.295$ times the 117 peak (0.32), or 0.73, and the total $CDCl_3^+$ ion abundance is 3.89. The 50-v monoisotopic spectrum is then normalized as before and is given in Table II, column 5. The complete 70-v spectrum (column 6) was obtained in a similar manner from the complete polyisotopic spectrum.

DISCUSSION

From Table I, the sensitivities of the most abundant ions of $CHCl_3$ and $CDCl_3$ for 50-v electrons are 76.4 and 80.1 divisions per micron, respectively. The sensitivities of the molecule ions may be computed from these values. For $CHCl_3$, the sensitivity of the molecule ion is $(76.4)(0.0185)=1.41$ divisions per micron. For $CDCl_3$, the 119 peak is first corrected for the $CCl_2^{35}Cl^{37+}$ ion contribution using the second term of the quadratic expansion given above. Then the sensitivity is $(80.1)(0.0174)=1.39$ divisions per micron. Thus, the molecule ion sensitivities are equal within the estimated (2 percent) experimental error. A similar result is obtained from the data at 70 v. These results are in agreement with previous observations on a number of sets of isotopic molecules including deuterohydrocarbons.

The sums of the principal ions from $CHCl_3$ and $CDCl_3$ at 50 v are 295 and 283, respectively, calculated on the basis of the spectra normalized to the maximum peak. However, on the basis of the molecule ion peaks (underlined in Table I) the ratio of the total ionizations is seen to be $(295/283)(0.0174/0.0185)=0.98$, which is unity within experimental error.

TABLE I. Portion of the polyisotopic mass spectra of $CHCl_3$ and $CDCl_3$ for 50-v and 70-v electrons. Correction is made for C^{13}.

	$CHCl_3$		$CDCl_3$	
m/e	50 v	70 v	50 v	70 v
35	22.1	20.1	22.6	20.2
36	2.63	2.20	...	...
37	6.81	6.15	8.66	7.86
38	0.84	0.69	...	...
39	...	...	0.59	0.51
47	39.3	37.1	37.0	35.0
48	16.7	15.9	...	...
49	12.4	11.7	27.5	25.8
50	5.40	4.82	...	...
51	...	...	5.19	4.93
70	1.04	0.80	0.96	0.78
72	0.68	0.53	0.65	0.52
74	0.12	0.10	0.11	0.09
82	3.86	3.63	2.22	2.17
83	100.0	100.0	...	...
84	2.43	2.25	100.0	100.0
85	63.4	64.0	...	...
86	0.40	0.39	63.2	63.3
87	10.2	10.2	...	...
88	...	...	10.0	9.92
117	1.03	1.08	0.32	0.30
118	1.85	1.85	...	...
119	1.00	1.02	2.04	2.02
120	1.66	1.69	...	...
121	0.34	0.33	1.67	1.66
122	0.53	0.53	...	...
123	0.05	0.04	0.52	0.52
124	0.07	0.05	...	...
125	...	...	0.07	0.05
Sensitivity*	76.4	83.1	80.1	87.7
Total ionization	295.	287.	283.	275.

* Ion current of principal peak per unit of pressure in the reservoir in arbitrary units.

TABLE II. Monoisotopic spectra of $CHCl_3$ and $CDCl_3$ for 50-v and 70-v electrons.

	$CHCl_3$			$CDCl_3$	
Ion	50 v	70 v	Ion	50 v	70 v
$CHCl^{++}$	0.07	0.06	$CDCl^{++}$	0.08	0.08
Cl^+	16.6	15.1	Cl^+	17.4	15.5
HCl^+	2.00	1.66	DCl^+	1.19	1.14
CCl_2^{++}	0.48	0.42	CCl_2^{++}	0.49	0.51
$CHCl_2^{++}$	0.78	0.80	$CDCl_2^{++}$	1.16	1.25
CCl^+	29.8	28.0	CCl^+	28.4	26.9
$CHCl^+$	12.7	11.9	$CDCl^+$	12.2	11.4
$CHCl_3^{++}$	...	0.11	$CDCl_3^{++}$	...	...
Cl_2^+	1.06	0.82	Cl_2^+	1.00	0.81
CCl_2^+	3.86	3.61	CCl_2^+	2.25	2.20
$CHCl_2^+$	100.0	100.0	$CDCl_2^+$	100.0	100.0
CCl_3^+	1.39	1.41	CCl_3^+	0.44	0.40
$CHCl_3^+$	2.37	2.37	$CDCl_3^+$	2.27	2.25

From the 50-v monoisotopic spectra in Table II, the values of the abundance ratios $CCl_3^+/CHCl_3^+$ and $CCl_3^+/CDCl_3^+$ are 0.58_6 and 0.19_4, respectively. The ratio of these values, 3.0_2, is a measure of the relative probability of dissociating a hydrogen atom from $CHCl_3$ compared with $CDCl_3$. Thus, for 50-v electrons the dissociation of a C—H bond is three times more frequent than the dissociation of a C—D bond. The data at 70 v confirm this result. This is comparable to the "π-effect" reported for monodeuteromethane[2] which amounts to a factor of about 2.6.

The abundance ratios $CCl_2^+/CHCl_3^+$ and $CCl_2^+/CDCl_3^+$ at 50 v are 1.63 and 0.99, respectively. The ratio of these values, 1.65, is a measure of the relative probability of dissociating an H and a Cl atom compared with a D and a Cl atom. It is interesting to note the ratio of the relative abundances $HCl^+/CHCl_3^+$(0.844) and $DCl^+/CDCl_3^+$(0.524) gives a very similar value, 1.61. This suggests that the CCl_2^+ ion is formed primarily by the dissociation of HCl or DCl molecules rather than by dissociation into the separate atoms. If the former alternative were the only mechanism operative, the isotope effect would be very small. If, however, the latter process were the only one, a factor of about three in the relative probabilities would be anticipated. The observed value of 1.6 suggests a process intermediate between these two limiting cases.

For the dissociation of a hydrogen atom and two chlorine atoms, the abundance ratios are equal within the estimated error. This is the result expected if an HCl or a DCl fragment and a chlorine atom were dissociated. There is some evidence for HCl_2^+ ions in the $CHCl_3$ spectrum. However, the abundance of these ions is very small and their origin is in doubt.

The probability of dissociating chlorine atoms is only slightly affected by the presence of an H or a D atom, since the abundance ratios $CHCl_2^+/CHCl_3^+$ and $CDCl_2^+/CDCl_3^+$ differ by only 4 percent. Furthermore, for the dissociation of two chlorine atoms the abundance ratios $CHCl^+/CHCl_3^+$ and $CDCl^+/CDCl_3^+$ are nearly identical.

The authors are grateful to Mr. W. M. Boyer and Mr. T. L. Brown for their assistance with the preparation of the deuterochloroform and to Dr. Fred L. Mohler for his valuable suggestions concerning the interpretations of the mass spectra.

THE JOURNAL OF CHEMICAL PHYSICS VOLUME 19, NUMBER 4 APRIL, 1951

Infrared Spectra of CH_2N_2 and CD_2N_2

BRYCE L. CRAWFORD, JR. AND WILLIAM H. FLETCHER*
School of Chemistry, University of Minnesota, Minneapolis, Minnesota

AND

D. A. RAMSAY
National Research Council, Ottawa, Canada

(Received November 2, 1950)

The infrared spectra of CH_2N_2 and CD_2N_2 have been investigated in the gas phase between 4500 and 400 cm^{-1} using a Perkin-Elmer spectrometer with LiF, NaCl, and KBr prisms.

The spectra have been correlated with a planar, nonlinear configuration for the diazomethane molecule with symmetry C_{2v}. The perpendicular type bands for both molecules are all overlapped or perturbed by neighboring absorption bands, so that no accurate values for the least moments of inertia have been obtained.

Two alternative schemes of assignments for the vibrational frequencies have been proposed and the thermodynamic functions for CH_2N_2 computed.

Potential-function calculations have been carried out.

INTRODUCTION

THE infrared spectrum of diazomethane is of interest, since it permits a complete assignment of the fundamental vibrational frequencies of the molecule and calculation of the thermodynamic properties. The physical properties of this molecule make it doubtful that these properties will ever be measured directly.

A preliminary investigation[1] has shown that the infrared spectrum is consistent with a planar, straight chain structure for the molecule, in agreement with the electron diffraction data.[2] The spectrum of the deuterated molecule has also been investigated and is in agreement with these conclusions. Complete assignments of vibration frequencies for the two molecules have been made and the potential function of the molecule calculated.

EXPERIMENTAL

Diazomethane was prepared by two different methods: (i) by the hydrolysis of nitrosomethylurea with NaOH, (ii) by the treatment of N-nitroso-β-methyl-

* Present address: Department of Chemistry, University of Tennessee, Knoxville, Tennessee. This paper is, in part, from a thesis submitted to the Graduate Faculty of the University of Minnesota by William H. Fletcher, in partial fulfillment of the requirements for the Ph.D. degree.

[1] D. A. Ramsay, J. Chem. Phys. **17**, 666 (1949).

[2] H. Boersch, Monatsh. **65**, 311 (1935).

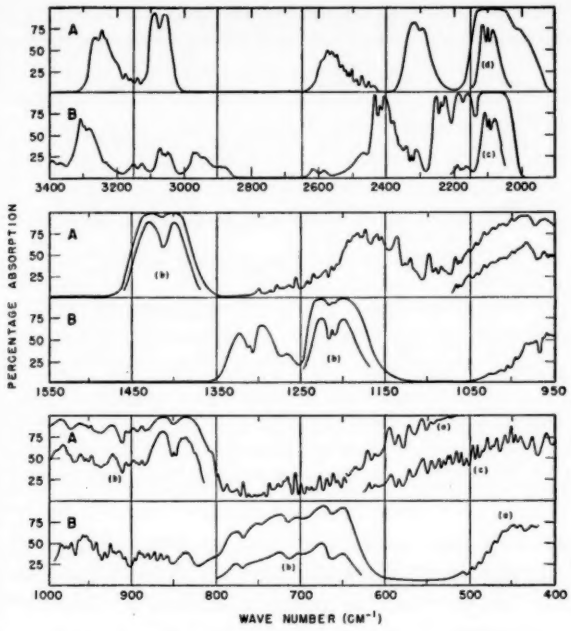

FIG. 1. Infrared spectra of (A) CH_2N_2, (B) CD_2N_2. Cell length = 10 cm. Temperature = 20°C. A. Pressure (a) 300-mm Hg, (b) 100-mm Hg, (c) 50-mm Hg, (d) 10-mm Hg. B. Pressure (a) 300-mm Hg, (b) 100-mm Hg, (c) 5-mm Hg.

aminoisobutylmethyl ketone with sodium dissolved in benzyl alcohol. Its spectrum was investigated independently in the two laboratories using Perkin-Elmer spectrometers with NaCl and KBr prisms. Glass absorption cells with KBr windows were used throughout, and vapor pressures of diazomethane from 5 to 650 mm Hg were investigated. The region above 2000 cm^{-1} was also examined under higher resolving power using a Perkin-Elmer spectrometer with a LiF prism in the one case and a quartz spectrometer in the other. In all cases the agreement between the spectra obtained was extremely good. The appropriate absorption curves are reproduced in Fig. 1, and the frequencies of the absorption peaks are given in Tables I and III.

Deuterated diazomethane, CD_2N_2, was prepared by the hydrolysis of nitroso-methyl-d_3-urea[3] with NaOD. Its vapor spectrum was investigated on a Perkin-Elmer spectrometer with NaCl, KBr, and LiF prisms (see Fig. 1 and Tables II and III). By comparison with the spectrum of CH_2N_2, it is seen that the amount of CH_2N_2 impurity in the CD_2N_2 is negligible. There is the possibility of $CHDN_2$ impurity, however.

Another attempt was made to prepare CD_2N_2 by decomposition of N-nitroso-β-methyl-d_3-aminoisobutylmethyl ketone with sodium dissolved in benzyl alcohol, but owing to an unexpected exchange with the solvent the deuterium in the intermediate was almost entirely lost in the last step of the preparation. The spectrum of this diazomethane sample, however, showed two ab-

[3] Leitch, Gagnon, and Cambron, Can. J. Research **28**, 256 (1950). The authors are indebted to Dr. Leitch for a sample of nitroso-methyl-d_3-urea.

TABLE I. Infrared frequencies and assignments for CH_2N_2.

cm^{-1}	Int.	Band type	Assignment[b,c]	
400–650[a]	*s*	⊥	$\nu_9(b_2)=487$ cm^{-1}	(I)
			$\nu_7(b_1)=586$ cm^{-1}	(I)
			$\nu_9(b_2)=456$ cm^{-1}	(II)
			$\nu_7(b_1)=487$ cm^{-1}	(II)
650–825[a]	*w*	⊥	$2\nu_7-\nu_9=685$ (B_2)	(I)
			$\nu_8-\nu_9=691$ (A_2)[d]	(II)
P 839				
Q 852	*s*	∥	$\nu_4(a_1)$	
R 864				
P 900				
Q —	*m*	∥?	$2\nu_9(A_1)$	(II)
R 926				
926	*m*	⊥?	$\nu_3-\nu_9=928$ (B_2)	(I)
875–1050[a]	*m*	⊥	$\nu_5(b_2)=920$ cm^{-1}	
P 962				
Q —	*m*	∥	$2\nu_9(A_1)$	(I)
R 986			$2\nu_7(A_1)$	(II)
1050–1325[a]	*m*	⊥	$\nu_6(b_1)=1147$ cm^{-1}	
P 1159				
Q —	*m*	∥?	$2\nu_7(A_1)$	(I)
R 1184				
P 1401				
Q —	*s*	∥	$\nu_3(a_1)$	
R 1429				
2016	*w*	?	$\nu_4+2\nu_7=2024$ (A_1)	(I)
			$\nu_4+\nu_6=1999$ (B_1)	
P 2087				
Q 2101	*vs*	∥	$\nu_2(a_1)$	
R 2115				
P 2290				
Q —	*m*	∥	$2\nu_6=2294$ (A_1)	
R 2315			$\nu_3+2\nu_9=2327$ (A_1)	(II)
2400–2650[a]	*m*	⊥	$\nu_2+\nu_9=2588$ (B_2)	(I)
			$\nu_2+\nu_7=2588$ (B_1)	(II)
			$\nu_3+\nu_6=2562$ (B_1)	
P 3062				
Q —	*s*	∥	$\nu_1(a_1)$	
R 3088				
Q 3140				
Q 3158	*w*	⊥	$\nu_5(b_1)=3150$ cm^{-1}	
Q 3175				
P 3245				
Q —	*m*	∥	$\nu_3+2\nu_8=3255$ (A_1)	
R 3266				
P 4168				
Q —	*m*	∥	$2\nu_2(A_1)$	
R 4193				
P 4275				
Q —	*w*	∥	$\nu_5+\nu_6=4297$ (A_1)	
R 4300				

[a] The frequencies of the absorption peaks in this region are given in Table III.
[b] I—Assignment I.
[c] II—Assignment II.
[d] Made active by Coriolis interaction.

TABLE II. Infrared frequencies and assignments for CD_2N_2.

cm^{-1}	Int.	Band type	Assignment	
<525[a]	s	⊥	$\nu_9(b_2)=406$ cm^{-1}	(I)
			$\nu_7(b_1)=502$ cm^{-1}	(I)
			$\nu_9(b_2)=382$ cm^{-1}	(II)
			$\nu_7(b_1)=423$ cm^{-1}	(II)
P 650				
Q —	s	∥	$\nu_4(a_1)$	
R 674				
701	m	?	$\nu_3-\nu_7=711$ (B_1)	(I)
724	m	?	$\nu_8+\nu_9-\nu_7=740$ (B_1)	(I)
P 753				
Q —	m	∥	$\nu_4(a')$ $(CHDN_2)$	
R 777				
800–1050[a]	m	⊥	$\nu_8(b_2)=836$ cm^{-1}	
			$\nu_6(b_1)=960$ cm^{-1}	
P 1200				
Q 1213	s	∥	$\nu_3(a_1)$	
R 1225				
1267	w	?	$\nu_2-2\nu_9=1284$ (A_1)	(I)
			$3\nu_7=1269$ (B_1)	(II)
P 1295				
Q 1311	m	∥	$\nu_3(a')$ $(CHDN_2)$	
R 1323				
P 1846				
Q —	w	∥	$\nu_3+\nu_4=1875$ (A_1)	
R 1869				
P 2081				
Q 2096	vs	∥	$\nu_2(a_1)$	
R 2107				
P 2164				
Q 2178	s	∥	$\nu_3+2\nu_7=2217$ (A_1)	(I)
R 2188			$2\nu_4+2\nu_7=2170$ (A_1)	(II)
P 2229				
Q 2241	s	∥	$\nu_1(a_1)$	
R 2253				
P 2318				
Q 2329	w	∥	$\nu_5(a')$ $(CHDN_2)$	
R 2341			$\nu_4+2\nu_8=2334$ (A_1)	
Q 2363				
Q 2373	w	⊥	$\nu_5(b_1)=2370$ cm^{-1}	
Q 2382				
P 2408				
Q 2420	s	∥	$2\nu_3(A_1)$	
R 2432				
2470	w	?	$\nu_5+\nu_7-\nu_9=2466$ (B_2)	(I)
			$\nu_2+\nu_9=2478$ (B_2)	(II)
P 2593				
Q —	w	∥	$2\nu_3=2622$ (A_1) $(CHDN_2)$	
R 2619			$\nu_4+2\nu_8=2582$ (A_1)	
2850–3000	w	?	$\nu_5+\nu_7=2872$ (A_1)	(I)
			$\nu_1+\nu_4=2903$ (A_1)	
			$\nu_2+\nu_8=2932$ (B_2)	
P 3046				
Q 3060	w	∥	$2\nu_3+\nu_4=3088$ (A_1)	
R 3072				

TABLE II.—*Continued*

cm^{-1}	Int.	Band type	Assignment
P 3124			
Q —	w	∥	$\nu_1(a')$ $(CHDN_2)$
R 3149			$\nu_3+2\nu_6=3133$ (A_1)
P 3283			
Q —	m	∥	$\nu_2+\nu_3=3309$ (A_1)
R 3306			
P 3368			
Q —	w	∥	$\nu_2+2\nu_4=3420$ (A_1)
R 3391			
P 4159			
Q —	w	∥	$2\nu_2=4192$ (A_1)
R 4181			

[a] The frequencies of the absorption peaks in this region are given in Table III.

sorption bands at 765 cm^{-1} and 1311 cm^{-1} not present in the spectrum of CH_2N_2 (see Fig. 2); in all other regions the spectrum of this sample was identical with

TABLE III. Absorption peaks in some perpendicular type bands of CH_2N_2 and CD_2N_2.

cm^{-1}	cm^{-1}	cm^{-1}	cm^{-1}
	(a) CH_2N_2 from 400 to 825 cm^{-1}		
413	512	637	729
429	516	650	739
441	525	658	746
448	528	663	750
454	533	672	755
460	538	679	763
470	547	684	770
474	557	689	777
480	573	694	789
485	586	701	801
493	597	709	809
499	615	717	825
506	622		
	(b) CH_2N_2 from 875 to 1325 cm^{-1}		
890	1013	1099	1207
900	1023	1121	1215
909	1034	1127	1223
926	1043	1137	1237
950	1051	1155	1245
956	1055	1161	1260
962	1064	1175	1268
986	1067	1179	1281
1002	1085	1184	1287
1008	1091	1195	1303
	(c) CH_2N_2 from 2400 to 2650 cm^{-1}		
2437	2500	2526	2570
2453	2507	2540	2587
2471	2514	2556	2599
2485			
	(d) CD_2N_2 from 425 to 525 cm^{-1}		
440	460	479	498
450	470	489	507
	(e) CD_2N_2 from 800 to 1050 cm^{-1}		
836	897	938	976
858	908	942	985
866	914	954	995
873	921	958	1005
881	924	962	1013
891	933	971	1027

that of pure CH_2N_2. These bands, also observed in the spectrum of the CD_2N_2 sample above, are presumably due to $CHDN_2$ impurity.

Several attempts were made to observe the Raman spectrum using 5461A excitation on solutions of CH_2N_2 in various inert solvents. Only small concentrations of CH_2N_2 were obtainable, and none of the plates showed any Raman lines which could be attributed to CH_2N_2.

ASSIGNMENT OF FREQUENCIES

Diazomethane is a planar, nonlinear pentatomic molecule with symmetry C_{2v}. The nine normal modes of vibration and their symmetry classes are shown in Fig. 3, the totally symmetric A_1 vibrations and the antisymmetric B_1 vibrations being drawn according to the subsequent normal-coordinate calculations. All the fundamental frequencies are theoretically active both in the infrared and in the Raman spectrum.

The contours of the infrared bands may be predicted as follows: taking the electron diffraction[2] values for the C−N and N−N bond lengths, *viz.*, $r_{C-N}=1.34\pm0.05$ A. U. and $r_{N-N}=1.13\pm0.04$ A. U., and assuming the C−H bond lengths to be 1.07 A. U., as in ethylene, and the H−C−H bond angle to be 120°, the principal moments of inertia for CH_2N_2 and CD_2N_2 are:

CH_2N_2	CD_2N_2
$I_A=2.9\times10^{-40}$ g cm^2	5.8×10^{-40} g cm^2
$I_B=76.6$	86.7
$I_C=79.5$	92.5

The molecules thus approximate very closely to symmetric tops. The type A_1 bands should show P, Q, R structures characteristic of "parallel" bands of a symmetric top, the intensity of the Q branch[4] being considerably less than the intensity of the P and R branches, owing to the small value of I_A/I_C. The PR spacings may be calculated from the equations of Gerhard and Dennison[5] and are found to be 25.3 cm^{-1} for CH_2N_2 and 24.3 cm^{-1} for CD_2N_2. The observed spacing of the parallel bands is in satisfactory agreement with these calculations.

For CH_2N_2 the four parallel fundamentals are readily assigned as $\nu_1^{CH}=3074$ cm^{-1}, $\nu_2^{NN}=2101$ cm^{-1}, $\nu_3^{CH_2}=1415$ cm^{-1}, and $\nu_4^{CN}=852$ cm^{-1}. For CD_2N_2 the assignment of $\nu_2^{NN}=2096$ cm^{-1} is quite clear, and the bands at 1213 cm^{-1} and 662 cm^{-1} appear to be $\nu_3^{CD_2}$ and ν_4^{CN}. The assignment of ν_1^{CD} is less certain, but by use of the product rule[6] it appears that the most probable assignment is $\nu_1^{CD}=2241$ cm^{-1}.

The type B_1 and B_2 bands should resemble perpendicular bands of a spindle-shaped symmetric top.[7] In the absence of any underlying absorption or perturbing influences, these bands should consist of series of approximately equally spaced Q branches belonging to the various subbands present, the spacing being 18.7 cm^{-1} for CH_2N_2 and 9.1 cm^{-1} for CD_2N_2. The intensities of the Q branches should decrease on either side of the band center according to a Boltzmann factor, approximately six or eight Q branches being observed on either side for the light molecule and about ten for the heavy molecule.

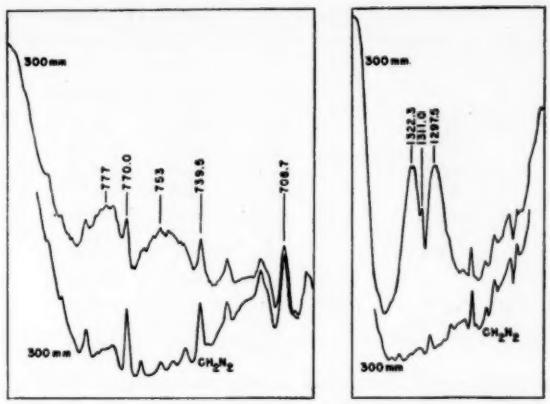

FIG. 2. The 765-cm^{-1} and 1311-cm^{-1} bands of $CHDN_2$.

For CH_2N_2 the H nuclei follow Fermi statistics, and the ratio of the number of molecules in the even and odd K rotational levels is 1:3, respectively. An intensity alternation in the Q branches of the perpendicular bands is therefore to be expected, the first peak on the long wavelength side of the band center being the strongest one. For CD_2N_2 the D nuclei follow Bose statistics and the corresponding ratio is 2:1. For this isotope the strongest peak will be on the short wavelength side of the band center.

Several perpendicular type bands are observed in the

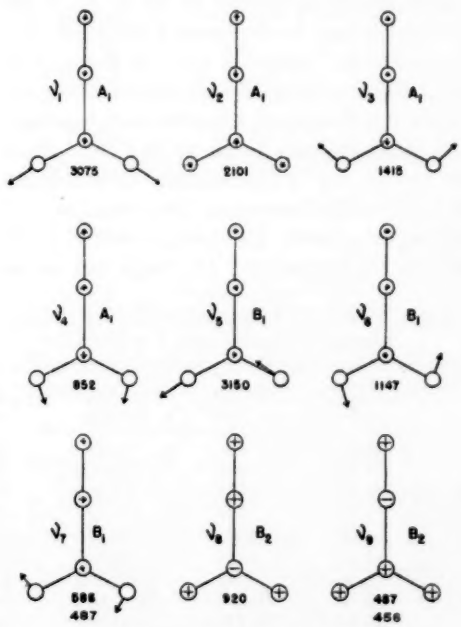

FIG. 3. Normal vibrations of CH_2N_2.

[4] G. Herzberg, *Infrared and Raman Spectra of Polyatomic Molecules* (D. Van Nostrand Company, Inc., New York, 1945), p. 421.
[5] S. L. Gerhard and D. M. Dennison, Phys. Rev. **43**, 197 (1933).
[6] E. Teller, quoted in J. Chem. Soc. **1936**, 966. O. Redlich, Z. physik. Chem. **B28**, 371 (1935).
[7] Reference 4, pp. 424–6.

TABLE IV. Observed and calculated frequencies (cm^{-1}).

		CH_2N_2			CD_2N_2			$CHDN_2$		
		obs	calc	percent error	obs	calc	percent error	obs	calc	percent error
A_1:	ν_1^{CH}	3075	3065	−0.32	2241	2238	−0.13	3137	3114	−0.73
	ν_2^{NN}	2101	2108	+0.33	2096	2091	−0.24		2104	
	$\nu_3^{CH_2}$	1415	1426	+0.78	1213	1208	−0.41	1311	1336	+1.9
	ν_4^{CN}	852	828	−2.8	662	686	+3.6	765	758	−0.93
B_1:	ν_5^{CH}	3150	3156	+0.35	2370	2365	−0.21	2329	2299	−1.3
	$\nu_6^{CH_2}$	1147	1147	0.0	960	956	−0.42		1043[c]	
	ν_7^{CNN}	586[a]	577	−1.5	502[a]	510	+1.6		534[c]	
		487[b]	484	−0.62	423[b]	425	+0.47			
B_2:	$\nu_8^{CH_2}$	920	923	+0.32	836	834	−0.24		877[c]	
	ν_9^{CNN}	487[a]	481	−1.2	406[a]	410	+1.0		452[c]	
		456[b]	455	−0.22	382[b]	386	+1.0			

[a] Assignment I; see text.
[b] Assignment II; see text.
[c] Calculated with the force constants of Assignment I.

spectra of both CH_2N_2 and CD_2N_2 but, unfortunately, all these bands are overlapped or perturbed by neighboring absorption bands. The antisymmetric C−H and C−D stretching bands are both overlapped by strong parallel bands, only three Q branches showing in each case. The Q branch spacings, however, agree with the values expected and the intensity alternation is clearly visible in the case of the C−H stretching band. The band centers cannot be located with certainty but are tentatively assigned as $\nu_5^{CH}=3150\ cm^{-1}$ and $\nu_5^{CD}=2370\ cm^{-1}$.

The complex absorption below 700 cm^{-1} for CH_2N_2 is presumably caused by the two skeletal vibrations, ν_7 and ν_9. The spacing, however, is highly irregular and probably indicates a Coriolis interaction between these two vibrations. Some indication of the positions of the band centers may be obtained from the overtones of these bands, but these are not conclusive. Indeed, two interpretations are possible, both of which seem equally reasonable. The two assignments are given below.

Two parallel bands appear to lie at 1172 cm^{-1} and 974 cm^{-1}, which may be reasonably assigned to $2\nu_7$, and $2\nu_9$, giving 586 cm^{-1} and 487 cm^{-1} as the apparent frequencies of the low-lying fundamentals (Assignment I). The alternative assignment is obtained by noting that a parallel band appears to be at 912 cm^{-1}, giving 456 cm^{-1} for one of the fundamentals. It is interesting to note that the latter frequency lies near the maximum of the absorption curve. Assigning ν_7 and ν_9 at 487 cm^{-1} and 456 cm^{-1} (Assignment II) does not explain the apparent parallel band at 1172 cm^{-1}, but the preceding assignment does not explain the one at 912 cm^{-1}. These two assignments will be discussed in more detail later.

The absorption in the region 1050–1300 cm^{-1} shows four well-defined Q branches at 1067, 1099, 1137, and 1175 cm^{-1} with a marked intensity alternation and may be assigned to the CH_2 rocking motion, $\nu_6(b_1)$, or to the CH_2 wagging motion, $\nu_8(b_2)$. The former assignment is favored by the appearance of a parallel combination band with $\nu_5^{CH}(b_1)$ at 4288 cm^{-1}. This, and a parallel overtone at 2303 cm^{-1}, support the choice of 1147 cm^{-1} as the band center.

The CH_2 wagging motion, $\nu_8(b_2)$, may be assigned to the perpendicular band in the region 1050–850 cm^{-1} or to the weak perpendicular band in the region 800–650 cm^{-1}. The former assignment is more likely because of the appearance of the parallel band, $\nu_3+2\nu_8$, at 3255 cm^{-1}, and this is supported by the spectrum of CD_2N_2. The band center is difficult to locate but has been

TABLE V. Thermodynamic functions for CH_2N_2 (hypothetical ideal gas, 1 atmos).

T °K	C_p^0 cal/degree/mole	$H^0-E_0^0$ cal/mole	$F^0-E_0^0$ cal/mole	S^0 cal/degree/mole
100	8.07	797	−3892	46.89
200	9.59	1668	−8906	52.87
298.16	11.68	2711	−14,309	57.08
300	11.73	2734	−14,415	57.16
400	13.66	4006	−20,317	60.81
500	15.25	5454	−26,547	64.00
600	16.56	7046	−33,106	66.92
800	18.60	10,570	−47,014	71.98
1000	20.13	14,454	−61,862	76.32

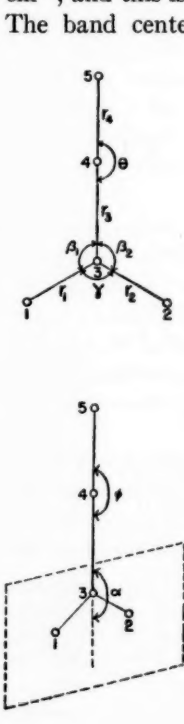

FIG. 4. Internal coordinates of diazomethane.

tentatively assigned as $\nu_8^{CH}=920$ cm^{-1}, which is near the strong Q branch at 909 cm^{-1}.

The assignments for CD_2N_2 are more difficult. One immediately notices two parallel bands, at 765 cm^{-1} and 712 cm^{-1}, which might be overtones of the low-lying fundamentals. However, the band at 765 cm^{-1} was observed in the sample obtained in the abortive attempt to prepare CD_2N_2, while the stronger bands at 1213 cm^{-1} and 662 cm^{-1} were absent. The band at 765 cm^{-1} must, therefore, be due to $CHDN_2$. A few calculations with the product rule show that 356 cm^{-1} is unreasonably low for a fundamental, so we are inclined to overlook the apparent parallel band at 712 cm^{-1}. In order to find values for the skeletal bending frequencies, it was necessary to assign frequencies to the CD_2 rocking and wagging motions and then use the product rule. The perpendicular bands in the region 800–1050 cm^{-1} are presumably caused by the two CD_2 motions, ν_6 and ν_8. The band center of the former has been assigned at 960 cm^{-1}, near the peak of the absorption curve, and the band center of the latter has been set at 836 cm^{-1}.

Both of the previously mentioned assignments for ν_7 and ν_9 in CH_2N_2 were used with the above assignments for the CH_2 and CD_2 motions to calculate the values of the skeletal bending frequencies in CD_2N_2 necessary to satisfy the product rule. With $\nu_7=586$ cm^{-1} and $\nu_9=487$ cm^{-1} for CH_2N_2, the corresponding frequencies for CD_2N_2 are 502 cm^{-1} and 406 cm^{-1}. If $\nu_7=487$ cm^{-1} and $\nu_9=456$ cm^{-1} for CH_2N_2, we find 423 cm^{-1} and 382 cm^{-1} for CD_2N_2.

The complete assignments of the fundamentals and overtones for CH_2N_2 and CD_2N_2 on the basis of Assignments I and II are given in Tables I and II. The most serious objection to Assignment I is that it predicts a rather strong fundamental for CD_2N_2 at 502 cm^{-1} in a region where little absorption is observed. On the other hand, Assignment II does not give a satisfactory interpretation of the perpendicular band for CH_2N_2 in the region 650–800 cm^{-1} or of the strong parallel band at 2178 cm^{-1} in the spectrum of CD_2N_2. In view of these facts, both of these proposed assignments are presented with some reserve. Unfortunately, the data available at this time do not afford a more satisfactory explanation of the observed spectra.

Supporting evidence for certain aspects of the assignment was gained by a normal-coordinate treatment and calculation of force constants. It will be noted in Table I that four bands in the spectrum of the CD_2N_2 sample (at 3137 cm^{-1}, 2329 cm^{-1}, 1311 cm^{-1}, and 765 cm^{-1}) are attributed to the presence of $CHDN_2$. The force constants obtained from the frequencies assigned to CH_2N_2 and CD_2N_2 were used to calculate the frequencies to be expected for $CHDN_2$. Satisfactory agreement was found for these four bands. While the force constants used for this were for Assignment I, it seems very probable that the set of force constants for Assignment II would give equally good results.

The observed and calculated frequencies for the three isotopic molecules are given in Table IV. In the A_1 group there is a discrepancy of 5.5 percent between the observed and theoretical product rule ratios. In the B_1 and B_2 groups the values taken for ν_7 and ν_9 in CD_2N_2 were about 1 percent less than the calculated values.

The thermodynamic functions for CH_2N_2 have been calculated for a number of temperatures on the basis of Assignment I and are given in Table V. The values of the constants given in the tables of the American Petroleum Institute, Project 44 (December 31, 1947), were used for these calculations. The vibrational contributions were obtained from the tables given in Taylor and Glasstone's *Treatise on Physical Chemistry*, Vol. I. If Assignment II is preferred, the corrections to be added vary from 0.03–0.33 cal/degree mole for C_p^0, 0–140 cal/mole for $H^0-E_0^0$, 0–300 cal/mole for $F^0-E_0^0$, and 0–0.44 cal/mole degree for S^0.

TABLE VI. Valence force symmetry coordinates (see Fig. 4).

$$S_{CH}=2^{-\frac{1}{2}}(\Delta r_1+\Delta r_2)$$
$$S_{CN}=\Delta r_3$$
$$S_{NN}=\Delta r_4$$
$$S_\gamma=6^{-\frac{1}{2}}r_1^0(2\Delta\gamma-\Delta\beta_1-\Delta\beta_2)$$
$$S'_{CH}=2^{-\frac{1}{2}}(\Delta r_1-\Delta r_2)$$
$$S_\beta=2^{-\frac{1}{2}}r_1^0(\Delta\beta_1-\Delta\beta_2)$$
$$S_\theta=r_3^0\Delta\theta$$
$$S_\phi=r_3^0\Delta\phi$$
$$S_\alpha=r_3^0\Delta\alpha$$

A_1 :

	S_{CH}	S_{CN}	S_{NN}	S_γ
S_{CH}	$\mu_+ + A\mu_C$	$2^{\frac{1}{2}}\eta\mu_C$	0	$-3^{\frac{1}{2}}\sigma\mu_0$
S_{CN}		$\mu_C+\mu_N$	$-\mu_N$	$-6^{\frac{1}{2}}D\mu_C$
S_{NN}			$2\mu_N$	0
S_γ				$3\mu_+ + 3B\mu_C$

B_1 :

	S'_{CH}	S_β	S_θ
S'_{CH}	$\mu_+ + B\mu_C$	$-bB\mu_C$	$-B^{\frac{1}{2}}\mu_C$
S_β		$\mu_+ + a^2B\mu_N + b^2B\mu_C$	$B^{\frac{1}{2}}b\mu_C + B^{\frac{1}{2}}a(1+p)\mu_N$
S_θ			$\mu_C + (2p^2+2p+1)\mu_N$

B_2 :

	S_ϕ	S_α
S_ϕ	$\mu_C + (2p^2+2p+1)\mu_N$	$-(1+q)\mu_C - (1+p)\mu_N$
S_α		$(q^2/2)\mu_+ + (1+q)^2\mu_C + \mu_N$

The symbols have the following meanings (Fig. 4):

$\mu_\pm = \frac{1}{2}(\frac{1}{m_1} \pm \frac{1}{m_2})$ $\quad$ $A = 1+\cos\gamma$

$\mu_C, \mu_N = \frac{1}{m_C}, \frac{1}{m_N}$ $\quad$ $B = 1-\cos\gamma$

$\eta = \cos\beta$ $\quad$ $D = \cos\beta\tan(\gamma/2)$

$\sigma = \sin\beta$ $\quad$ $p = r_3/r_4$

$a = r_1/r_3\sin\beta$ $\quad$ $q = r_3/r_1\cos(\gamma/2)$

$b = a - \mathrm{ctn}\beta$

FIG. 5. G matrix elements for CH_2N_2 and CD_2N_2.

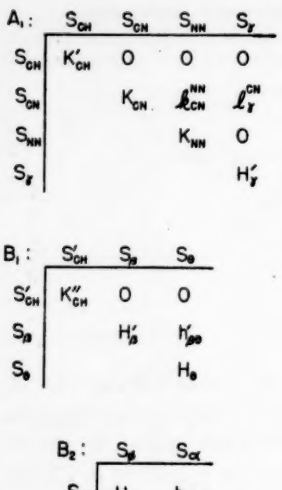

FIG. 6. *F* Matrix for diazomethane.

TABLE VII. Force constants for diazomethane, 10^5 dynes/cm.

Force constant		Assignment I	Assignment II
$K_{CH'}$	(C−H stretch)	5.32	same
K_{NN}	(N−N stretch)	17.75	same
K_{CN}	(C−N stretch)	5.11	same
$H_{\gamma'}$	(CH_2 deformation)	0.290	same
$k_{CN}{}^{NN}$	(interaction)	0.94	same
$l_{\gamma}{}^{CN}$	(interaction)	0.25	same
$K_{CH''}$	(C−H stretch)	5.23	same
$H_{\beta'}$	(in-plane CH_2 rocking)	0.518	0.481
H_{θ}	(in-plane CNN bend)	0.503	0.401
$h_{\beta\theta'}$	(interaction)	0.04	0.107
H_{ϕ}	(out-of-plane CNN bend)	0.451	0.435
H_{α}	(out-of-plane CH_2 wag)	0.083	0.079
$h_{\phi\alpha}$	(interaction)	−0.058	−0.065

NORMAL COORDINATE TREATMENT

The secular equations were set up by the $\mathcal{F}$ and $\mathcal{G}$ matrix method of Wilson.[8] The internal coordinates are shown in Fig. 4. The valence-force symmetry coordinates (VFSC) used in forming the irreducible representations of the point group C_{2v} are given in Table VI. These were chosen to be orthogonal to the redundancy involving the angles β_1, β_2, and γ. Those coordinates involving angles were defined as the product of the angular displacement and the equilibrium length of an adjacent bond so all force constants would have the same dimensions.

The $\mathcal{G}$ matrix for the VFSC is given in Fig. 5. The blocks given utilize the symmetry factoring for the point group C_{2v}. In the case of $CHDN_2$, point group C_s, the A_1 and B_1 blocks are connected by two interaction terms: between $S_{CH}(A_1)$ and $S'_{CH}(B_1)$ we have $\mathcal{G}_{CH,CH'} = \mu_-/2$, and between $S_\gamma(A_1)$ and $S_\beta(B_1)$ we have $\mathcal{G}_{\gamma\beta} = -3^{\frac{1}{2}}\mu_-/2$.

The $\mathcal{F}$ matrix ($2V = \tilde{S}\mathcal{F}S$) is given in Fig. 6. The only interaction terms which were discarded were those involving C−H or C−D stretching motions, and the one involving the N−N stretching and the CH_2 or CD_2 deformation, the last being omitted because these two groups do not have an atom in common.[9]

The force constants were obtained from the secular equations by the usual algebraic methods. Since the algebraic equations obtained from the observed frequencies are somewhat inconsistent, least-square treatments were used to get better sets of force constants for the A_1 and B_1 groups. The force-constant sets obtained from the two assignments are given in Table VII.

The pairs of frequencies, 586 cm^{-1} and 487 cm^{-1}, and 487 cm^{-1} and 456 cm^{-1}, were assigned to species B_1 and B_2, respectively. The reverse assignment was considered in both cases, but this leads to less satisfactory sets of force constants. H_θ and H_ϕ might be expected to have similar magnitudes, and this is more nearly true for the assignments chosen than for the reverse ones.

The unsymmetric molecule, $CHDN_2$, belongs to point group C_s and, therefore, has seven vibrations in the totally symmetric species. The roots of this seventh-order secular equation were found by forming the $\mathcal{GF}$ product and then applying an iteration process.[10]

ACKNOWLEDGMENTS

The work at Minnesota was carried out during the tenure of a Kimberley-Clarke Fellowship by one of us (W.H.F.). The research also received support from the Office of Naval Research through contract N5ori-147, T.O. 2.

One of us (D.A.R.) wishes to express his thanks to Dr. R. N. Jones, who kindly placed the infrared spectrometer at his disposal, and to Dr. G. Herzberg for helpful discussion.

[8] E. B. Wilson, Jr., J. Chem. Phys. **7**, 1047 (1939); **9**, 76 (1941).
[9] B. L. Crawford, Jr. and S. R. Brinkley, J. Chem. Phys. **9**, 69 (1941).
[10] Frazer, Duncan, and Collar, *Elementary Matrices* (The MacMillan Company, New York, 1947), pp. 142–5.

The Crystal Structure of $NaPt_3O_4$

JÜRG WASER AND EDWIN D. MCCLANAHAN, JR.
Department of Chemistry, The Rice Institute, Houston, Texas
(Received November 16, 1950)

The structure of a microcrystalline platinum compound is derived from x-ray data. Space group O_h^3-Pm3n, $a_0=5.69$A, with 6 Pt at $\pm(\frac{1}{4}\,0\,\frac{1}{2},\ \circlearrowleft)$, 8 O at $\pm(\frac{1}{4}\,\frac{1}{4}\,\frac{1}{4},\ \frac{1}{4}\,\frac{3}{4}\,\frac{3}{4},\ \circlearrowleft)$, and 2 Na at $(000,\ \frac{1}{2}\,\frac{1}{2}\,\frac{1}{2})$, corresponding to the formula $NaPt_3O_4$. The coordinations are as follows: platinum 4 O and 2 Pt, oxygen: 3 O and 2 Na, sodium: 8 O. The substance is an ionic conductor.

THE preparation of an oxide of platinum by fusion of sodium chloroplatinate with sodium carbonate has been reported by Jörgensen.[1] The oxygen content of the compound was determined by finding the weight lost on ignition with a result corresponding to the formula Pt_3O_4. Repeating this work Wöhler[2] found that all his preparations contained small and varying amounts of sodium and water in addition to platinum and oxygen. The amount of water given off upon heating was determined directly, and found to vary between 1 and 5 percent. The sodium content varied between 3 and $4\frac{1}{4}$ percent. The oxygen percentage depended on the history of the sample but was always between the extremes corresponding to PtO and PtO_2. Wöhler concluded that the product of the reaction described was a mixture of PtO and PtO_2. He did not try to account for the sodium and assumed the water to be water of hydration.

Our structure determination by x-rays shows that a compound actually is formed and that it has the composition $NaPt_3O_4$.

PREPARATION AND PROPERTIES

One part of finely divided anhydrous sodium chloroplatinate was thoroughly mixed with four parts of powdered anhydrous sodium carbonate. The mixture was heated in a platinum crucible, the crust forming on top being constantly pushed back into the main body of the melting material. The heating was stopped as soon as the whole mass was molten. After cooling, the unreacted sodium carbonate was dissolved in dilute nitric acid. The resulting black powder was washed with water and dried over phosphorus pentoxide. An x-ray powder diagram showed, besides other lines, those of metallic platinum. Only repeated grinding followed each time by extraction with hot aqua regia, which does not react with the compound investigated, eliminated all but traces of metallic platinum.

Analysis of the compound gave the following inconclusive results. Like Wöhler we found water to be present to the extent of 2.6 percent, even after drying for 24 hours at 110°C in a high vacuum. The platinum was determined as residue with the two results 84.69 percent and 86.51 percent which is to be compared with the theoretical value 87.07 percent for $NaPt_3O_4$. In order to completely eliminate the oxygen in this analysis a final introduction of hydrogen around 500°C was necessary. This produced a vigorous exothermic reaction causing the substance to heat up to a dull red and completely eliminated any sodium that had not escaped in the previous heating. No attempt was made to determine analytically the sodium content of the compound.

The compound is a jet black powder which is reasonably stable at room temperature but decomposes slowly over a period of several months. No solvent action is observed for aqua regia or concentrated mineral acids. The oxide does react, however, with reducing agents such as KI or $SnCl_2$ in a strongly acid medium. One of the reaction products appears to be colloidal platinum.

DETERMINATION OF CRYSTAL STRUCTURE

Powder diagrams taken with CrK_α as well as CuK_α radiation showed a set of very sharp lines that could be indexed on a simple cubic lattice with a unit cell of edge $a_0=5.69$A based on extrapolation to $\vartheta=90°$. The first two columns of Table I contain the spacings observed together with the indices (*hkl*). On all our photographs there appeared a very weak diffuse line at a spacing of 4.55A. With cubic cells of twice or three times the edge of our cell this line can be indexed, but the line is diffuse and seems to vary in intensity for different preparations. There is no other evidence pointing to a larger cell.

Accurate intensities for CuK_α radiation were determined for $\vartheta\leq 45°$ employing a Norelco Geiger counter instrument whose linearity in the range used had been established by calibration with a set of nickel foils. For each reflection counts were determined at about twenty different ϑ-values, starting and ending at a constant background. The area between a curve drawn smoothly through these points and a suitable background line was taken as a measure of the integrated intensity, and is listed in column 3 of Table I (except for a constant factor). Visual intensity data for CuK_α radiation were obtained by a multiple film technique.[3] These values were corrected for absorption by using as calibration points reflections (*hkl*) for which $h+k+l=2n+1$. Only the Pt-atoms contribute to these reflections and they can be placed in the unit cell by the use of extinction criteria alone (compare below). The logarithms of the ratios of calculated and observed intensities were plotted

[1] S. M. Jörgensen, J. Prakt. Chem. **16**, 344 (1877).
[2] L. Wöhler, Z. anorg. u. allgem. Chem. **40**, 450 (1904).
[3] De Lange, Robertson, and Woodward, Proc. Roy. Soc. (London) **A171**, 398 (1939).

TABLE I. The crystal structure of $NaPt_3O_4$.[a]

hkl	*d*, A	I_G	I_v	I_{c4}		I_{c1}	I_{c2}	I_{c3}
—	4.55		v.v.w.					
110	4.03	334	(440)	419		566	485	566
200	2.84	68	(88)	71		111	73	48
210	2.54	1395	(1420)	1417		1417	1417	1417
211	2.32	306	(364)	342		268	259	268
220	2.00	27	(29)	26		83	64	39
310	1.79	97	(91)	93		122	155	122
222	1.64	344	(364)	305		273	286	329
320	1.58	364	(321)	321		321	321	321
321	1.52	215	(162)	175		140	160	140
400	1.42	194	(175)	165		130	124	154
411	1.34	64	(43)	37	56	47	50	47
330	1.34			19		24	14	24
420	1.27	30	(29)	29		39	42	22
421	1.24	325	(291)	291		291	291	291
332	1.21	37	(27)	42		34	25	34
422	1.16	21	(10)	13		31	32	18
510	1.115		51	22	67	28	23	28
431	1.115			45		55	53	55
520	1.055		292	101	302	101	101	101
432	1.055			201		201	201	201
521	1.038		45	57		47	43	47
440	1.004		162	127		104	105	120
530	0.973		26	18	36	22	30	22
433	0.973			18		22	25	22
600	0.947		24	5	23	6	8	4
442	0.947			18		23	23	15
610	0.933		83	92		92	92	92
532	0.921		86	55	83	47	55	47
611	0.921			28		23	25	23
620	0.898		12	12		24	30	16
541	0.876		42	42		50	49	50
622	0.857		383	266		248	238	282
630	0.848		455	117	350	117	117	117
542	0.848			233		233	233	233
631	0.839		59	72		60	52	61
444	0.821		286	124		105	105	119
550	0.804		252	18	125	21	17	21
710	0.804			36		42	42	42
543	0.804			71		84	79	84
640	0.789		57	45		57	52	37
641	0.781		902	601	902	601	601	601
720	0.781			301		301	301	301

[a] I_G: Geiger counter intensity; I_v: visual intensity; I_{ci} ($i=1, 2, 3, 4$): calculated intensity, with $i=1$: contributions of Pt only; $i=2$: oxygens in 8*e* of T_d^4, $u=0.322$; $i=3$: oxygens in 8*e* of O_h^3; $i=4$: final structure including Na. All forms not listed have vanishing structure factor.

for these reflections against $\sin^2\vartheta$. A smooth curve drawn with the aid of these points served for absorption correction and is shown in Fig. 1. The visual intensities corrected in this manner are listed in column 4 of Table I. The visual values for $\vartheta \leq 45°$ are included for comparison with the Geiger counter values only and were not subsequently used in the determination of the structure.

Systematic absence of reflections (*hhl*) with *l* odd led to the probable space groups $O_h^3 - Pm3n$ and $T_d^4 - P\bar{4}3n$.[4] It was found that besides satisfying this space group criterion reflections *hkl* occurred if and only if one of the following conditions was satisfied: (1) $h+k+l=2n$, (2) $h=4n$, $k=4n+2$, and $l=2n+1$. These are exactly the conditions required by the two equivalent sets of 6-fold positions 6*c*, $\pm(\frac{1}{4}\,0\,\frac{1}{2}, \circlearrowleft)$ and 6*d*, $\pm(0\,\frac{1}{4}\,\frac{1}{2}, \circlearrowleft)$[5] in O_h^3 or T_d^4.[4] Intensities calculated with Pt-atoms in one of these sets, e.g., 6*c*, show satisfactory agreement with the observed values (column 6, Table I) so that there are six Pt-atoms in the unit cell. In particular, placing six more Pt-atoms in the set 6*d* would lead to unsatisfactory intensities and too short Pt-Pt distances. Another possibility not violating condition (1) would be to introduce two more Pt-atoms in positions 2*a* of O_h^3, $(000, \frac{1}{2}\,\frac{1}{2}\,\frac{1}{2})$, which would make the arrangement of Pt-atoms identical with that of W-atoms in β-wolfram.[6] It is ruled out since for it the Pt-amplitudes would cancel for ten lines which are actually present with normal intensities. The intensities calculated for Pt-atoms in positions 6*c* were used as described above to correct the visual intensities.

Even with heavy exposures, no faint lines were detected that did not satisfy either of the above extinction rules (1) and (2). Condition (1) is that for a body-centered lattice while the aggregate of conditions (1) and (2) is that of either of the two sets 6*c* and 6*d* discussed above, of which 6*c* has been filled with Pt-atoms and 6*d* is no longer available because of space requirements. The remaining atoms are thus arranged on a body-centered lattice. Nevertheless, all non-body-centered as well as body-centered 6-fold, 8-fold, and 12-fold sets of the cubic system[7] were systematically investigated in the placement of the relatively weakly scattering O-atoms. Only two possibilities were found that did not lead either to spatial difficulties or to otherwise unsatisfactory structures. These were the two related 8-fold sets 8*e* of T_d^4, $(000, \frac{1}{2}\,\frac{1}{2}\,\frac{1}{2}) \pm(u\,u\,u,\ u\,\bar{u}\,\bar{u}, \circlearrowleft)$ and 8*e* of O_h^3, $(000, \frac{1}{2}\,\frac{1}{2}\,\frac{1}{2}) \pm(\frac{1}{4}\,\frac{1}{4}\,\frac{1}{4},\ \frac{1}{4}\,\frac{3}{4}\,\frac{3}{4}, \circlearrowleft)$, both of them body-centered.

The unit cell therefore contains eight oxygen atoms. Neglecting the volume of the Pt-atoms one arrives at a volume of $23A^3$ taken up by each O-atom. This is in fair agreement with the value of $25A^3$ found for PtO.[8] Indeed, taking $6A^3$ for the volume occupied by each Pt-atom one obtains $19A^3$ for the volume taken up by one O-atom in either compound, which is in excellent agreement with the values found by Zachariasen in a

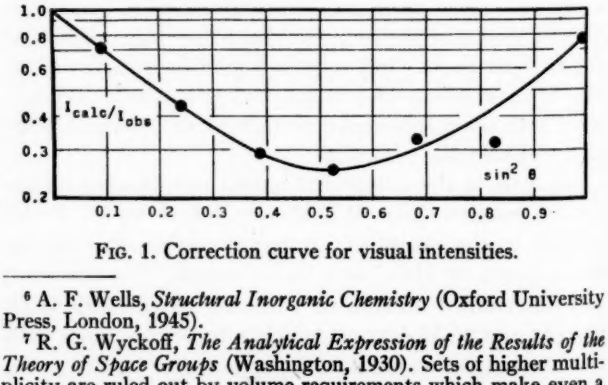

FIG. 1. Correction curve for visual intensities.

[4] *Internationale Tabellen zur Bestimmung von Kristallstrukturen*, Berlin, 1935. Volumes 1 and 2.

[5] The symbol $\circlearrowleft$ stands for cyclical permutation.

[6] A. F. Wells, *Structural Inorganic Chemistry* (Oxford University Press, London, 1945).

[7] R. G. Wyckoff, *The Analytical Expression of the Results of the Theory of Space Groups* (Washington, 1930). Sets of higher multiplicity are ruled out by volume requirements which make even a 12-fold set very unlikely (compare below).

[8] W. J. Moore, Jr., and L. Pauling, J. Am. Chem. Soc. **63**, 1392 (1941).

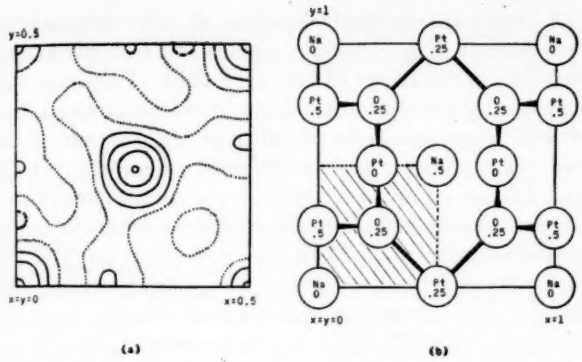

FIG. 2. (a) Projection $\rho'(x, y)$ on (001) plane. Contours in arbitrary units, zero contour dotted and negative contour dashed. (b) View of unit cell along c-axis. Numbers are z-parameters, with the additional stipulation that the value 0.25 indicates an atom at $z=0.75$ also. Only Pt–O bonds are shown.

number of oxides.[9,10] Intensities were calculated for either set of oxygen coordinates mentioned above, 8*e* of T_d^4 and 8*e* of O_h^3. These are listed in columns 7 and 8 of Table I. The parameter u for the former set was given the value 0.322, which leads to satisfactory packing and places the O-atoms at the centers of regular tetrahedra formed by the Pt-atoms. The value of the quantity

$$\frac{\sum\|F_{obs}|-|F_{calc}\|}{\sum|F_{obs}|}$$

for either of the two possible oxygen positions is listed in Table II for the Geiger counter intensities alone, as well as for the whole set of intensities. The agreement is better for the set 8*e* of O_h^3 in which the oxygens are arranged on a simple cubic lattice of unit cell edge $a_0/2$.

The holes in the center of some of the oxygen cubes appeared suspicious and indeed filling these holes with some scattering matter further improved the agreement between calculated and observed intensities. It was decided to investigate this question further by the aid of a fourier projection on the xy-plane in which the platinum atoms have been removed. This was accomplished by using for coefficients the values of $sgn(F_{hk0}^{Pt})\{|F_{hk0}^{obs}|-|F_{hk0}^{Pt}|\}$ where $|F_{hk0}^{obs}|$ is the magnitude of the observed structure factor obtained from the intensities in the usual way, F_{hk0}^{Pt} is the structure factor for the Pt atoms alone and $sgn(F_{hk0}^{Pt})$ its sign. For the atomic structure factor of Pt an average was used of the values based on the Thomas-Fermi model[4] and those of Pauling and Sherman.[11] The intensity of reflections that superimposed was distributed in the ratios of the frequency factors among the forms involved.

Figure 2 shows (a) the resulting fourier projection for one-quarter of the unit cell and (b) for comparison, the projection of the full unit cell of the final structure. The peak at the center of the fourier projection represents two superimposed oxygen atoms. The ratio of the peak at the origin to the oxygen peak is approximately 0.7. This fits reasonably well to sodium, the only possible candidate in the reaction mixture, for which a ratio of about $0.64=11/16=Na/(2$ superimposed O) (or 10/16 for Na in the ionized state) would be expected. The fact that, if anything, the peak at the origin is somewhat higher than this, strongly indicates that practically all the holes in the oxygen cubes corresponding to the twofold set of positions 2*a* of O_h^3 (000, $\frac{1}{2}\frac{1}{2}\frac{1}{2}$) are filled with sodium. Several minor peaks of spurious nature are also in evidence. They are probably due to such things as breaking-off error, improper apportioning of intensities for superimposed lines, and the difficulties involved in subtracting such a heavy atom as Pt. Intensities were calculated including the sodium contributions. They are listed in column 5 of Table I and appear to be in excellent agreement with the observed intensities. Significant improvement of

$$\frac{\sum\|F_{obs}|-|F_{calc}\|}{\sum|F_{obs}|}$$

(Table II) over the values not including sodium is noted.

CONDUCTIVITY EXPERIMENTS

The presence in the structure of infinite strings of Pt atoms (compare below) induced us to make conductivity measurements expecting the compound to exhibit metallic conduction. A sample of about 5 mm length was placed in a glass capillary tube of about 2 mm i.d. and clamped between two spring loaded brass electrodes. The conductivity was roughly determined at −196°C, 30°C, and 110°C and showed marked temperature de-

TABLE II. $\Sigma\|F_{calc}|-|F_{obs}\|^a/\Sigma|F_{obs}|^b$ for several structures.[b]

	c_1	c_2	c_3	c_4
Geiger counter intensities	0.144	0.132	0.091	0.061
Geiger counter and visual intensities	0.168	0.166	0.126	0.102

[a] Superposed reflections were excluded.
[b] The symbols c_i ($i=1, 2, 3, 4$) are explained in the footnote to Table I.

[9] W. H. Zachariasen, Acta Cryst. **1**, 281 (1948).

[10] An oxide of the formula Pt_3O_4 has been reported by Galloni and Roffo [E. E. Galloni and A. E. Roffo, Jr., J. Chem. Phys. **9**, 875 (1941)]. The diffraction pattern published by G. and R. is entirely different from that characteristic of our substance. The x-ray evidence on which the formula for their compound is based does not appear to us to be conclusive. Indeed, assuming that the compound investigated by G. and R. is a platinum oxide, one is tempted to conclude it to be PtO_2 by the following consideration. The cell volume reported is 240A³. Assuming 20A³ per O-atom one comes to 12 oxygens per unit cell. Since G. and R. show that 6 Pt-atoms in the set 6*b* of O_h^9 (reference 4) reproduce the major traits of the observed intensities one arrives at the composition PtO_2.

In a more recent publication [Z. Naturforsch. **56**, 130 (1950)] R. Busch confirms the lines reported by G. and R. as due to a platinum oxide. He also refers to work on the structure of an oxide PtO_2. (Busch, Cairo, Galloni, and Raskovan, Reunion A. Fisika Arg., La Plata, 1949, to be published.) We find that the lines listed by Busch (see above) for this compound coincide with lines calculated for the unit cell of the platinum oxide whose structure, as reported by Moore and Pauling, fits the formula PtO (reference 8).

[11] L. Pauling and J. Sherman, Z. Krist. **81**, 1 (1932).

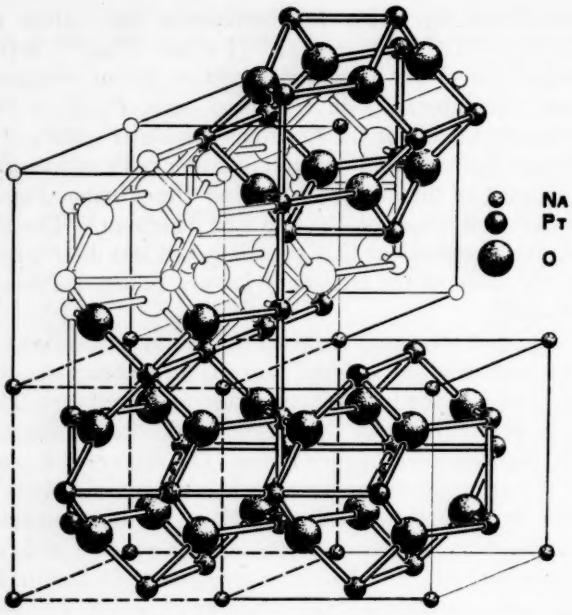

FIG. 3. Three-dimensional representation of relationship of atoms in $NaPt_3O_4$. Unit cube dashed at lower left corner.

pendence, being much smaller the lower the temperature. At −196°C there was a steady decrease in current immediately after application of a potential to the electrodes. Replacing the emf by a short-circuit loop caused current to flow in the opposite direction. Reversing the polarity of the electrodes reversed the effect. This polarization was less marked at room temperature and still less so at 110°C. The specific resistance at room temperature was of the order of 10^4 ohm cm, but since it was impossible to obtain sintered samples no attempts were made to place the measurements on an exact basis. It is quite possible that the grains of $NaPt_3O_4$ are actually much better conductors than would correspond to this magnitude. It appears clear that the conduction is of ionic character, and that the loosely fitting Na^+-ions (compare below) are the carriers.

DISCUSSION

The crystal structure derived above corresponds to the stoichiometric formula $NaPt_3O_4$ assuming that all oxygen cubes which do not already contain Pt-atoms are filled with Na-atoms, as is strongly implied by the magnitude of the fourier peak at the origin of Fig. 2a. The formula corresponds to 3.42 percent Na 9.51 percent O and 87.07 percent Pt which is well within the values of Wöhler's and the accuracy of our analyses. The variation in the oxygen content might be due to the presence of varying amounts of an amorphous oxide or of adsorbed oxygen, in as far as it is not caused by the experimental difficulties of analysis. The same holds for the water found. Attempts to prepare a Na free compound or to replace the Na with K or Li have so far been unsuccessful. The x-ray density of the compound is calculated to be 12.13 g/cm³.

A three-dimensional drawing of the structure is presented in Fig. 3. Infinite chains of Pt-atoms extend parallel to the edges of the unit cube. They are tied together by the O-atoms to form interlocking cages, two of which are shown by shading at the bottom of the figure and another one in different orientation at the top. At the centers of these cages are sodium ions which have as closest neighbors eight oxygen atoms at 2.46A arranged on a cube of half the unit cell edge. Each of these O-atoms has as neighbors three Pt-atoms at 2.01A forming the corners of an isosceles triangle and two Na-ions at 2.46A above and below the center of this triangle. The Pt-atoms are at the center of a square of O-atoms at 2.01A above and below which are two Pt-atoms at 2.85A, which are part of the chains of Pt-atoms already mentioned.

All atoms of a given kind are equivalent in this structure. In particular the Pt-atoms all have the unusual oxidation number 7/3. There is some covalent bonding of the Pt-atoms of a chain, the interatomic distance of 2.85A leading to a bond number 0.38.[12] The Pt−O distance corresponds essentially to a single bond between these two atoms being within 0.01A of the Pt−O distance found in PtO (2.02A).[8] It is interesting to note that this bond is not significantly shortened by a possible resonating double bond as usually formed for oxygen with trigonal hybridization. There are, however, hardly enough orbitals available in the Pt valence shell to accept such double bonds, and the p_z-lobes of the oxygen orbitals might find some compensation forming half-bonds to the sodiums towards which they are directed (compare e.g., the oxygen atom in lower left of Fig. 3). Nevertheless, the sodium must have a good deal of ionic character being responsible for the ionic conductance. The surrounding of the Na-ions by eight cubically arranged oxygens is the same as in Na_2O which has the antifluorite structure and in which the Na−O distance is 2.40A.[13] The analogous distance observed in $NaPt_3O_4$ (2.46A) indicates a somewhat looser fit of the Na-ions in $NaPt_3O_4$ than in Na_2O. The closest approach of the non-bonded O-atoms (2.85A) at the edges of these cubes as well as of the cubes containing Pt-atoms is very close to a van der Waals' contact (expected at 2.80A).

This substance reminds one somewhat of the wolfram bronzes $MeWO_3 \cdot xWO_3$, with Me an alkali metal, discussed most recently by Straumanis and co-workers,[14] and by Kupka and Sienko.[14] In the sodium bronzes the sodium is surrounded octahedrally by O-atoms at a distance of 2.72A, which is even larger than the Na−O distance in $NaPt_3O_4$. The sodium wolfram bronzes show metallic conductivity, but the lithium bronzes conduct by an ionic mechanism.[14]

[12] L. Pauling, J. Am. Chem. Soc. **69**, 542 (1947).
[13] Zintl, Harder, and Dauth, Z. Elektrochem. **40**, 588 (1934).
[14] M. E. Straumanis and S. S. Hsu, J. Am. Chem. Soc. **72**, 4027 (1950) etc., F. Kupka and M. J. Sienko, J. Chem. Phys. **18**, 1296 (1950), and reference 6.

THE JOURNAL OF CHEMICAL PHYSICS VOLUME 19, NUMBER 4 APRIL, 1951

Energy Transfer in the Photo-Sensitization of Silver Halide Photographic Emulsions: Optical Sensitization, Supersensitization, and Antisensitization*

W. West and B. H. Carroll
Kodak Research Laboratories, Rochester, New York
(Received November 24, 1950)

Many facts concerning optical sensitization of silver halide photographic emulsions point to the importance in the sensitization process of the migration of excitation energy from a dye molecule primarily excited by radiation to neighboring molecules in a cooperative layer. Individual dye molecules, however, appear capable of transferring energy to the silver halide without the intervention of energy migration, often with high efficiency, as is shown by relatively high quantum yields of sensitization at low concentrations of dye. If, as a result of increase in the concentration of dye, the sharp absorption bands indicative of exciton migration appear, the efficiency of transfer tends, in fact, to fall. Dyes in the cooperative state, however, are most susceptible to the increase of sensitization caused by *supersensitizers*. The regular periodic field which favors exciton migration decreases the probability of energy transfer to the halide, and the supersensitizer appears to act as a perturbation of this field at which the moving exciton is slowed down so as to facilitate transfer. Consistent with this explanation is the high quenching power of supersensitizers on the fluorescence sometimes exhibited in solution and in the adsorbed state by cooperative aggregates of dye molecules. The inverse of supersensitization, *antisensitization* by relatively small amounts of nonplanar dyes, is also observed. Here the migrating energy in the cooperative layer is dissipated as heat by the perturbing molecule, and is prevented from reaching the silver halide. Experimental evidence supporting these conclusions is furnished in detail, including correlations between optical sensitization and supersensitization with the type of absorption spectrum of the adsorbed dye; the relations between the concentration of sensitizer, supersensitizer, and antisensitizer, and the efficiency of super- and antisensitization; the quenching of fluorescence of sensitizers by both types of perturbing molecules; and effects of nonplanar dyes on the photoconductivity of optically sensitized silver halide emulsions analogous to their photographic effects.

INTRODUCTION

It is well known that the silver halide grains of a photographic emulsion, when carrying an adsorbed film of certain dyes, are rendered photo-sensitive to light absorbed by the dye. Substances which, by virtue of the absorption of light, confer photographic sensitivity at wavelengths longer than those absorbed by the silver halide are called "optical sensitizers."

The sensitizing effect of a mixture of two dyes is seldom additive. Often the sensitization produced by the mixture is less than the sum of the sensitizations of the components, which are then noncommittally described as "interfering." Some dye mixtures, or even mixtures of a dye with a colorless compound, show a sensitization much greater than the sum of the individual effects, a phenomenon termed by Mees "supersensitization."[1] The effect of the supersensitizer is often manifest at low concentrations of supersensitizer relative to sensitizer. To clarify the phenomenon, it may be well to refer to an example of the effect in its simplest form. The dye, 1,1′-diethyl-2,2′-cyanine iodide (Dye I, Table VIII), in a bromoiodide emulsion of medium speed is only a moderately good sensitizer, with a sharp sensitization maximum at 575 mμ, coinciding with its absorption maximum on the silver halide grain; the sensitivity of an experimental emulsion containing the dye alone at the sensitization maximum was 9.77, expressed as the reciprocal of the incident energy in ergs per cm² of emulsion surface required to produce a developed density of 0.6 above fog.† The merocyanine dye, XXIV,[2] whose absorption band on the grain is in the blue-green region of the spectrum, and which does not itself confer sensitivity at 575 mμ, added to the 2,2′-cyanine dye, produced a sensitivity of 169 at 575 mμ, an increase of 17-fold over that produced by the sensitizer alone. The enhancement of sensitivity is known, experimentally, not to be caused by any corresponding increase in the absorption of light by the combination, and the action of the supersensitizer must lie in its increasing the efficiency of transfer of the energy absorbed by the sensitizer to the silver halide grain. In the example cited, the quantum efficiency of sensitization, in terms of light absorbed at 575 mμ, relative to the quantum yield of light absorbed directly by the silver halide, increased from 0.05 with the dye alone to practically 1.0 in the presence of the supersensitizer.[3]

Supersensitization in general seems to be a complex of effects, and among the numerous examples known, increase in sensitivity attributable to increased absorption or to decreased desensitization by the sensitizing dye, as well as to increased efficiency of transfer, can be recognized. The latter effect is, however, the most common, and the present article is concerned only with supersensitization of this kind.

Recently, the inverse of supersensitization has been observed—a great depression of sensitization by a relatively small amount of certain dyes without any corresponding decrease in absorption. This effect differs from normal "interference" in the great effect of a small

* Communication No. 1382 from the Kodak Research Laboratories.

[1] C. E. K. Mees, U. S. Pat. 2,075,046–8 (1937). C. E. K. Mees, *The Theory of the Photographic Process* (Macmillan Company, New York, 1942), pp. 975, 1070.

† We are indebted to Dr. J. Spence for the quantitative data in this example.

[2] Carroll, Brooker, and Spence, Brit. Pat. 625,466 (1949).

[3] See J. Spence and B. H. Carroll, J. Phys. and Colloid Chem. **52**, 1090 (1948), for the details of measuring the relative quantum efficiency.

amount of the inhibiting dye, and is distinguishable from desensitization by the fact that the depressant action of the inhibiting foreign dye is much greater on the sensitivity conferred by the other dye than on that associated with the absorption band of the silver halide. As will be discussed in detail, the effect is related to supersensitization and can conveniently be termed "antisensitization." The structural factor common to antisensitizers is the lack of planarity of the atoms in the chromophoric chain of the dye.

The experiments described in this paper indicate that supersensitization and antisensitization, antithetical though they may appear, have their origin in a common cause, the migration of the energy of electronic excitation from molecule to molecule within the layer of sensitizing dye.

The concept of energy migration from molecule to molecule of a light-absorbing substance by resonance interaction between unexcited and excited molecules has been qualitatively familiar since J. Perrin pointed out its possibility,[4] and F. Perrin,[5] with the aid of the considerations adduced by Kallmann and London,[6] advanced a quantum-mechanical theory of the process. Another theoretical step in the development was the introduction of the concept of the exciton by Frenckel[7] and its elaboration by Peierls.[8] This is a very quick propagation of electronic excitation energy through the molecules of a crystal so that any particular molecule retains the energy for a short time in comparison with the period of a vibration. The general subject of energy propagation in condensed systems has been more recently discussed by Franck and Teller,[9] Förster,[10] and Franck and Livingstone.[11] The latter authors, in particular, emphasize the distinction between exciton migration, with its very close coupling between neighboring molecules, and slower migration processes, typified by sensitized fluorescence, in which, under conditions of nearly exact resonance, energy can be transferred from one resonance-partner to another over distances of 50A or more.[5,6]

Many of the phenomena of interest in this discussion are illustrated by the sensitizing dye, 1,1′-diethyl-2,2′-cyanine iodide (Dye I). This dye, as chloride in sufficiently concentrated aqueous solution, has a remarkably sharp absorption band at about 575 mμ, bathochromic to the spectrum of an assembly of isolated molecules in dilute alcoholic or aqueous solution, whose maximum is at 520 mμ.[12,13] The sharp band has been termed a "*J*-band."[14] The observations, particularly of Scheibe and co-workers, have shown that the condition of the state characterized by the *J*-band is a polymer of high molecular weight, constituted of oriented molecules held by van der waals forces so that the molecular planes are parallel to one another.[15] The molecules line up to form fiber-like aggregates in which the direction of the fiber is at right angles to the axis joining the nitrogen atoms of the quinoline nuclei (I), and the molecular planes are probably tilted from the normal with respect to the fiber direction.

Absorption in the *J*-band of 1,1′-diethyl-2,2′-cyanine is accompanied by a strong fluorescence at nearly the same wavelength,[12,13] which is appreciably quenched by resorcinol at very low concentrations in comparison with that of the dye. From this and other observations, Scheibe *et al.*[16] concluded that the excitation energy primarily absorbed by a molecule in the aggregate must be able to migrate from molecule to molecule of the polymer. This concept of energy-wandering through the macromolecular aggregate is consistent with the peculiarity that, in the *J*-band, light is absorbed with highest intensity when the direction of the electric vector is parallel to the direction of the fiber and perpendicular to the N^+—N axes of the individual molecules,[17] the general picture suggested being of a kind of macromolecular optical unit formed by overlapping of the π-orbitals of the chromophoric chain in which the oscillating charge associated with absorption moves along the fiber axis. Franck and Teller[9] pointed out that the extreme narrowness of the *J*-absorption band suggested exciton motion, and Franck and Livingstone[11] regard the dye aggregates which exhibit these bands as probably the only known instances in which exciton motion occurs. Much more common are other cases of energy migration, illustrated by sensitized fluorescence, in which the absorption bands are not particularly sharp. The migration here is slower and less extensive spatially than in exciton propagation.

AGGREGATION AND SENSITIZATION

In the adsorbed state on the silver halide grain, Dye I, along with many others which do not form *J*-aggregates in aqueous solution, or only after addition of electrolyte, shows a relatively sharp *J*-band absorption[18–20] which is reproduced in optical sensitization (Fig. 1, curve 3). It seems probable that the characteristic exciton propagation of the aggregate in solution is retained in the

[4] J. Perrin, *2me conseil de chimie Solvay, Brussels (1924)* (Gauthier-Villars, Paris, 1925), p. 322.
[5] F. Perrin, Ann. chim. et phys. **17**, 283 (1932).
[6] H. Kallmann and F. London, Z. physik. Chem. (B) **2**, 207 (1928).
[7] J. Frenckel, Phys. Rev. **37**, 17 (1931). J. Frenckel, Physik. Z. Sowjetunion **9**, 158 (1936).
[8] R. Peierls, Ann. d. Physik **13**, 905 (1932).
[9] J. Franck and E. Teller, J. Chem. Phys. **6**, 861 (1938).
[10] Th. Förster, Ann. Physik **6**, 2, 55 (1948).
[11] J. Franck and R. Livingstone, Revs. Modern Phys. **21**, 505 (1949).
[12] E. E. Jelley, Nature **138**, 1009 (1936).
[13] G. Scheibe, Z. angew. Chem. **50**, 51 (1937).
[14] S. E. Sheppard, Revs. Modern Phys. **14**, 303 (1942).
[15] G. Scheibe, Z. Elektrochem. **52**, 283 (1948).
[16] Scheibe, Schöntag, and Katheder, Naturwiss. **27**, 499 (1939).
[17] E. E. Jelley, Nature **139**, 631 (1937).
[18] Leermakers, Carroll, and Staud, J. Chem. Phys. **5**, 878 (1937).
[19] G. Schwarz, Science et inds. phot. (2) **10**, 233 (1939).
[20] B. H. Carroll and W. West, *Photographic Processes* (Butterworths Scientific Publications, Ltd., London), to be published.

adsorbed layer. As already mentioned, the sensitization of Dye I can be increased manyfold by the addition of suitable supersensitizers. Susceptibility to supersensitization to some degree can be taken as a fairly general expectation for dyes which exhibit *J*-bands on the silver halide grain. Supersensitization, however, is by no means limited to dyes forming *J*-aggregates on the grain. For example, Dye II, Table VIII, is derived from Dye I by substituting methyl for ethyl on the nitrogen atoms, and its absorption spectrum as an assembly of isolated molecules is very similar in position and intensity to that of the diethyl compound. The two dyes in alcoholic solution show absorption maxima at 522 and 524 mμ, respectively. Adsorbed on silver halide, the dimethyl dye sometimes shows a *J*-band of low intensity, which may indeed be absent, the main absorption band being a broad band at about 485 mμ, hypsochromic to the molecular band, and a broad band at about 540 mμ. (See Fig. 1, curves 1 and 2.) Systematic observation has shown[20] that on the grain, as the concentration of a sensitizing dye increases, the absorption spectrum tends to pass through a sequence of stages, the first, at low concentrations, identifiable with the absorption spectrum of the isolated molecule, as modified by adsorption (i.e., a bathochromic shift of about 30 mμ from the maximum in alcoholic solution), then a polymeric stage characterized by hypsochromic displacement of the band from the position of the molecular band, following which, with increasing concentration, the sharp *J*-maximum may appear. The aggregates characterized by the broad hypsochromic bands can be conveniently termed "*H*-aggregates," or polymers, and the corresponding bands, "*H*-bands."

The band in adsorbed 1,1′-dimethyl-2,2′-cyanine iodide at 485 mμ is such an *H*-band, while the band at about 540 mμ may be the molecular band as modified by adsorption. Table I contains sensitometric data on chlorobromide emulsions sensitized with dimethyl- and diethyl-2,2′-cyanine iodides, at a concentration of 20 mg per liter of emulsion,‡ with and without the supersensitizer, *p*-diethylaminostyrylbenzothiazole (Dye XXIII), at a concentration of 2.5 mg per liter. The sensitivity, *S*, is expressed at various wavelengths, λ, as the reciprocal of the incident energy in ergs per

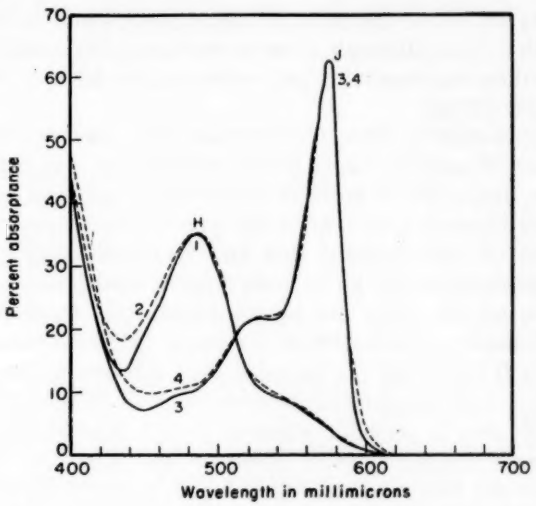

FIG. 1. Absorption spectra of 1,1′-dimethyl-(Dye II) and of 1,1′-diethyl-2,2′-cyanine (Dye I) iodides in a chlorobromide emulsion, with and without a supersensitizer: 1. Dye II, 20 mg per liter; 2. Dye II, 20 mg per liter+supersensitizer, 2.5 mg per liter; 3. Dye I, 20 mg per liter; 4. Dye I, 20 mg per liter+supersensitizer, 2.5 mg per liter.

cm² required to produce a developed density of 0.8 above fog; the percentage absorption of the emulsion coatings at these wavelengths is denoted by *A*, and the quantum yield relative to that at 420 mμ, at which only the silver halide absorbs, is denoted by $\phi_r = S_\lambda/S_{420} \cdot A_{420}/A_\lambda \cdot 420/\lambda$.[3] The left-hand part of the table contains the data for the dyes without supersensitizer and the right-hand part for the dye in the presence of a small quantity of a nearly colorless supersensitizer which itself confers only a very low sensitivity at 490 mμ and none at longer wavelengths. The data and Fig. 1 show clearly that the absorption of the two sensitizers is only slightly altered by the supersensitizer and that the marked increase in sensitivity to the light absorbed by the sensitizers is caused by an increased quantum efficiency for the sensitization process. Supersensitization is effected both on the dimethyl dye, in which the absorption is concentrated mostly in the *H*-band about 490 mμ and on the diethyl dye, with the pronounced *J*-maximum at 575 mμ. In this example, the quantum yields for the supersensitized mix-

TABLE I. Relative quantum efficiencies of sensitization of 1,1′-dimethyl (Dye II)- and of 1,1′-diethyl (Dye I)-2,2′-cyanine iodides in a chlorobromide emulsion.

		Sensitizer alone			Sensitizer + supersensitizer		
Sensitizer	λ (mμ)	420	490	550	420	490	550
Dye II	Sensitivity, *S*	0.98	0.23	0.06	1.45	1.75	0.52
20 mg/liter	Absorption (%) *A*	20.5	35.0	8.5	23.6	35.1	9.5
	ϕ_r	1.00	0.12	0.12	1.00	0.70	0.68
	λ (mμ)	420	540	575	420	540	575
Dye I	Sensitivity, *S*	1.05	0.02	0.06	1.38	1.12	3.65
20 mg/liter	Absorption (%)	20.8	21.2	62.5	23.1	22.3	62.4
	ϕ_r	1.00	0.016	0.013	1.00	0.65	0.72

‡ The dyes are added to the liquid emulsion before coating, and in this communication, dye concentrations are expressed as mg of dye per liter of liquid emulsion.

tures are about the same for the dimethyl and for the diethyl dyes, although, in most emulsions, the dimethyl dye does not respond to supersensitization quite as well as the diethyl.

Dyes differ in the extent to which their spectra in the adsorbed state on silver halide change with concentration, and a survey of much experimental material indicates a correlation between the type of absorption spectrum of the adsorbed dye and its susceptibility to supersensitization. Three main types of absorption spectrum on the grain can be recognized—(1) those predominantly constituted of a *J*-band, (2) those mostly of an *H*-band, and (3) those not very different in shape, over a wide range of concentration, from the spectrum of the dye in alcoholic solution, with a general bathochromic displacement of about 30 mμ. The first two types are illustrated in Fig. 1 for Dyes I and II. Dye XVIII, 3,3′-diethylthiacarbocyanine iodide, is an example of the latter class. In alcoholic solution, the absorption maximum of this dye is at 558 mμ; adsorbed to the grain at a concentration of 1.5 mg per liter of a bromoiodide emulsion, corresponding to less than one percent coverage of the grain surface, it exhibits an absorption maximum at 585 mμ, and at approximately the optimum sensitizing concentration of 20 mg per liter, the main maximum is at 590 mμ with an accompanying *H*-band at 540 mμ. The bathochromic shift from 558 to 585 mμ seems to be the normal result of adsorption on the spectrum of the isolated molecule, and it seems that in dyes showing the spectral characteristics on the grain of Dye XVIII most of the molecules in the adsorbed layer retain essentially the spectrum of the isolated molecule.

In general, dyes like XVIII, whose spectrum in the adsorbed state on silver halide resembles the molecular spectrum, are least susceptible to supersensitization; those with strong *J*-bands are most responsive to supersensitization; and those showing predominantly *H*-bands occupy an intermediate position. In this discussion it should be remarked that while some substances act as supersensitizers towards more than one type of sensitizing dyes, most sensitizer-supersensitizer combinations are highly individualistic.

These observations and others to be described suggest that sensitization and supersensitization are intimately connected with the migration of excitation energy throughout the adsorbed layer of dye molecules.

At the normal sensitizing concentration used in photographic emulsions, approximately half of the total surface of the emulsion grain is covered by dye.[21] The nature of the adsorption isotherm and the manner in which the absorption spectrum of the adsorbed dye changes with concentration[21] suggest that at the normal sensitizing concentration, efficient sensitizers of the cyanine classes are held to the surface in islands of closely packed oriented molecules with relatively bare spaces intervening. The conditions are therefore favorable to the propagation of energy throughout these islands from any molecule primarily excited by the absorption of radiation. Even if at half coverage of the grain the dye molecules were uniformly distributed over the surface, the mutual propinquity of the molecules would permit migration of excitation energy by a process analogous to sensitized fluorescence. Under the normal sensitizing conditions of photographic practice, it seems probable that some migration of excitation energy can always occur. The rapidity and extent of the migration no doubt differ from dye to dye. In so far as the sharp *J*-band is the sign of exciton migration,[9] the migration will be fastest and extend over the greatest number of individual molecules in adsorbed layers showing this type of spectrum. The breadth of the *H*-band indicates greater interaction between molecular oscillations and the electronic motion in the *H*-aggregate than in the *J*-aggregate, leading to a greater probability of thermal degradation and correspondingly shorter path length for the moving excitation state, while for the dyes in which the mutual interaction between the electronic motion in neighboring molecules is small enough to preserve the energy levels largely unchanged, the extent of the migration will be least. The behavior of sensitizers exhibiting these various types of spectra on the grain towards supersensitization and antisensitization is in general agreement with these deductions.

Franck and Teller[9] pointed out that the very rapid flow of excitation energy from molecule to molecule associated with exciton migration would leave the excited state in the neighborhood of any foreign energy-accepting point for too short a period for a transfer-interaction to occur; photo-chemical sensitization would be unlikely to occur so long as the exciton was rapidly moving, but would be facilitated at an impurity. Frenckel[7] also indicated that an exciton would be slowed down and "trapped" at a foreign singularity in the lattice, and the suggestion was made by West and Carroll[22] and by Mott[23] that a photographic supersensitizer acted by furnishing a singularity in the regular potential field of the adsorbed sensitizing dye at which the propagation of excitation would be disturbed so as to facilitate transfer to the silver halide grain. In this way the effect of small quantities of supersensitizer in comparison with that of the sensitizer is explained, and some of the requirements of a supersensitizer can be seen. It must be sufficiently different from the sensitizer to form an effective singularity in the potential field, but it must be capable of entering into the adsorbed layer in a kind of "solid solution" in the two-dimensional lattice, instead of aggregating by itself outside the layer of sensitizer. Moreover, it must not itself permanently acquire the energy of excitation, either by degrading it

[21] Adsorption studies made in these Laboratories in preparation for publication.

[22] W. West and B. H. Carroll, J. Chem. Phys. **15**, 529 (1947).
[23] N. F. Mott, Phot. J. **88B**, 119 (1948).

thermally or utilizing it chemically. It is probably not, in general, necessary for the excitation energy to be acquired by the supersensitizer, but if it is, it must be passed on to the halide lattice. These criteria are in general agreement with the known sensitizer-supersensitizer combinations. The supersensitizer may be a dye, but of a different class from the sensitizer, or if a colorless compound, it usually contains a nucleus similar to one of the nuclei in the sensitizer, attached to a part unrepresented in the sensitizer, so that the supersensitizer could reasonably be incorporated in "solution" in the adsorbed layer of sensitizing dye.

EFFECT OF SENSITIZER CONCENTRATION ON OPTICAL SENSITIZATION AND SUPERSENSITIZATION

In the mechanism of supersensitization just described, an all-important role is played by a cooperative layer of sensitizer molecules; it follows that at sufficiently low concentration of sensitizer, when the dye is present as isolated molecules scattered over the surface, supersensitization should diminish. Some dyes, such as Dye I, are so readily *J*-aggregated that, at the lowest concencentration at which adequately precise measurements of absorption can be made for the computation of relative quantum efficiencies of sensitization, the adsorbed layer shows predominantly the *J*-band, and for these, since cooperative patches begin to be built up at very low concentrations, no great variation of the efficiency of supersensitization with the concentration of sensitizer is to be expected. Even for these sensitizers, however, there is an indication of decreased efficiency of supersensitization at very low concentrations. The case becomes much more certain for dyes which exhibit a well-marked change in absorption, from the molecular type at low concentration to the *J*-type at higher, and relative quantum yields of sensitization have been measured for a number of these sensitizers, at different concentrations, with and without supersensitizers. Table II, summarizing measurements of the relative quantum yield of sensitization for 3,3′-dimethyl-9-ethylthiacarbocyanine bromide (XX) and for 3,3′-9-triethylselenacarbocyanine iodide (XXII), with and without a supersensitizer, is representative of the results.

At the lowest concentrations, corresponding to less than one percent coverage of the grain surface, the absorption spectra are those of the individual molecules as modified by adsorption to the silver halide, whereas at higher concentrations *J*-bands are prominent. A number of sensitizer-supersensitizer combinations have been examined in this way, with the invariable result that supersensitization at low concentrations of sensitizers was less efficient than at higher concentrations. The tendency exhibited by Dye XX to sensitize when alone with lower efficiency as the concentration is increased is also found in other examples. From the observations as a whole, it can be concluded that (a) the isolated molecule can act as an optical sensitizer, often with high efficiency, (b) aggregation in itself, with concomitant energy-wandering, tends to lower rather than to increase the efficiency of sensitization, and (c) the aggregated state is peculiarly susceptible to supersensitization.

TABLE II. Relative quantum yields, ϕ_r, at different concentrations of sensitizer.

Dye	Conc. mg/liter		Sensitizer alone			Sensitizer and supersensitizer		
3,3′-Dimethyl-		(λ)	540	570	630	540	570	630
9-ethylthia-	1.0	ϕ_r	—	0.41	—	—	0.30	—
carbocyanine	2.0	ϕ_r	—	0.24	—			
bromide (XX)	10.0	ϕ_r	0.22	0.25	0.22	0.30	0.48	0.47
3,3′,9-Triethyl-		(λ)	585			585		
selenacarbo-	1.0	ϕ_r	0.34			0.41		
cyanine iodide	10.0	ϕ_r	0.33			0.60 (600 mμ)		
(XXII)								

A fact which strongly supports the view that in supersensitization the supersensitizer is incorporated into some kind of excitation unit with the sensitizer is the observation that, in the combination, the characteristic absorption shown on the silver halide by the supersensitizer alone is sometimes wholly or partly suppressed. Figure 2 illustrates this effect. In this figure, reflectance minima correspond to absorption maxima. The sensitizer is Dye XX, and the supersensitizer, a

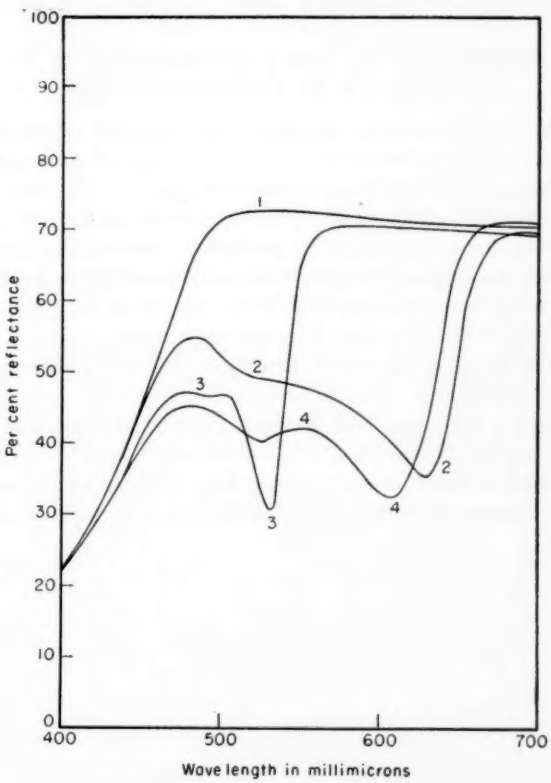

FIG. 2. Reflectance spectra of emulsion coatings containing the sensitizer, 3,3′-dimethyl-9-ethylthiacarbocyanine (XX), and supersensitizer, 1′-ethyl-3-methylthia-2′-cyanine (XV): 1. Silver halide alone; 2. Dye XX alone, 20 mg per liter; 3. Dye XV alone, 20 mg per liter; 4. Dye XX+Dye XV, each 20 mg per liter.

TABLE III. Quenching of fluorescence in *J*-band by supersensitizer in fine-grained emulsion.

Conc. of sensitizer mg per liter	Conc. of supersens. mg per liter	Relative intensity of fluorescence
0	0	0
50	0	50
100	0	100+
200	0	100
0	(a) 5	0
50	(a) 5	5
100	(a) 5	5
200	(a) 5	5
0	(b) 100	0
100	(b) 100	1
100	(b) 50	4
100	(b) 20	6

thia-2′-cyanine which can itself sensitize with a maximum at 530 mμ, is Dye XV. The adsorbed sensitizer alone has a *J*-maximum at 630 mμ (curve 2) and the supersensitizer, one at 530 mμ (curve 3). In the combination, the maximum of the sensitizer is hypsochromically displaced to about 610 mμ, and the intensity of absorption of the supersensitizer within its characteristic band is considerably reduced (curve 4). The case is analogous to that of mixed polymers, reported by Scheibe,[24] according to which two dyes, each showing *J*-bands alone, when mixed had a single sharp absorption band of intermediate wavelength, variable with composition, between the bands of the components.

QUENCHING OF THE FLUORESCENCE OF A *J*-AGGREGATE BY SUPERSENSITIZERS

Another fact that suggests the capacity of supersensitizers to interfere with the migration of excitation energy throughout a cooperative layer of sensitizer is the marked effect of supersensitizers in quenching the characteristic fluorescence of Dye I, the maximum of which corresponds very closely in position with the *J*-absorption maximum, both in concentrated aqueous gel and in the adsorbed state on silver halide grains. The feeble fluorescence of the adsorbed dye can be observed conveniently in coatings of very fine grained emulsions in which reflection and scattering are minimized. Table III contains data on the fluorescence intensity in the *J*-band of emulsions containing Dye I with and without the supersensitizers, *p*-diethylaminostyrylbenzothiazole,

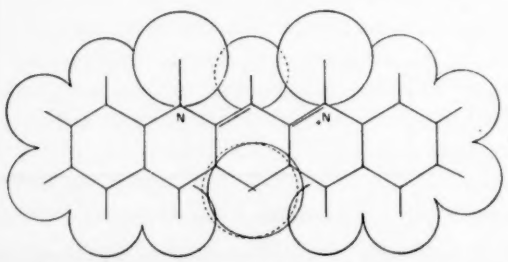

FIG. 3. 1,1′,3,3′-tetramethyl-2,2′-cyanine cation.

[24] Scheibe, Mareis, and Ecker, Naturwiss. **25**, 474 (1937).

Dye XXIII (a),[25] and the merocyanine, XXIV (b). The exciting radiation was the mercury green line 546 mμ, and the fluorescence was observed through a Kodak Wratten No. 22 Filter, which transmits the fluorescent light but absorbs most of the exciting light.

On the other hand, merocyanines somewhat similar, structurally, to XXIV but which have small supersensitizing capacity, quenched the fluorescence of the adsorbed sensitizer only slightly, and, in general, a marked correlation was found between the quenching powers of dyes on the fluorescence of the sensitizer and their capacity to cause supersensitization.

ANTISENSITIZATION BY NONPLANAR DYES

The suggestion of Sheppard, Lambert, and Walker[26] that molecular planarity was an important requirement for efficient optical sensitization has been amply confirmed by the study of a number of dyes prepared in these Laboratories under the direction of Dr. L. G. S. Brooker, and a great variety of nonplanar cyanines and other dyes are now available. An example of a nonplanar 2,2′-cyanine is 1,1′,3,3′-tetramethyl-2,2′-cyanine iodide (VII) (Fig. 3).

As a result of the mutual impingement of the methyl groups in the 3- and 3′-positions, the nuclei joined by the methine bridge are forced from co-planarity. The existence of crowding in a dye can be recognized by well-marked effects on the intensity and often in the position of the absorption bands.[27]

It was suggested by the view of supersensitization just described that a molecule of the tetramethyl-2,2′-cyanine introduced into the cooperative layer of 1,1′-diethyl-2,2′-cyanine (I) might act as a singularity leading to supersensitization. While this expectation has been verified by definite supersensitization by the nonplanar 2,2′-cyanine of certain dyes of other classes than the 2,2′-cyanines, the effect on Dye I was a large suppression of the sensitization. Within limits discussed in some detail in later paragraphs, small amounts of nonplanar dyes are found, in general, strongly to depress the sensitization produced by optical sensitizers. This effect is to be distinguished from general desensitization of the emulsion, indicated by depressed sensitivity towards blue light, nor is it associated with any corresponding depression of light absorption in the optically sensitized region of the spectrum. It is therefore a reduction in the efficiency of transfer of excitation energy to the silver halide and can be conveniently termed *antisensitization*.

Examples are shown in Table IV of the antisensitizing action of various nonplanar dyes on 2,2′-cyanines and thiacarbocyanines. The sensitivities in the regions absorbed by the sensitizer and by the silver halide are

[25] B. H. Carroll and J. A. Leermakers, U. S. Pat. 2,313,922 (1943).

[26] Sheppard, Lambert, and Walker, J. Chem. Phys. **9**, 96 (1941).

[27] Brooker, White, Sprague, Dent, Jr., and VanZandt, Chem. Revs. **41**, 325 (1947).

arbitrarily set at 100 for emulsions containing sensitizer only, and it will be seen that small amounts of the crowded dyes depress optical sensitization much more than they do the "natural" sensitivity to blue light. In this table, 5,6-benzo-2,2′-cyanine (VIII) and its 3,4-benzo-isomer (IX) form an interesting pair. The former is an efficient sensitizer, while the latter, distorted from planarity by the impingement of the 3,4-benzene ring on the quinoline nucleus at the other end of the methine bridge, does not sensitize.[26,28] A small quantity of the nonplanar dye added to its planar isomer greatly diminishes the sensitization of the latter dye. Many examples have shown the generality of the phenomenon of antisensitization among a variety of dye types, including 2,2′-cyanines and carbocyanines, 4,4′-cyanines, thiacyanines, thia-2′-cyanines, thiacarbocyanines, and thiadicarbocyanines.

Antisensitization is exerted at relative concentrations of antisensitizers and sensitizers lower than 1:100; small quantities of antisensitizer have relatively the greatest effect, and, analogous to the quenching of fluorescence by foreign substances, the degree of antisensitization is approximately a hyperbolic function of the concentration of the antisensitizer. If S_0 is the sensitivity of an emulsion to light absorbed by the sensitizer alone, and S the sensitivity in the presence of a concentration c of antisensitizer, $S=S_0/(1+kc)$.[20]

The dyes most susceptible to antisensitization are those with well-pronounced J-maxima which, alone or in the presence of supersensitizers, are highly efficient optical sensitizers. In accord with this, a given dye is relatively less strongly antisensitized at low concentration on the halide grain, at which the rounded maxima characteristic of isolated adsorbed molecules or of lower and less extensively cooperative aggregates predominate, than at higher concentrations exhibiting pronounced J-maxima in absorption and sensitization. Table V contains examples.

TABLE IV. Antisensitization by nonplanar dyes.

Sensitizer (conc. =20 mg/l)	Antisensitizer	Relative sensitivity in optically sensitized region	Relative sensitivity in region of silver salt absorption
1,1′-diEt-2,2′-cyanine (I)	—	100	100
	nonplanar 2,2′-cyanines 2 mg per liter		
	1,1′,9-triMe (V)	25	100
	1-Et-1′,3-diMe (VI)	18	85
	1,1′,3,3′-tetraMe (VII)	12	85
	nonplanar 4,4′-cyanine 2 mg per liter		
	1,1′,3,3′-tetraMe (XIII)	30	100
	nonplanar thia-2′-cyanine 2 mg per liter		
	1,3′-diEt-3-Me (XVII)	35	100
1,1′-diEt-5,6-benzo-2,2′-cyanine (VIII)		100	100
	nonplanar benzo-2,2′-cyanine (IX)	36	100
3,3′-diEt-9-Me-thiacarbocyanine (XIX)		100	100
	nonplanar 2,2′-carbocyanines		
	1,1′-diEt-10-Me (XI)	25	47
3,3′-diMe-9-Et-thiacarbocyanine (XX)		100	100
	1,1′-diMe-10-Ph (XII)	13	53

In Table V, "efficiency of antisensitization" is measured by the ratio of the sensitivity in the absorption region of the sensitizer without the antisensitizer to that with the antisensitizer. In addition to their effect in inhibiting optical sensitization, some antisensitizers diminish sensitivity to blue light absorbed by the silver salt. It is assumed that this general desensitizing action occurs also in the optically sensitized region of the sensi-

TABLE V. Effect of concentration of sensitizer on antisensitization.

Sensitizer	Antisensitizer	Efficiency of antisensitization	Nature of absorption spectrum of sensitizer
1,1′-diEt-2,2′-cyanine (I)	1,1′,3,3′-tetraMe-2,2′-cyanine (VII)		
20 mg per liter	2 mg per liter	6.7	Strong J-max
1 mg per liter	2 mg per liter	2.0	Weak J-max
3,3′,9-triEt-5,5′-diClthiacarbocyanine (XXI)	1,1′-diEt-10-Me-2,2′-carbocyanine (XI)		
20 mg per liter	5 mg per liter	4.0	Strong J-max, 650 mμ
1 mg per liter	5 mg per liter	2.8	Weak J-max, 650 mμ
1 mg per liter	1 mg per liter	1.6	Strong rounded max, 580 mμ
3,3′-diMe-9-Et-thiacarbocyanine (XX)	1,1′-diMe-10-phenyl-2,2′-carbocyanine (XII)		
20 mg per liter	5 mg per liter	9.5	Strong J-max, 650 mμ Weaker rounded max, 590 mμ
1 mg per liter	5 mg per liter	2.8	Rounded max, 570 mμ
1 mg per liter	1 mg per liter	1.4	Rounded max, 570 mμ

[28] L. G. S. Brooker and G. H. Keyes, J. Am. Chem. Soc. **58**, 659 (1936).

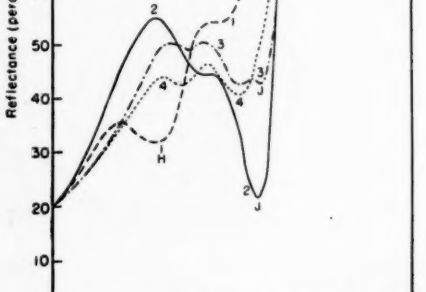

FIG. 4. Reflectance spectra of 2,2′-cyanines in emulsion: 1. 1,1′-dimethyl-2,2′-cyanine (I); 2. 1,1′-diethyl-2,2′-cyanine (II); 3. 1,1′-diamyl-2,2′-cyanine (III); 4. 1,1′-diphenyl-2,2′-cyanine (IV).

tivity spectrum, and, in the table, the figures for efficiency of antisensitization are corrected for any general desensitizing action of the nonplanar dye.

The fact that antisensitization occurs at a low molecular ratio of antisensitizer to sensitizer, and that it is most efficient at high concentrations of sensitizer, suggests that antisensitization involves the interruption of the flow of excitation energy in a cooperative layer of adsorbed sensitizer molecules and its degradation by the antisensitizer. The phenomenon is therefore very similar to transfer-supersensitization, the essential difference being that, in supersensitization, the excitation energy trapped in the vicinity of the foreign molecule is ultimately transferred to the silver halide grain, while in antisensitization, it is degraded, presumably by excitation of vibrations, within the foreign molecule itself.

Since the sharp *J*-absorption band seems to be associated with the greatest mobility of the excited state throughout the layer and the greatest extent of migration from the primarily excited molecule, both supersensitization and antisensitization should be most pronounced with sensitizers showing this type of absorption, as is found to be true.

An interesting example of the relation between the type of absorption spectrum and susceptibility to supersensitization and to antisensitization is afforded by the series of 2,2′-cyanines containing the groups, methyl (II), ethyl (I), amyl (III), and phenyl (IV), on the nitrogen atoms (Table VIII).

Each of these dyes is known from measurements of the adsorption isotherm to form a packed layer of adsorbed molecules oriented "edge-on" to the halide surface, but as shown in Fig. 4, the absorption spectra of the adsorbed dyes on the grains of a bromoiodide emulsion are quite different. (In Fig. 4 reflectance minima are absorption maxima.) In this emulsion, the diethyl dye has a very strong *J*-band (curve 2), the dimethyl a weak *J*- and a strong *H*-band (curve 1), the diamyl a *J*-band with a companion in the position to be expected for the absorption of individual molecules as modified by adsorption (curve 3), and the diphenyl dye, with no *J*-band (curve 4), shows only bands corresponding to relatively low degrees of optical cooperation. Probably all four dyes are adsorbed as layers of laterally interacting molecules, but the effect on the absorption spectra is least for the diphenyl dye, increasing for the diamyl, dimethyl, and diethyl dye. Migration of excitation energy will extend only over a few molecules of the diphenyl dye and be greatest in the diethyl. The diphenyl dye can be supersensitized, but to a smaller degree than the dimethyl which usually does not respond as well as the diethyl dye. Similarly, the efficiency of antisensitization by the nonplanar 1,1′,3,3′-tetramethyl-2,2′-cyanine (VII) in the ratio of 1:10 in each of these dyes in the series, diethyl, diamyl, dimethyl, and diphenyl, is 5.5, 2, 1.6, 1.2, measured as before. The order of the efficiency of antisensitization is the order of intensity of the *J*-absorption bands.

ENERGETIC RELATIONS IN ANTISENSITIZATION

A nonplanar dye can act as an efficient antisensitizer towards a sensitizer whose absorption maximum is at a shorter wavelength than that of the antisensitizer, or not more than about 70 mμ longer, i.e., the essential energetic condition to be fulfilled is that the electronically excited sensitizer must possess enough energy to bring about the electronic excitation of the antisensitizer. There is a steady decrease in the efficiency of a given antisensitizer towards a series of sensitizers as the absorption bands of the sensitizers occur at longer and longer wavelengths. There is no sign of decreased efficiency of antisensitization as the absorption bands of the nonplanar dyes are chosen at wavelengths successively longer than that of the sensitizer. The large number of vibrational degrees of freedom in the excited antisensitizer are apparently able to utilize any excess energy transferred from the sensitizer above that required for pure electronic excitation.

The existence of antisensitization when the absorption maximum of the antisensitizer is somewhat shorter than that of the sensitizer no doubt has various origins—the absorption bands may be broad and overlap so that sharp resonance may occur between sensitizer molecules absorbing at the short-wave end of the sensitizer spectrum and antisensitizer molecules absorbing at the long-wave end of the antisensitizer spectrum, and a certain deficiency in excitation energy on the part of the sensitizer can be compensated for by utilizing thermal energy, as in anti-Stokes fluorescence and Raman excitation.

Some examples of the energetic relations in antisensitization are shown in Table VI, illustrating the diminish-

ing efficiency of a given antisensitizer towards sensitizers absorbing farther and farther at longer wavelengths. The interval by which the wavelength of the absorption maximum of the adsorbed sensitizer is longer than that of the adsorbed antisensitizer is denoted by $\Delta\lambda$.

The sensitizers are:

Dye XIV, 3,3′-diethyl-4,5,4′,5′-dibenzothiacyanine, λ max = 500 mμ.

Dye XV, 1′-ethyl-3-methylthia-2′-cyanine, λ max = 530 mμ.

Dye XVI, 1′,3-diethyl-6′-methoxythia-2′-cyanine, λ max = 540 mμ.

Dye I, 1,1′-diethyl-2,2′-cyanine, λ max = 575 mμ.

Dye VIII, 1,1′-diethyl-5,6-benzo-2,2′-cyanine, λ max = 585 mμ.

Dye X, 1,1′-diethyl-5,6,5′,6′-dibenzo-2,2′-cyanine, λ max = 600 mμ.

Dye XX, 3,3′-dimethyl-9-ethylthiacarbocyanine, λ max = 640 mμ.

Lists such as those in Table VI usually contain certain irregularities, such as that shown by the lower efficiency of antisensitization of Dye XIV by the antisensitizing Dye VII, than for Dyes XV and XVI. Irregularities are to be expected, partly because the breadth of the bands does not make $\Delta\lambda$ max a very good measure of the divergence from energetic equivalence between sensitizer and antisensitizer, and also because structural as well as energetic factors must intervene. Numerous examples, however, leave no doubt of the correctness of the energetic relation.

It will be observed that when the absorption maximum of the sensitizer is about 100 mμ longer than that of the nonplanar dye, not only is antisensitization inefficient, but the optical sensitization may actually be increased by the nonplanar dye. A given nonplanar dye may therefore act as an antisensitizer towards one sensitizer and a mild supersensitizer towards another, depending on whether the optically excited sensitizer has sufficient energy to excite the foreign dye or not. The possibility of supersensitization by nonplanar dyes is consistent with the perturbation mechanism of supersensitization already described, the nonplanar molecule representing a singularity in the regular potential field of the sensitizer layer at which the migration of excitation energy is disturbed and slowed up, allowing increased probability of transfer to the silver halide at that point.

Nonplanar cyanine dyes are in themselves practically devoid of sensitizing properties, although sometimes the presence of supersensitizers, of the same type as are effective with planar dyes of the same class, induces appreciable sensitization. It is therefore interesting that when they act as antisensitizers towards sensitizing dyes, a small but definite sensitivity within the absorption band of the antisensitizer is sometimes observed. The antisensitizer, which may have greatly reduced the sensitivity conferred by the sensitizer, is itself supersensitized. The inability of the nonplanar dye to sensitize implies very ready thermal degradation of the energy of excitation. If, however, the nonplanar dye is imbedded in a dye layer in which ready migration of excitation energy occurs, there is a small probability that excitation energy absorbed by the crowded dye will be transferred to the layer and escape thermal degradation. Since the absorption level of the sensitizer is higher than the absorption level of the antisensitizer in the examples in which supersensitization of the antisensitizer has been observed, this explanation requires thermal activation to fulfill energetic requirements.

TABLE VI. Wavelength relations in antisensitization.

Antisensitizer	Sensitizer	$\Delta\lambda$max mμ	Efficiency of antisensitization
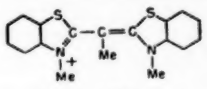 λmax 475 mμ	XIV	25	2.8
	XV	55	1.2
	XVI	65	0.0
	I	100	Trace of supersensitization
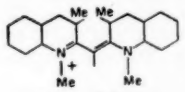 λmax 530 mμ	XIV	−30	2.8
	XV	0	8
	XVI	10	5.5
	I	45	4
	X	70	0 (slight supersensitization)
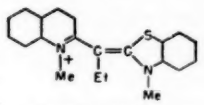 λmax 542 mμ	X	110	0 (supersensitization)
	I	33	13
	VIII	43	4
	X	58	2

ANTISENSITIZATION IN PHOTOCONDUCTIVITY OF DYED SILVER HALIDE

Whatever be the detailed nature of the transfer of excitation energy from an adsorbed dye layer to the silver halide, the final result is the appearance of an electron in the conduction band of the silver halide, which then participates in the formation of the latent image in a manner essentially similar to, if not identical with, that of the photoelectrons produced by direct absorption by the silver salt. Sensitizing dyes therefore sensitize the photoconductivity of silver halide in a

TABLE VII. Antisensitization and supersensitization in photoconductivity.

Dye	Relative photocurrents λ459 mμ	Relative photocurrents λ575 mμ	Photographic sensitivity Blue filter	Photographic sensitivity Green filter
Sensitizer 20 mg/liter	165	30	2000	355
Sensitizer +antisensitizer 5 mg/liter	135	5	2000	60
Sensitizer +supersensitizer 5 mg/liter	157	290	2000	2800
Sensitizer +supersensitizer +antisensitizer	140	210	2000	1700

TABLE VIII. Dye formulas.

For cyanine dyes, only the cations are named and formulated.

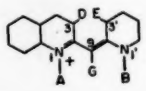

I 1,1′-diethyl-2,2′-cyanine, A=B=Et, G=D=E=H
II 1,1-dimethyl-2,2′-cyanine, A=B=Me, G=D=E=H
III 1,1′-diamyl-2,2′-cyanine, A=B=Am, G=D=E=H
IV 1,1′-diphenyl-2,2′-cyanine, A=B=Ph, G=D=E=H

Nonplanar 2,2′-cyanines

V 1,1′,9-trimethyl-2,2′-cyanine, A=B=G=Me, D=E=H
VI 1-ethyl-1′,3-dimethyl-2,2′-cyanine, A=Et, B=D=Me, G=E=H
VII 1,1′,3,3′-tetramethyl-2,2′-cyanine, A=B=D=E=Me, G=H

VIII 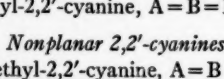

1,1′-diethyl-5,6-benzo-2,2′-cyanine (planar)

IX 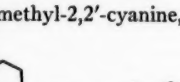

1,1′-diethyl-3,4-benzo-2,2′-cyanine (nonplanar)

X 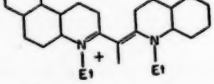

1,1′-diethyl-5,6,5′,6′-dibenzo-2,2′-cyanine (planar)

Nonplanar 2,2′-carbocyanines

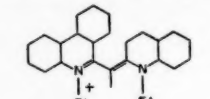

XI 1,1′-diethyl-10-methyl-2,2′-carbocyanine, A=B=Et, G_1=Me
XII 1,1′-dimethyl-10-phenyl-2,2′-carbocyanine, A=B=Me, G_1=Ph

Nonplanar 4,4′-cyanine

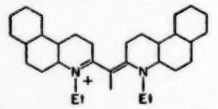

XIII 1,1′,3,3′-tetramethyl-4,4′-cyanine

Thiacyanine

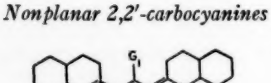

XIV 3,3′-diethyl-4,5,4′,5′-dibenzothiacyanine

Thia-2′-cyanines

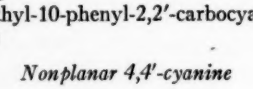

XV 1′-ethyl-3-methylthia-2′-cyanine, A=Me, B=Et, G_1=D=H

TABLE VIII.—*Continued.*

For cyanine dyes, only the cations are named and formulated.

XVI 1′,3-diethyl-6′-methoxythia-2′-cyanine, A=B=Et, D=OMe, G_1=H
XVII 1,3′-diethyl-3-methylthia-2′-cyanine (nonplanar), A=B=Et, G_1=Me

Thia- and Selenacarbocyanines

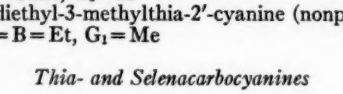

XVIII 3,3′-diethylthiacarbocyanine, Y=S, A=B=Et
XIX 3,3′-diethyl-9-methylthiacarbocyanine, Y=S, A=B=Et, G_1=Me
XX 3,3′-dimethyl-9-ethylthiacarbocyanine, Y=S, A=B=Me, G_1=Et
XXI 3,3′,9-triethyl-5,5′-dichlorothiacarbocyanine, Y=S, A=B=G_1=Et, D=D′=Cl
XXII 3,3′,9-triethylselenacarbocyanine, Y=Se, A=B=Et, G_1=Et

Supersensitizers

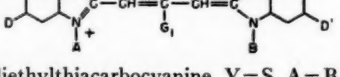

XXIII 2-*p*-diethylaminostyrylbenzothiazole

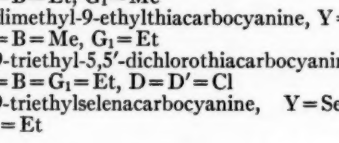

XXIV Merocyanine dye
4-[(3-ethyl-2(3H)-benzothiazolylidene)isopropylidene]-3-methyl-1-(*p*-sulfophenyl)-5-pyrazolone

manner parallel to their action on photographic sensitivity, and the phenomenon of photographic supersensitization has its counterpart in photoconductivity.[22] It is therefore to be expected from the mechanism of antisensitization adduced that the phenomenon should occur in photoconductivity. This is true, as is illustrated in Table VII, containing the relative photocurrents excited in emulsion coatings containing the sensitizing dye (I) with and without a supersensitizer and antisensitizer, excited by blue light and at the absorption maximum of the sensitizer. The corresponding photographic sensitivities are indicated in terms of $10/i$ speed, where i is the inertia of the emulsion.[29] The exciting energy used in the measurements of photoconductivity is comparable to that of the photographic exposures.

There is a fair parallelism between the photoconductive and photographic sensitivities; the antisensitizer reduces the sensitized photoconductivity with only a minor effect on the photoconductivity excited by blue light. The figures also illustrate the general observation that antisensitization of a supersensitized combination is less efficient than that of the sensitizer alone.

[29] C. E. K. Mees, *Theory of the Photographic Process* (Macmillan Company, New York, 1942), p. 204.

QUENCHING OF FLUORESCENCE BY NONPLANAR DYES

The "resonance" fluorescence of 1,1′-diethyl-2,2′-cyanine in the aqueous gel of this dye is vigorously quenched by the nonplanar 1,1′,3,3′-tetramethyl-2,2′-cyanine (VII) (see Table VIII) consistent with capture of the energy of excitation by the crowded dye and its subsequent thermal degradation. As another example, the dye 3,3′-diethyl-4,5,4′,5′-dibenzothiacyanine (XIV) shows strong fluorescence as a polymer in dilute aqueous solution strongly quenched by nonplanar thiacyanines.

One outstanding phenomenon remains little understood, the reason for the lack of sensitization of nonplanar dyes and their powerful antisensitizing properties. As will be discussed in detail in another publication, the lack of sensitization cannot be accounted for either by lack of adsorption to the halide grain or by inadequate absorption of light. A great tendency towards thermal degradation of excitation energy in nonplanar dyes is implied by their photographic behavior, by their quenching of fluorescence, and by the general weakness of fluorescence of nonplanar dyes when corresponding planar dyes are strongly fluorescent. One difference to be expected in the pattern of the normal vibrations of nonplanar and planar dyes is the presence in the former of strong torsional vibrations about the axis of twist, and it is possible that these are concerned in the energy degradation which exhibits photographic sensitization.

The observations described in this paper show how the concept of the migration of excitation energy from molecule to molecule in condensed systems of compounds containing conjugated chains, and the interruption of the migration at singularities, gives a unified picture of diverse phenomena in photographic sensitization by dyes and its enhancement and inhibition, in fluorescence of dyes, and in photoconductivity of dyed silver bromide. Interesting and important as the phenomena are in the theory and practice of optical sensitization of the photographic emulsion, their significance is probably not limited to photographic systems, and analogous phenomena are probably to be found in the general study of the photochemistry of condensed systems.

THE JOURNAL OF CHEMICAL PHYSICS VOLUME 19, NUMBER 4 APRIL, 1951

The Thickness of Shock Fronts in Argon and Nitrogen and Rotational Heat Capacity Lags*

E. F. GREENE, G. R. COWAN,† AND D. F. HORNIG
Metcalf Research Laboratory, Brown University, Providence, Rhode Island

(Received December 12, 1950)

Shock front thicknesses in argon and nitrogen have been measured at Mach numbers of approximately 1.12, 1.28, and 1.40 by the reflectivity method. These thicknesses are significantly greater than predicted by Thomas and demonstrate the need for an improved theory which will cover the whole range of shock strengths. Reflectivity measurements have also been used to detect distortions of shock fronts in nitrogen owing to the lag of the rotational heat capacity. About 20 collisions are required for the rotational relaxation of nitrogen at room temperature.

INTRODUCTION

COWAN and Hornig[1] have recently introduced an experimental method for studying the region of abrupt temperature, pressure, and density rise in the fronts of gaseous shock waves. From many points of view this region is so narrow (*ca* 10^{-5} cm) that the assumption of an abrupt discontinuity is satisfactory. However, the molecular composition of gases makes it clear that shock fronts cannot be vanishingly thin but must extend for a distance of at least a few mean free paths. This new method, which involves the reflectivity of visible light from the shock front, provides a way of studying processes occurring in a very small number of collisions.

Within a limited range of conditions, Cowan and Hornig found that the thickness of shock fronts in nitrogen was significantly greater than predicted theoretically. In the present investigation these studies were extended to argon, a gas to which theories assuming hard sphere molecules should apply; and both argon and nitrogen were studied over a greater pressure range and with somewhat greater precision. It proved possible to detect the delay in equilibration of rotational degrees of freedom, i.e., rotational heat capacity lags, in shock fronts in nitrogen and to ascertain that roughly 20 collisions are required to obtain rotational equilibration.

Lagging vibrational heat capacities have been extensively studied[2–4] by means of the dispersion of velocity and the absorption of high frequency sound

* The work reported here was supported by the ONR under Contract N7 onr-358, Task 3.

† Present address: Department of Physical Chemistry, University of Minnesota, Minneapolis, Minnesota.

[1] G. R. Cowan and D. F. Hornig, J. Chem. Phys. **18**, 1008 (1950).

[2] H. O. Kneser, Ann. Physik **16**, 337 (1933).

[3] van Itterbeek, de Bruyn, and Mariëns, Physica **6**, 511 (1939).

[4] J. L. Stewart, Rev. Sci. Instr. **17**, 59 (1946).

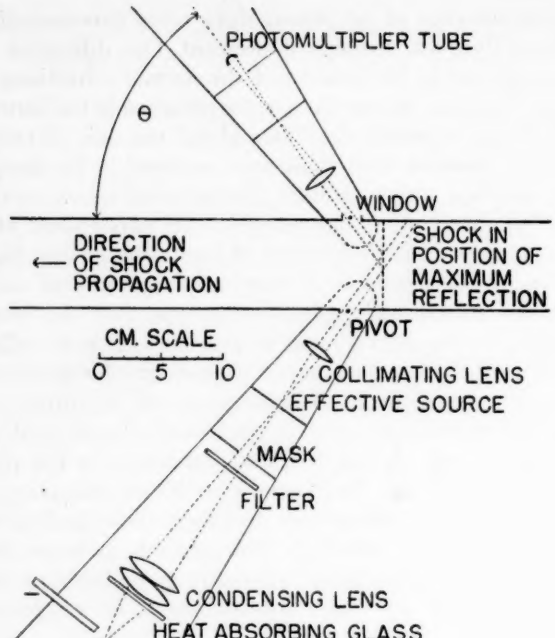

FIG. 1. Schematic drawing of optical system.

waves and also by the rapid compression of gas at an impact tube.[5]

Stewart,[6] Rhodes,[7] and Huber and Kantrowitz[8] have applied these methods to the study of rotational relaxation.

For hydrogen, Stewart found a relaxation time of approximately 1.8×10^{-8} sec (1 atmos and 25°C), which corresponds to 270 collisions, while Huber and Kantrowitz report 1.07×10^{-8} sec (1 atmos and 12°C) or 159 collisions. The latter authors also attempted to measure the rotational heat capacity lag in nitrogen and reported an upper limit of 10^{-9} sec (or 7 collisions) for the relaxation time at room temperature and atmospheric pressure. Recently Braithwaite and Werner[9] have found a region of rotational dispersion in dry air at room temperature which corresponds to a relaxation time of 1.28×10^{-8} sec (about 90 collisions). The results of the present investigation indicate that a value between these extremes is more likely for nitrogen.

APPARATUS

In principle, the apparatus used for this work was the same as that of Cowan and Hornig although most of the details were redesigned. The shock tube was made of stainless steel tubing of 2.75-in. inside diameter and $\frac{1}{8}$-in. wall thickness in four two-foot sections, the ends of which were silver-soldered to steel flanges. The flanges and end plates were machined with tongue and groove joints and bolted together. Lead gaskets provided gas tight seals.

The optical system was carefully designed to give improved reproducibility of settings of the angles of incidence and reflection and also to eliminate all possible stray light. Figure 1 shows the arrangement used. The carbon arc source (8-mm positive carbon) was run just below the hissing stage, at about 15 amp, because this has been recommended as giving the steadiest light.[10] To a first approximation, changes in current through the arc merely change the size of the positive crater, so that by focusing on only the central fraction of the crater, the illumination is less sensitive to current fluctuations. A piece of heat-absorbing glass protected the condensing lens, which focused the positive crater of the arc on the rectangular effective source. The size of this slit (5 mm high by 1.8 mm wide) was determined by the degree of divergence allowable in the beam after collimation by the next lens. This divergence was set at 1° for the horizontal and 3° for the vertical half-angles. This shape of source slit was chosen to provide a compromise between maximal illumination of the shock front and minimal divergence of the beam in the horizontal plane, which was the critical one for the angle measurements.

The approximately collimated beam was reflected in the center of the shock tube and then passed through similar optical components in reversed order until it was finally received by a photo-multiplier tube. The change in length of the optical path when the angle of incidence was varied was not important for the range of angles used. The optical components on both sides of the shock tube were mounted on movable sections pivoted just below the respective windows ($\frac{1}{4}$-in. plate glass) of the tube. This allowed adjustment of angle without the need of changing the position of the windows in the tube. Masks were placed in each beam to reduce stray light. The desired wavelengths were obtained by interference filters.‡ The effective wavelengths for maximum transmission and the band widths were slightly greater than the nominal values, since the filters were used in converging light. A half-angle of 9°, the maximum value, gave a shift in the maximum transmission of approximately 6 mμ for the outer edge of the beam.

With this system the background of scattered light seen by the photo-multiplier tube was well below 10 percent of the signal for the larger signals (nearest to grazing incidence and for strong shocks). Nevertheless, the scattered light and the noise associated with the light of the signal itself rather than the dark current still determined the ultimate noise level. The 1P21 photo-multiplier tube output was developed across a load

[5] A. Kantrowitz, J. Chem. Phys. **14**, 150 (1946).
[6] E. S. Stewart, Phys. Rev. **69**, 632 (1946).
[7] J. E. Rhodes, Jr., Phys. Rev. **70**, 932 (1946).
[8] P. W. Huber and A. Kantrowitz, J. Chem. Phys. **15**, 275 (1947).
[9] J. W. Braithwaite and F. D. Werner, University of Minnesota, Department of Aeronautical Engineering, Research Report 58, "Thermodynamic properties of air (gamma-study)," ONR Contract N6onr-246, Task VII (1950).

[10] C. S. Rupert and J. Strong, J. Opt. Soc. Am. **40**, 455 (1950).
‡ Farrand Optical Company, Inc., New York, New York, and Baird Associates, Inc., Cambridge, Massachusetts.

resistor of 250 k ohms and then fed to a 6J5 cathode follower to reduce the integrating effect of shunt capacitance in the connections and input of the Dumont 304-H oscilloscope. An integrated signal has the advantage of improved signal-to-noise ratio because of the narrower band pass, but has the disadvantage that the magnitude of the signal then depends on the shock velocity as well as the reflectivity.

EXPERIMENTAL

The main drawback of the earlier experiments was the lack of reproducibility of the measured reflectivities; a series of successive experiments at a given angle of incidence had an average deviation from the mean of 10–15 percent. Therefore, it was hoped that the new, more carefully built apparatus would eliminate much of the fluctuation.

Real improvement appeared only in that it was now possible to plot reflectivities as a function of the angle of incidence with about the same consistency as at a constant angle. Reflectivities at any given angle were not noticeably more accurate than previously; and, although considerable effort was concentrated on finding the source of the fluctuations, no single factor appeared responsible.

In order to reduce the effect of variations in the source intensity a sample beam was separated from the main one and passed around the shock tube into the photo-multiplier by a system of mirrors. This signal was chopped 500 times a second and thus provided a calibrating step signal on the photo-multiplier. This system reduced the average deviation slightly—to about 10 percent.

The measuring point in the shock tube was 3.5 ft from the diaphragm; and, although Bleakney *et al.*[11] report this as well beyond the point where the shock is formed, it might have been insufficient for the present measurements. However, placing another two-foot section between the diaphragm and the windows produced no noticeable improvement. In order to speed the release of gas when the diaphragm ruptured, the copper diaphragm used in the earlier work was replaced by a brass one which withstood a greater pressure difference for the same weight and tended to shatter instead of shearing; and 70–30 brass shim stock of 0.002–0.005-in. thickness, half-hard temper, and small grain size was used. Previously, a post had been used to catch the ruptured diaphragm; but for these experiments the post was removed so that the gas might expand more freely. Instead of relying on spontaneous bursting of the diaphragm it was ruptured with a spring-loaded needle to make the bursting pressure more definite. To insure rapid disintegration the diaphragm was thus ruptured at a pressure only 10 percent below the average spontaneous bursting pressure.

[11] Bleakney, Weimer, and Fletcher, Rev. Sci. Instr. **20**, 807 (1949).

Velocity measurements served as a partial check on the strengths of successive shocks, but the observed variations of about 0.2 percent in the shock velocity were insufficient to explain the fluctuations in reflectivity. The net effect of all these changes was to reduce the average deviations in the reflectivity from about 15 to 8 percent.

The experimental procedure was basically the same as that of Cowan and Hornig. It involved receiving the reflected light pulse from the shock wave on a photo-multiplier tube, feeding the signal through a cathode follower to an oscilloscope, and photographing the trace. No preamplifier was necessary and the wide range of gains required was easily obtained by changing the voltage on the dynodes of the photo-multiplier. The sweep of the oscilloscope was triggered by a piezoelectric gauge taped to the outside of the shock tube ahead of the measuring windows. The duration of the signal was approximately 20 microseconds, and the sweep length was maintained at 4 milliseconds to allow the presence of two calibrating steps.

The pressures in the compression and expansion chambers of the shock tube were measured by Bourdon gauges which had been calibrated in the range up to 3 atmos absolute with a mercury manometer and up to 21 atmos with a dead weight tester in which the pressure was measured by weights placed on a vertical piston of known cross-sectional area. The absolute accuracy of readings of the expansion chamber pressure was estimated at ± 100 mm, while relative pressures in successive experiments could be matched to approximately 10 mm.

The temperature was that of the room which varied between 24.5 and 27°C. After the shock tube was filled to the desired pressure, time was always allowed for the temperature of the gas to return to its equilibrium value. One-half minute was usually enough.

The interference filters were calibrated on a Beckmann spectrophotometer (Model DU) and found to coincide with the maker's ratings as to wavelength of maximum transmission and band width (approximately 15 mμ at one-half maximum transmission). The effective wavelength depended on the product of the emission curve of the carbon arc, the filter transmission (corrected for a slightly convergent beam), and the sensitivity curve of the 1P21 photo-multiplier tube. Since all the corrections together produced a negligible effect on the final plots, the wavelength was simply taken as that of the rated maximum transmission for the filter.

The shock strength, as measured by the ratio of pressure or density behind to that before the front, may be calculated from the original pressures on both sides of the diaphragm (e.g., see references 1 and 11). However, an appreciable correction must be allowed for the non-ideal nature of the bursting process. For this reason, measurements of the velocity of the shock wave are important, since they can give the actual shock strength

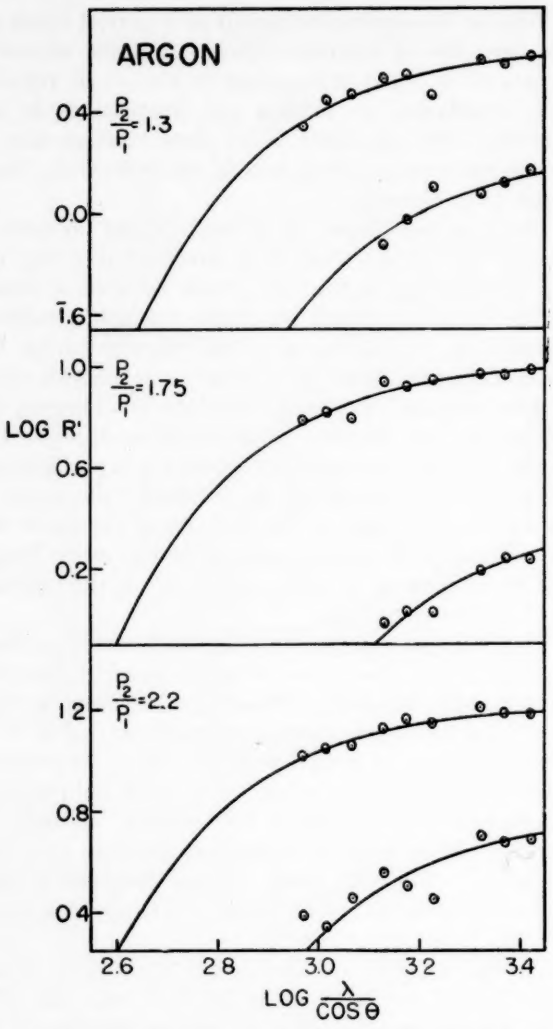

FIG. 2. Measured shock front reflectivities for argon. Solid lines are theoretical curves.

directly from the hydrodynamic relations. Because the present apparatus was not suited for simultaneous velocity and reflection measurements, the velocity data were obtained from separate runs under similar conditions. The following procedure[11,12] was adopted. Two collimated light beams were passed through the shock tube normal to its length, and slits were arranged to block part of the stationary beams from their respective photo-multiplier tubes. As the shock wave passed through a beam, the reflected and refracted beam moved so as to produce a pulse of light on the photo-multiplier tube. These signals were superimposed on a slow (400 cps) sawtooth sweep and fed to the vertical plates of an oscilloscope. The horizontal plates carried a 10-kc/sec sine wave from an oscillator whose frequency was checked with a crystal which had been calibrated against Station WWV of the Bureau of Standards. The two beams were 64.40±0.05 cm apart and included the point in the tube which contained the windows for the reflection measurements. The average deviation of similar runs was approximately 0.2 percent. Four experiments were run for each shock wave, and the average used for computing the shock strength. The average velocities should be accurate within ±0.2 percent.

[12] University of Michigan, Engineering Research Institute Report, 1949. F. W. Geiger and C. W. Mautz, "The shock tube as an instrument for the investigation of transonic and supersonic flow patterns," ONR Contract N6onr-232, Task Order IV.

SHOCK THICKNESS

Shocks of pressure ratios across the front of approximately 1.3, 1.75, and 2.2 (Mach numbers approximately 1.12, 1.28, and 1.40) were investigated in argon and nitrogen, in each case at two different initial pressures. The reason for the choice of these two gases was that they were inert, inexpensive, and available and, above all, could provide a direct comparison of the

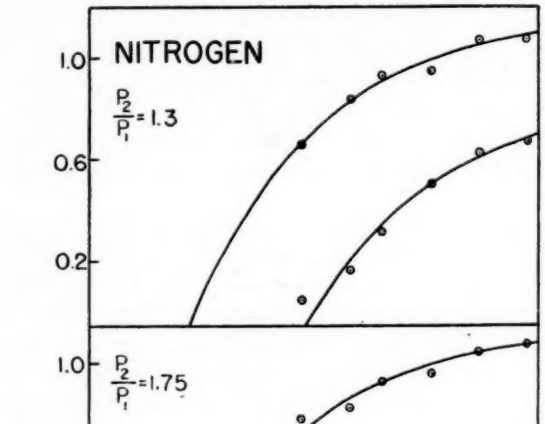

FIG. 3. Measured shock front reflectivities for nitrogen. Solid lines are theoretical curves.

TABLE I. Thickness of shock fronts in argon and nitrogen.

Gas	P_1 (atmos)	P_2 (atmos)	Velocity (km/sec)	Mach No.	P_2/P_1	ρ_2/ρ_1	Thickness (10^{-5} cm)	Thickness scaled to $P_1=1$ atmos (10^{-5} cm)	Thickness (mean free paths ahead of shock)
A	7.27	11.7	0.3574	1.113	1.299	1.169	2.15	15.6	23
	10.73	17.4	0.3582	1.115	1.304	1.172	1.43	15.3	22
	6.66	18.8	0.4046	1.259	1.734	1.384	1.24	8.2	12
	3.20	9.5	0.4104	1.275	1.782	1.405	2.50	8.0	12
	6.11	26.7	0.4424	1.377	2.120	1.548	1.12	6.8	10
	3.48	16.1	0.4476	1.393	2.176	1.570	1.80	6.3	9
N_2	11.00	19.3	0.3971	1.128	1.318	1.217	1.86	20.5	32
	6.73	12.1	0.4011	1.139	1.347	1.235	2.48	16.7	26
	2.62	8.9	0.4523	1.285	1.760	1.488	2.59	6.8	10
	5.19	17.4	0.4530	1.286	1.767	1.491	1.63	8.5	13
	2.62	14.9	0.4978	1.414	2.167	1.712	2.20	5.7	9
	4.63	26.1	0.4993	1.418	2.181	1.720	1.38	6.4	10

behavior of a monatomic and a diatomic gas. Thus, argon is a good approximation to the ideal hard sphere model, while nitrogen includes the additional complication of rotational energy.

The expression for the reflectivity of the front assuming Cowan and Hornig's Model II

$$\rho=\rho_1+(\rho_2-\rho_1)/[1+\exp(-4x/L)] \tag{1}$$

is

$$R=\frac{1+\tan^4\theta}{4}(\Delta n)^2\left[\frac{\pi^2 L\cos\theta/\lambda}{\sinh(\pi^2 L\cos\theta/\lambda)}\right]^2, \tag{2}$$

where L is the shock thickness defined by

$$L=(\rho_2-\rho_1)/(d\rho/dx)_{\max}, \tag{3}$$

ρ is the density (with the subscripts 1, 2 indicating the limiting values ahead of and behind the front), λ the wavelength of the incident light, θ the angle of incidence (measured from the direction of shock propagation), and Δn the change in refractive index across the shock. In determining the thickness it is convenient to take

$$R'=4R/(1+\tan^4\theta)(\Delta n)^2 \tag{4}$$

and plot $\log R'$ *vs* $\log(\lambda/\cos\theta)$. Then L may be estimated by comparing the experimental points with the theoretical curve for $\log R'$ *vs* $\log\lambda/\pi^2 L\cos\theta$. The reference ordinates for each pressure ratio are arbitrary and serve only for internal comparison. Figures 2 and 3 show the results for argon and nitrogen, respectively, at three different pressure ratios. For argon each point is the average of four runs, there being three different wavelengths (439, 490, and 552 mμ) for each pressure, while for nitrogen each point is the average of six runs, only two wavelengths (439 and 552 mμ) being used for each pressure. Reflectivities were measured at angles of incidence, θ, of 62, 71, and 78°. On each plot the theoretical reflectivity curve is drawn in for comparison with the experimental points. For each shock, Table I lists the pertinent data and the thickness, in which the estimated error is ±15 percent. P_1, P_2, and P_3 are, respectively, the pressures ahead of the shock wave, behind the shock but ahead of the rarefaction, and in the compression chamber before the rupture of the diaphragm. ρ_1 and ρ_2 are the densities ahead of and behind the shock.§ The scaling of thicknesses to a desired P_1 is accomplished by using the relation LP_1 = constant for any given P_2/P_1. The Mach number is the ratio of the shock propagation velocity to the velocity of sound ahead of the shock.

In order to compare the results with the various theoretical treatments it is convenient to plot the inverse of the thickness *versus* the Mach number and to measure thickness in terms of the mean free path before the shock. This is done in Figs. 4 and 5 for argon and nitrogen. Figure 6 shows the behavior of the theoretical curves for argon at higher Mach numbers. The mean

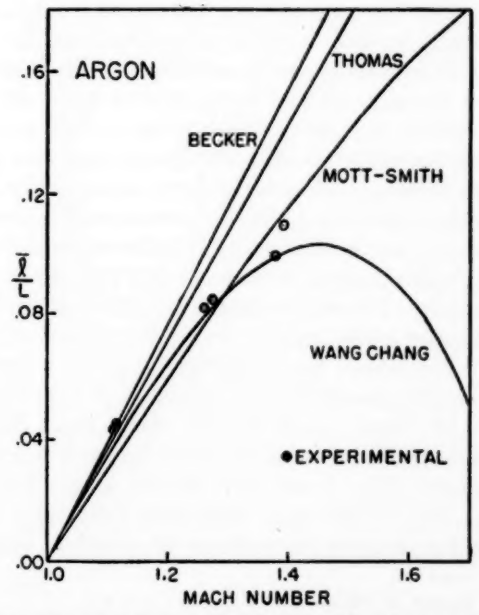

FIG. 4. Experimental shock front thicknesses in argon as a function of Mach number. Solid lines are theoretical curves.

§ In determining ρ_2 from the velocity, $\gamma_{N_2}=1.404$ and $\gamma_A=1.668$.

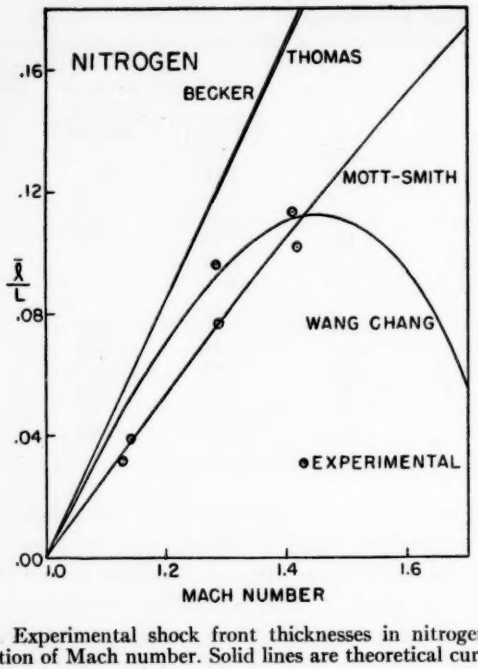

FIG. 5. Experimental shock front thicknesses in nitrogen as a function of Mach number. Solid lines are theoretical curves.

free path before the shock is defined as

$$\bar{l}=(\pi/2)^{\frac{1}{2}}\eta/0.998(P_1\rho_1)^{\frac{1}{2}}, \tag{5}$$

where η is the viscosity.

The basis for all of the theoretical approaches to the solution of the shock front problem has been the Boltzmann equation. Its integration yields a generalized form of the hydrodynamic equations, including the complete stress tensor and heat flux vector; but their solution for this case has not been carried out, and all treatments involve various approximations. In zero order the equations are the hydrodynamic equations without viscosity or heat conductivity, and their solution predicts the shock front to be a discontinuity. Becker[13] investigated the next order by solving the hydrodynamic equations including viscosity and thermal conduction, treating both as constants. His solution applies only to the case $\eta C_p/\lambda'=0.75$, where C_p is the specific heat at constant pressure and λ' is the thermal conductivity. The experimental values of this ratio for nitrogen and argon are 0.77 and 0.66, respectively; but Libby[14] has shown by numerical integration that the solutions are insensitive to variations in this ratio for shocks of Mach numbers less than two. Becker's treatment yielded reasonable results for weak shocks but vanishingly thin fronts for strong ones. Thomas[15] showed that if the same equations were used but a proper temperature dependence of η and λ' were included, the thickness remained finite even for strong shocks. His results, of course, were also obtained for $\eta C_p/\lambda'=0.75$.

Wang Chang[16] has recently treated the case of monatomic gases, using the Enskog-Chapman[17] solution of the Boltzmann equation up to Burnett and third-order terms. Her solution is in the form of a power series in $M-1$, where M is the Mach number. She has shown that through the term in $(M-1)^2$ her solution is identical with that of Thomas. However, this method is nonconvergent even for fairly weak shock waves and, because of the labor involved in the computation of higher order terms, it does not appear capable of extension to stronger shocks. In any case, the Enskog-Chapman expansion seems fundamentally unsound for strong shocks, since it is essentially an expansion in the gradients and they become very large in strong shocks.

Mott-Smith[18] started from the limiting case of a discontinuity rather than a homogeneous gas. In this limit the gas on either side of the front is in equilibrium, and there is a discontinuity in the distribution function at the front. To represent a real case he has chosen a distribution function

$$f=af_1+bf_2, \tag{6}$$

where f_1 is the distribution function describing the gas before the front, f_2 is that describing the gas behind the front, and a and b are parameters which vary from $a=1$, $b=0$ before the front to $a=0$, $b=1$ behind the front. In the front, the description is essentially that of a mixture of two gases having different temperatures and mass

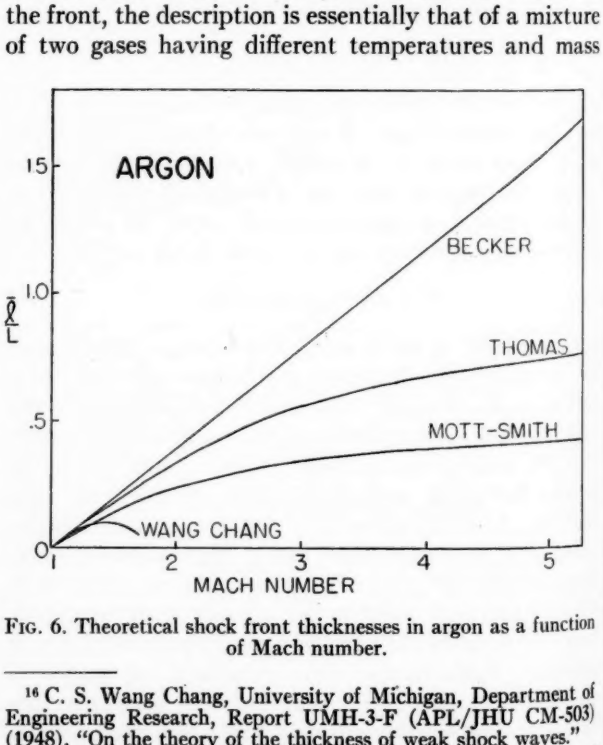

FIG. 6. Theoretical shock front thicknesses in argon as a function of Mach number.

[13] R. Becker, Z. Physik 8, 321 (1922).
[14] P. A. Libby, Polytechnic Institute of Brooklyn, Department of Aeronautical Engineering and Applied Mechanics Report No. 152 (1949), "The structure of a one dimensional shock wave according to the Navier-Stokes equations," Contract No. N6ori-206, Task Order I.
[15] L. H. Thomas, J. Chem. Phys. 12, 449 (1944).
[16] C. S. Wang Chang, University of Michigan, Department of Engineering Research, Report UMH-3-F (APL/JHU CM-503) (1948), "On the theory of the thickness of weak shock waves."
[17] S. Chapman and T. G. Cowling, *The Mathematical Theory of Non-Uniform Gases* (Cambridge University Press, Cambridge, England, 1939).
[18] H. M. Mott-Smith, "Kinetic theory treatment of a shock wave" (unpublished manuscript).

velocities. This treatment should give increasingly good results for very strong shocks, so that his limiting value for the thickness, which is greater than that of Thomas, appears to be more reliable. On the other hand, his solution should fail for weak shocks; and, indeed, his limiting values for vanishingly weak shocks differ from those of Becker, Thomas, and Wang Chang, which must be correct in this limit. Mott-Smith's curve in Figs. 4 through 6 is for the hard sphere case; and the thickness is determined from the consideration of the transport of u^2, where u is the mass velocity.

The inaccuracy of the experimental results precludes a definite statement about the various theories. However, in agreement with Cowan and Hornig, the thickness seems significantly greater than that predicted by Thomas. Within the range of validity of Wang Chang's results, there is agreement with experiment; and, in general, there is good indication that a theory which fits Wang Chang's and Mott-Smith's treatments in the limits of low and high Mach numbers, respectively, will be in reasonable agreement with the experimental points. The necessity for an adequate theoretical approach which will cover the intermediate range of shock strengths is apparent, and it seems likely that it must come from an approach of the general nature of that of Mott-Smith rather than by extension of the usual gas kinetic methods.

EQUILIBRATION OF ROTATIONAL ENERGY

When the molecules of a diatomic gas pass through the shock front, they are compressed and heated. If there is a delay in the transfer of energy to the rotational degrees of freedom, the heat capacity is initially that of a monatomic gas but later rises to the equilibrium value. It may be anticipated that the effect of such a delay is to distort the shock front, in that the temperature increase is greater and the density increase is less than for the same gas in equilibrium. At later times both quantities approach their equilibrium values.

Three possible cases are illustrated in Fig. 7. The top curve (1) is the density profile for a shock in which the rotational temperature of the diatomic gas is equal to the translational temperature at all times (Cowan and Hornig's Model II). The bottom curve (3) shows the case of negligible excitation of rotational energy within the region of the front. It is again of the form of Model II; but the density increase is much less, and the thickness of the front is greater than before. At greater distances from the front the density rises to the same value as in the first case. The density behind the front in this case of no rotational equilibration can be obtained from the following considerations. It was shown by Lord Rayleigh[19] that the velocity at which a plane shock wave is propagated depends only on the initial and final conditions in the gas and on the equation of state (equilibrium conditions), provided that the process is

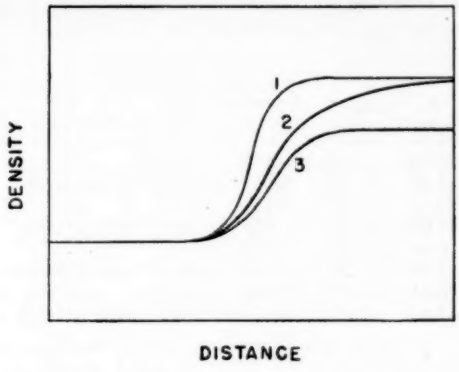

FIG. 7. Shock wave density profiles: 1. Complete rotational heat capacity equilibration. 2. Partial equilibration. 3. No equilibration.

stationary in time. However, if the process is a stationary one, the propagation velocity of the initial front in which γ, the ratio of specific heats, is characteristic of a monatomic gas must be the same as that calculated from the final conditions. In that case, if ρ_2 is used to designate the density behind the front and ρ_F the final density, one obtains

$$\rho_2=\frac{1+\gamma_2}{\gamma_2}\rho_1\Big/\left[\frac{\rho_1}{\rho_F}\left(\frac{1+\gamma_F}{\gamma_F}\right)+\frac{\gamma_2-\gamma_F}{\gamma_2\gamma_F}\right]. \quad (7)$$

This case, of a relaxation region long compared with the front thickness, has been discussed by Stepanov[20] who derived formulas for the density, pressure, and temperature changes across the front.

Both Wang Chang and Thomas find the thickness of a shock front proportional to $\gamma^{\frac{1}{2}}$ for a given Mach number. This means that for negligible excitation of rotational energy the front is thicker than that for the equilibrium case not only by a factor $(1.667/1.4)^{\frac{1}{2}}=1.09$, but also because of the lower effective Mach number for the quasi-monatomic molecules. This Mach number is that given by the ρ_2 of the preceding paragraph.

The middle curve in Fig. 7 shows schematically how the density changes when equilibration occurs in a region comparable to the front itself. There is no theoretical basis for its exact shape at the present time.

There are two ways in which the extreme cases, presence or absence of rotational equilibration in the front, could be distinguished in our experiments: (1) from the difference in thickness of the front, for which the accuracy of the experiments is not adequate, and (2) from the total density change across the front. The latter method was used, since the effect is considerably greater and the measurements can be made with fair precision.

At grazing incidence, or at very long wavelengths, the reflectivity is independent of the profile of the front and

[19] Lord Rayleigh, Proc. Roy. Soc. (London) **84A**, 268 (1910).

[20] P. E. Stepanov, J. Exptl. Theoret. Phys. (U.S.S.R.) **17**, 377 (1947).

TABLE II. Evidence for rotational heat capacity lag in nitrogen.

Gas	P_1 (atmos)	Mach No.	Calculated $\Delta\rho/\rho_1$ $\gamma=1.667$	$\gamma=1.4$	Exptl. $\Delta\rho/\rho_1$	Number of collisions in shock front
A	10.73	1.115	0.172	...	...	...
N_2	11.00	1.128	0.053	0.217	0.225±0.006	48
A	13.31	1.119	0.178	...	...	...
N_2	11.01	1.131	0.057	0.222	0.224±0.004	48
A	6.66	1.259	0.384	...	...	...
N_2	5.19	1.286	0.268	0.491	0.446±0.011	22
A	6.11	1.377	0.548	...	...	...
N_2	4.63	1.418	0.443	0.720	0.675±0.012	19

is given by the expression

$$R=(1+\tan^4\theta)(\Delta n)^2/4. \tag{8}$$

Since for small changes in the density we can also write

$$\Delta n=(n_1-1)\Delta\rho/\rho_1, \tag{9}$$

this limiting reflectivity affords a direct measurement of $\Delta\rho$. The method is probably valid in this simple form whenever the equilibration region is of the order of ten or more times greater than for the shock front transition. If it is not extremely great compared with the shock front, it may be expected that the reflectivity curve will first approach a constant value, characteristic of a monatomic gas, as $\lambda/\cos\theta$ is increased, but that at still greater values of this parameter the reflectivity will again rise to the limit for the diatomic gas. This means that at appropriate intermediate values of $\lambda/\cos\theta$ the density can be measured behind the front but before appreciable relaxation has occurred.

Since the apparatus was not capable of measuring absolute reflectivities, the measurements were made by direct comparison between nitrogen and argon. From Eq. (9) one obtains the expression

$$\left(\frac{\Delta\rho}{\rho_1}\right)_{N_2}=\left(\frac{\Delta\rho}{\rho_1}\right)_A\frac{[(n_D-1)P_1]_A}{[(n_D-1)P_1]_{N_2}}\cdot\frac{R_{N_2}^{\frac{1}{2}}}{R_A^{\frac{1}{2}}}; \tag{10}$$

and since all of the quantities on the right are either known or measured, an experimental value can be obtained for $(\Delta\rho/\rho_1)_{N_2}$. The quantities (n_D-1) for argon and nitrogen were taken as 281×10^{-6} and 297×10^{-6}, respectively. The reflectivities of nitrogen and argon were compared at the same three pressure ratios used in the thickness determination but only at the higher of the two initial pressures. The measurements were made at an angle of incidence of 82° and a wavelength of 593 mμ. Under these conditions the reflectivity is so near to the limiting value that only a slight extrapolation along the theoretical curve obtained from Model II is necessary to find the apparent limit.

The results of four such determinations are tabulated in Table II. Each determination is the mean of ten runs. In the two weaker shocks the final density is in excellent agreement with that calculated for complete rotational equilibration. It may, therefore, be concluded that equilibration is substantially complete after 48 collisions.[‖]

On the other hand, the final densities in the two stronger shocks have values intermediate between the two limiting cases. The difference between the observed values and the equilibrium values are well outside the experimental error and there can be no doubt that equilibrium was not reached in these two cases. The situation must, therefore, resemble the intermediate curve in Fig. 7. In this case it is not legitimate to extrapolate along a Model II reflectivity, curve but the extrapolation has so little effect that the qualitative conclusion stands. Since the fronts were each about 20 collisions thick, it seems very likely that rotational equilibration in nitrogen requires more than seven collisions, the upper limit set by Huber and Kantrowitz, and that it requires about the same number of collisions as the shock front transition in these shocks, approximately 20 collisions.

To establish this quantity more precisely, it will be necessary to obtain accurate reflectivity curves in the region of large $\lambda/\cos\theta$ and to derive the density curves from them, since the simple limiting theory does not apply. However, these experiments do make it certain that the process of rotational equilibration can be studied by this method and the task of obtaining accurate results lies ahead.

ACKNOWLEDGMENT

We wish to thank Dr. H. M. Mott-Smith for his kindness in allowing us to use the results of his work. We also owe much to Mr. T. L. Dawson for his assistance in the design and construction of the apparatus.

‖ The number of collisions a molecule makes in passing through a shock front is greater than the thickness of the front measured in mean-free-paths-before-the-shock both because the density increases in the shock wave and because the molecules do not travel only in the direction of shock propagation. In Table II the number of collisions in the front was calculated as

$$N_L=N_{\rho_1,T}\int(\rho/\rho_1)dt,$$

where the limits of integration are the times when the molecule is at $x=-L/2$ and when the molecule is at $x=L/2$.

$N_{\rho_1,T}$ is the number of collisions one molecule makes per second at a density ρ_1 and temperature T, the mean of the temperatures before and after the shock. For nitrogen, N_1 atmos, 15°C was taken as 7.44×10^9/sec.

Mobile Multilayer Adsorption of a Bose-Einstein Gas: Helium*

WILLIAM BAND
Department of Physics, The State College of Washington, Pullman, Washington
(Received September 22, 1950)

The quantum properties of a Bose-Einstein gas give rise to a critical adsorption into a mobile film. If the energy of adsorption is assumed to decrease with thickness according to a simple power law, the theory gives an isotherm in good agreement with observations on helium adsorption at temperatures above the lambda-temperature of liquid helium, for all gas pressures higher than 10 percent saturation.

With mixtures of He^3 and He^4 isotopes the theory predicts appreciable adsorption of He^3 only in the first or localized monolayer; all mobile monolayers should be practically pure He^4 at all gas pressures. Comparison is suggested with the known isotopic constitution of the Rollin film below the lambda-temperature.

I. INTRODUCTION

IT is well known that the theory of multilayer adsorption due to Brunauer, Emmett, and Teller[1] suffers from several inherent defects.[2] In particular, it is assumed in the BET theory that the energy of adsorption on any atom is independent of the number of atoms already adsorbed on neighboring sites, and is always equal to the latent heat of evaporation from the liquid phase, independent of the thickness of the film except for the first layer to be adsorbed. It is also assumed that every adsorbed atom immediately becomes a site for further adsorption.[3]

If satisfactory corrections for these defects are included in the beginning, the deduction of the adsorption isotherm becomes prohibitively complicated if not actually impossible. A correction for anomalous packing in the first layer can be included, however,[4] and the resulting isotherm can be made to agree fairly well with observed isotherms for helium at low temperatures.[5]

This in itself is most surprising if not fortuitous, because, in fact, the BET adsorption process is one in which the adsorbed atoms are localized on definite sites, the translational energy or mobility of the film being entirely neglected; whereas the adsorbed helium film is presumably mobile, and below T_λ even superfluid.[6]

In view of this highly unsatisfactory situation, it was felt to be of interest to study the adsorption equilibrium between a quantum degenerate Bose-Einstein three-dimensional gas and the corresponding two-dimensional gaseous film. Whereas the BET theory neglects mobility entirely, the suggested theory would exaggerate mobility by treating the liquid film as an ideal gas trapped in a potential well.

It turns out that the adsorption on such a film is small until a critical pressure is reached at which a Bose-Einstein condensation occurs into the adsorbed film. In making this statement it is not implied that the particles that get condensed into the film are at the same time condensed in momentum space in the sense of an ordinary Bose-Einstein condensation. They are simply removed from the momentum space of the three-dimensional gas and so play exactly the same role as do the particles condensed into the zeroth state in an ordinary Bose-Einstein condensation. The quantum properties of the Bose-Einstein gas result in the sudden adsorption into the film at a critical temperature. One calculates this critical temperature in precisely the same way as one calculates the lambda-point temperature for an ordinary Bose-Einstein condensation. The film plays the same role as the zeroth state in this calculation; and, because its energy is lower than the lowest energy in the three-dimensional gas, the transition temperature is higher than the lambda-temperature of the gas.

The critical nature of this adsorption process allows us to outline a satisfactory picture of multilayer adsorption of helium at less than saturated vapor pressures. The first layer to be adsorbed definitely goes on to the adsorbate as an immobilized two-dimensional solid phase, even below T_λ, having an anomalously high surface density;[4] but already in the second layer at least part of the adsorbed atoms are mobile.[6] For the first one or two layers we may therefore use the BET theory of adsorption. We assume that the energy of adsorption falls off with some power law, presumably the third power[7] from the maximum energy of adsorption into the first layer down to the latent heat of evaporation at sufficiently thick films. Because of this decrease of energy of adsorption, the critical pressure at which condensation into the uppermost mobile monolayer takes place steadily increases as the number of layers increases. Suppose the pressure in the gas is set at the critical pressure for adsorption into the nth layer; this pressure is less than the critical pressure for the $(n+1)$st layer, so there will be negligible adsorption in the $(n+1)$st layer. The adsorption into the nth layer continues until it is full in the sense that the energy of further adsorption into the nth layer drops

* This work was supported by the ONR.
[1] Brunauer, Emmett, and Teller, J. Am. Chem. Soc. **60**, 309 (1938).
[2] T. L. Hill, J. Chem. Phys. **15**, 767 (1947). A. B. D. Cassie, Trans. Faraday Soc. **44**, 575 (1947). S. J. Gregg and J. Jacobs, Trans. Faraday Soc. **45**, 615 (1948).
[3] J. R. Arnold, J. Am. Chem. Soc. **71**, 104 (1949).
[4] W. Band, Phys. Rev. **76**, 441 (1949).
[5] E. A. Long and L. Meyer, Phys. Rev. **76**, 440 (1949).
[6] E. A. Long and L. Meyer, Phys. Rev. **79**, 1031 (1950).
[7] E. Huckel, *Adsorption und Kapillarkondensation* (Akademische Verlag., Leipzig, 1928), Chapter III.

below the energy of adsorption into the next layer. During this process the gas pressure must increase to take care of the decreasing energy of adsorption and critical condensation begins in the $(n+1)$st layer on top of the full nth layer. This condensation proceeds until the $(n+1)$st layer is in turn full in the same sense, and critical condensation then begins in the $(n+2)$nd layer, and so on. If the energy of adsorption in any layer were independent of the population in that layer until full, adsorption would occur in sudden steps. It will rather be assumed that the energy of adsorption in any layer is a function of the population in that layer, of such a form as to ensure a smooth isotherm; the precise form of this function will not be considered. Since the film is mobile, a smoothed-out treatment of the effect of neighbor interaction is permissible.

The process of adsorption with increasing gas pressure continues until there is no further decrease of adsorption energy with increasing thickness, and by then the process has become that of condensation into the liquid phase with the latent heat of evaporation at the saturated vapor pressure. This identification of a Bose-Einstein condensation with the condensation into a liquid phase has already been made on the basis of the clustering theory of phase condensation,[8] and may be taken as a point in favor of the present picture of adsorption.

II. MOBILE MONOLAYER ADSORPTION OF A BOSE-EINSTEIN GAS

Let W be the energy of adsorption in the monolayer, N_g be the number of atoms in the gas, N_f in the film. Then[9]

$$N_g = V(2\pi mkT/h^2)^{\frac{3}{2}}\sum_{j=1}(1/j)^{\frac{3}{2}}e^{j\mu/kT}, \quad (1)$$

$$N_f = A(2\pi mkT/h^2)\sum_{j=1}(1/j)e^{j(\mu+W)/kT}, \quad (2)$$

where V is the volume of the gas, A the area of the film, and where μ is determined by

$$N_g = N_f = N = \text{constant}. \quad (3)$$

First we note that for helium atoms at temperatures near 4°K, N_f is negligible in Eq. (3). We may then determine μ as a function of V simply by equating N to N_g given by Eq. (1). This demands a negative value for μ that increases towards zero as V decreases. However, inspection of Eq. (2) shows that if μ increases too far, becoming equal to $-W$ then the series in Eq. (2) approaches $\sum_{j=1}(1/j)$, which actually diverges to infinity, so that we should no longer be justified in neglecting N_f.

This situation is exactly similar with that appearing in the Bose-Einstein lambda-transition in an ideal gas, with the film monolayer playing the same role as the zero state in the gas. We define a volume V_1 by the equation

$$N = V_1(2\pi mkT/h^2)^{\frac{3}{2}}\sum_{j=1}(1/j)^{\frac{3}{2}}e^{-jW/kT}. \quad (4)$$

Above this volume μ is determined accurately by

$$V > V_1: \quad N = V(2\pi mkT/h^2)^{\frac{3}{2}}\sum_{j=1}(1/j)^{\frac{3}{2}}e^{j\mu/kT}, \quad (5)$$

and the number in the film can be neglected. At the volume V_1 Eq. (4) coincides with Eq. (5), while as soon as $V \leqslant V_1$, the number in the film becomes significant. Equation (10) prevents μ from going any higher than $-W$. Instead, μ approaches $-W$ more and more closely as V goes down below V_1 in order to satisfy Eq. (2), while Eq. (1) may still be used with μ equal just to $-W$ to fix the number in the gas:

$$V \leqslant V_1: \quad N_g = V(2\pi mkT/h^2)^{\frac{3}{2}}\sum_{j=1}(1/j)^{\frac{3}{2}}e^{-jW/kT}. \quad (6)$$

The number in the film is then determined simply by Eqs. (6) and (3). After this we could evaluate the small difference $\mu+W$ from the value of N_f and Eq. (2), although for our present purpose this is of no interest. Combining Eqs. (6) and (4), we may write

$$N_f/N = 1 - V/V_1, \quad (7)$$

so the density of the gas remains constant if V_1 does, while condensation proceeds.

The pressure exerted by the gas is obtained by using the general theorem[11] that $PV = 2E/3$. The result is

$$V \geqslant V_1: \quad P = kT(2\pi mkT/h^2)^{\frac{3}{2}}\sum_{j=1}(1/j)^{5/2}e^{j\mu/kT}. \quad (8)$$

The pressure required to give critical adsorption at any prescribed temperature is therefore

$$P_c = kT(2\pi mkT/h^2)^{\frac{3}{2}}\sum_{j=1}(1/j)^{5/2}e^{-jW/kT}. \quad (9)$$

III. MOBILE MULTILAYER ADSORPTION ISOTHERM

Let the energy of adsorption in the nth layer be W_n, a function of the number of particles in the layer such that it decreases rather quickly when the layer fills to the normal superficial density in the liquid phase. Let the initial energy of adsorption for any layer depend on the numerical depth of the layer above the adsorbate:

$$W_n - W_\infty = (W_1 - W_\infty)/n^q, \quad (10)$$

where q is a constant presumably about equal to 3. The nth layer will be counted as full when the energy of further adsorption in the nth layer has decreased to the energy of initial adsorption in the $(n+1)$st layer.

The pressure for critical adsorption into the nth layer is given by Eq. (9):

$$P_n = kT(2\pi mkT/h^2)^{\frac{3}{2}}\sum_{j=1}(1/j)^{5/2}\exp(-jW_n/kT), \quad (11)$$

where W_n is given by Eq. (10) and represents the energy of adsorption when the nth layer first starts to form. As the population of the nth layer increases, the energy of adsorption decreases and increased pressure will be needed; and when the nth layer is full, the pressure has reached that needed for critical adsorption in the $(n+1)$st layer. This step-by-step process continues until

[8] W. Band, Phys. Rev. **79**, 871 (1950).
[9] J. E. Mayer and M. G. Mayer, *Statistical Mechanics* (John Wiley and Sons, Inc., New York, 1940), p. 416.

no further decrease of adsorption energy is possible, when we shall have arrived at the saturated vapor pressure:

$$P_\infty = kT(2\pi mkT/h^2)^{\frac{3}{2}} \sum_{j=1}(1/j)^{5/2} \exp(-jW_\infty/kT). \quad (12)$$

Taking the ratio between Eqs. (11) and (12) yields

$$P_n/P_\infty = X_n(5/2;T) : X_\infty(5/2;T), \quad (13)$$

where

$$X_n(5/2;T) = \sum_{j=1}(1/j)^{5/2} \exp(-jW_n/kT). \quad (14)$$

Calculation of the value of this series as a function of n through Eq. (10) leads easily to a graphical representation of n as a function of the pressure ratio P_n/P_∞, and this is the adsorption isotherm desired.

In applying this theory to helium we may accept the observational data given by Keesom[10] on W_1 and W_∞ and calculate the isotherm for some assumed value of q. In making these calculations it is assumed that the first layer is present before mobile adsorption begins, and that this first layer contains four times as many atoms as are needed to fill any subsequent layer:[5] the mobile isotherm is simply shifted to take care of this.

Figure 1 shows the curves for a temperature about 2.4°K, and for comparison the modified BET theory[4] curve is also drawn for the same energy values and the same compression in the first layer. The dotted curve shows the experimental data[5] at temperatures just above the lambda-point.

Evidently, according to the present picture, the observed isotherm ought to follow the BET curve only for the first adsorbed layer, $0<A/B<1$, and to cross over from the BET curve to the mobile curve between the first and second layer, $1<A/B<1.25$. The mobile curve for $q=2$ gives a decidedly better agreement than that with $q=3$, and is quite convincingly better than the BET curve beyond the first layer; but if we restrict ourselves to the theoretically more justifiable value $q=3$, the mobile isotherm is not really superior to the BET curve, and this leaves the question somewhat open.

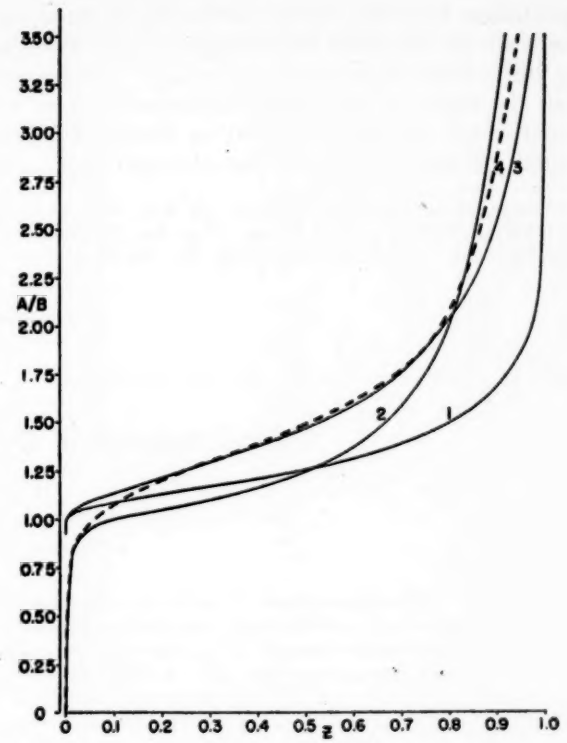

FIG. 1. A/B = total number of atoms adsorbed/number of sites in first layer. $Z=P/P_{sat}$ = pressure of gas in equilibrium with film/saturated vapor pressure. Curves 1 and 3 calculated from Bose-Einstein condensation adsorption theory for inverse cube and inverse square law on energy of adsorption, respectively. Curve 2 calculated from modified BET theory. Curve 4: experimental curve, reference 5. All curves are drawn on the assumption that the number of sites is four times the number of atoms filling the second or any higher layer. Note: $A/B=1$ corresponds to the first layer filled; $A/B=1.25$ to the second layer filled; $A/B=3.5$ to the eleventh layer filled.

IV. DISCUSSION

If the present theory is substantially correct, some interesting selective adsorption phenomena should be observed in mixtures of He^4 and He^3 isotopes: the critical adsorption in the higher (mobile) layers should favor He^4 over He^3. No critical adsorption can occur with He^3. No selective adsorption should occur in the first immobilized layer except in so far as the energies of adsorption of the isotopes differ. The selective adsorption of He^4 in the mobile film occurs even with no difference in the energies of adsorption. The theory predicts the relative concentration of He^3 isotope in the mobile film, *even above the lambda-temperature of liquid helium*, to be much less than the concentration in the gas or vapor with which the film is in equilibrium. According to the BET theory, on the other hand, any selective adsorption in the film could be due only to differences in adsorption energies and should persist throughout the film: there should be no marked difference between concentrations in the first localized layer and the upper mobile ones. This difference between the two theories is probably more decisive than the shapes of the isotherms.

The phenomena observed below the lambda-temperature of liquid helium[5] demand further consideration, for it is now known that the lambda-transition occurs even in the unsaturated film as well as in the liquid phase.[6] A mobile monolayer, as treated in the above theory, cannot undergo a lambda-transition itself; and mobility must be included across the layers of the film.[11] Equilibrium between such a quasi-liquid film and the parent gas will have to be studied, and this work is reserved for a later paper.

One remark may be permitted at the present time. Since the mobile multilayer adsorbed film above the lambda-temperature of liquid helium is due to critical condensation of the Bose-Einstein gas, it appears reasonable to regard the superfluid Rollin film, below the lambda-temperature of liquid helium as not only in

[10] W. H. Keesom, *Helium* (Elsevier, New York, 1942), pp. 127, 231.

[11] M. F. M. Osborne, Phys. Rev. **76**, 396 (1949).

equilibrium with the "z-fluid" of the liquid phase, but also with the saturated Bose-Einstein vapor. Whether the film is actually produced by "leakage" of the z-fluid from the liquid or by critical condensation from the Bose-Einstein gas would depend on fortuitous experimental circumstances. Also, the observed fact[12] that He^3 is not present in the Rollin film may be regarded as the result of the selective adsorption process described above just as reasonably as the result of a "filtering" effect of the film-liquid junction.

The writer wishes to thank Mr. E. B. Emery for making the computations needed for Fig. 1. He is very grateful to Dr. E. A. Long and Dr. L. Meyer for communicating the manuscript of their letter, quoted above[6] in advance of publication.

[12] Daunt, Probst, Johnston, Aldrich, and Nier, Phys. Rev. **72**, 502 (1947). P. V. Rollin and J. Hatton, Phys. Rev. **74**, 508 (1948). Lane, Fairbank, Aldrich, and Nier, Phys. Rev. **75**, 46 (1949).

THE JOURNAL OF CHEMICAL PHYSICS VOLUME 19, NUMBER 4 APRIL, 1951

Optical Rotation of Quartz in the Infrared to 9.7μ

H. S. GUTOWSKY
The Noyes Chemical Laboratory, University of Illinois, Urbana, Illinois
(Received December 12, 1950)

The optical rotation of quartz has been observed in the infrared from 2.2 to 9.7μ. The measurements were made with a selenium film transmission polarizer and a similar analyzer; a Perkin-Elmer Model 12B infrared spectrometer was used as the monochromator and detector. Anomalous rotatory dispersion was found at wavelengths longer than 3.7μ. A tentative qualitative interpretation of the anomaly is suggested.

INTRODUCTION

THE value of rotatory dispersion data in the infrared lies mainly in connection with the nature of optical activity, which contemporary theory[1] associates almost exclusively with electronic absorption bands in the ultraviolet and visible regions of the spectrum. This theoretical view reflects the fact that in those few instances where rotation data have been obtained in the infrared, the optical rotation decreases steadily with increasing wavelength, showing no anomalies even in the vicinity of infrared absorption bands.[2] Furthermore, the technical difficulties of measuring accurately the small optical rotations in the infrared have limited such observations and most observation extend only to the near infrared.

The development in recent years of very sensitive efficient infrared monochromators, as well as the rapidly expanding use of polarized infrared in the investigation of molecular orientation, suggested that some reconsideration might be given to optical rotation in the infrared. α-quartz, the low temperature form, was chosen for initial study, as it has an unusually large specific rotation,[3–5] previously known to be large enough for observation in the near infrared.[6]

The most extensive and also most recent observations on quartz in the infrared are those of Lowry and Snow,[6] who found no anomalies in measurements extending to 3.21μ, excluding the region from 2.79 to 3.18μ where measurements were prevented by an absorption band. Herein are presented data extending from 2.2 to 9.7μ. Quartz was found to exhibit anomalous rotatory dispersion at wavelengths longer than 3.7μ, where absorption becomes appreciable.

EXPERIMENTAL PROCEDURE AND RESULTS

The optical rotations were measured with a Perkin-Elmer Model 12B infrared automatic recording spectrometer, used as a monochromator and detector, in conjunction with two selenium film infrared polarizers. In this "infrared polarimeter," the conventional functions of polarizer and analyzer were reversed. The polarizer was rotatable, and the analyzer was fixed. They were constructed by essentially the method of Elliott, Ambrose, and Temple[7] and each contained six selenium films. The analyzer was composed of rectangular films[7] in a fixed mount. It was placed in the monochromator between the exit slit and the thermocouple. The polarizer was made by mounting the selenium films on elliptical sections $\frac{1}{32}$ in. thick, cut at an angle of 65° from $1\frac{1}{4}$-in. brass tubing. These were then inserted in a larger tube, a graduated dial attached to one end, and the assembly mounted so it could be rotated. The polarizer was placed before the entrance slit of the monochromator, with the sample between the polarizer and the slit.

[1] Kauzmann, Walter, and Eyring, Chem. Revs. **26**, 339 (1940).
[2] T. M. Lowry, *Optical Rotatory Power* (Longmans, Green and Company, London, 1935).
[3] R. B. Sosman, *The Properties of Silica* (The Chemical Catalog Company, Inc., 1927).
[4] R. Servant, J. phys. radium [8], **3**, 90 (1942).
[5] T. Radhakrishnan, Proc. Indian Acad. Sci. **25A**, 260 (1947).
[6] T. M. Lowry and C. P. Snow, Proc. Roy. Soc. (London) **127A**, 271 (1930).
[7] Elliott, Ambrose, and Temple, J. Opt. Soc. Am. **38**, 212 (1948).

The transmission of the system, at a given wavelength, was obtained at 10° intervals in the angular position of the polarizer, with the spectrometer shutter closed to give a zero between settings. The recorded transmission values over a 180° range about a transmission maximum were plotted *vs* polarizer angles and a smooth curve drawn. Figure 1 gives a typical plot made at 2.7μ, with no sample, used to determine the zero of the polarimeter. The crosses are the experimental values and the circles are the function $(I_{max}-I_{min})\cos^2\theta+I_{min}$. This function is the theoretical relation between transmission and orientation of the polarizer; it is the law of Malus.[8] The excellent agreement indicates the satisfactory operation of the polarimeter. In this instance, the polarization is 98.5 percent complete; similar performance was observed throughout the investigated range from 1 to 25μ.

The bisected horizontal chords in Fig. 1 indicate the method used to locate the angular position of a maximum. The change in transmission with the angular position of the polarizer is greatest at 45° from the maximum. By bisecting several chords about this angle, values differing by no more than 1° were obtained. The average of these values was rounded off to the nearest half-degree, which represents the accuracy of the set-up as used.

The specific rotations in degrees rotation per mm of quartz, listed in Table I, were obtained from room temperature observations on a pair of single crystals, set 2, of the highest available purity, kindly supplied by Francis P. Phelps and L. T. Sogn of the Quartz Research Laboratory at the National Bureau of Standards. The right-handed crystal is 25.73 mm long and the left-handed is 24.99 mm long. Both crystals are approximately 1.5 cm square in cross section, and the polished faces are off from perpendicular to the optic axis by no more than 6′. The rotations observed for the left-handed crystal were consistently about 5 to 8 percent larger than for the right-handed crystal. The values in Table I are averages of the values for the two crystals.

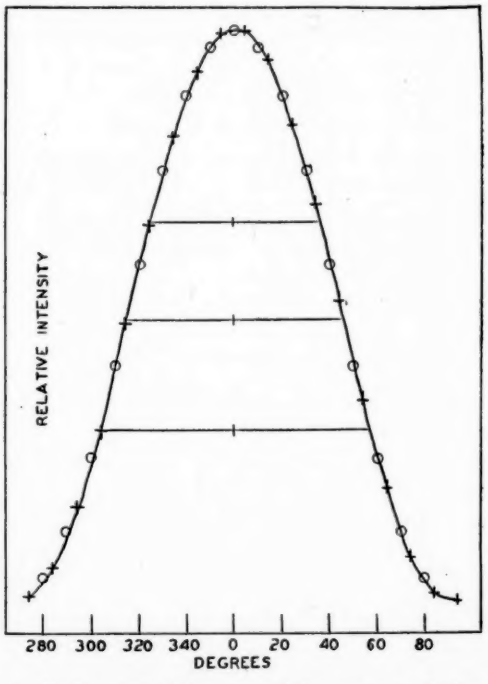

FIG. 1. Light transmission of polarimeter *vs* polarizer angle, without sample, at a wavelength of 2.7μ. The crosses are experimental points, and the circles are the theoretical function $(I_{max}-I_{min})\cos^2\theta+I_{min}$. The bisected horizontal lines indicate the method of locating the angle corresponding to maximum transmission.

TABLE I. Specific rotation of quartz from 2.2 to 9.7μ.

cm^{-1}	μ	α (deg./mm)
4525	2.210	1.29
4260	2.347	1.14
4035	2.478	1.03
3850	2.597	0.92
3680	2.717	0.82
3535	2.829	0.74
3410	2.933	0.66
3290	3.040	0.59
3170	3.155	0.54
3065	3.263	0.49
2965	3.373	0.44
2870	3.484	0.40
2795	3.578	0.37
2720	3.676	0.34
2650	3.774	0.39
2590	3.861	0.38
2525	3.960	0.39
2470	4.049	0.43
2420	4.132	0.57
2325	4.301	0.88
2150	4.651	1.08
2005	4.988	1.13
1893	5.283	1.19
1798	5.562	1.23
1462	6.840	1.28
1264	7.911	1.30
1129	8.857	1.31
1030	9.709	1.31

In measurements made on a similar pair of crystals, set 1, also from the National Bureau of Standards, the specific rotations from 2.2 to 5μ agree within experimental error for the two crystals. They agree also with the values in Table I from set 2. At wavelengths longer than 5μ, the left-handed crystal in set 1 gave increasingly larger specific rotations than did the right-handed; at 9.7μ the two crystals differed by about 25 percent. These differences probably are due to lack of purity, inasmuch as the absorption spectra of the crystals in set 1 were markedly different. However, in each of the crystals in both sets and in several other crystals examined in preliminary experiments, the rotatory dispersion exhibits the same trends as the data in Table I.

The data in Table I are shown graphically in Fig. 2, which includes observations of Lowry and Snow,[6] at wavelengths from 2.2 to 3.21μ. The slit widths we used are indicated by the pairs of horizontal lines in Fig. 2.

[8] F. A. Jenkins and H. E. White, *Fundamentals of Optics* (McGraw-Hill Book Company, Inc., New York 1950), p. 492.

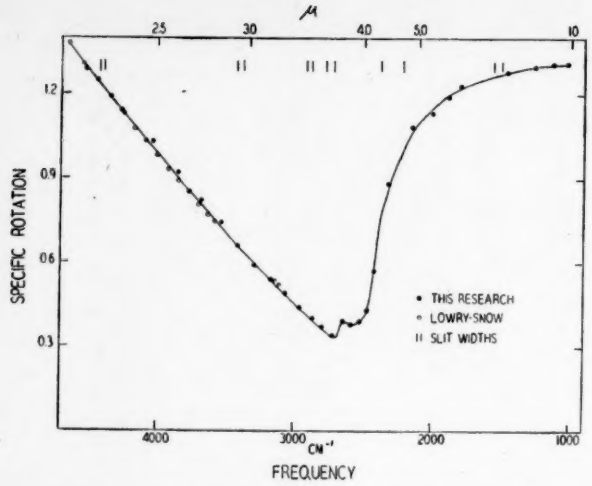

FIG. 2. The rotatory dispersion of quartz from 2.21 to 9.71μ. The plotted values are optical rotation in degrees/mm quartz.

At 2.2 and 3.2μ, there is excellent agreement between our results and the previous ones. The systematic differences in the vicinity of 2.7μ are slightly in excess of the stated errors in the polarization angle measures. The calibration of our spectrometer is accurate to ± 20 cm^{-1} in this region, and part of the discrepancy could be from systematic errors in the calibration. A more likely interpretation is that differences in the quartz samples themselves are responsible; the variability we observed among the samples was greater than the differences between our data and that of Lowry and Snow. The optical system of the spectrometer itself introduces an appreciable amount of polarization, varying from about 10 percent at 2.5μ to about 20 percent at 10μ. However, this effect should introduce no error, since the zero of the polarimeter is independent of frequency.

DISCUSSION

The apparent anomalous rotatory dispersion of quartz at wavelengths longer than 3.7μ seems to be a real effect. Not only the general features of the optical activity, but even the small hump in specific rotation at 3.79μ appeared in all single crystals examined, although in some an inflection point was found at 3.79μ rather than a true maximum. It is difficult to visualize any manner in which the optical system itself might be responsible, although the polarizing effects of the optics undoubtedly complicate the transmission characteristics of the polarimeter. The magnitude of the apparent anomaly is about fifty time larger than the experimental error, as indicated by the small spread of the plotted points from the smooth curve drawn in Fig. 2. Furthermore, there is the correlation among samples of observed differences in absorption and in specific rotation. This then appears to be the first reported instance of appreciable anomalous rotatory dispersion in the vicinity of absorption bands corresponding to vibrational transitions.

If the anomalous optical rotation by quartz is of the usual variety, there should be a reversal in the sign of rotation in the vicinity of the active absorption band. The strong absorption by quartz at long wavelengths prevented the extension of our observations past 10μ; however, a consideration of the dichroism of quartz[9] suggests that such a reversal may occur. Quartz shows appreciable dichroism at wavelengths of about 10μ, and it extends throughout the long wavelength region. For example, observed absorption maxima for the ordinary and extraordinary rays occur at 12.52 and 12.87μ, and for a band at long wavelengths at 21.0 and 19.7μ. The dichroism should be related to the optical rotation, and since the dichroism reverses direction between 10 and 20μ, the optical rotation may also reverse.

It is beyond the scope of this report to attempt a complete theoretical interpretation of the anomaly. However, a few general observations are relevant. Quartz owes its optical activity ultimately to the arrangement of the silica tetrahedra in a left- or right-handed spiral about the optical axis of the crystal. Each oxygen atom is shared by two tetrahedra, thereby providing strong coupling between the vibrations of atoms in adjacent tetrahedra.[9] The Kuhn and Born theories of optical activity[2] are based on the existence of such coupled oscillators, and the strong coupling of vibrational modes in quartz suggests this may be the mechanism responsible for the optical activity in the infrared. Hylleraas[10] has made calculations for β-quartz based on this point of view. The treatment considers optical rotation in the visible region, and the results are at least in general agreement with observation. Similar calculations for α-quartz in the infrared would be of interest.

ACKNOWLEDGMENT

I wish to express my indebtedness to Dr. Charles J. Hoffman and Miss Elizabeth M. Petersen for their able and generous assistance in this research. Dr. Hoffman constructed the polarizers; Miss Petersen made a number of the observations and also measured the recordings and plotted the transmission curves.

[9] B. D. Saksena, Proc. Indian Acad. Sci. **12A**, 93 (1940), gives a very complete bibliography and discussion of the infrared and Raman spectra.

[10] E. A. Hylleraas, Z. Physik 44, 871 (1927).

The Reactions of Radicals Produced by the Action of Sodium on Alkyl Iodides

A. A. COMSTOCK AND G. K. ROLLEFSON
Department of Chemistry, University of California, Berkley, California
(Received December 21, 1950)

The products of the reactions of sodium vapor with methyl and ethyl iodide vapors have been analyzed. It has been found that in the reaction with methyl iodide the principal product is ethane, but considerable amounts of methane, ethylene, and hydrogen are also formed. With ethyl iodide the principal product was butane, with lesser amounts of ethane, ethylene, methane, and hydrogen. It was also noted that in the latter system considerable amounts of propane appeared which could be accounted for as a pyrolysis product of the butane formed. The results have been compared with those obtained by others with similar systems and with the results obtained in the photolyses of mercury dimethyl and mercury diethyl. It is concluded that at low temperatures the dominant reaction for both ethyl and methyl radicals is for two to combine to form a saturated hydrocarbon. At higher temperatures, disproportionation reactions and reactions of the radicals with other molecules must be taken into account and eventually become the dominant reactions.

FOR many years it has been a common practice to assume the existence of various free radicals as intermediates in the thermal or photochemical reactions involving organic molecules. In setting up mechanisms for these reactions, various possibilities have been suggested for the formation of the products from these radicals, but, as a rule, it has not been possible to make a unique decision between two or more methods of achieving the ultimate result. Furthermore, we find such anomalies as the assumption by one author that methyl radicals react to form ethane, whereas another assumes that they form methane and a methylene radical. In this paper we wish to report the results on the reactions of methyl and ethyl radicals prepared under conditions such that the possibility of complicating side reactions has been reduced to a minimum.

The radicals were prepared by the action of sodium vapor on the vapor of the appropriate alkyl iodide. Polanyi[1] has studied these reactions extensively in the presence of a carrier gas and has concluded that reaction occurs at about every collision between a sodium atom and an alkyl iodide molecule. He has not investigated the subsequent reactions of the radicals. Saffer and Davis[2] studied the products produced by heating liquid sodium in the presence of about 200-mm pressure of various alkyl iodides. They believed that the reaction occurred in the gas phase but did not vary the experimental conditions or in any way exclude the possibility that reactions could occur at the surface of the sodium. Bawn and Tipper[3] have studied the products produced when sodium vapor reacts with ethyl or methyl iodide in a stream of hydrogen or nitrogen gas at temperatures of 300 to 363°C. Their results are related to ours and will be discussed in detail later.

Most thermal and photochemical reactions in which methyl or ethyl radicals have been assumed as intermediates offer too many possibilities for these radicals to react with other molecules for the results to be comparable with those to be presented in this paper. However, there are some simple systems which are comparable. The photolysis of methyl iodide has been studied by Schultz and Taylor[4] and also by West and Schlessinger.[5] The latter authors have also studied the photolysis of ethyl iodide. The photolysis of dimethyl mercury has been studied by Gomer and Noyes,[6] Phibbs and Darwent,[7] and Cunningham and Taylor.[8] The photolysis of diethyl mercury has been studied by Moore and Taylor.[9] In all of these cases, the results can be related to those presented in this paper; therefore, they will be discussed in detail later. In these photochemical studies the number of radicals formed has been quite small compared to the total number of molecules present. The experiments which we are about to describe were designed to make the number of radicals present large compared to the number of other molecules and thus greatly increase the probability of radicals reacting with each other rather than with some other molecule.

APPARATUS

Since radicals probably react at a glass surface, a five liter flask was used to enclose our reaction system and thus favor, as much as possible, the occurrence of homogeneous reactions. Figure 1 illustrates the experimental arrangement. *D* is the flask with the tube *G* extending from the ground glass joint *H*, through the neck, to the center of the flask. *G* is about 4.5 cm in diameter and is connected at the top by a Dewar seal to the tube *S*, which is concentric to it. *G* and *S* differ sufficiently in diameter to permit the insertion of the single chromel heater winding, *I*, covered with baked

[1] For example, see H. von Hartel and M. Polanyi, Z. physik. Chem. **B11**, 97 (1930).
[2] A. Saffer and T. W. Davis, J. Am. Chem. Soc. **64**, 2039 (1942).
[3] C. E. H. Bawn and C. F. H. Tipper, Faraday Soc. Discussions **2**, 104 (1947).
[4] R. D. Schultz and H. A. Taylor, J. Chem. Phys. **18**, 194 (1950).
[5] W. West and L. Schlessinger, J. Am. Chem. Soc. **60**, 961 (1938).
[6] R. Gomer and W. A. Noyes, Jr., J. Am. Chem. Soc. **71**, 3390 (1949).
[7] M. K. Phibbs and B. deB. Darwent, Trans. Faraday Soc. **45**, 541 (1949).
[8] J. P. Cunningham and H. S. Taylor, J. Chem. Phys. **6**, 359 (1938).
[9] W. J. Moore and H. A. Taylor, J. Chem. Phys. **8**, 396 (1940).

out wet asbestos paper. The current through the heater is controlled by a variac. At the bottom of *S* is a small thermocouple well. *J* is a cylindrical bulb containing the sodium; it is concentric to *G* and *S* but not attached to either. The bottom of *J* is shaped to fit over the thermocouple well in *S*, and the top is drawn down to form a jet of about 5 mm internal diameter.

At the top of the bulb *D* is the tube *C* in which the rod *B* can be slid up and down by means of a magnet operating on the piece of soft iron *A*. At the lower end of *B* is a cover which fits over the opening in the sodium tube *J*. *F* is a thermocouple well which was placed in the exit tube *T* in order to measure the temperature at the surface of the flask.

It was desired to calculate a material balance for the reactions; hence, it was necessary to know the amount of iodide introduced in each experiment. The iodide was degassed by successive freezing and thawing and pumping off the liberated gas while the iodide was frozen. When a sample was not being taken, the reserve of the iodide was kept frozen. To introduce a sample into the reaction vessel, the reservoir was brought to 0°C by surrounding it with ice and water. The iodide was allowed to vaporize into a doser bulb, volume not greater than 100 ml, until the equilibrium vapor pressure at 0° was attained. Then the doser bulb was shut off from the reservoir, and the vapor expanded into the reaction vessel *D*. With ethyl iodide, the vapor pressure was so low at 0° that, in order to obtain enough vapor for the higher pressure runs, it was necessary to collect two or more doses by freezing them out in a side tube and then, finally, vaporizing the entire amount into the reaction vessel.

The apparatus used for handling the reaction products differed slightly for methyl and ethyl iodides. It was not necessary to fractionate the products of the methyl

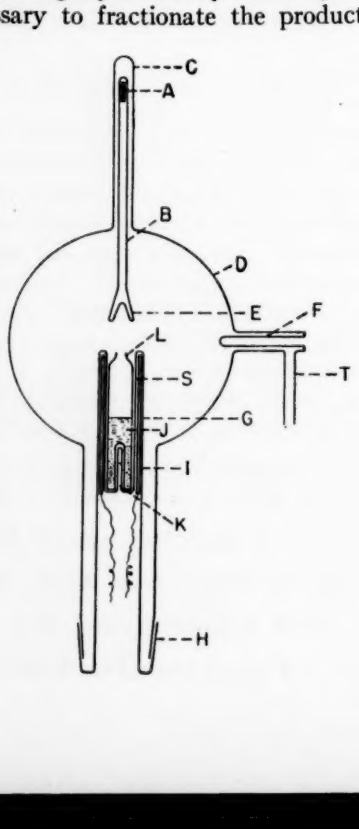

FIG. 1.

iodide reaction (excess sodium was always used so there was no residual methyl iodide); hence, after the reaction was completed, the products were pumped from the reaction bulb into a storage bulb by means of a mercury vapor pump. This process was facilitated by cooling a side tube on the storage bulb during the pumping, thus condensing some of the products. After the transfer was complete, the condensable products were vaporized and mixed with the others before they were transferred to the analytical apparatus.

The arrangement used to fractionate the products from the ethyl iodide reaction is shown in Fig. 2. The products first passed through the trap *I*, which was cooled with liquid nitrogen. The noncondensable portion was collected and analyzed on the assumption that it contained only hydrogen and methane. The method used for the separation of the condensable products was essentially the same as that used by Saffer and Davis, except that instead of using freezing mixtures we used the arrangement shown. The trap *O* is surrounded by a chromel heating element the leads for which pass through the seal *M* in the tube *J*. *J* is concentric with *O*. The air pressure between *O* and *J* can be varied by opening the stopcock *K* to the atmosphere or by connecting it to a mechanical vacuum pump. *L* is a thermocouple well so that the temperature of the inner trap *O* can be measured. The condensable products were transferred from *I* to *O* by surrounding *J* with liquid nitrogen and opening *K* to the atmosphere. When the thermocouple indicated that *O* was approximately at liquid nitrogen temperature, *I* was warmed until the products had passed over to *O*. The temperature of *O* was then varied by reducing the pressure in *J* and sending a small current through the chromel wire heater. The products which vaporized with *O* held at 135°K were analyzed on the assumption that they were only methane, ethane, and ethylene. The next fraction was taken off at 195°K and analyzed as a mixture of ethane, ethylene, propane, and propylene. The remainder was treated as a mixture of propane, propylene, butane, and butylene.

GAS ANALYSIS

The gas mixtures were analyzed by means of an apparatus in which the essential features of the low pressure arrangement designed by C. H. Prescott[10] were utilized. Certain additional units were added to make the equipment suitable for the analysis of the gases obtained in our experiments. With this arrangement, a sample of the gases to be analyzed was measured in a gas burette and mixed with oxygen or whatever other gas was needed as a reagent in the analytical procedure. The usual practice was to run a combustion and determinations of hydrogen and olefins.

For combustion, the sample was mixed with excess oxygen and compressed into a small tube fitted with a

[10] C. H. Prescott, Jr., J. Am. Chem. Soc. **50**, 3237 (1928).

platinum filament. This filament was welded to the ends of some heavy platinum leads which in turn were silver soldered to the tungsten leads which were sealed through the glass. The filament was sufficiently far removed from the silver solder and tungsten that neither of them would be heated enough to cause any oxidation during the course of a combustion. In order to insure complete combustion, the filament was heated for ten minutes, then the gas was returned to the gas burette and the volume redetermined. Next, this gas was passed through a coil immersed in a dry ice-acetone bath to remove water vapor, and the volume was measured again. Finally, the gas was passed through a coil immersed in liquid nitrogen to freeze out carbon dioxide and the volume remeasured. In this manner the number of moles of carbon dioxide formed per mole of sample and the number of moles of oxygen required per mole of sample were determined.

Hydrogen and the olefins could be determined by catalytic hydrogenation. The catalyst was prepared by saturating shredded asbestos with molten nickel nitrate hexahydrate. Heating with either a Bunsen burner or a gas-oxygen hand torch dehydrated and decomposed the nitrate, leaving nickel oxide on the asbestos. The oxide coated asbestos was placed in a Pyrex tube in an electric heater, and hydrogen passed through it overnight. The asbestos was then transferred to a small tube on the gas analysis apparatus. Since, in this last step the catalyst was exposed to air, a final reduction and activation was carried out after it was installed in the apparatus. For this purpose, a small heater was placed around the tube and a considerable amount of hydrogen admitted. After fifteen or twenty minutes of heating, the catalyst was allowed to cool, and the hydrogen was pumped off. Activation was always necessary after any exposure of the catalyst to air or oxygen. It was also found that mercury poisoned the catalyst permanently. Frequent tests of the activity of the catalyst were made by running blank hydrogenations of ethylene by hydrogen.

The olefinic content of a sample was determined by mixing it with a known excess volume of hydrogen and exposing the mixture to the action of the catalyst for ten minutes. The decrease in volume measured the number of moles of olefin present. Correspondingly, if an excess of ethylene was added to a different sample and exposed to the catalyst, the decrease in volume measured the amount of hydrogen present.

MATERIALS

The methyl and ethyl iodides were washed to remove iodine and other impurities and dried with phosphorus pentoxide. Then they were fractionated in a Vigreux column and the middle fraction, which boiled within ±0.5° of the accepted boiling point, was kept for use. After distillation the iodides were stored in the dark over a few drops of mercury.

The sodium was cut from large pieces of the laboratory supply and melted under a vacuum. While in the molten state, it was allowed to flow through a constriction into a tube of the form shown at *J* in Fig. 1. It was heated until the evolution of gas appeared to be complete, then the tube was sealed off at the constriction. Later, this tube was cut off in the constricted part so as to leave it in the condition described in connection with Fig. 1. Air entered at this stage but only for a brief interval, since the tube was immediately placed in the indicated position in the reaction assembly and the system evacuated. The sodium was degassed further by heating it in place in the reaction system. Even with these precautions, it was found impossible to completely eliminate the evolution of gas from the molten metal, and this fact prevented us from making runs at very low pressures.

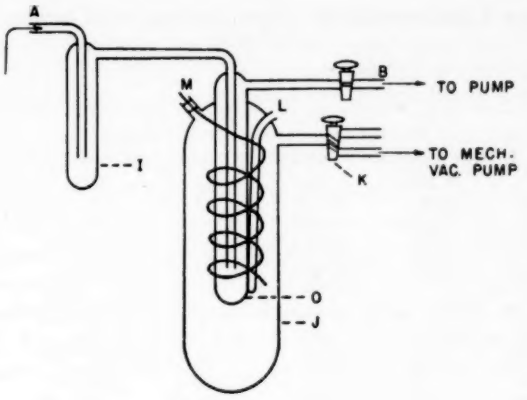

FIG. 2.

EXPERIMENTAL PROCEDURE AND RESULTS

The general procedure was to heat the sodium until it reached a certain desired temperature, which was always at least 400°C. Then the dose of iodide needed to give the desired pressure was introduced. Next, the cover *E* was lifted; the sodium vapor came out as a small sphere, which expanded rapidly to fill the flask. The course of the sodium vapor was followed by observing the fluorescence which was excited by illuminating the reaction vessel with the light of a sodium vapor lamp. The reaction was complete in ten to fifteen seconds or less. When excess sodium was present, the cover was replaced on *L* and the products pumped out as rapidly and completely as possible. It was found necessary to flame the reaction bulb after the reaction in order to obtain all of the gaseous products.

Some sodium leaked out from under the cover, *E*, and condensed on the walls of the large bulb during the preliminary heating. This fact did not lead to any complication, since the temperature of the wall never exceeded 150°C. At this temperature no appreciable reaction occurs between the methyl iodide and the sodium on the wall in the time required for an experiment.

The experiments with methyl iodide were carried out under three sets of conditions, as indicated in Table I.

TABLE I. Products obtained from the reaction of sodium with methyl iodide.

Moles of product/moles of methyl iodide used				Percent yield	
H_2	CH_4	C_2H_4	C_2H_6	H[a]	C[a]
I. Methyl iodide pressure=0.47 mm; sodium at 420°C.					
0.025	0.187	0.094	0.312	101	100
0.070	0.185	0.070	0.312	101	95
0.040	0.247	0.040	0.297	100	91.5
0.070	0.191	0.077	0.300	100	94.5
0.055	0.286	0.048	0.293	104	96.5
II. Methyl iodide pressure=2.35 mm; sodium at 485°C.					
0.036	0.271	0.079	0.217	92	86
0.020	0.354	0.049	0.228	101	91
0.007	0.541	0.015	0.180	104	93
0.000	0.450	0.028	0.188	101	88
III. Methyl iodide pressure=2.35 mm; sodium at 450–460°C.					
0.000	0.250	0.033	0.332	96.5	91
0.012	0.292	0.021	0.284	99.5	90
0.012	0.340	0.030	0.234	97	87
0.006	0.218	0.028	0.322	98	92

[a] Percent yield of hydrogen is the number of gram atoms of hydrogen contained in the gaseous products, divided by the number of gram atoms of hydrogen in the methyl iodide used, and multiplied by 100. Percent yield of carbon is calculated in a similar manner.

Under the sets of conditions designated as I and III, the course of the reaction, as manifested by the sodium fluorescence, was essentially the same. Under these conditions, when the cover *E* was lifted, a sphere of sodium vapor formed, remained at constant diameter for a brief interval, and then expanded to fill the entire vessel. The reaction was complete in from ten to fifteen seconds. In the set of runs designated as II, the reaction was complete in about one second. As soon as the reaction was complete the products were pumped out of the reaction vessel and the total volume of the gases measured in a gas buret. Combustions and hydrogenations were carried out as previously described, and the composition of the gas was calculated from the data thus obtained.

TABLE II. Products obtained from the reaction of sodium with ethyl iodide.

Moles of product/moles of ethyl iodide used							Percent yield	
H_2	CH_4	C_2H_6	C_2H_4	C_3H_8	C_4H_{10}	C_3H_8 +C_4H_{10}	H	C
I. Pressure of ethyl iodide=0.69 mm; sodium at 380°C.								
0.049	0.013	0.137	0.069	0.232	0.117	0.349	85.5	79.5
0.072	0.013	0.168	0.095	0.000	0.352	0.352	102	97
0.058	0.016	0.123	0.143	0.000	0.350	0.350	99.5	97
not det.		0.166	0.040	0.034	0.301	0.335	not det.	
II. Pressure of ethyl iodide=2.78 mm; sodium at 445°C.								
0.066	0.024	0.13	0.07	0.075	0.247	0.322	87.5	82
0.049	0.005	0.157	0.016	0.12	0.199	0.319	81.4	75.4
0.080	0.007	0.155	0.021	0.00	0.313	0.313	86.9	80.8
0.056	0.019	0.142	0.022	0.124	0.230	0.354	88.5	82
0.043	0.007	0.158	0.049	0.000	0.318	0.318	90.6	85
III. Pressure of ethyl iodide=2.78 mm; sodium at 460–470°C.								
0.07	0.008	0.217	0.029	0.046	0.184	0.230	76	69
0.055	0.004	0.151	0.085	0.000	0.250	0.250	77.5	73.8
0.097	0.003	0.108	0.108	0.111	0.181	0.292	80	75
IV. Pressure of ethyl iodide=2.78 mm; sodium at about 490°C.								
0.086	0.032	0.095	0.185	0.263	0.077	0.340	91	85

The general procedure was the same in the experiments with ethyl iodide. The specific differences in experimental conditions are indicated, along with the results, in Table II. The products were fractionated and analyzed as already described. One noticeable difference from the methyl iodide experiments was that, in this case, chemiluminescence accompanied the reaction. In the fastest reactions, a white luminescence appeared as a long ellipsoidal flame above the jet for a brief interval after the cover was lifted. Otherwise, the color was the characteristic sodium yellow of lower intensity, decreasing in intensity as the reaction proceeded. The products were fractionated, as previously described, and the compositions of the various fractions were determined by measuring the total volume, the numbers of moles of carbon dioxide formed, and the numbers of moles of oxygen used in combustion.

DISCUSSION OF RESULTS

It is apparent from a survey of the results listed in Table I that the principal products obtained in the experiments with methyl iodide are methane and ethane. Furthermore, the material balance shows that no major product has been missed. These results are in qualitative agreement with the results of Saffer and Davis[2] and those of Bawn and Tipper,[3] although both of them reported relatively larger percentages of methane. The temperatures in our experiments were not as well defined as those in the experiments of Bawn and Tipper, since we did not use a carrier gas. However, even in their experiments there is some question as to the actual temperature in the reaction zone. The reactions of alkyl iodides with sodium vapor are exothermic by a considerable number of kilocalories, and this energy must be distributed between the alkyl radical and sodium iodide molecule which are produced. An appreciable amount of time is required to reduce the energies of these "hot" molecules to a normal thermal distribution. It was shown by Berry and Rollefson[11] that fast moving sodium atoms require many collisions to reduce their speeds to values characteristic of the temperature of the gas in which they are moving. The effective temperature in the reaction zone in our experiments was probably somewhat above the value registered by the thermocouple at *F* (Fig. 1). Actually, the results fall within the range defined by Gomer and Noyes[6] at low temperatures and those of Bawn and Tipper at higher temperatures.* Furthermore, in the series II experiments in which the rate was so much faster than in I or III, the methane/ethane ratio was distinctly higher, as might be expected if, due to lack of temperature equilibrium, the effective average temperature was higher than in the slower

[11] N. E. Berry and G. K. Rollefson, Phys. Rev. **38**, 1599 (1931).

* In the case of the latter authors, the pressures of carrier gas were so low that the recorded temperatures probably should be considered as minimum values.

experiments. Considering all of these experiments, it seems justifiable to conclude that at low temperatures and over a wide range of pressures the dominant reaction for methyl radicals under these varied conditions is the formation of ethane. As the temperature is raised, the possibility of the methyl radical capturing a hydrogen atom from another radical, or some hydrogen containing molecule, increases corresponding to an activation energy for this reaction, which is about nine[3, 6] kilocalories greater than that for the formation of ethane. The latter activation energy is usually assumed to be zero, but no conclusions concerning its value can be drawn from these experiments.

The variations in the yields of the substances found in smaller amounts in these experiments may be due, in part, to errors in analysis but may also be caused by slight variations in conditions which alter the relative importance of the various possible secondary reactions, although not affecting the principal association reaction of the radicals.

The results tabulated in Table II show that the products obtained as a result of the reaction of ethyl iodide with sodium in the vapor state consist of principally ethane, propane, and butane, with smaller amounts of ethylene, methane, and hydrogen. This is a greater variety than reported by Bawn and Tipper, who list only ethane, ethylene, and butane. There is no apparent reason for their failure to find the other products listed by us since, in this case, they give a material balance which is about the same as we have been able to get. It is noticeable in our results that although the absolute amounts of propane and butane show considerable variation, the sum of the two is reasonably constant. This fact suggests that the propane may not be a primary product but may result from the pyrolysis of butane. In order to check this idea, one of our fourth fractions, which analyzed as pure butane, was returned to the reaction vessel with the temperatures of the various parts set the same as for a regular run. After a short time the gas was pumped out, fractionated, and analyzed. It was found to contain about twenty-five percent propane. In view of this result, we believe that we are justified in considering the sum of the propane and butane as a measure of the amount of butane produced in the primary processes. On this basis it appears, from the results listed in Table II, that about twice as many moles of butane are produced as there are of ethane. Bawn and Tipper report that with ethyl iodide they obtained about two moles of ethane for each mole of butane over a range of temperature from 300 to 370°C with no apparent variation with temperature. This difference could still be explained as a temperature effect, as was done for the methyl iodide results above, if we consider that the trend is so much smaller in this case that it would be masked by experimental errors in the short range of temperatures covered by Bawn and Tipper. Saffer and Davis reported considerable quantities of ethane and propane with much smaller quantities of butane, butene, and propylene in their experiments with ethyl iodide. In view of our experience with the pyrolysis of butane, we are inclined to think that their reported values for three and four carbon hydrocarbons should be lumped together as a measure of the amount of butane formed originally. If this is done, their result agrees quite well with those of Bawn and Tipper for the same temperature. Our fastest runs (series VI), which presumably occurred at higher temperatures than the slower ones, seem to show some trend in the direction of higher ethane/butane ratios which would be in accord with the idea that the difference is due to difference in temperature in the reaction zone. However, the effect is too small to be considered certain.

Another point of difference between our results and those published previously is that we find considerably less ethylene. This fact can also be explained on a temperature dependence basis if we assume that the normal reaction of the ethyl radicals at low temperatures is to form butane, but at higher temperatures the disproportionation reaction and reaction with some other molecule to form ethane become important. For this explanation to hold it is necessary that the latter two possibilities require slightly higher activation energies than the formation of butane, which may not require any. This seems like a reasonable assumption.

At this point it seems desirable to review the work on the photolyses of mercury dimethyl and mercury diethyl. With regard to the former, both Cunningham and Taylor[8] and Gomer and Noyes[6] find that, at low temperatures, the dominant product is ethane with relatively little methane. As the temperature is increased, the methane/ethane ratio increases. The data of the latter authors may be plotted as log(methane/ethane) *vs* $1/T$ to give a reasonably good straight line. In this manner their data may be extrapolated to the temperatures used by Bawn and Tipper, and it is found that they correspond to lower ratios than the latter give by about a factor of three. On the other hand, the extrapolated values are a little closer to the values obtained by Cunningham and Taylor in the thermal decomposition of mercury dimethyl at 348°C. They are also more in accord with our results. Although it has been postulated in this earlier work that the radicals might enter into reactions with the excess mercury dimethyl or a $HgCH_3$ radical, the results, when compared to those obtained from the reaction of sodium with methyl halides, seem to indicate that there is little, if any, specific effect of this nature.

A similar comparison can be made between the results obtained by Moore and Taylor[9] for the photolysis of mercury diethyl and our results. Their butane/ethane ratio is a little lower than that found by us and decreases as the temperature is raised. The highest temperature they used was 250°C, at which their values were definitely below those obtained by Bawn and Tipper at 300° and higher. However, the discrepancy is not great, and it seems justifiable to conclude that the

action of the radicals in this type of system is essentially the same as in the reactions of sodium with the ethyl iodide, whether the experiments are carried out at high or low pressures or in the presence of an inert carrier gas.

The variety of products reported in other systems in which methyl or ethyl radicals have been assumed as intermediates is probably due, to some extent at least, to specific interactions with the other molecules present, such as aldehydes or ketones. The system which does not seem capable of a simple explanation in terms of the results discussed in this paper is the photolysis of ethyl iodide in the presence of silver. West and Schlessinger reported finding only ethane and ethylene, although we would have expected a mixture of these substances with a considerable amount of butane. Since this is the only case in which butane is not reported, it must be considered an exception, possibly due to the reaction occurring at the surface of the silver. In this connection, it may be mentioned that Bawn and Whitby[12] reported that the decomposition of silver ethyl in alcohol solution at −40°C yielded ethane and ethylene as well as some butane. If we were to extrapolate the other results discussed in this paper to such a temperature, we would not expect any appreciable amount of ethane and ethylene.

[12] C. E. H. Bawn and F. J. Whitby, Faraday Society Discussions 2, 228 (1947).

THE JOURNAL OF CHEMICAL PHYSICS VOLUME 19, NUMBER 4 APRIL, 1951

The Bonding of Trihalide and Bifluoride Ions by the Molecular Orbital Method

GEORGE C. PIMENTEL
Department of Chemistry and Chemical Engineering, University of California, Berkeley, California
(Received November 13, 1950)

A simple molecular orbital treatment is presented to explain the bonding in trihalide ions, X_3^-, XY_2^-, and XYZ^-, and bifluoride ion, HF_2^-. The M.O.'s are formed from linear combinations of $np\sigma$ halogen orbitals, and the $1s$ hydrogen orbital and stable bonding M.O.'s are obtained without the introduction of higher atomic orbitals. Applications are suggested in prediction of other stable species and low energy reaction intermediates.

THE trihalide ions, X_3^-, XY_2^-, and XYZ^-, and bifluoride ion, HF_2^-, offer an interesting opportunity to test theories of molecular bonding. Both molecular halogen, X_2, and the halide ion, X^-, have the appropriate number of electrons to provide completed octets. Hence, the formation of an additional covalent bond in X_3^- provides an excess of electrons over the number required to fill the outermost occupied p orbitals. Consequently, a description of the electronic arrangement using only hydrogen atom orbitals must introduce at least one orbital of higher energy. Similarly, hydrofluoric acid, HF, and fluoride ion, F^-, have electronic arrangements predicted to be particularly stable by the widely applicable Lewis covalent bond description. Bifluoride ion, with an additional bond, may be described in the conventional bonding scheme only if covalent bonds are abandoned (i.e., "ionic" bonding is assumed) or if an additional orbital contributes to the bonding. In HF_2^- the only available atomic orbitals are of higher principle quantum number and are presumably of much higher energy.

The electronic arrangements of I_3^-, ICl_2^-, IBr_2^-, and $ClIBr^-$ have been discussed by Pauling,[1] and Kimball[2] has considered I_3^-. Both authors utilize bond hybridization arguments to rationalize the use of a higher energy $5d$ or $6s$ orbital. Pauling[1] discusses the HF_2^- ion with an ionic bond description, averting the problems introduced by a covalent bond model.

X-ray studies of trihalide salts have been made for $CsICl_2$,[3] and for $N(CH_3)_4ICl_2$, NH_4I_3, and NH_4ClIBr.[4] Except for NH_4I_3, the trihalide group is found to be linear. The I_3^- group may deviate from linearity by a few degrees, and the central iodine atom seems to be nonequidistant from the end iodine atoms. The experimental halogen-halogen bond lengths, d, are slightly longer than predicted from the sums of the covalent radii, Σr, as given by Pauling.[1] The lowest ratio of $d/\Sigma r$ is found for $N(CH_3)_4ICl_2$ to be 1.01; and the largest ratio for the larger I−I distance in NH_4I_3, is 1.16. The latter is much larger than the average ratio, 1.06. The trihalide bonds are apparently slightly longer and presumably slightly weaker than the corresponding halogen bonds.

Four bifluoride salts have been studied by x-ray analysis, KHF_2,[5] $NaHF_2$,[6] $TlHF_2$,[7] and NH_4HF_2.[8] The

[1] L. Pauling, *The Nature of the Chemical Bond* (Cornell University Press, Ithaca, New York, 1940).
[2] G. E. Kimball, J. Chem. Phys. 8, 188 (1940).
[3] R. W. G. Wyckoff, J. Am. Chem. Soc. 42, 1100 (1920).
[4] R. C. L. Mooney, Z. Krist. (A) 100, 519 (1939); 90, 143 (1935); Phys. Rev. 47, 807 (1935).
[5] R. M. Bozorth, J. Am. Chem. Soc. 45, 2128 (1923); L. Helmholz, and M. T. Rogers, J. Am. Chem. Soc. 61, 2590 (1939).
[6] Rinne, Hentzchel, and Leonhardt, Z. Krist. 58, 629 (1923); C. Anderson and O. Hassel, Z. physik Chem. 123, 151 (1926).
[7] L. Pauling, Z. Krist. 85, 380 (1933).
[8] O. Hassel and H. Kringstad, Z. anorg. u. allgem. Chem. 191, 36 (1930).

hydrogen atoms have not been located by x-ray methods, and the early workers assumed a central location. Recently, Westrum and Pitzer[9] have presented convincing evidence that the proton in HF_2^- is centrally located, i.e., the potential along the fluorine-fluorine axis has but a single minimum. The bond lengths in these compounds are considerably longer than predicted from covalent radii; the average value of $d/\Sigma r$ is 1.27. The extreme values of this ratio are found for KHF_2 to be 1.20, and for $NaHF_2$, 1.36.

The feasibility of the bond hybridization argument may be indicated to some extent by the spacing of the spectral energy levels of monatomic halogens. For each halogen, the energy levels involving the orbital $(n+1)s$ are lower in energy than those involving the orbital nd. For example, the spectrum of $Br(g)$[10] indicates the energies:

$$\cdots 4s^2 4p^5\ {}^2P \rightarrow \cdots 4s^2 4p^4 5s \quad {}^4P_3 \Delta E = 181.2 \text{ kcal/mole}$$
$$\cdots 4s^2 4p^5\ {}^2P \rightarrow \cdots 4s^2 4p^4 4d \quad {}^4D_4 \Delta E = 256.7$$
$$Br_2(g) \rightarrow 2Br(g) \qquad \Delta H = 45.24.$$

Comparing the energy of dissociation of gaseous bromine,[11] it is readily seen that the gain in bonding energy to be expected is very small relative to the level spacing in the atoms, a condition which is common to all the halogens.

The molecular orbital method may be applied to trihalide ions, and even though the complexity of the problem and the numerous approximations may render quantitative calculations almost meaningless, certain qualitative conclusions may be drawn. In particular, it is of interest to consider the qualitative features of the molecular orbitals formed from a set of p orbitals, without contribution from additional higher orbitals. In the simplest approximation, four of the electrons may be considered to be taking part in the bonding and occupying molecular orbitals formed from linear combinations of three $np\sigma$ orbitals, one associated with each atom. The atomic orbitals may be, but do not have to be, taken as hydrogen atom orbitals. Slater functions are used to provide estimates of overlap magnitudes, merely because the integrals are conveniently available. For the qualitative conclusions drawn, the only specific characteristics assumed for the orbitals will be the symmetry properties of $p\sigma$ orbitals, shown in Fig. 1A. All of the remaining electrons are considered to occupy nonbonding $np\pi$ orbitals, ns orbitals, or orbitals of lower principle quantum number. A justification for neglecting the $np\pi$ orbitals may be based upon the smaller overlap between $5p\pi$ orbitals, 0.063, relative to that between $5p\sigma$ orbitals, 0.234, at the average I—I distance in I_3^-, 1.96A, using Slater type functions and published tables of overlap integrals.[12]

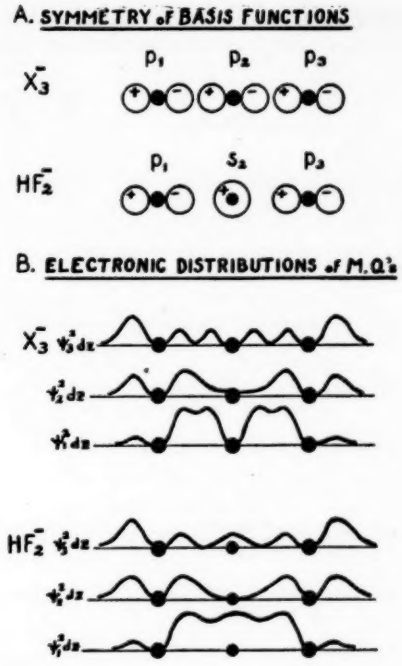

FIG. 1. (A). Symmetry of basis functions. (B). Electronic distributions of molecular orbitals along the molecular axis.

The secular determinant obtained is of third order and may be factored by use of the symmetry $D_{\infty h}$ into first- and second-order determinants. The integrals encountered are symbolized as follows:

$$Q_i = \int p_i H p_i d\tau \qquad s_i = \int p_i p_i d\tau = 1$$

$$\beta = \int p_1 H p_2 d\tau = \int p_3 H p_2 d\tau \qquad s_\beta = \int p_1 p_2 d\tau = \int p_3 p_2 d\tau$$

$$\gamma = \int p_1 H p_3 d\tau \qquad s_\gamma = \int p_1 p_3 d\tau.$$

To make the problem more tractable, it is convenient to make the assumptions that $Q_1 = Q_3 \sim Q_2 = Q_p$ and that $\gamma \sim s_\gamma \sim 0$. The first assumption seems to be quite reasonable for the trihalide X_3^-, although it would be questionable if applied to X_2Y^- or XYZ^- trihalides. The validity of the second approximation may be tested by use of the tables of the overlap integrals, again using Slater functions, with the distance parameter appropriate to the extreme I—I distance in I_3^-. With the interatomic distance 5.92A, the overlap is less than 0.01. The unnormalized wave functions and energy levels obtained in this approximation are given in Table I, and the qualitative features of the electronic distribution along the molecular axis for $2p$ orbitals are shown in

[9] E. F. Westrum, Jr. and K. S. Pitzer, J. Am. Chem. Soc. **71**, 1940 (1949).

[10] C. C. Kiess and T. L. de Bruin, U. S. Bur. Standard's J. of Research **4**, 667 (1930).

[11] F. R. Bichowski and F. D. Rossini, *The Thermochemistry of the Chemical Substances* (Reinhold Publishing Corporation, New York, 1936).

[12] Mulliken, Rieke, Orloff, and Orloff, J. Chem. Phys. **12**, 1248 (1949).

TABLE I. M.O. Wave functions and energy levels.

X_3^-

$$\psi_3=p_1+\sqrt{2}p_2+p_3 \qquad W_3=\frac{Q_p+\sqrt{2}\beta}{1+\sqrt{2}s}$$
$$\psi_2=p_1-p_3 \qquad W_2=Q_p$$
$$\psi_1=p_1-\sqrt{2}p_2+p_3 \qquad W_1=\frac{Q_p-\sqrt{2}\beta}{1-\sqrt{2}s}$$

HF_2^-

$$\psi_3=a_3(p_1-p_3)+b_3s_2 \qquad W_3=\frac{Q_1+\sqrt{2}\beta}{1+\sqrt{2}s}$$
$$\psi_2=p_1+p_3 \qquad W_2=Q_p$$
$$\psi_1=a_1(p_1-p_3)+b_1s_2 \qquad W_1=\frac{Q_1-\sqrt{2}\beta}{1-\sqrt{2}s}$$

$$\lim_{\Delta\to 0}\left\{\frac{a_1}{b_1}=-\frac{1}{\sqrt{2}};\quad \frac{a_3}{b_3}=+\frac{1}{\sqrt{2}};\quad Q_1=Q_p=Q_s\right\}$$

$$\lim_{\Delta^2\to 0}\left\{\frac{a_1}{b_1}=-\frac{1}{\sqrt{2}}\frac{(\beta-sQ_p+s\Delta/2)}{(\beta-sQ_p+\Delta/2\sqrt{2})};\right.$$
$$\left.\frac{a_3}{b_3}=+\frac{1}{\sqrt{2}}\frac{(\beta-sQ_p+s\Delta/2)}{(\beta-sQ_p-\Delta/2\sqrt{2})};\quad Q_1=\tfrac{1}{2}(Q_p+Q_s)\right\}$$

Fig. 1B. Since only qualitative conclusions are drawn, no attempt was made to arrive at a self-consistent field solution, and the final wave functions have not been antisymmetrized.

In this approximation, the ground configuration of X_3^- would be $\Psi_0=\psi_1^2\psi_2^2$. The lowest orbital ψ_1 is definitely bonding, while the second ψ_2, although formally nonbonding, does tend to place the electrons between atoms 1 and 3 without introducing a node and probably contributes to the stability of the bond.

An analogous molecular orbital treatment for HF_2^- can be made by forming the orbitals from two $2p\sigma$ orbitals, one from each fluorine atom, and the hydrogen $1s$ orbital. The symmetry properties assumed for the orbitals are shown in Fig. 1A. The integrals of interest are symbolized as follows:

$$Q_p=\int p_iHp_id\tau \qquad s_i=\int p_ip_id\tau=\int s_2s_2d\tau=1$$

$$Q_s=Q_p-\Delta=\int s_2Hs_2d\tau$$

$$\beta=\int p_iHs_2d\tau \qquad s_\beta=\int p_is_2d\tau$$

$$\gamma=\int p_1Hp_3d\tau \qquad s_\gamma=\int p_1p_3d\tau.$$

As in the earlier treatment, the approximation $\gamma\sim s_\gamma\sim 0$ is quite reasonable. As a zero-order approximation, we can assume that $\Delta=Q_p-Q_s\sim 0$. Since this term is probably small but not negligible, the next approximation can be made that Δ is sufficiently small so that terms of the order of $(\Delta/\beta-sQ)^2$ may be neglected. The wave functions and energy levels for HF_2^- are given for both assumptions. Figure 1B shows the qualitative features of the electronic distributions of the resulting molecular orbitals, applicable to either case.

As in trihalide ion, the ground state $\Psi_0=\psi_1^2\psi_2^2$ involves a definitely bonding orbital ψ_1 and a formally nonbonding orbital ψ_2. In this instance, ψ_2 has a node at the central atom, and the orbital probably does not aid in the bonding, possibly offering an explanation of the higher ratio of $d/\Sigma r$ for the bifluorides compared to that of the trihalides. In either case, the bond stability provided by the lowest M.O. ψ_1 results in a prediction of stable but relatively weak bonds.

The treatment presented here seems to offer a satisfactory qualitative explanation of the bonding in trihalide and bifluoride ions without the introduction of higher orbitals. In addition, it is possible to predict the stability of other molecular species possessing similar electronic arrangements. Those species which are isoelectronic with X^-, such as OH^-, NH_2^-, H_2O, NH_3, HX, noble gases, etc., should be able to combine with groups similar in electronic character to X_2, such as H_2O_2, N_2H_4, etc. For example, one might expect such reactions as:

$$H_2O_2+OH^-=(OH)_3^-,$$
$$N_2H_4+NH_2^-=(NH_2)_3^-.$$

Some hydrates might owe their stability to such bonds, e.g.:

$$N_2H_4+H_2O=NH_2-NH_2-OH_2.$$

It is to be expected that a rare gas could form complexes with halogens. It is interesting to speculate that the halogen rare gas compounds (of unknown composition), reported by Boomer[13] and later by von Antropoff, Weil, and Frauenhof,[14] might be due to bond formation similar to that in the trihalides. The rare gas-halogen mixtures which may form compounds include helium-iodine, argon-chlorine, krypton-chlorine, and krypton-bromine.

Even though the molecular orbitals described previously may sometimes fail to give rise to stable molecular species, they may suggest low energy excited states which aid in deducing reaction mechanisms.

The author would like to thank Professor R. E. Connick for suggesting the consideration of the foregoing problem.

[13] E. H. Boomer, Proc. Roy. Soc. (London) **109**, 198 (1925).
[14] von Antropoff, Weil, and Frauenhof, Naturwiss. **20**, 688 (1932).

Near Infrared Pleochroism. II. The 0.8−2.5μ Region of Some Linear Polymers

L. GLATT*† AND J. W. ELLIS
Department of Physics, University of California, Los Angeles, California
(Received July 21, 1949)

Polarized radiation is used to study the pleochroism of aligned specimens of polythene, Nylon, polyvinyl alcohol, polyvinyl chloride, and polyvinylidene chloride, in the 0.8−2.5μ overtone and combination region. Assignments of observed absorption bands to various vibration modes of (coupled) $>CH_2$, N−H, and C=O groups are attempted. The symmetry of an infinite planar-zigzag $>CH_2$ chain is discussed as an approximation to that of polythene and, to a lesser extent, Nylon. Some limitations in the interpretation of observed pleochroism and in the application of selection rules are discussed. A pleochroism study, with *unpolarized* radiation, is made of the molecular alignment in oriented "Parowax." A study is made also of the rupture of the intermolecular N−H···O bonds in molten and premolten Nylon.

I. INTRODUCTION

INFRARED absorption is, for a given vibration mode, most intense when the exciting *E*-vector is parallel to the direction (for degenerate modes, *directions*) of the oscillating electric moment increment characteristic of that mode. The infrared pleochroism of a specimen, or variation of absorption intensity with respect to the *E*-vector, can often yield considerable information as to the vibration modes which are responsible for the various observed absorption bands and also concerning the orientation of the molecules in the specimen. This is, naturally, true only for a crystalline or ordered substance in which, moreover, the molecules have some element of symmetry.

Several investigations early in the century used polarized infrared radiation to study crystals of inorganic salts. Schaefer and Matossi summarized, in 1930, the results of investigations on carbonates, nitrates, and other ionic crystals.[1] Ellis and Bath, in this laboratory, were perhaps the first to use infrared pleochroism for the correlation of the vibration spectra of *organic* substances with their structures.[2,3] Several such studies have been conducted recently, in England for the most part. Reference will be made later to these contemporary investigations.

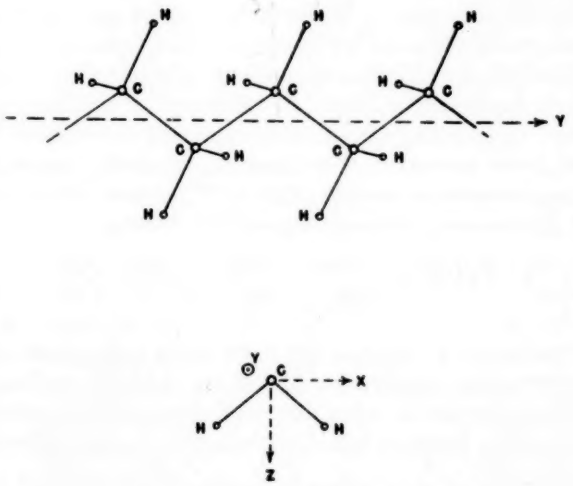

FIG. 1. Section of a $>CH_2$ chain.

The present report is concerned with some linear polymers that were semi-aligned by mechanically stretching or rolling the specimens. Polythene, "Parowax," 6.10 polyamide (a "Nylon"), polyvinyl alcohol, polyvinyl chloride, and polyvinylidene chloride are the substances discussed in this paper. Later papers will deal with single-crystal as well as with polymer specimens. Whenever possible, the authors have attempted the assignment of observed absorption bands to the various vibration modes of (coupled) $>CH_2$, O−H, N−H, and C=O groups. In making these assignments, it was attempted to correlate the observed pleochroism with available data on molecular orientation and with symmetry selection rules.

Figure 1 shows a diagram of a normal saturated $>CH_2$ chain. The carbon atoms form a planar zigzag. The planes of the CH_2 groups, shown in projection, are normal to the chain axis. The four single bonds about each carbon atom are distributed essentially at the tetrahedral angle. Schematic diagrams for the three fundamental modes of a free CH_2 group (not to scale) are shown in Fig. 2. Similar figures are shown for the three restricted rotation modes that result when the $>CH_2$ group is attached to the rest of the molecule.

Spectrograms of all the specimens were made on a quartz prism recording spectrograph, which was used in the overtone and combination band region between 0.6 and 2.7μ.[4] The fundamental X−H bond stretching region in between roughly 2.7μ and 4.0μ. A Glan-Thompson type calcite polarizer was used with this instrument.

It is not possible, unfortunately, to send plane polarized radiation through a non-isotropic medium with the *E*-vector vibrating in any arbitrarily chosen direction. The cross section of the index ellipsoid parallel

* Most of this material was taken from a dissertation presented in partial satisfaction of the requirements for a Ph.D. degree.
† Now at the Cryogenic Laboratory, Ohio State University.
[1] C. Schaefer and F. Matossi, *Das Ultrarote Spektrum* (Verlag. Julius Springer, Berlin, Germany, 1930).
[2] J. W. Ellis and J. Bath, J. Chem. Phys. **6**, 221 (1938); **7**, 862 (1938).
[3] J. W. Ellis and J. Bath, J. Am. Chem. Soc. **62**, 2859 (1940).
[4] J. W. Ellis, Rev. Sci. Instr. **4**, 123 (1933).

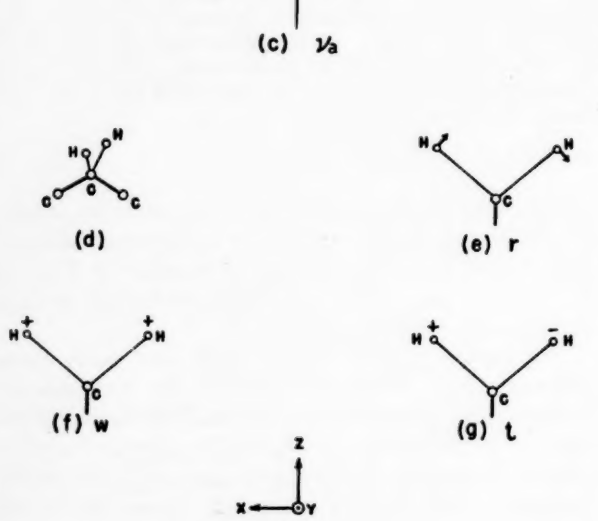

FIG. 2. The three vibration and the three restricted rotation modes of a $>CH_2$ oscillator.

to the transmitting surface is, in general, an ellipse, the major and minor axes of which are, for normal incidence, the only two vibration directions for which plane polarized radiation can be transmitted as such. If a vibration direction for the incident beam other than one of the above two mutually perpendicular ones is chosen, then *elliptically* polarized light is transmitted through the specimen. This limitation upon the use of polarized radiation has not always been appreciated.

The converging beam of the quartz spectrograph has a semi-angle of about 10°. This causes most of the light to impinge upon the specimen at slightly oblique incidence. The alignment between specimen and polarizer is seldom reliable to better than 3°. These deviations from the ideal condition cause the *E*-vector within the specimen to vibrate in a compact bundle with slightly varying azimuths and hence tend to diminish the variation in absorption intensity with respect to polarization direction.

II. PREPARATION AND CRYSTAL NATURE OF THE SPECIMENS

The specimens were mostly in the form of aligned multilayers imbedded in CCl_4 to minimize scattering loss. The total thickness of the various specimens ranged from 0.04 to 0.5 mm. The two polarization directions used were those perpendicular and parallel, respectively, to the direction in which the films had been stretched or rolled.

Untreated polymer films exist in a composite phase in which both crystalline and amorphous regions are distributed at random.[5,6] Treatments such as stretching, rolling, pressing, and annealing tend to increase greatly the ratio of ordered to amorphous regions. A small percentage of amorphous regions remain even in fully stretched or rolled specimens. Short side groups, if present, tend to disrupt the ordered structure in their vicinity. Longer side chains line up with the parent chain.[5]

1. Polythene and "Parowax"[7]; $-(CH_2)_n-$

Oriented specimens of polythene were graciously supplied by Dr. Wilfried Heller, now at Wayne University, and his former co-worker at the University of Chicago, Dr. Hans Oppenheimer. These specimens were plastic films which had been stretched until the alignment of the molecular chain axes was as closely parallel to the stretch direction as possible.[8]

Unoriented specimens of "Parowax" were sliced from a block. Semi-crystalline specimens were prepared by slow cooling of a melt on a hot water surface. To minimize disorientation caused by the heat of the beam, these latter specimens were placed at the *exit* slit of the instrument.

The crystal structure of polythene has been determined by C. W. Bunn[9] and by A. Charlesby.[10] Two chain molecules pass through a unit cell, which contains four CH_2 units. The CH_2 planes are all parallel to the $c(001)$ plane, but the symmetry axes of the CH_2 triangles that belong to different chains are *not* parallel to each other. The planes of the zigzag carbon backbones are all parallel to the c-axis, but those of the two adjacent chains passing through the same unit cell form angles of $\sim 82°$ with each other. The symmetry axes of the CH_2 triangles lie in the carbon planes and are thus also inclined at $\sim 82°$ to those of adjacent chains. In the stretched specimens the various microcrystals have their c-axes aligned with the direction of stretch, but have their a-axes (and b-axes) randomly distributed in the plane normal to this direction. Charlesby found in his specimens an average angle of 9° between the c-axes of the microcrystals and the stretch direction.

2. Nylon[11]; $-[NH-(CH_2)_6-NH-CO-(CH_2)_8-CO]_n-$

A sheet of 6.10 polyamide 0.095 to 0.12 mm thick was very kindly supplied by Mr. R. B. Aken of DuPont. Fully stretched or rolled films were approximately 0.045 mm thick. Strips of rolled or pressed Nylon tennis string

[5] E. M. Frith and R. F. Tuckett, Trans. Faraday Soc. **40**, 251 (1944).
[6] S. D. Gehman, Chem. Revs. **26**, 203 (1940).
[7] L. Glatt and J. W. Ellis, J. Chem. Phys. **15**, 884 (1947).
[8] W. Heller, Phys. Rev. **69**, 53 (1946).
[9] C. W. Bunn, Trans. Faraday Soc. **35**, 482 (1939).
[10] A. Charlesby, Proc. Phys. Soc. (London) **57**, 496 (1945).
[11] L. Glatt and J. W. Ellis, J. Chem. Phys. **16**, 551 (1948).

were also examined. Nylon tennis string, as sold commercially, is pre-stretched. Some unstretched tennis string, desirable for testing the orientation effects of pressing, was also supplied by Mr. Aken. Spectrograms were also made of molten Nylon specimens. A heated absorption cell[12] was used.

The crystal structure of two polyamides, 66 and 6.10, have been fully determined by C. W. Bunn and E. V. Garner.[13] There is only one chain molecule passing through each unit cell. In a Nylon crystalloid, the molecular backbone planes are thus all parallel to one another. The chain axes are parallel to the crystallographic *c*-axis. The oxygen atoms of one molecule lie on the same level as the NH units of the next; the molecules are linked into parallel sheets by intermolecular N—H···O bonds which extend perpendicularly to the *c*-axis. Excellent structure diagrams are given by Bunn and Garner.[13]

3. Polyvinyl Alcohol; $-(CH_2-CHOH)_n-$

Dr. Maurice L. Huggins of the Eastman Kodak Company supplied us with clear films of polyvinyl alcohol. To orient the films, they were either rolled between heated rollers or stretched under the heat of a commercial infrared lamp. Spectrograms were made for specimens oriented by each method.

An x-ray study of the structure of this substance has been made by R. C. L. Mooney.[14] Some features of her synthesized model have been objected to by Bunn and Peiser,[15] and by M. L. Huggins (in a correspondence with the authors). It seems probable, however, that Mooney was correct in concluding that the molecular chains are in pairs linked together by hydrogen bonds, with the C—C bonds in each molecular zigzag and the O—H···O bonds between the two molecules both tending to be in the (101) plane. The molecular chains have their axes parallel to the crystallographic *b*-axis. It is likely that there are departures of considerable magnitude from this orientation resulting chiefly from a randomness relative to the plane of the carbon zigzag of the oxygen atoms in each chain;[15] there are two alternative positions for each O—H group. This randomness was not considered by Mooney in her structure analysis.

Strips of polyvinyl alcohol that are rolled between heated rollers become doubly oriented with the (101) planes preferentially in or near the plane of the strip and with the *b*-axes in the direction of roll. In stretched specimens the double chains lie along the stretch direction but in random orientation about it. Dr. Huggins was so gracious as to communicate the above information to the authors.

[12] A. E. Richards and H. W. Thompson, Trans. Faraday Soc. **41**, 185 (1945).
[13] C. W. Bunn and E. V. Garner, Proc. Roy. Soc. (London) **A189**, 39 (1947).
[14] R. C. L. Mooney, J. Am. Chem. Soc. **63**, 2828 (1941).
[15] C. W. Bunn and H. S. Peiser, Nature **159**, 161 (1947).

4. Polyvinyl Chloride; $-(CH_2-CHCl-CH_2-CClH)_n-$ and Polyvinylidene Chloride; $-(CH_2-CCl_2)_n-$

Both of these substances, in the form of amorphous sheets, were obtained from Dr. M. L. Huggins. Specimens were oriented by warming somewhat with a heat lamp and then stretching. The long chain molecules of the vinyl-polymer have their carbon backbones in a planar zigzag; the fiber repeat distance is, however, 5.0A, approximately twice that for polythene and polyvinyl alcohol. This has been interpreted as implying that the chlorine atoms are alternately placed, first on one side and then on the other with respect to the plane of the zigzag.[16]

The crystal structure of polyvinylidene chloride has been investigated by R. C. Reinhardt;[17] his results indicate that the carbon backbones are neither planar zigzags nor uniform spirals. He postulates a sort of serpentine configuration of the C-atoms with the C—C—C bond angles at 122° rather than the usual 109°–112°. This sort of a configuration would cause the CH_2- (and the CCl_2-) planes to have an appreciable inclination toward the chain axis, and thus considerably diminish the pleochroism in the CH_2 bands. It is therefore significant that the $>CH_2$ bands in polyvinylidene chloride exhibit considerably less pleochroism than do those of any of the other, planar zigzag, polymers investigated (see Fig. 9), this, in spite of the fact that oriented polyvinylidene chloride specimens have a very high degree of crystallinity and very little branching in the chains.[17]

III. SELECTION RULES AND COUPLING FOR AN EXTENDED INFINITE $>CH_2$ CHAIN

Consider an infinite normal $>CH_2$ chain with the planar zigzag carbon backbone in the *yz* plane (see Figs. 1 and 2). The full spatial symmetry of such a chain forms a "strip-group" of infinite order whose factor group is isomorphic to the finite point group D_{2h}. There is point symmetry $C_{2v}(z)$ about a *z*-axis through *each* carbon atom.

The normal modes of a $>CH_2$ chain containing *n* links[18] can be subdivided into nine sets of *n*-fold multiplets; one multiplet set corresponding to each of the three true vibration, three restricted rotation, and three restricted translation modes characteristic of a $>CH_2$ vibrator. The multiplet component of a given set differ in the phase relations between the various $>CH_2$ links; their frequencies can be expected to be closely packed or overlapping. It is evident, even without resort to group theory, that the net dipole moment increment of the chain can be expected to be negligible for most of these multiplet components.

[16] M. L. Huggins, J. Chem. Phys. **13**, 37 (1945).
[17] R. C. Reinhardt, Ind. Eng. Chem. **35**, 422 (1943).
[18] Whitcomb, Nielsen, and Thomas, J. Chem. Phys. **8**, 143 (1940).

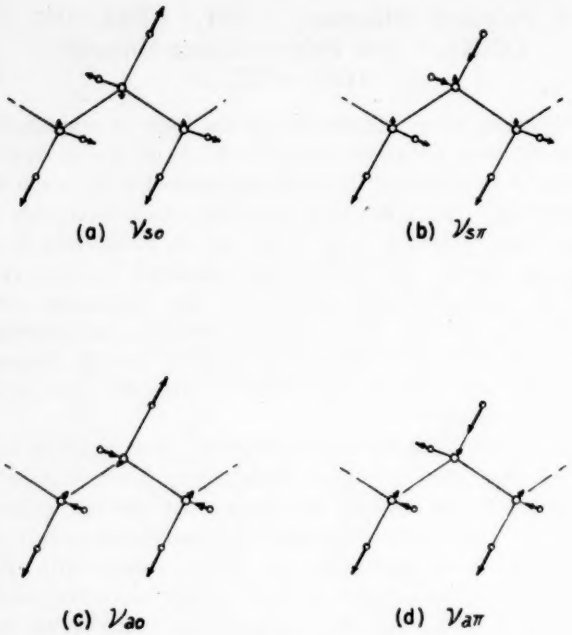

FIG. 3. O- and π-coupled C−H bond stretching modes in a $>CH_2$ chain.

Winston and Halford[19] have analyzed the classification of motions of a crystal and the selection rules for spectra according to *space* symmetry. Their analysis shows, implicitly, that each of the nine sets of n-fold multiplets contains either one normal mode only or none at all with a non-zero dipole moment increment. The sets containing an active fundamental can be identified by analyzing modes of one $>CH_2$ group under its local point symmetry $C_{2v}(z)$. The active member of the corresponding set is the mode that belongs to the totally symmetric representation of the (invariant) translation sub-group of the strip-group. This means that for infrared active fundamentals there must be zero phase difference between the motions of all $>CH_2$ units that are interchangeable by pure translations. Adjacent $>CH_2$ units are oppositely directed and cannot be interchanged by *pure* translations. It is evident that for infrared activity, the dipole moment increments of adjacent units must reinforce rather than negate one another. Of the modes shown in Fig. 3, for example, $\nu_{s\pi}$ and $\nu_{a\pi}$ are infrared active while ν_{s0} and ν_{a0} are inactive. This would also follow from an analysis under the D_{2h} factor group representations.

The analysis of combination (and overtone) modes of the CH_2 chain is considerably complicated by the C−C coupling of the chain units. Whereas the selection rules for fundamentals permit infrared activity by, *at most*, *one* component from each of the nine n-fold multiplets, the space symmetry selection rules permit activity, for *any* binary multiplet, by essentially n among the n^2 pairs of components that can be formed. Thus, *no* composite transition corresponding to an arbitrary pair (or triplet, etc.) of multiplet sets is *strictly* forbidden by symmetry considerations.[19]

Although it can be expected that most of these above modes will have very weak absorption, if n is large and they lie in a narrow frequency range, they may accumulate to produce considerable absorption. Thus, even neglecting anharmonicity, the center of the envelope for a doubly excited mode need not fall at the sum of the two active components. If the active fundamentals were both the lowest members of their respective sets, then the active combinations could well appear at frequencies exceeding their sum. If the active fundamentals were the highest frequencies of their respective multiplet sets, the converse could be true. It has been suggested by a reviewer of this paper that the hypothesis outlined above may account for the apparently anomalous shifts from predicted positions, assuming normal anharmonicities, of some of the observed absorption bands discussed later in this paper.

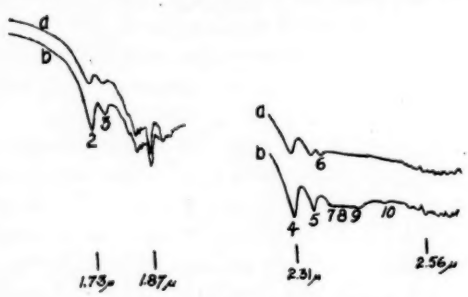

FIG. 4. Spectrograms with polarized radiation of stretched polythene film: (a) $E \parallel$ stretch direction; and (b) $E \perp$ stretch direction.

TABLE I. Selection rules and band assignments frequencies of polythene bands.

$C_{2v}(z)$	Fundamentals Mode	Fundamentals Freq. (cm^{-1})	Binary combinations Mode	Computed freq. (cm^{-1})	Observed freq. (cm^{-1})	Band numbers
A_1; M_z	ν_s	2853	$2\nu_a$	5790	?{5782	2
	δ	1460	$2\nu_s$	5650	{5782	2
			$\nu_s+\delta$	4250	4247	5
			ν_a+w	4180 or 4250		
A_2; f	t	(1300)	ν_s+t	4100		
B_1; M_x	ν_a	2925	$\nu_a+\nu_s$	5720	5671	3
	r	725	$\nu_a+\delta$	4325	4322	4
B_2; M_y	w	1310 (or 1375)	ν_s+w	4110 (or 4180)	4216	6
			ν_a+t	4180		

The space symmetry representations of the n permitted binary transitions, for *each* pair of n-fold multiplets, contain *all* factor group, and thus also all activity, representations of the space group. It is to be expected, therefore, that there will be a diminution of the pleochroism as well as possible apparent violations

[19] H. Winston and R. S. Halford, J. Chem. Phys. 7, 607–616 (1949).

of the factor group and "site" symmetry selection rules. It is nevertheless proposed, in line with arguments advanced by Winston and Halford, to use as a suitable approximation the selection rules of the "site" symmetry, $C_{2v}(z)$, of the $>CH_2$ units.

The $C_{2v}(z)$ selection rules will be applied, therefore, to the observed $>CH_2$ type bands of polythene and the other polymers. It is realized, of course, that the above discussion for an infinite extended $>CH_2$ chain is only approximately applicable, even for polythene. Aside from the finite length of the polymer chains, there is some branching, and also some units other than $>CH_2$ exist to cause complications. There is the possibility, moreover, that coupling by the crystal field between adjacent chains cannot be neglected safely in comparison to the coupling by the C—C bonds within a chain.

The symmetry species of some of the more important $>CH_2$ oscillator type modes are cataloged in Table I. These symmetry species were derived from the character

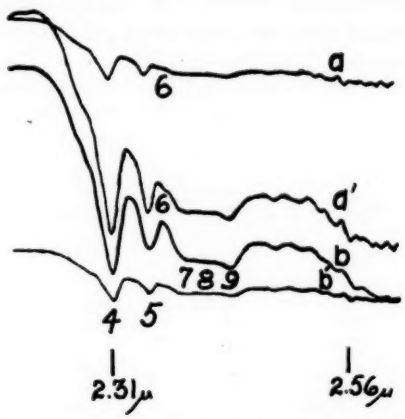

FIG. 5. Spectrograms with unpolarized radiation of "Parowax:" (a) specimen with molecules randomly oriented [(a') wide slits]; and (b') specimen prepared from a melt on the surface of hot water [(b) wide slits].

tables of the irreducible representations for the $C_{2v}(z)$ point group.[20] The symbols for the dipole moment components are listed adjacently to those of the irreducible representations to which they belong, f meaning that infrared activity is forbidden by the "site" symmetry (but not strictly forbidden by the full spatial symmetry). The wave number frequencies given for the fundamental modes (see Fig. 2) are consensus values from the literature for polythene. The alternate 1375 cm^{-1} frequency for the $>CH_2$ "wagging" mode w is more usually assigned to the symmetrical deformation mode of the methyl units which are said to be present in small quantities on the side chains of polythene.[21,22] This 1395 cm^{-1} band shows, however, the y-type activity expected of a $>CH_2$ w mode and has been so assigned by

[20] J. E. Rosenthal and G. M. Murphy, Revs. Modern Phys. **8**, 317 (1936).

[21] H. W. Thompson and P. Tarkington, Proc. Roy. Soc. (London) **184A**, 3 (1945).

[22] Elliott, Ambrose, and Temple, J. Chem. Phys. **16**, 875 (1948).

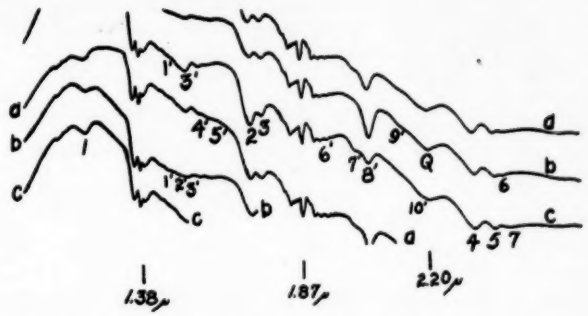

FIG. 6. Spectrograms of stretched Nylon (6.10): (a) unpolarized radiation; (b) $E \parallel$ stretch direction; and (c) $E \perp$ stretch direction.

at least one investigator, T. Simanouti,[23] who gives arguments for questioning the methyl assignment.

The predicted frequencies given in Table I for the binary combination and overtone modes were computed by adding the observed frequencies of the appropriate pairs of fundamentals and subtracting approximately 50 or 60 cm^{-1} as an anharmonicity term. It was pointed out previously that the n-fold multiplicity of *permitted* components in a composite binary transition can cause a significant shift from frequencies computed in the above fashion.

A discussion of the proposed band assignments given in the last column of Table I, together with some possible alternative assignments, is given in the following sections of this paper. The arbitrary band numbers listed after the observed (polythene) frequencies are those assigned to the absorption bands in Figs. 4–9.

IV. RESULTS AND THEIR INTERPRETATIONS

This section of the report shows reproductions of spectrograms made on the quartz-prism instrument. All of the spectrograms show several atmospheric water vapor bands, and the band at 2.20μ caused by the quartz prisms. The numbered bands are those caused by

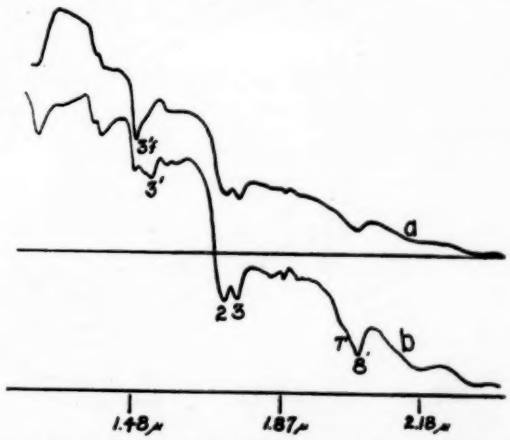

FIG. 7. Spectrograms with unpolarized light of Nylon (6.10): (a) molten specimen kept at 300°C; and (b) solid specimen kept at 200°C.

[23] T. Simanouti, J. Chem. Phys. **17**, 734–7 (1949).

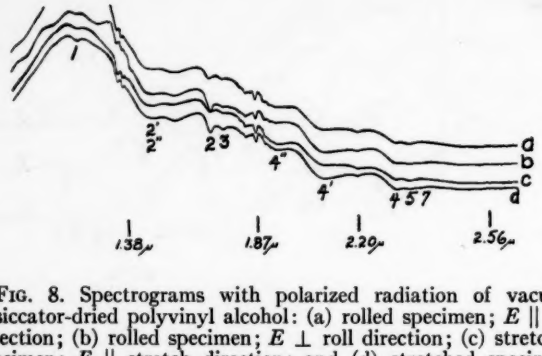

FIG. 8. Spectrograms with polarized radiation of vacuum desiccator-dried polyvinyl alcohol: (a) rolled specimen; $E \parallel$ roll direction; (b) rolled specimen; $E \perp$ roll direction; (c) stretched specimen; $E \parallel$ stretch direction; and (d) stretched specimen; $E \perp$ stretch direction.

absorption in the specimens. The positions and relative intensities of the numbered bands are listed in tables. Owing to causes which will be discussed later, it was often quite difficult to determine these relative intensities with any degree of accuracy. The comparative intensities of widely separated bands are accurate to only one significant figure. The relative intensities listed were, in general, averaged from several spectrograms rather than taken from the particular spectrogram shown in the figures.

1. Bands in the 1.7μ (5900 cm^{-1}) and 2.3μ (4300 cm^{-1}) Regions

Designations on the spectrograms reproduced in Figs. 4–9 make it evident which of the absorption bands of the other polymers correspond to those of polythene. The positions of these $>CH_2$ type bands are tabulated in Table II; Table III gives their relative intensities.

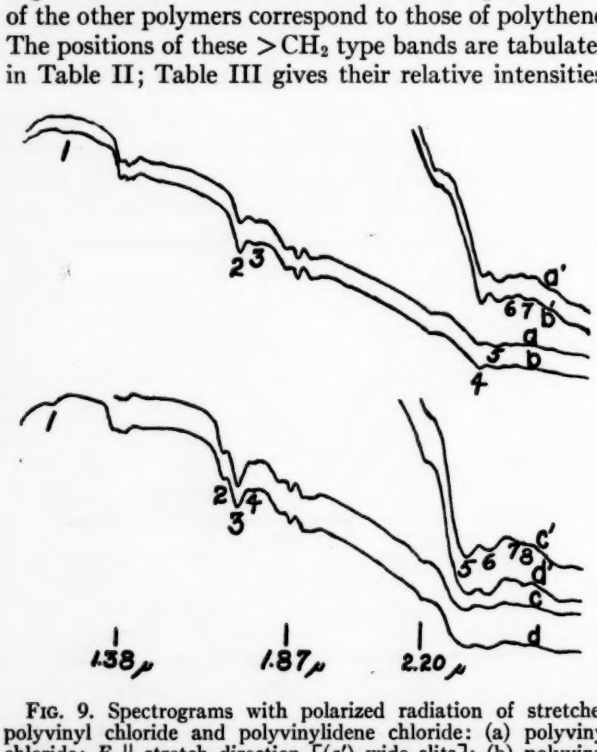

FIG. 9. Spectrograms with polarized radiation of stretched polyvinyl chloride and polyvinylidene chloride: (a) polyvinyl chloride; $E \parallel$ stretch direction [(a') wide slits]; (b) polyvinyl chloride; $E \perp$ stretch direction [(b') wide slits]; (c) polyvinylidene chloride; $E \perp$ stretch direction [(c') wide slits]; (d) polyvinylidene chloride; $E \parallel$ stretch direction [(d') wide slits].

The values for polyvinylidene chloride are tabulated separately in Table IV.

a. Pleochroism in Nylon

Bunn and Garner[13] outline procedures for obtaining doubly oriented strips of Nylon film with the backbone planes almost parallel to the surface. A specimen of this sort would be expected to exhibit a considerably reduced absorption for "x-active" and a somewhat enhanced absorption for "z-active" modes. It will be recalled that the x-axis was chosen normal to the plane of the carbon backbone, and the z-axis parallel to the symmetry axes of the CH_2 triangles.

Nylon (6.10 polyamide) specimens initially in the form of unoriented films, stretched fibers, and unstretched fibers were variously treated, after the fashions outlined by Bunn and Garner, in an attempt to obtain double orientation. Unfortunately, only a limited degree of double orientation was achieved. There was very little significant contrast between the spectrograms of the singly oriented stretched specimens and those of any of

TABLE II. Positions of the $>CH_2$ bands.

Band No.	Polythene freq. (cm^{-1})	Nylon freq. (cm^{-1})	Polyvinyl alc. freq. (cm^{-1})	Polyvinyl chl. freq. (cm^{-1})
1	8237	8292	8319	8333
2	5782	5804	5838	5828
3′	—	—	—	5740
3	5671	5695	5688	5708
4′	—	—	—	4360
4	4322	4342	4329	4329
5	4247	4257	4255	4279
6	4216	4219	—	—
7	4184	4202	4202	4211
8	4130	—	—	4161
9	4095	—	—	4100
10	4018	4010	4010	4075

the specimens in which it had been attempted to produce double orientation. Some of the pressed fiber specimens did, however, appear to show a slight *decrease* in the intensity of band 3 relative to band 2 (see Fig. 6). This intensity change, which was in the opposite direction from that expected on the basis of the relative positions of the bands, may have been only apparent. It was difficult to estimate the correct background from which to measure the intensity of the bands involved.

b. Pleochroism in Polyvinyl Alcohol

More definite evidence can be had by comparing the spectrograms of stretched, with those of rolled polyvinyl alcohol. It was remarked earlier that the rolled specimens are believed to have the zigzag carbon backbones, and thus the CH_2 z-direction preferentially located in or near the plane of the sheet. It is evident from Fig. 8 and Table III that the ratio of the intensity of band 3 to that of band 2 is definitely diminished in rolled as compared to the stretched specimens. The intensity ratio of band 5 to band 4 is, on the other hand, slightly

increased. This last is, however, somewhat unreliable. The energy background in the 2.3μ region changes too abruptly and is pulled down too severely by the overlying O—H···O absorption to allow accurate determinations of relative intensities. These same handicaps also restrict the accuracy of the relative intensity determinations in the 1.7μ region but not to so great an extent. The relative intensities listed in Table III are fairly reliable for the comparison of bands in the near vicinity of each other. For widely separated bands the listed intensities serve merely as orders of magnitude. This is particularly true of the polyvinyl alcohol bands.

c. Assignments

The above discussed pleochroism observed in the polyvinyl alcohol bands gives an admittedly flimsy basis for the assignment of the 1.7μ and the 2.3μ doublets to vibration modes. The interpretation is further complicated by the existence of the carbinol C—H units. The pleochroism evidence is the weakest for the 2.3μ doublet; it appears safe, however, to assign band 4 to the "x-active" $\nu_a+\delta$ type modes and band 5 to the "z-active" $\nu_s+\delta$ type modes (see Table I). These assignments are in good agreement with positions, separations, and relative intensities of the observed bands.

Four possible assignments, none of them completely satisfactory, are shown below for the 1.7μ doublet.

	Band 2 (apparently "z-active")	Band 3 (apparently "x-active")
(1)	$2\nu_s$ type; "z-active"	$\nu_a+\nu_s$ type; "x-active"
(2)	$2\nu_a$ type; "z-active"	$\nu_a+\nu_s$ type; "x-active"
(3)	$2\nu_a$ type; "z-active"	$2\nu_s$ type; "z-active"
(4)	$\nu_a+\nu_s$ type; "x-active"	$2\nu_s$ type; "z-active"

None of the above assignments is completely forbidden by the $C_{2v}(z)$ selection rules. The last two are, however, in disagreement with the evidence from the pleochroism observed in polyvinyl alcohol (and perhaps in Nylon). The third of the assignments is the only one for which the observed band positions are in good agreement with the frequencies computed from the *active components* of the fundamental multiplets. This is evident from Table I. It is difficult, however, to reconcile so strong an activity as that observed in band 2 with what would be expected from a "z-active" mode compounded out of "x-active" and inactive multiplet components. This latter criticism also holds for the second assignment, which, however, is in agreement with the observed pleochroism.

The first assignment is in agreement with the observed pleochroism and does not incur the difficulties mentioned above. It is therefore somewhat hesitantly favored by the authors even though it gives the poorest agreement between observed and computed frequencies. A justification, in terms of multiplet structure, has already been advanced for the assumption of such large frequency shifts. In addition, there is a precedent, from the spectra of water vapor, for the assumption of an extraordinarily large negative anharmonicity term for the $\nu_a+\nu_s$ type combinations.[24] The authors have also found a like phenomenon in the $>CH_2$ bands of many of the organic crystals that will be discussed in a later paper. There is precedent also for the possible assumption of a *positive* anharmonicity term for the $2\nu_s$ type mode. In the ν_s type vibration of methane, CH_4, a positive anharmonicity term is associated with the repulsive forces between the H-atoms which approach one another as they move on the surface of a hypothetical sphere.[25] In $2\nu_s$ type modes of $>CH_2$ oscillators, the two H-atoms approach one another as the C—H lengths contract, and a repulsive force probably is present.

TABLE III. Relative intensities of the $>CH_2$ bands.

Band No.	Stretched polythene ⊥	Stretched polythene ∥	Stretched Nylon ⊥	Stretched Nylon ∥	Stretched pvl. alc. ⊥	Stretched pvl. alc. ∥	Rolled pvl. alc. ⊥	Rolled pvl. alc. ∥	Stretched pvl. chl. ⊥	Stretched pvl. chl. ∥
1	0.6	0.2	0.7	0.4	0.5	0.3	0.5	0.3	0.3	0.2
2	4	1.9	3.2	1.3	3	1.2	3.6	1.5	4	2.5
3′	—	—	—	—	—	—	—	—	0.05	0.05
3	1.7	1	2.2	1.2	1.7	0.7	1.2	0.9	1.6	1.3
4′	—	—	—	—	—	—	—	—	0.1	0.2
4	10*	6	10*	7	10*	6	10*	7	10*	7
5	8	5	10⁻	7⁻	9⁻	5	10⁻	6	4	3.5
6	0	3	0	1.7	—	—	—	—	—	—
7	5⁺	0.5	6	0	4	0	5	0	6	5
8	2		—	—	—	—	—	—	5	4
9	5⁺	0.5	—	—	—	—	—	—	4	3
10	2	0	?	?	5	5	5	5	2	1

* Intensity arbitrarily set at 10.
⊥ E-vector perpendicular to stretch (or roll) direction.
∥ E-vector parallel to stretch (or roll) direction.

d. Polyvinyl Chloride and Polyvinylidene Chloride.

The absorption bands in these two polymers will not be discussed in detail. The 1.7μ region in the former is very similar to those in polythene, Nylon, and polyvinyl alcohol. There is no distinct band that can be attributed to the C—H bond in the CHCl units; this is similar to what was found in polyvinyl alcohol. The bands in the region beyond 2.2μ are too broad to be conveniently classified with those of polythene and the other polymers.

The 1.7μ region in polyvinylidene chloride is markedly different from that of the other polymers. This difference

TABLE IV. The polyvinylidene chloride bands.

Band No.	Freq. (cm^{-1})	Relative intensity ⊥	Relative intensity ∥
1	8439	0.4	0.4
2	5924	1.4	1.2
3	5787	4	3
4	5624	9	8
5	4370	10*	8⁺
6	4272	8	10⁻
7	4172	4	6
8	4125	3	5

[24] G. Herzberg, *Infrared and Raman Spectra* (D. Van Nostrand Company, Inc., New York, 1945), p. 282.
[25] D. M. Dennison, Revs. Modern Phys. **12**, 207 (1940).

TABLE V. The perturbed N−H···O and C=O bands in stretched Nylon (6.10).

Band Nos.	Frequency (10^{-3}·cm^{-1})	Relative intensities* ⊥	∥	Assignments
1′	6.789	0.01	0.02	Perturbed 2ν(N−H)
2′	6.636	0.01	0.02	
3′	6.523	1.4	0.5	
3′f	6.757	0	0	Free 2ν(N−H)
4′	6.373	0.7	0.4	?Perturbed 2ν(N−H)
5′	6.223	0.4	0.4	
6′	5.13	?	?	$\nu+\delta$(O−H) of bound H_2O
7′	4.975	2	0	3ν(C=O)
8′	4.883	2.3	5	$\nu+\delta$(N−H)
9′	4.70	0	0.03	?
10′	4.591	0.04	0	?

* The listed intensities are relative to the arbitrary value 10 for the CH_2 band number 4.

is very probably caused by the difference in skeletal structure.[16] Band 2 (Fig. 9, c and d), which is definitely absent from the spectrograms of the other polymers, may be caused by the $2\nu_a$ type mode. Bands 3 and 4 are quite broad and probably complex. This is also true of the longer wavelength bands.

A comparison of the spectrograms of polyvinylidene chloride with those of the other spectrograms shows that there is a greatly reduced pleochroism, particularly in the 1.7μ region. It has been pointed out in an earlier section of this paper that this decrease in pleochroism is a logical result of the altered structure of the carbon backbone. The authors wish to suggest that pleochroism studies of this sort might prove to be a useful implement to x-ray and electron diffraction methods in investigating the structure of long chain compounds. It may be that the pleochroism in some of the longer wavelength, skeletal type modes would give a fairly sensitive indication as to whether the backbone structure was a planar zigzag, a uniform spiral, etc.

2. Unusual Pleochroism in the 2.372$^-$ (4216 cm^{-1}) Band

The weak band 6, at 4216 cm^{-1} in polythene, is excited *only* by the *E*-component vibrating *parallel* to the molecular chain axes. The pleochroism exhibited by this "*y*-active" band is thus not only the most pronounced but also is in the direction opposite to that of any of the other $>CH_2$ bands. Figure 6 shows that this "*y*-active" band also appears, considerably diminished, at 4219 cm^{-1} in oriented Nylon specimens. It is too weak to be evident in the unpolarized spectrograms of Nylon, and is completely absent from the spectrograms made of polyvinyl alcohol and of polyvinyl chloride.

Since band 6 appears distinctly for polythene specimens as thin as 50μ, the mode responsible for it very probably involves displacements within the CH_2 units. Table I shows that possible assignments of this band are to the "*y*-active" ν_s+w or ν_a+l type modes. The first of these assignments is the more attractive. The w_τ mode is essentially a coupled motion of the entire chain in which all the hydrogens vibrate against all the carbons in a direction parallel to the chain axis. The oscillations could be expected to be restricted severely by the presence of the alternate CHX links in vinyl polymers, and to a lesser extent by the −CO−NH− links in Nylon. The above might also hold true for certain combinations of w and ν type modes, particularly for $\nu_{s0}+w_\tau$. This would explain the decreased intensity of band 6 in Nylon and its failure to appear in the vinyl polymers. The previously discussed "multiplet structure" of composite transitions can again be called upon to justify the fact that the observed frequency is about 36 or 106 cm^{-1} *higher* than that computed from the *active* fundamentals, depending upon the choice between the two w frequencies listed in Table I.

Band 6 could possibly be assigned to the ν_a+l type modes. One would, however, expect this type of mode to be active only very weakly, if at all, since none of the component ν_a or l type fundamentals belongs to a "*y*-active" representation. It is, in fact, questionable whether the fundamentals of the $>CH_2$ "twisting" type modes have been observed at all in the infrared.

3. Additional $>CH_2$ Bands

Band 1, which occurs at 8237 cm^{-1} in polythene, is very likely caused by some sort of a 3ν type mode. A comparison of the position of this band with that of the fundamental ν_a and ν_s modes shows that a rather large (negative) anharmonicity term occurs. Bands 7, 8, 9, and 10 may result from combinations of the $>CH_2$ type modes with some frequencies of the carbon backbone. There is a slight possibility that some of these bands, possibly 8 and 9, which are apparently absent from Nylon and the vinyl polymers, originate in the methyl side groups.

4. "Parowax"

The findings for "Parowax" are an example of a pleochroism study made with unpolarized radiation. The spectrograms made for amorphous "Parowax" specimens (Fig. 5; a, a′) are essentially identical with those of unoriented polythene. The unpolarized light spectrograms made for the crystalline specimens give convincing proof of an excellent alignment of the chain axes normal to the surface of the films.[7,26] As is shown in Fig. 5, b and b′, the "parallel" band 6 at 4216 cm^{-1} is completely missing and the intensity ratios and general appearance of the observed bands are unmistakably like those of the spectrograms made for oriented

[26] J. J. Trillat and T. V. Hirsch, Compt. rend. **195**, 215 (1932).

polythene when the *E*-vector was directed perpendicularly to the chain axes.

5. N—H···O and C=O Absorption in Nylon

The perturbed N—H···O and C=O bands in Nylon were discussed in an earlier preliminary report;[11] so also was the change in structure of certain of these bands in molten specimens and in specimens kept at 200°C, below the 260° melting point. The preliminary report did not, however, show spectrograms. The N—H···O and C=O bands are indicated in the spectrogram of Fig. 6 by primed numbers. The positions and relative intensities of these bands are tabulated in Table V. This table also gives assignments for some of the bands. Figure 7 shows spectrograms of molten and of 200°C specimens. Band $3'f$, which appears at 6757 cm^{-1} in these spectrograms, is caused by the *free* 2ν(N—H) bond stretching mode. The N—H···O bond ruptures in the molten specimens, and apparently to some extent in the hot unmolten specimens.[27]

The perturbed O—H···O bands in polyvinyl alcohol were discussed in a preceding report.[28]

[27] Fuller, Baker, and Pope, J. Am. Chem. Soc. **62**, 3275 (1940).
[28] Glatt, Webber, Seaman, and Ellis, J. Chem. Phys. **18**, 413 (1950).

THE JOURNAL OF CHEMICAL PHYSICS VOLUME 19, NUMBER 4 APRIL, 1951

An Absolute Theory of Solid-State Luminescence*

FERD E. WILLIAMS
General Electric Research Laboratory, Schenectady, New York
(Received December 26, 1950)

The absorption and emission spectra of the thallium-activated potassium chloride phosphor at various temperatures has been computed theoretically. An ionic model is used. The radial charge densities of free Tl^+ in the ground $^1S_0$ state and in the excited $^3P_1^0$ state are evaluated using the Sommerfeld modification of the Fermi-Thomas method for the core and the Hartree self-consistent field method for the two outershell electrons. From these wave functions and from the known ionic radius, polarizability, and repulsion energy constant ρ for the ground state, these parameters are evaluated for the Tl^+ in the excited state interacting with Cl^-. The variation of repulsion energy with interatomic distance a is shown to be equal to the variation of S^2/a with a, where S is an overlap integral. The Tl^+ in the $^1S_0$ and the $^3P_1^0$ states are substituted in dilute concentrations for the K^+ in KCl, and the change in total energy of the system is calculated as a function of the change in the Tl^+ nearest Cl^- distance Δa with the condition that the remainder of the lattice rearranges to minimize the total energy. Madelung, exchange repulsion, van der waals, ion-dipole and coulomb overlap interactions are included. The absorption spectrum is computed by recognizing that the various atomic configurations of the system in the ground state have probabilities in accord with a Boltzmann function. The emission spectrum is similarly determined by summing over configurations of the system in the excited state. The computed spectra at various temperatures are found to be in good agreement with experiment. In addition, new insight is obtained on the detailed mechanism of solid-state luminescence.

I. INTRODUCTION

THE quantitative interpretations of solid-state luminescent phenomena have been phenomenological. Fundamental interpretations based on the electronic theory of solids have produced only qualitative results. Detailed atomistic explanations frequently have been based on a configuration coordinate model.[1]

Diagrams of potential energy *versus* a position coordinate have been applied to problems of molecular spectra[2] and rates of chemical reactions.[3] In these applications, the position coordinate can be precisely specified as an interatomic distance. To describe the atomic rearrangements involved in electronic processes in solids requires, in principle, energy contours in configuration space having three times as many coordinates as there are particles involved. In describing the transitions and rearrangements occurring during luminescence, a useful simplification consists of defining a "center" as the excited atom plus the group of associated atoms participating in the rearrangements and then vaguely describing the coordinates of the center by a single average configuration coordinate. Seitz,[4] Gurney and Mott,[5] and Pringsheim[6] have used such potential energy diagrams to illustrate qualitatively various effects in the luminescence of solids, and Williams and Eyring[7] have correlated phenomenologically various diverse properties of luminescent solids with calculations based on a simple configuration coordinate model.

The use of a model involving potential energy plotted against an unprecise coordinate to describe the lu-

* Presented October 10, 1950 at the National Academy Meeting in Schenectady. See Science **112**, 428 (1950) and Phys. Rev. **80**, 306 (1950).
[1] F. E. Williams, J. Opt. Soc. Am. **39**, 648 (1949).
[2] A. G. Gaydon, *Dissociation Energies* (Dover Publications, New York, 1950).
[3] Glasstone, Laidler, and Eyring, *Theory of Rate Processes* (McGraw-Hill Book Company, Inc., New York, 1941).
[4] F. Seitz, J. Chem. Phys. **6**, 150 and 454 (1938).
[5] R. W. Gurney and N. F. Mott, Trans. Faraday Soc. **35**, 69 (1939).
[6] P. Pringsheim, Revs. Modern Phys. **14**, 132 (1942).
[7] F. E. Williams and H. Eyring, J. Chem. Phys. **15**, 289 (1947).

minescence of phosphors is unsuitable for quantitative theoretical interpretations and is open to criticism for even qualitative explanations. The general approach would be strengthened by judiciously selecting a single real coordinate in the lattice of a simple luminescent solid and demonstrating that important properties can be quantitatively evaluated by plotting the energy of various states of the system as a function of this coordinate. The calculation would be a basis for an absolute theory of solid-state luminescence in the sense that luminescent properties are computed utilizing first principles and the properties of the constituent ions only.

An atomistic calculation of this type is clearly most feasible for evaluating properties that depend on the simplest localized rearrangements largely confined to the immediate environment of the activator ion. The long wavelength absorption and the emission spectra of phosphors are properties of this type. Particularly for absorption and emission in which the electrons remain relatively tightly-bound to the activator ion even in the emitting state are the atomic rearrangements localized.

The calculation of the energy of a system consisting of a lattice containing activator ions in both ground and excited states for various atomic configurations is feasible for ionic crystals. Mayer[8] has calculated the lattice energies of alkali and thallium halides to within a few percent using an ionic model, and von Hipple[9] has computed the absorption of pure alkali halides to within seven percent by an electron transfer process between ions of the lattice. Both properties are primarily dependent on the least tightly bound electrons of the ions comprising the lattice. The luminescence of ionic phosphors differs principally in that the excited states, as well as the ground state, of impurity ions are involved.

Potassium chloride containing less than a few hundredths of a percent thallium is an ideal phosphor for an absolute calculation of absorption and emission spectra. The phosphor consists of an ionic lattice containing thallous ions substituted in dilute concentration for potassium ions. Optical absorption of the potassium chloride begins at 1650A. The thallium introduces two clearly resolved bell-shaped absorption bands peaking at 1960A and 2490A, and a broader bell-shaped emission band peaking at 3050A for 25°C. That excited states of the thallous ion, rather than electron transfer processes, are responsible for the absorption and emission bands is demonstrated by the absence in these spectra of the doublet characteristic of the halide ions, by the trivial dependences of peak positions on temperature, by the close similarity of thallium-activated alkali halides containing different anions, and by energy considerations. Even in the emitting state, the least tightly bound electron of the thallous ion is bound by several electron volts to the activator so that atomic rearrangements following optical absorption and emission are localized.

[8] J. E. Mayer, J. Chem. Phys. **1**, 270, 327 (1933).
[9] A. von Hipple, Z. Physik **101**, 680 (1936).

II. FORMULATION

The most probable thallous ion states responsible for the absorption and emission bands of KCl:Tl can be determined from the free Tl^+ spectra and the selection rules. The ground state is $6s^2\,{}^1S_0$ for free Tl^+ and for ionic compounds of Tl^+. The lowest excited states $6s6p$ consist of three triplet states ${}^3P_0{}^0$, ${}^3P_1{}^0$, and ${}^3P_2{}^0$ and one singlet state ${}^1P_1{}^0$ in order of increasing energy and separated by approximately an electron volt.[10] Because the coupling is not pure LS but is in part JJ, the multiplicity selection rule $\Delta S=0$ is not stringent. However, the dipole radiation selection rules for angular orbital momentum $\Delta L=\pm 1$ and for total angular momentum $\Delta J=0,\ \pm 1$ (except $J=0\rightarrow J'=0$) and for parity are applicable.[11] Therefore, it is tentatively deduced that the absorption bands of KCl:Tl at 1960 and 2490A, having oscillator strengths of approximately 0.1, arise from ${}^1S_0\rightarrow{}^1P_1{}^0$ and ${}^1S_0\rightarrow{}^3P_1{}^0$ transitions, respectively. The emission band at 3050A has a transition probability greater than 10^4 sec^{-1} and is similarly attributed to the ${}^3P_1{}^0\rightarrow{}^1S_0$ transition. Because a quantitative configuration coordinate model approach is expected to be most feasible for the ground and lowest excited states, the calculation will be confined to the ${}^1S_0$ and ${}^3P_1{}^0$ states. The results of the calculation should refute or confirm the tentative conclusions as to the origin of the 2490A absorption band and of the 3050A emission band, as well as being a critical test of the model.

The substitution in dilute concentration of Tl^+, either in the ${}^1S_0$ or ${}^3P_1{}^0$ state, for K^+ in KCl produces localized distortion of the perfect lattice. The spherically symmetrical ${}^1S_0Tl^+$ interacting with Cl^- has a different ionic radius r_0, polarizability α, and exponential variation of repulsion energy $1/\rho$ than K^+; therefore, the six nearest Cl^- neighbors will be equally displaced radially from the Tl^+ from the perfect KCl lattice positions to new positions of equilibrium. More distant ions will be similarly displaced. However, the displacements will be rapidly reduced with distance from the Tl^+. The energy changes accompanying these displacements will be even more rapidly decreased because of the parabolic dependence of energy on displacement. The nonspherically symmetrical free ${}^3P_1{}^0Tl^+$ on substitution for K^+ in the KCl will suffer partial quenching of the orbital angular momentum so that similar symmetric displacements will occur to a different equilibrium atomic configuration dependent on the r_0, α, and ρ of the excited state and on possible

[10] R. F. Bacher and S. Goudsmit, *Atomic Energy States* (McGraw-Hill Book Company, Inc., New York, 1932).
[11] E. U. Condon and G. H. Shortley, *Theory of Atomic Spectra* (Cambridge University Press, London, 1935).

coulomb overlap effects arising from the more diffuse total radial charge density of the excited state.

The only interaction energies strongly dependent on the state of the Tl^+ are those between the $Tl^+(000)$† and the six nearest Cl^- neighbors (100 and equivalent sites). Therefore, the Tl^+ nearest Cl^- neighbor distance is clearly the significant configuration coordinate. The symmetric displacement of the six Cl^- from the perfect KCl lattice positions is defined as Δa. The energy of the system as a function of Δa is uniquely determined only if specific restrictions are placed on the displacements of the remainder of the ions in the lattice. The required restriction is, of course, that the remainder of the ions in lattice, are displaced to positions minimizing the total energy. A good approximation to this condition is found to require only the displacement of the six K^+ (200 and equivalent sites) radially from the nearest Cl^- to the position of minimum energy. The symmetric displacement of the six K^+ from the perfect KCl lattice positions is defined as $\Delta a'$, and the position of minimum energy is $\Delta a_m'$. The displacement $\Delta a_m'$ is a function of Δa and is independent of the state of the Tl^+. The greater importance of this displacement compared to the displacement of the nearest K^+ (110 and equivalent sites) arises from the $(100)Cl^-$ being displaced toward the $(200)K^+$.

The optical absorption process occurs in accord with the Franck-Condon principle; that is, the transition from the $^1S_0$ to $^3P_1^0$ state occurs maintaining the atomic configurations characteristic of the $^1S_0$ state. Following absorption, because the lifetime of the excited state is long compared to the period of a lattice vibration, the system will come to thermal equilibrium with the lattice for the Tl^+ in the $^3P_1^0$ state. Emission will then occur in accord with the Franck-Condon principle maintaining the atomic configurations characteristic of the excited state; and following emission, rearrangement energy will again be given to the lattice. For both absorption and emission, all configurations accessible through thermal vibrations must be summed to obtain the complete spectra.

For the system of $^1S_0Tl^+$ substituted in dilute concentration for K^+ in KCl, the changes in total energy of the system can be readily calculated as a function of Δa and $\Delta a'$ because the values of ionic radius r_0, polarizability α, and exponential variation of repulsion energy ρ have been determined by Mayer.[8] The energy changes consist of a component arising from substituting the Tl^+ for K^+ in the perfect KCl lattice and a component arising from the distortion Δa, $\Delta a'$. Madelung, exchange repulsion, van der waals, and ion-induced dipole interactions are included.

For the system of $^3P_1^0Tl^+$, r_0, α, and ρ are not measurable and have not previously been computed. Therefore, prerequisite to evaluating the changes in total energy of the system as a function of Δa and $\Delta a'$, a theoretical basis for these parameters must be formulated, tested on the ground states of ions, and then applied to the excited state of Tl^+. In addition, the possibility of additional interaction energies peculiar to excited ionic states, such as coulomb overlap interactions, must be investigated.

† xyz coordinates in units of the interatomic distance.

III. PROPERTIES OF THE EXCITED THALLOUS ION

The parameters r_0 and α are properties of the individual ion and therefore functions of the radial charge density of the ion, and ρ is a property of two interacting ions and therefore a function of the radial charge densities of the interacting ions. The success of the Born-Mayer[8] model of ionic crystals and the approximate invariance of α for the free and combined ion[12] suggests that r_0, α, and ρ can be computed from the radial charge density of the free ion. If these parameters can be evaluated theoretically for K^+ and Tl^+ in the ground state interacting with Cl^-, it is justified to apply the same theory to evaluate these parameters for $^3P_1^0Tl^+$. The radial charge densities $\sum_i P_i^2$ for free K^+ and free Cl^- have been evaluated by the Hartree self-consistent field method[13] by Hartree and Hartree.[14,15] However, $\sum_i P_i^2$ have not been evaluated for $^1S_0Tl^+$ or for $^3P_1^0Tl^+$. The parameters r_0, α, and ρ, as well as coulomb overlap effects, are primarily a function of the contribution to the radial charge density of the outershell electrons. Therefore, the radial charge densities of the $6s^2$ electrons for $^1S_0Tl^+$ and the $6s6p$ electrons for $^3P_1^0Tl^+$ will be evaluated quite accurately by the Hartree self-consistent field method, whereas the total radial charge density of the 78 electrons $1s^2\cdots5d^{10}$ of the core will be evaluated approximately by the Sommerfeld modification[16] of the Fermi-Thomas statistical method.[17]

For the Fermi-Thomas method applied to central fields the radial charge density of the core P_c^2 is related to the potential of the core V_c:

$$P_c^2=[2me(V_c-V_0)]^{\frac{1}{2}}32\pi^2r^2/3h^3. \qquad (3\text{–}1)$$

The calculation of V_c is handled differently depending on r, the distance from the nucleus. For $r<0.75$,‡ V_c is essentially the same as for neutral Tl^0, and is

$$V_c=Ze\chi(r)/r, \quad r<0.75, \qquad (3\text{–}2)$$

where $\chi(r)$ is the solution of the ordinary Fermi-Thomas equation,

$$r^{\frac{1}{2}}d^2\chi(r)/dr^2=\chi(r)^{\frac{3}{2}}, \qquad (3\text{–}3)$$

[12] J. H. Van Vleck, *Theory of Electric and Magnetic Susceptibilities* (Oxford University Press, New York, 1932), p. 222.
[13] D. R. Hartree, Proc. Cambridge Phil. Soc. **24**, 89, 111 (1928).
[14] D. R. Hartree and W. Hartree, Proc. Roy. Soc. (London) **166A**, 460 (1938).
[15] D. R. Hartree and W. Hartree, Proc. Roy. Soc. (London) **156A**, 59 (1936).
[16] A. Sommerfeld, Z. Physik **78**, 283 (1932).
[17] Reference 11, p. 335.
‡ Radial distances are expressed in atomic units,

$$1 \text{ atomic unit}=h^2/4\pi^2me^2=0.5292\text{A}.$$

TABLE I. Potential and normalized total radial charge density of trivalent thallium by the Sommerfeld modification of the Fermi-Thomas method.

r (au)*	V (au) Fermi-Thomas	Sommerfeld	ΣP_n^2 (au^{-1})
0.0189	3810		122.6
0.0306	2209		140.4
0.0500	1228		155.5
0.0757	722.1		159.1
0.1200	379.9		153.4
0.189	190.7		134.9
0.250	119.5		117.5
0.340	68.6		92.07
0.500	32.04		61.73
0.633	19.39	(19.62)	46.60
0.750		12.84	33.4712
1.00		6.871	21.3083
1.10		5.5733	
1.20		4.6217	
1.40		3.3448	
1.50			9.9276
1.70		2.3136	
2.00		1.7211	5.1000
2.40		1.3105	
2.50		1.2426	2.6768
2.80		1.0813	
3.00			0.9705
3.20		0.9224	
3.782 (r_0)		0.7937	0.0000

* Atomic units.

and has been computed numerically,[17] and Z is the atomic number. The values of V_c and P_c^2 obtained from Eqs. (3–2) and (3–1) are tabulated in columns 2 and 4 of Table I. For $r>0.75$ the Sommerfeld modification[16] for ions must be used and V_c is

$$V_c=(Ze/r)\psi(r)+\sigma e/r_s, \quad 0.75<r<r_s, \tag{3–4}$$

$$V_c=\sigma e/r, \quad r>r_s, \tag{3–5}$$

where σ is the valence of the ion; r_s is the Sommerfeld radius of the ion and is

$$r_s=(h^2/4\pi^2me^2)(9\pi^2/128Z)^{\frac{1}{3}}12^{\frac{1}{3}}z_0^{\frac{1}{3}},$$

in which z_0 is obtained from

$$z_0/(1+z_0)^{\frac{1}{2}\lambda_1+1}=\sigma/\lambda_1 Z$$

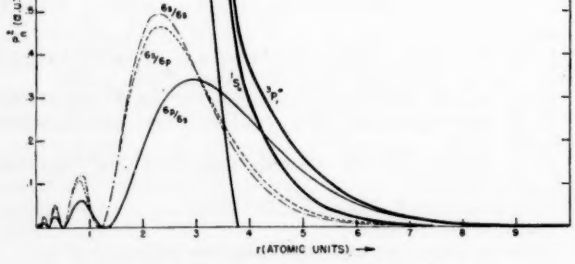

FIG. 1. Radial charge densities of $^1S_0$ and $^3P_1{}^0Tl^+$.

and $\psi(r)$ is

$$\Psi(r)=\frac{1}{(1+z)^{\frac{1}{2}\lambda_1}}\left[1-\left(\frac{1+z}{1+z_0}\right)^{\lambda_1/\lambda}\right]. \tag{3–6}$$

The parameter z is

$$z=1.5482r^{\lambda},$$

and λ and λ_1 are constants equalling 7.772 and 0.772, respectively. The values of V_c and P_c^2 for Tl^{+++} obtained from Eqs. (3–4) and (3–6) and from Eq. (3–1) are tabulated in columns 3 and 4 of Table I. Incidentally, V_0 for the ion is equal to $\sigma e/r_s$. For $r>r_s$, V_c is coulombic and P_c^2 is zero. In the region of r_s, P_c^2 is plotted on Fig. 1.

For the calculation of the radial charge density P_i^2 of the i outershell electron in the potential of the core V_c and the potential of the other outershell electron V_j, the Hartree[13] form of the Schroedinger equation is used:

$$(d^2P_i/dr^2)+[-2(V_c+V_j)-\epsilon_i - l_i(l_i+1)/r^2]P_i=0, \tag{3–7}$$

where ϵ_i is the eigenvalue for the i electron and l_i is the angular orbital momentum quantum number. V_j and P_j^2 are related:

$$V_j=-\int_r^{\infty}\left(\left[1-\int_r^{\infty}P_j^2dr\right]\Big/r^2\right)dr; \tag{3–8}$$

P_c^2 and V_c are considered invariant. However, P_i^2 and therefore V_i are dependent on V_j; and, consequently, the outer shell electrons must be treated self-consistently. Initial P_i^2 and P_j^2 are obtained from the Sommerfeld-Fermi-Thomas treatment of Tl^+, Tl^{++}, and Tl^{+++} and are substituted in Eq. (3–8) to provide tentative V_i and V_j. The V_c and tentative V_i and V_j are substituted in Eq. (3–7), which is numerically integrated to provide improved values of P_i^2 and P_j^2. In the detailed calculations, modified forms[13] of Eq. (3–7) are used at very small and very large r. ϵ_i and ϵ_j are adjusted to provide continuous and finite P_i^2 and P_j^2, respectively. The improved P_i^2 and P_j^2 are normalized and substituted in Eq. (3–8), and the numerical integration including adjustment of ϵ_i and ϵ_j recalculated. The procedure is repeated until the initial and final P_i^2 and P_j^2 are identical. For $^1S_0Tl^+$, both i and j are 6s, so that l is 0; for $^3P_1{}^0Tl^+$, i and j are 6s and 6p, so that l is 0 and 1, respectively. Final V_c, V_i, and V_j are tabulated in Table II and final P_i^2 and P_j^2 for the $^1S_0$ and $^3P_1{}^0$ states are tabulated in Table III. In addition, the normalized radial charge densities P_n^2 of the 6s in the field of the core and the 6s, the 6s in the field of the core and the 6p, and the 6p in the field of the core and the 6s are plotted on Fig. 1. The resultant total radial charge densities of the $^1S_0Tl^+$ and $^3P_1{}^0Tl^+$ are also plotted.

From examination of the total radial charge densities of $^1S_0Tl^+$ and $^3P_1{}^0Tl^+$, the following conclusions are

TABLE II. Potential due to core and individual outershell electrons for monovalent thallium.

r (au)	Tl^{+++} (core)	V (au) $6s/6p$	$6s/6s$	$6p/6s$
1.1	+5.5733			
1.2	4.6217	−0.3990	−0.3947	−0.3124
1.4	3.3448	−0.3938	−0.3894	−0.3094
1.6			−0.3843	
1.7	2.3136	−0.3853	−0.3813	−0.3058
1.8			−0.3779	
2.0	1.7211	−0.3736	−0.3695	−0.3013
2.2			−0.3591	
2.4	1.3105	−0.3509	−0.3472	−0.2923
2.6			−0.3342	
2.8	1.0813	−0.3237	−0.3207	−0.2796
3.0			−0.30707	
3.2	0.9224	−0.2960	−0.2936	−0.2645
3.4			−0.2806	
3.6	0.8329	−0.2699	−0.2681	−0.2484
3.78	0.7937			
3.8			−0.2562	
4.0	0.7500	−0.2465	−0.2451	−0.2322
5.0	0.6000	−0.2001	−0.1994	−0.1951
5.8			−0.1723	
6.0	0.5000	−0.1674		−0.1654
6.2			−0.1613	
7.0	0.4286	−0.1436	−0.1430	−0.1425
8.0	0.3750		−0.1250	−0.1249
8.2		−0.1220	−0.1220	
9.0	0.3333	−0.1111	−0.1111	−0.1111
10.0	0.3000	−0.1000	−0.1000	−0.1000
11.0	0.2727			−0.09091

deduced as characterizing the excited Tl^+ compared to unexcited Tl^+:

(1) Because the radial charge density of $^3P_1{}^0Tl^+$ is more diffuse, it is apparent that the polarizability α is greater. (2) The charge density is greater at distances r comparable with or greater than the ionic radius of the ground state; therefore, it is concluded that the ionic radius r_0 of $^3P_1{}^0Tl^+$ is greater. (3) Because the derivative of charge density with radial distance is everywhere less, the $^3P_1{}^0$ is more compressible; that is, ρ is greater. The exact calculation of α, r_0, and ρ of $^3P_1{}^0Tl^+$ depends on theories relating these parameters quantitatively to radial charge density.

The polarizability of $^3P_1{}^0Tl^+\alpha'$ is calculated in three ways. The first two methods utilize the formula of Kirkwood:[18]

$$\alpha = -K\left[\sum_i \int_0^\infty r^2 P_i^2 dr\right]^2, \qquad (3\text{–}9)$$

where K is a constant for ions containing the same number of electrons. The polarizability of $^1S_0Tl^+\alpha$ is known experimentally.[10] The ratio α'/α is a function only of the P_i^2 for all electrons. However, the individual P_i^2 have been determined only for the outershell electrons so that, although these electrons contribute most to the polarizability, the contribution of the core must be treated approximately. If the polarizability of the core is considered negligible, α' is computed to be

[18] J. G. Kirkwood, Physik. Z. 33, 57 (1932).

TABLE III. Normalized Hartree radial charge densities of the outershell electrons in field of the core and the other outshell electrons for free monovalent thallium.

r (au)	P_n^2 (au^{-1}) $6s/6p$	$6s/6s$	$6p/6s$
0.01	0.00493	0.00451	
0.025	0.00003	0.00003	
0.035			0.00575
0.05	0.01207	0.01104	
0.08			0
0.09	0	0	
0.10	0.00202	0.001848	0.00407
0.14			0.01185
0.15	0.02494	0.02282	
0.20	0.00560	0.00512	0.00108
0.22			0.00007
0.225	0	0	
0.25	0.00600	0.005487	
0.27			0.01023
0.30	0.03614	0.033074	0.01884
0.34			0.02465
0.35	0.05050	0.046212	
0.40	0.03523	0.03224	0.01808
0.45	0.01084	0.009922	0.00685
0.50	0	0	0.00028
0.55	0.01105	0.010107	0.00272
0.60	0.03886	0.035555	0.01331
0.65	0.07256	0.066119	0.02828
0.70	0.10059	0.092048	0.04331
0.80	0.11990	0.109716	0.06180
0.85			0.06300
0.90	0.09118	0.083436	0.05928
1.00	0.04454	0.04076	0.042111
1.1	0.00881	0.008047	0.02114
1.2	0.00106	0.000978	0.00542
1.3	0.02462	0.02261	0.00001
1.4	0.07419	0.06800	0.00631
1.5	0.14059	0.12874	0.02336
1.6	0.21371	0.19599	0.04895
1.7	0.28537	0.26238	0.07970
1.8	0.34974	0.32251	0.11402
1.9	0.40332	0.37309	0.14923
2.0	0.44450	0.41256	0.18349
2.1	0.47297	0.44064	0.20891
2.2	0.48947	0.45793	0.24467
2.3	0.49523	0.46541	0.270214
2.4	0.49161	0.46430	0.29192
2.5	0.48036	0.45601	0.30964
2.6	0.46213	0.44290	0.32337
2.7		0.42622	0.33321
2.8	0.41523	0.40580	0.339428
2.9		0.38452	0.34236
3.0	0.36004	0.36206	0.34238
3.2	0.30378	0.31274	0.33467
3.4	0.25072	0.26458	0.31900
3.6	0.20330	0.22036	0.29886
3.8	0.16234	0.18062	0.27533
4.0	0.12789	0.14612	0.24991
4.2	0.09957	0.11683	0.22371
4.4	0.07672	0.09236	0.19769
4.6	0.05849	0.07235	0.17273
4.8	0.04422	0.05605	0.14938
5.0	0.03316	0.04323	0.12798
5.5	0.01543	0.02178	0.08399
6.0	0.00715	0.01058	0.05287
6.5	0.00317	0.00498	0.03213
7.0	0.00147	0.00229	0.01897
7.5	0.00058	0.00103	0.01092
8.0	0.00024	0.00046	0.00616
8.5	0.00010	0.00020	0.00340
9.0	0.00004	0.00008	0.00186
9.5		0.00004	0.00099
9.8	0.00001	0.00002	
10.0			0.00053
ϵ (au)	1.25	1.150	0.770

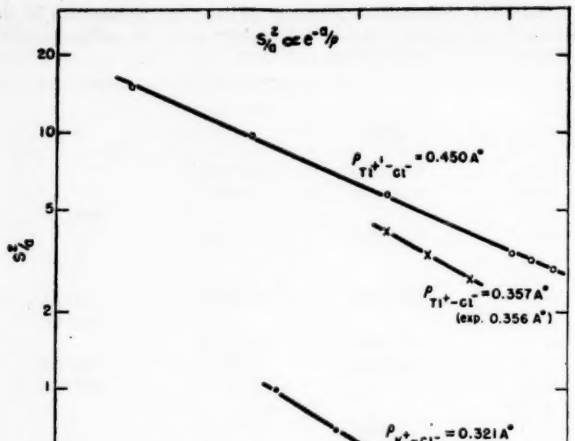

FIG. 2. Dependence of overlap integral S on interatomic distance a.

5.56A³; whereas, if the mean square radii of the core electrons are considered identical and determined by the Fermi-Thomas radial charge density, α' of 5.03A³ is obtained. The third method utilizes the empirical observation that electronic polarizability is proportional to the fourth power of the ionic radius, and from the ionic radius of $^3P_1{}^0Tl^+$ derived in the following section, α' is evaluated as 5.52A³. It is gratifying that the three values agree within 10 percent. The numerical average 5.37A³ will be used in the lattice energy calculations involving $^3P_1{}^0Tl^+$.

The repulsion energy of two interacting ions separated by the distance a is:

$$E_R = b \exp[-(a-a_0)/\rho], \tag{3-10}$$

where b is determined by the valences and numbers of outershell electrons of the ions, a_0 is the sum of the ionic radii and is obtained from lattice constants, and ρ is related to compressibility. For one ion in an excited state, the ionic radius of the excited ion r_0' and ρ' characteristic of the ion pair must be determined from theoretical considerations. A simple procedure will first be used to estimate r_0', and then a more refined procedure will be used to evaluate r_0' and ρ' simultaneously. A simple criterion for r_0' of $^3P_1{}^0Tl^+$ is the radius beyond which the total charge

$$\int_{r_0'}^{\infty} \sum_i P_i^2 dr$$

is identical with total charge beyond the known ionic radius, 1.49A, or $^1S_0Tl^+$. From the data of Tables I and II and Fig. 1, r_0' is computed to be 1.638A. This method is limited because equal weight is assigned charge at just beyond and at large distances beyond the ionic radius, whereas actually the latter contributes more effectively to the exchange repulsion. An improved r_0' and also ρ' can be evaluated from overlap integrals. A plausible form of the exchange repulsion energy is:

$$E_R = K'S^2/a, \tag{3-11}$$

where K' is a constant and S is an overlap integral defined:

$$S = \int_V \varphi_A \varphi_B dV, \tag{3-12}$$

where φ_A is the square root of the total charge density of the unperturbed A ion at a distance r_A from the nucleus:

$$\varphi_A = (\sum P_A{}^2)^{\frac{1}{2}}/r_A, \tag{3-13}$$

and the integration is over all space. Equation (3-12) is simplified in Appendix I to yield:

$$S = \frac{2\pi}{a} \int_0^r r(a-r)\varphi_A dr \int_{(a-r)}^{\infty} \varphi(y) dy. \tag{3-14}$$

Equation (3-14) can be integrated numerically for $^3P_1{}^0Tl^+$ and $^1S_0Tl^+$ interacting with Cl^- from the data of Tables I and III and the P^2 for Cl^- of Hartree and Hartree,[15] and with the condition:

$$S'^2/a_0' = S^2/a_0; \tag{3-15}$$

r_0' is computed to be 1.64A. In addition, S^2/a is computed, tabulated in Table IV, and plotted in Fig. 2 as a function of a for K^+, $^1S_0Tl^+$, and $^3P_i{}^0Tl^+$ interacting with Cl^-. The P^2 for K^+ are obtained from Hartree and Hartree.[14] From Eq. (3-10) and the computed S^2/a, theoretical values of ρ for K^+-Cl^- and $^1S_0Tl^+-Cl$ within 2 percent of the experimental values are obtained and shown on Fig. 2 in striking confirmation of Eq. (3-11). It is therefore warranted to use the theoretical ρ' of 0.450A, as well as the theoretical r_0' of 1.64A, for the lattice energy calculations.

TABLE IV. Overlap integrals *versus* interionic distance.

Ion pair	Distance, a (au)	Overlap integral, S	S^2/a
K^+-Cl^-	5.733	2.376_6	0.985_2
K^+-Cl^-	5.933	2.032_5	0.696_3
K^+-Cl^-	6.133	1.765_3	0.508_1
Tl^+-Cl^-	6.096	4.99_5	4.09_3
Tl^+-Cl^-	6.236	4.57_9	3.36_2
Tl^+-Cl^-	6.376	4.15_3	2.70_5
$Tl^{+\prime}-Cl^-$	5.250	8.83_8	14.86
$Tl^{+\prime}-Cl^-$	5.650	7.38_1	9.63
$Tl^{+\prime}-Cl^-$	6.100	5.90_3	5.71
$Tl^{+\prime}-Cl^-$	6.516	4.69_5	3.38_3
$Tl^{+\prime}-Cl^-$	6.579	4.57_5	3.18_1
$Tl^{+\prime}-Cl^-$	6.656	4.41_8	2.93_2

IV. LATTICE ENERGY CALCULATIONS

With the polarizabilities, ionic radii, and rates of exponential variation of repulsion energy determined for K^+, $^1S_0Tl^+$, and $^3P_1{}^0Tl^+$, the change in total energy of the system resulting from substituting in dilute concentration $^1S_0Tl^+$ or $^3P_1{}^0Tl^+$ for K^+ in KCl can be calculated. The energy change E for $^1S_0Tl^+$ and E' for $^3P_1{}^0Tl^+$ are computed as a function of Δa and $\Delta a'$. Madelung, exchange repulsion, van der waals, and ion-induced dipole interactions are included. The energy difference between the configuration Δa, $\Delta a'$ with the substituted Tl^+ and the perfect KCl lattice is computed in each case. In addition, because of the more diffuse radial charge density of $^3P_1{}^0Tl^+$ evidenced by Fig. 1, a coulomb overlap interaction will be included in E'. Also, E' includes the difference in electronic energies of the free $^3P_1{}^0Tl^+$ and $^1S_0Tl^+$.

The change in Madelung energy or coulombic energy of a system of point ions is readily computed. The Madelung energy is independent of the state of the ions and is a function only of their valences and of Δa and $\Delta a'$. Because coulomb energies vary only as the reciprocal of separation distance, a large number of interactions with quite distance ions must be included.

The repulsion energy change is markedly dependent on ρ and a_0 as shown by Eq. (3–10), and is therefore different for $^1S_0Tl^+$ and $^3P_1{}^0Tl^+$. The repulsion energy rapidly decreases with separation distance so that relatively few interaction energy changes need be computed.

Both dipole-dipole and quadripole-dipole interaction terms are included in the changes in van der waals energies. The total van der waals energy is[8]

$$E_D=-\frac{[S_6'c_{+-}+S_6''(c_{++}+c_{--})/2]}{a^6}-\frac{[S_8'd_{+-}+S_8''(d_{++}+d_{--})/2]}{a^8}, \quad (4\text{–}1)$$

where the S_N result from summing over the ions and are determined by the crystal structure, and the c and d are characteristic of individual ion pairs and are functions of the polarizability and ionization energy of the ions. The c and d for KCl and $^1S_0TlCl$ have been tabulated by Mayer[8] and for $^3P_1{}^0TlCl$ are readily evaluated from α' and free ion spectra.[10] In computing the changes in van der waals energies it is convenient to evaluate the energy change resulting from the substituted Tl^+ interacting with all other ions except the displaced neighbors by using the sums S_N and the energy changes resulting from the displaced ions interacting with all other ions individually.

In a perfect crystal lattice the ion-induced dipole interaction is zero because the dipole that is induced on an ion from one neighbor will be exactly canceled by the dipole induced by the neighbor on the opposite side equally distant. In the distorted crystal with nonzero Δa and $\Delta a'$, an ion-induced dipole interaction exists. The moment of the induced dipole is:

$$M=\alpha\sum_i e_i\bar{a}_i/a_i^3, \quad (4\text{–}2)$$

where α is the polarizability of the polarized ion, a_i is the distance from the i ion to the dipole, and $\bar{a}_i$ is the component of the distance from the i ion to the dipole in the direction of the dipole. The interaction energy is[19]

$$E_P=-\tfrac{1}{2}eM\sum_i \bar{a}_i/a_i^3. \quad (4\text{–}3)$$

Because the diffuse radial charge density of the $^3P_1{}^0Tl^+(000)$ extends beyond the (100) position, the effective charge e_i creating the dipole in the (100) ion is not equal to e; therefore, the ion induced dipole energy will be a function not only of Δa and $\Delta a'$ but also dependent on the state of the Tl^+.

The coulomb overlap interaction for E' is computed as a difference in coulomb overlap energies for the $^3P_1{}^0Tl^+$ and the $^1S_0Tl^+$ from the total radial charge densities $\sum_i P_i^2$ of the free ions. The components of the coulomb overlap energies for spherically symmetrical ions are derived in Appendix II and are

TABLE V. Coulomb overlap energies.

Δa(A)	$\Delta\epsilon_1$	$\Delta\epsilon_2$	$\Delta\epsilon_3$	$\Delta\epsilon_4$	$\Delta\epsilon$ (ev)
−0.36	−4.2205	+0.0412	−4.4687	+5.8014	−2.8465
−0.16	−2.9453	+0.0262	−2.6845	+3.6968	−1.9069
0	−1.9816	+0.0137	−1.7562	+2.3137	−1.4104
+0.16	−1.5086	+0.0066	−1.1731	+1.5793	−1.0959

$$\Delta\epsilon_1=\frac{1}{4a}\int_0^\infty[\varphi^2{}_{Tl^{+\prime}}(r_1)-\varphi^2{}_{Tl^+}(r_1)]\times\int_{|a-r_1|}^{a+r_1} r_1r_2\varphi^2{}_{Cl^-}(r_2)[r_1+r_2-a]^2dr_2dr_1,$$

$$\Delta\epsilon_2=\int_0^\infty r_1^2[\varphi^2{}_{Tl^{+\prime}}(r_1)-\varphi^2{}_{Tl^+}(r_1)]\times\int_{a+r_1}^\infty r_2^2\varphi^2{}_{Cl^-}(r_2)\left[\frac{1}{a}-\frac{1}{r_2}\right]dr_2dr_1,$$

$$\Delta\epsilon_3=\int_0^\infty r_2^2\varphi^2{}_{Cl^-}(r_2)\int_{a+r_2}^\infty r_1^2[\varphi^2{}_{Tl^{+\prime}}(r_1)-\varphi^2{}_{Tl^+}(r_1)]\left[\frac{1}{a}-\frac{1}{r_1}\right]dr_1dr_2,$$

$$\Delta\epsilon_4=Z_{Cl^-}\int_a^\infty r_1^2[\varphi^2{}_{Tl^{+\prime}}(r_1)-\varphi^2{}_{Tl^+}(r_1)]\left[\frac{1}{a}-\frac{1}{r_1}\right]dr_1, \quad (4\text{–}4)$$

where $\Delta\epsilon_1$, $\Delta\epsilon_2$, $\Delta\epsilon_3$, and $\Delta\epsilon_4$ are, respectively, the cou-

[19] O. K. Rice, *Electronic Structure and Chemical Binding* (McGraw-Hill Book Conpany, Inc., New York, 1940), p. 462.

TABLE VI. Energy changes E(ev) for $Tl^{+\prime}(^3P_1{}^0)$ and $Tl^+(^1S_0)$ in KCl *versus* Δa(A°) and $\Delta a'$(A°).

Δa	Madelung	Repulsion	Van der Waals	Ion dipole	Coulomb overlap	Total energy change
$Tl^{+\prime}(^3P_1{}^0)$	$\Delta a'=0$					
−0.36	+0.465146	+3.8287	−2.4097	−0.13024	−2.8465	+5.3974
−0.25	+0.214243	+2.7931	−1.8602	−0.07204	−2.2762*	+5.2889*
−0.16	+0.084074	+2.1803	−1.5283	−0.02499	−1.9069	+5.2942
0	0	+1.5126	−1.1252	−0.00168	−1.4104	+5.4653
−0.16	+0.071281	+1.3136	−0.9014	−0.06830	−1.0959	+5.8093
$Tl^+(^1S_0)$	$\Delta a'=0$					
−0.36	$+0.46514_6$	+3.6310	−1.6613	−0.2865		+2.1483
−0.16	$+0.08407_4$	+1.6821	−1.0299	−0.0514		+0.6849
0	0	+0.9695	−0.7533	0		+0.2162
+0.06	$+0.01069_5$	$+0.8607_0$	-0.6922_4	-0.0065_2		$+0.1726_4$
+0.10	$+0.02905_9$	$+0.8192_2$	-0.6428_8	−0.0164		$+0.1889_9$
+0.16	$+0.07128_1$	$+0.8158_8$	-0.6143_9	-0.0447_7		+0.2280
+0.24	$+0.15331_6$	$+0.9194_3$	-0.5872_6	-0.0956_4		$+0.3898_5$
$Tl^+(^1S_0)$	$\Delta a'=+0.06$					
0	$+0.00047_1$	+1.0020	-0.7545_6	-0.0086_2		$+0.2392_9$
+0.06	$+0.02628_4$	$+0.8556_8$	-0.6903_0	-0.0201_4		$+0.1715_2$
+0.10	$+0.05538_8$	$+0.7949_2$	-0.6377_9	-0.0325_9		$+0.1799_3$
+0.16	$+0.11479_7$	$+0.7578_7$	-0.6046_5	-0.0667_4		$+0.2012_8$
+0.24	$+0.22195_8$	$+0.8070_1$	-0.5670_9	-0.1206_6		$+0.3412_1$
$Tl^+(^1S_0)$	$\Delta a'=+0.12$					
+0.24	$+0.29056_6$	+0.7543	−0.56209	−0.14975		$+0.3330_3$

* Coulomb overlap energy determined by interpolation.

lomb overlap correction for intersecting spherical shells of charge, shells of Cl^- charge encircling Tl^+ shells, shells of Tl^+ charge encircling Cl^- shells, and shells of Tl^+ encircling the nuclear charge Z_{Cl^-}. The numerical values are tabulated as a function of Δa in Table V.

In Table VI the lattice energies are tabulated for $^3P_1{}^0Tl^+$ and $^1S_0Tl^+$ as a function of Δa and $\Delta a'$. Because the only interactions peculiar to the state of the Tl^+ involve the nearest Cl^- neighbors, $\Delta a_m'$ is a function only of Δa, and for small displacements must be proportional to Δa. Also, the energy must be parabolic with Δa and $\Delta a'$ for small displacements about the equilibrium positions. The following form is therefore indicated:

$$E=A(\Delta a-\Delta a_0)^2+B(\Delta a'-d\Delta a)^2+E_0, \quad (4\text{–}5)$$

where B and d are independent of the state of the Tl^+ and are evaluated by the method of least squares to be 6.41 ev/A² and 0.4264/A, respectively. The total energy changes of the system can now be transformed to the $\Delta a_m'$ plane; that is, the energy change as a function of the Tl^+ nearest Cl^- distance with the condition that the lattice rearranges to minimize the total energy. The results of the transformation are tabulated in Table VII and plotted on Fig. 3. Striking confirmation of Eq. (4–5) is demonstrated on Fig. 3 by the excellent agreement with the computed points of the plotted parabolas fitted by the method of least squares.

TABLE VII. Energy changes for $Tl^+(^1S_0)$ and $Tl^{+\prime}(^3P_1{}^0)$ *versus* Δa for $\Delta a_m'$.

Δa (A°)	$\Delta E_{\Delta a_m'}$ (ev)	$\Delta E'_{\Delta a_m'}$ (ev)
−0.36	1.9849	5.2463
−0.25		5.2161
−0.16	0.6526	5.2644
0	0.2162	5.4653
0.06	0.1663	5.7795
0.10	0.1773	
0.16	0.1981	
0.24	0.3255	

V. ABSORPTION AND EMISSION SPECTRA

The plots and analytic expressions for total energy E *versus* the configuration coordinate Δa shown in Fig. 3 for the $^1S_0Tl^+$ and $^3P_1{}^0Tl^+$ systems can be used to evaluate absorption and emission spectra. The transition energy is

$$\Delta E=E'-E=-5.2070(\Delta a)^2+3.3278(\Delta a)+5.2120. \quad (5\text{–}1)$$

The absorption spectrum is determined by the probability $P(\Delta E)$ of the transition energy ΔE from the $^1S_0Tl^+$ system to the $^3P_1{}^0Tl^+$ system. $P(\Delta E)$ is a function of the probability of the configuration of the $^1S_0Tl^+$ resulting in the transition energy ΔE and of the variation in transition energy ΔE with configuration. Because the configuration Δa refers to atomic coordinates, a Boltzmann distribution of configurations is appropriate. Therefore, for absorption:

$$P(\Delta E)=C\exp[-(E-E_0)/kT]d(\Delta a)/d(\Delta E)=C\frac{\exp[-8.244_5(\Delta a-0.0950)^2/kT]}{[3.3278-10.414\Delta a]}, \quad (5\text{–}2)$$

where C is a normalization constant and E_0 is the minimum energy of the $^1S_0Tl^+$ system. The emission spec-

trum is determined by the probability $P'(\Delta E)$ of the transition energy ΔE from the $^3P_1{}^0Tl^+$ system to the $^1S_0Tl^+$ system. $P'(\Delta E)$ is a function of a Boltzmann distribution of configurations characteristic of the $^3P_1{}^0Tl^+$ system and of the variation of transition energy ΔE with configuration. Therefore, for emission

$$P'(\Delta E)=C'\exp[-(E'-E_0')/kT]d(\Delta a)/d(\Delta E)$$

$$=C'\frac{\exp[-3.217_5(\Delta a+0.2684)^2/kT]}{[3.3278-10.414\Delta a]}, \quad (5\text{–}3)$$

where C' is a normalization constant and E_0' is the minimum energy of the $^3P_1{}^0Tl^+$ system. In Fig. 4 $P(\Delta E)$ and $P'(\Delta E)$ for 298°K are plotted as a function of ΔE and compared with the experimental[20] absorption and emission spectra. The agreement is satisfactory. The theoretical peak absorption, peak emission, and half-width of absorption agree within 10 percent of experimental values. The broader theoretical emission spectrum may arise from using free ion radial charge densities for calculating the coulomb overlap interaction for the $^3P_1{}^0Tl^+$ system, or from neglecting the rearrangement energies of neighbors more distant than (200) for configurations of large $|\Delta a|$. The asymmetry of the theoretical spectra are also in accord with experiment.

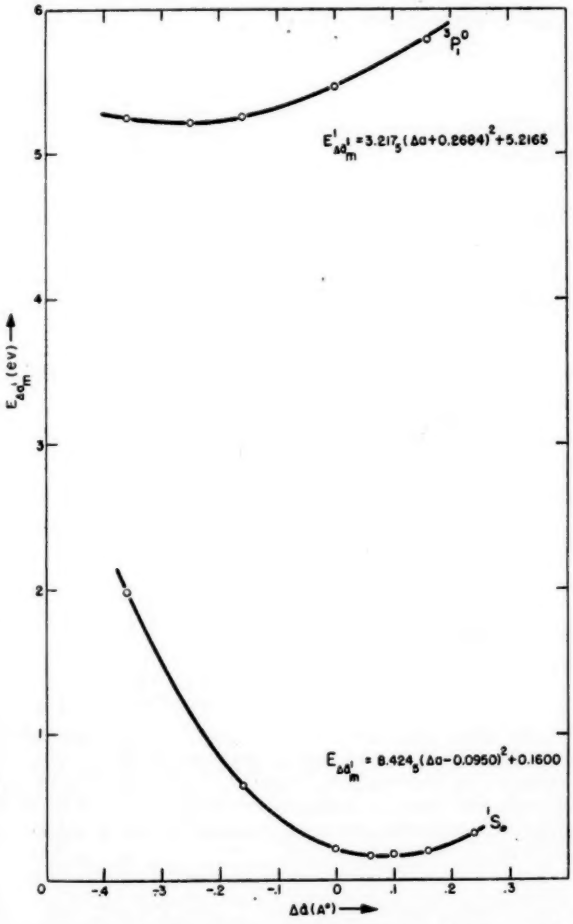

FIG. 3. Total energy changes E for $^1S_0Tl^+$ and E' for $^3P_1{}^0Tl^+$ as a function of configuration coordinate Δa.

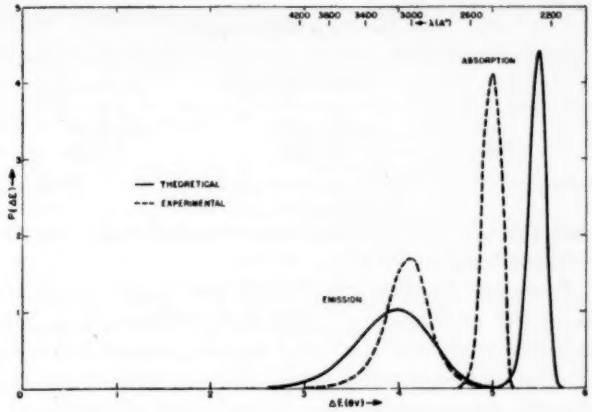

FIG. 4. Theoretical and experimental absorption and emission spectra of KCl:Tl.

From Eqs. (5–2) and (5–3) the absorption and emission spectra can be calculated at any temperature. The dependence of peak absorption and emission energies on temperature is very small and arises primarily from thermal expansion of the lattice, an effect not included in the theory. The dependence of half-width of absorption and emission spectra on temperature is quite pronounced, and arises from the Boltzmann factors of Eqs. (5–2) and (5–3). The half-widths at any temperature may be calculated by solving Eqs. (5–2) and (5–3) for the configurations Δa's resulting in probabilities $P(\Delta E)$ and $P'(\Delta E)$ equal to one-half and then substituting these values of Δa in Eq. (5–1). In Table VIII are tabulated the theoretical half-widths at various temperatures. In accord with experiment, the half-widths of both absorption and emission are halved on reducing the temperature from 298 to 80°K.§ Measurements of the spectra at 4 and 20°K are now in progress.

VI. CONCLUSIONS

It has been demonstrated in this paper that the significant luminescent properties of simple ionic phosphors can be derived quantitatively from theory. Specifically, the absorption and emission spectra of KCl:Tl at various temperatures have been quantitatively evaluated; and the agreement with experimental results confirms the interpretation that the $^1S_0\rightarrow{}^3P_1{}^0$ transition is responsible for the absorption band at 2490A and the $^3P_1{}^0\rightarrow{}^1S_0$ transition is responsible for the emission band at 3050A. It is concluded indirectly

[20] W. Koch, Z. Physik **57**, 638 (1929); W. von Meyeren, Z. Physik **61**, 321 (1930); P. D. Johnson, unpublished data of this laboratory.

§ *Note added in proof:*—Recognizing from Fig. 3 that both the ground and excited systems are harmonic oscillators, the quantum-mechanical zero point energy is computed to be 0.00830 ev for the ground state and 0.00513 ev for the excited state; therefore, negligible reduction in band widths at temperatures below 80°K is predicted.

TABLE VIII. Temperature dependence of half-widths of absorption and emission.

T °K	$\Delta E_{\frac{1}{2}}$ (abs.) ev	$\Delta E_{\frac{1}{2}}$ (em.) ev
80	0.1159	0.4729
298	0.2147	0.9142

that the $^1S_0 \rightarrow {}^1P_1{}^0$ transition is responsible for the absorption band at 1960A.

From the detailed calculations new insight is gained as to the mechanism of solid-state luminescence. The localized character of atomic rearrangements following absorption and emission is emphasized. Only the energy changes accompanying the displacement of the nearest Cl^- neighbors (100) are appreciably dependent on the state of the Tl^+; and the displacements are sufficiently small and rapidly attenuated with distance from the Tl^+, so that only the displacement of the $K^+(200)$ need also to be included for a good approximation to the condition that the remainder of the lattice rearranges to minimize the total energy. An unexpected result evident from Fig. 3 is that the equilibrium configuration characteristic of the $^3P_1{}^0Tl^+$ has a smaller $Tl^+(000)$ nearest Cl^- neighbor (100) separation than the $^1S_0Tl^+$ system. This arises from the greater polarizability, compressibility, and coulomb overlap interaction for the excited state. Obviously, for higher excited states of Tl^+, particularly for the ionized state Tl^{++}, the equilibrium configuration involves an even smaller activator nearest neighbor distance $(a_0+\Delta a)$.

Incidental to the calculation of absorption and emission spectra, it has been shown that the repulsion energy E_R is proportional to S^2/a, where S is an overlap integral and a is the separation distance. Also coulomb, overlap interactions between spherically symmetrical ions have been formulated, calculated, and demonstrated to be important for systems involving ions in excited states.

Finally, it has been demonstrated that the configuration coordinate model is useful for quantitative interpretations of solid-state luminescence.

The author is indebted to E. Alden, C. Carter, D. Cusano, J. Marinace, J. Martens, R. Speck, and L. Stevens for performing the detailed calculations, and to M. H. Hebb for helpful suggestions.

APPENDIX I. EVALUATION OF OVERLAP INTEGRAL S

$$dS=\varphi_A(r)\varphi_B(y)dv,$$

where r and y are, respectively, the distance from the volume element dv to the nucleus A and the nucleus B. Integration will be over spherical rings of radius r; therefore,

$$dv=2\pi r^2 \sin\theta dr d\theta,$$

where θ is the angle r makes with the line connecting nucleus A and nucleus B. The total overlap integral is obtained by integrating θ from 0 to π and r from 0 to a, where a is the distance separating the nuclei.

$$S=2\pi\int_0^a r^2\varphi_A(r)\int_0^\pi \sin\theta\varphi_B(y)d\theta dr.$$

The important overlap occurs at small θ where $\sin\theta\simeq\theta$, and

$$y=(r^2-2ar\cos\theta+a^2)^{\frac{1}{2}}\simeq(r^2-2ar+a^2+ar\theta^2)^{\frac{1}{2}}$$
$$\simeq\{(a-r)^2[1+ar\theta^2/(a-r)^2]\}^{\frac{1}{2}}\simeq(a-r)[1+ar\theta^2/2(a-r)^2],$$

and

$$S=\frac{2\pi}{a}\int_0^a r(a-r)\varphi_A(r)\int_{(a-r)}^\infty \varphi_B(y)dydr.$$

APPENDIX II. COULOMB OVERLAP INTERACTIONS

1. Intersecting Spherical Shells, $r_2+r_1>a>r_2-r_1$ $(r_2>r_1)$

For two intersecting spherical shells of charge $r_1^2\varphi_A^2(r_1)$ and $r_2^2\varphi_B^2(r_2)$ at distances r_1 and r_2 from their respective nuclei A and B, separated by the distance a, the correction to the Madelung energy for overlap is from geometrical considerations:

$$d\epsilon_1=\frac{r_1^2r_2^2\varphi_A^2(r_1)\varphi_B^2(r_2)}{2}\left\{\frac{1}{r_2^2}\int_0^{\theta_m}\sin\theta d\theta - \int_0^{\theta_m}\frac{\sin\theta d\theta}{(a^2+r_1^2-2ar_1\cos\theta)^{\frac{1}{2}}}\right\},$$

where θ is the angle r_1 makes with the line connecting the nuclei, and θ_m is

$$\theta_m=\cos^{-1}[(a^2+r_1^2-r_2^2)/2ar_1].$$

Integration over θ yields

$$d\epsilon_1=-r_1r_2\varphi_A^2(r_1)\varphi_B^2(r_2)(r_1+r_2-a)^2/4a,$$

and integration over r_1 and r_2, preserving the conditions for intersection, yields

$$\epsilon_1=-\frac{1}{4a}\int_0^\infty r_1\varphi_A^2(r_1)\int_{|a-r_1|}^{a+r_1} r_2\varphi_B^2(r_2)[r_1+r_2-a]^2dr_2dr_1.$$

2. Encircled Spherical Shells, $|r_2-r_1|>a$ $(r_2>r_1)$

Within the spherical shell $r_2^2\varphi_B^2(r_2)$ the potential is constant, so that the correction to the Madelung energy for interaction with the encircled shell $r_1^2\varphi_A^2(r_1)$ is

$$d\epsilon_2=r_1^2r_2^2\varphi_A^2(r_1)\varphi_B^2(r_2)\left[\frac{1}{a}-\frac{1}{r_2}\right],$$

and integration over r_1 and r_2 yields

$$\epsilon_2=\int_0^\infty r_1^2\varphi_A^2(r_1)\int_{a+r_1}^\infty r_2^2\varphi_B^2(r_2)\left[\frac{1}{a}-\frac{1}{r_2}\right]dr_2dr_1.$$

The coulomb overlap interaction energy ϵ_3 for spherical shells of electronic charge of A encircling electronic charge of $B(r_1>r_2)$ is obtained by interchanging A and B, and r_1 and r_2 in ϵ_2. Also, the coulomb overlap interaction ϵ_4 for spherical shells of electronic charge of A encircling the nuclear charge Z_B of B is apparent from ϵ_2.

THE JOURNAL OF CHEMICAL PHYSICS VOLUME 19, NUMBER 4 APRIL, 1951

On the Distribution Function in Phase Space, with Application to the Statistical Theory of Liquids

ERNEST IKENBERRY*
Louisiana State University, Baton Rouge, Louisiana
(Received January 23, 1951)

A simple form for the expansion of the distribution function in phase space, by means of modified hermite polynomials, is set up. Expressions for the density, temperature and the components of the mass current, of the strain tensor, and of the heat current, in terms of the coefficients in the expansion, are obtained. A simple method for obtaining the infinite set of integro-differential equations imposed upon the coefficients in the expansion of the distribution function by the Gibbs' principle of conservation of density-in-phase is outlined. Results obtained for the dissipative processes of heat conduction and of viscosity in liquids are summarized.

INTRODUCTION

IN applying the Gibbs' principle of conservation of density-in-phase[1] in the development of a statistical theory of liquids, as in the application of the Boltzmann integro-differential equation[2] to the statistical theory of gases, one may use either the procedure of operating entirely with average values, or one may first expand the distribution function, and then compute average values from this expansion. The two methods should give the same results for statistically defined, physically significant quantities, provided the calculations are carried out to terms of the same order. The first method, which is the more direct since it does not require determination of the coefficients in an assumed expansion, was introduced by Maxwell[3] and used also by Boltzmann[4] in their kinetic theory of gases. Boltzmann, however, also introduced the second method[5] by treating the anisotropic distribution function in position-velocity space as being only slightly different from the maxwellian distribution function. The latter was modified by multiplying it by a series progressing by powers of the components of the velocities. Relations among the coefficients were then obtained by requiring that the assumed distribution function should satisfy the Boltzmann integro-differential equation. From these relations among the coefficients there were readily obtained relations between the heat current and the temperature gradient, and between the surface forces and the velocity gradients.

The method of operating with averages predominates in the kinetic theory of liquids recently developed by Born and Green.[6] On the other hand, Jaffé,[7] in his application of the Gibbs' principle of conservation of density-in-phase to the dissipative processes of heat conduction and of viscosity in liquids, proceeded by multiplying Gibbs' canonical distribution function[1] by a multiple power series progressing by powers of the resultant linear momenta and total kinetic energy of the system. Numerical values for the coefficients of heat conductivity and of viscosity were then computed for ten representative liquids, by the use of previously determined potential functions.[8] Jaffé anticipated that better numerical results would be obtained by carrying the calculations out to terms of higher order. However, the calculations tend to become very tedious as terms beyond those of the third order are included in the power series expansion.

Since statistically defined, physically significant quantities are calculated from the distribution function by integrations in phase space, an expansion of the distribution function by means of an orthogonal set of functions in the momentum coordinates is suggested. Such an expansion offers the following advantages over a power series expansion:

1. The calculations do not necessarily tend to become more complicated as additional terms are included in the expansion.
2. The value of each coefficient, when once obtained, is complete in the sense that it remains unaffected and does not have to be recomputed each time an additional term is included in the expansion.
3. The approximation to the distribution function obtained by breaking the expansion off at any given term oscillates about the actual distribution function for all values of the momentum coordinates, rather than approximating it closely only in the neighborhood of some particular values of these coordinates.[9]
4. Expressions for statistically defined quantities, in terms of the coefficients in the expansion, are readily obtained.

The feasibility of expanding the distribution function in position-velocity space by means of an orthogonal set of functions was first demonstrated by Jaffé,[10] in a

* Now at Alabama Polytechnic Institute.
[1] J. W. Gibbs, *Collected Works*, Vol. II, Part I, Chapter 1 (1931).
[2] L. Boltzmann, *Vorlesungen über Gastheorie*, I Theil, 98–115.
[3] J. C. Maxwell, Phil. Mag. **35**, 4th ser. 185–217 (1868).
[4] See reference 2, pp. 141–184.
[5] See reference 2, pp. 184–190.
[6] M. Born and H. S. Green, Proc. Roy. Soc. (London) **A188**, 10–18 (1946), and subsequent papers.
[7] G. Jaffé, Phys. Rev. **75**, 184–196 (1949).
[8] G. Jaffé, Phys. Rev. **62**, 463–476 (1942).
[9] A. Sommerfeld, *Partial Differential Equations in Physics* (Academic Press, Inc., New York, 1949), pp. 26–27.
[10] G. Jaffé, Ann. Physik 5. Folge, Bd. **6**, 195–252 (1930).

treatment of the Boltzmann integro-differential equation. A transformation from cartesian to spherical coordinates was made, and an expansion of the distribution function for a gas, in terms of spherical harmonics, was obtained. More recently, an expansion for the distribution function in phase space by means of hermite polynomials has been set up and applied to the kinetic theory of gases by Grad.[11] However, it seems to the present author that the notation used by Grad is unnecessarily complicated and that the form of expansion which was used by the author in his doctoral dissertation[12] is much more suitable, not only for application to gases but also to liquids.

THE DISTRIBUTION FUNCTION

We shall consider a system consisting of N identical particles, each of mass m. Let q_{3a-2}, q_{3a-1}, q_{3a}, $a=1, 2, \cdots N$, be the rectangular position coordinates of particle a, and let $p_i=mdq_i/dt$, $i=1, 2, \cdots 3N$, be the corresponding momentum coordinates. Let polynomials $H_{ni}=H_n(hp_i)$ be defined[13] by

$$\int_{-\infty}^{\infty} \exp(-h^2p_i^2)H_n(hp_i)\cdot H_m(hp_i)dp_i = \pi^{\frac{1}{2}}h^{-1}\delta_{nm}, \quad n, m=0, 1, 2, \cdots, \quad (1)$$

where $\delta_{nm}=1$ or 0 according as $n=m$ or $n\neq m$, and $h>0$ is a parameter whose significance will be indicated later. The polynomials $H_n(hp_i)$ are made to differ from the customary hermite polynomials by factors $(2^n n!)^{-\frac{1}{2}}$ in order to simplify the notation. As a form for the expansion of the distribution function we shall write

$$f_h=(h^2/\pi)^{3N/2}\cdot\exp\left(-h^2\sum_{i=1}^{3N}p_i^2\right)\left\{a+\sum_{i=1}^{3N}b_iH_{1i} +\sum_{i=1}^{3N}c_iH_{2i}+\frac{1}{2}\sum_{i,j=1}^{3N}c_{ij}H_{1i}H_{1j}+\sum_{i=1}^{3N}d_iH_{3i} + \sum_{i,j=1}^{3N}d_{ij}H_{1i}H_{2j}+\cdots\right\}. \quad (2)$$

The coefficients a, b_i, etc., in (2) are, in general, functions of the $3N$ position coordinates, as well as of the time. For convenience, we shall let $c_{ij}=c_{ji}$ and $c_{ii}=d_{ii}=0$. However, in general, $d_{ij}\neq d_{ji}$. A subscript h is placed on f in (2) to indicate that the rapidity of convergence depends on h. Due to the closure property[13] of the hermite polynomials, the expansion (2) may be made to approximate the actual distribution function arbitrarily closely, by proper choice† of the coefficients and by the inclusion of a sufficient number of terms in the expansion. For the coefficients there is obtained, for example,

$$a=\int f d\omega,$$

$$b_i=\int fH_{1i}d\omega=\sqrt{2}h\int fp_i d\omega,$$

$$c_i=\int fH_{2i}d\omega=(1/\sqrt{2})\int f(2h^2p_i^2-1)d\omega,$$

$$c_{ij}=\int fH_{1i}H_{1j}d\omega=2h^2\int fp_ip_j d\omega,$$

$$d_i=\int fH_{3i}d\omega=(h/\sqrt{3})\int fp_i(2h^2p_i^2-3)d\omega,$$

$$d_{ij}=\int fH_{1i}H_{2j}d\omega=h\int fp_i(2h^2p_j^2-1)d\omega,$$

$$i, j=1, 2, 3, \cdots, i\neq j, \quad (3)$$

where

$$d\omega=\prod_{i=1}^{3N}dp_i$$

and we integrate from $-\infty$ to $+\infty$ with respect to each of the momentum coordinates.

It is evident that calculation of the coefficients in the expansion (2) requires knowledge of the microscopic distribution of the systems of the virtual ensemble in phase space. Such complete knowledge of the distribution of systems in phase space is available only for certain very idealized systems. In practice, it is necessary to operate entirely with observable quantities which are statistically defined in terms of integrations performed over the subspace of phase space obtained by assigning specified values to the position coordinates of a representative particle, say particle No. 1. Upon using the conventional definitions for the density n, the components mnu_i of the mass current, the temperature T, and the components S_{ij} and H_i of the strain tensor and of the heat current, we obtain:

$$n=(N/\mathbf{N})\int a dQ_1,$$

$$mnu_i=(1/h\sqrt{2})(N/\mathbf{N})\int b_i dQ_1,$$

$$S_{ii}=(1/2h^2m)(N/\mathbf{N})\int(a+c_i\sqrt{2})dQ_1, \quad i, j=1, 2, 3,$$

$$S_{ij}=(1/2h^2m)(N/\mathbf{N})\int c_{ij}dQ_1, \quad i\neq j$$

[11] H. Grad, Com. on Pure and Applied Math. **2**, 331–407 (1949).
[12] E. Ikenberry, "The conservation of systems in phase space as applied to the liquid state," doctoral dissertation, Louisiana State University (1950).
[13] G. Szegö, *Orthogonal Polynomials* (Am. Math. Soc., New York, 1939), pp. 101–106.

† By minimizing $\int \exp\left(h^2\sum_{i=1}^{3N}p_i^2\right)(f-f_h)^2d\omega$.

$$nkT=(1/6h^2m)(N/\mathbf{N})\int\{3a+\sqrt{2}(c_1+c_2+c_3)\}dQ_1,$$

$$H_1=(1/4h^3m^2)(N/\mathbf{N})\int(\sqrt{3}d_1+d_{12}+d_{13}+5b_1/\sqrt{2})dQ_1, \quad (4)$$

where

$$dQ_1=\prod_{i=4}^{3N}dq_i$$

and $\mathbf{N}$ is the total number of systems in the virtual ensemble. The ranges of the position coordinates in the integrations over dQ_1 are determined by the physical volume occupied by the particles of the system. In the case of a dense gas or of a liquid, the preceding expressions for the components of the strain tensor and of the heat current must be augmented by terms arising from molecular interactions.[6,14] Terms in the expressions defining the temperature and the components of the strain tensor and of the heat current, which arise from mass currents, have been neglected in (4). These terms may be included by replacing each p_i by $p_i'=p_i-(\int fp_i d\omega/\int f d\omega)$ in an expansion for the distribution function similar to that of (2). Then the coefficient of each first-order polynomial $H_1(hp_i)$ in the resulting expansion will vanish.

From (3) it is seen that the coefficients in (2) are functions of h. The author has shown[12] that the results obtained for statistically defined, physically significant quantities are independent of the manner of selecting h. However, the orders of magnitude of various coefficients in the expansion (2) depend upon the value of h. It is evidently desirable to choose h as a function of statistically defined quantities in such a way as to obtain most rapid convergence of the multiple series (2). As the only statistically defined, observable quantities which do not vanish when the system is in static equilibrium are the density and the temperature, it is desirable that the condition to be imposed on h be expressed in terms of either or both of these two quantities. Inspection of the preceding expressions for n and T shows that $\int(c_1+c_2+c_3)dQ_1=0$ if $h^2=1/(2mkT)$. This manner of selecting h is closely analogous to the method originally used by Boltzmann[5] in his expansion of the distribution function in position-velocity space. In the case of a canonical distribution of systems in phase space the expansion (2) reduces to Gibbs' canonical form, when we let $h^2=1/(2mkT)$.

APPLICATION TO THE STATISTICAL THEORY OF LIQUIDS

Members of the infinite set of linear, first-order, partial differential equations imposed upon the coefficients in the expansion (2) by the Liouville equation,

$$Df\equiv\frac{\partial f}{\partial t}+\sum_{i=1}^{3N}\left\{\frac{\partial}{\partial q_i}\left(f\frac{dq_i}{dt}\right)+\frac{\partial}{\partial p_i}\left(f\frac{dp_i}{dt}\right)\right\}=0, \quad (5)$$

may be readily obtained by multiplying (5) by products of the orthogonal polynomials $H_n(hp_i)$ and integrating over $d\omega$. The equations thus obtained may be integrated over dQ_1 and the resulting integro-differential equations combined linearly in any desired manner. The difficulties arising from the presence of the $3N$ terms in the summation, and from the complicated manner in which the coefficients in (2) depend upon the position coordinates, were resolved by Jaffé[7] by the assumption that the distribution function and the potential depend only upon the coordinates of the center of mass of the system. The author has obtained similar results by applying a very general boundary condition[14] to the distribution function, leading to the equation of transport:

$$\frac{\partial}{\partial t}\int\int f\phi d\omega dQ_1+\frac{1}{m}\sum_{i=1}^{3}\frac{\partial}{\partial q_i}\int\int fp_i\phi d\omega dQ_1=\int\int f(D\phi)d\omega dQ_1, \quad (6)$$

where ϕ is any multinomial in the momentum coordinates. Since any polynomial in a momentum coordinate p_i may be expressed as a linear combination of the polynomials $H_n(hp_i)$ in p_i, the equations obtained by taking multinomials in the p_i for ϕ are linear combinations of those obtained by taking products of such combinations in the $H_n(hp_i)$. The process of obtaining a solution for the coefficients, and then forming any desired linear combination of the coefficients, may thus be replaced by first taking for ϕ any desired multinomial, such as those occurring in the definitions of S_{ij}, nkT, H_i, etc.

The author has carried out both methods of obtaining solution, and obtained by each method the expressions[12]

$$\sigma=5nk^2T(B^*+D-1)/2m\lambda_T,$$
$$\eta=nkT(B^*-D)/D\lambda_v, \quad (7)$$

for the coefficients of heat conductivity and of viscosity, respectively, where[7] $B^*=(1/Nk)\partial U/\partial T$, $D=(-T/n)\partial n/\partial T$, and λ_T and λ_v are the time constants for the decay of a local disturbance in the temperature and velocity distributions, respectively. Values of B^* and D and the potential functions $\varphi(r_{ij})$ computed by Jaffé[7,8] were used. The contributions arising from molecular interactions were not included, and terms of higher than the first order in the temperature and velocity gradients were neglected. Solution of the appropriate equations for the time constants, which arise as maximum eigenvalues, gave

$$\lambda_T=\{(B^*+D-1)K/mB^*\}^{\frac{1}{2}},$$
$$\lambda_v=\{(2B^*-3D)K/mB^*\}^{\frac{1}{2}}, \quad (8)$$

where

$$K=\left\langle\sum_{a=2}^{N}\frac{\partial^2\varphi(r_{1a})}{\partial q_1^2}\right\rangle_{Av}$$

[14] E. Ikenberry, Quart. Appl. Math. **IX**, No. 2 (1951).

is the mean value of the curvature of the potential function $\varphi(r)$, evaluated for all microscopic distributions of the particles consistent with the observed macroscopic distribution.

For the numerical calculations, it was assumed that the zero order term for the density distribution in the neighborhood of a particle is given by the Boltzmann expression $n=n_0\cdot\exp(-\varphi(r)/kT)$ and use was made of the generalization[15] by Jaffé of Hertz' formula[16] for the most probable number of particles in a small element of volume surrounding a given particle. In general, the calculated values of σ and η did not agree as closely with experimental values as did the values computed by Jaffé.[7] The failure to obtain improved results is attributed, in large part, to the different method used for computing the mean curvature of the potential function. In the treatment by Jaffé, the value of $\varphi(r_0)$ for one particle, evaluated at the equilibrium distance r_0, was used. Numerical calculations indicate that the potential functions used allow for the penetration of too many particles within the equilibrium distance of any one particle. Jaffé has suggested that the calculations might be improved by the use of x-ray data for the distribution of particles in the neighborhood of any one particle. However, the author is postponing the lengthy computations necessary, pending the outcome of attempts to evaluate the contributions arising from molecular interactions and to solve the differential equations to terms of higher order.

[15] G. Jaffé, Phys. Rev. **58**, 968–976 (1940).
[16] P. Hertz, Math. Ann. **68**, 387–398 (1909).

THE JOURNAL OF CHEMICAL PHYSICS VOLUME 19, NUMBER 4 APRIL, 1951

Calculated Thermochemical Properties for Hydrazine–Hydrogen Peroxide Reaction at High Pressures

W. J. Barr and E. Justin Wilson, Jr.
Experiment Incorporated, Richmond, Virginia
(Received January 25, 1951)

A liquid bireactant system, consisting of a stoichiometric mixture of anhydrous hydrazine and hydrogen peroxide, is evaluated in terms of the resultant equilibrium temperature-pressure-density relationship corresponding to chamber pressures over the range 10,000 to 185,000 pounds per square inch. The analysis is based on the use of the reactants both at constant volume and at constant pressure, and data pertaining to the mole fractions of components of the product gas, its molecular weight and covolume are included for each case.

THE use of highly reactive liquid chemicals for miscellaneous gas generating purposes[1–3] ordinarily involves chamber pressures up to 1000 pounds per square inch under normal operating conditions. Since future attempts to improve performance or develop new uses by proceeding to much higher reaction chamber pressures may be anticipated, the present work was undertaken to provide the necessary background of thermodynamic data for a particular bireactant combination. This paper, then, contains the results of calculations for a system employing self-igniting stoichiometric mixtures of 100 percent hydrazine and 100 percent hydrogen peroxide, in the course of which values for equilibrium reaction temperature T_e, mole fractions n_i of the various product components, covolume b' and molecular weight M of the gas were determined as functions of the reaction pressure P. The latter quantity in turn has been related to the reactant (or loading) density, Δ, i.e., mass of the reactants per unit volume of reactor. Reactant densities amounting to 5 percent to 50 percent of the maximum possible were employed in order to produce pressures extending over the range of 10,000 to 185,000 pounds per square inch.

It was reasonable to expect that closed chamber tests to ascertain relative mixing, ignition and reaction rate properties would be required in any experimental study; under such conditions, the combustion of fuel and oxidizer takes place at constant volume. On the other hand, effective use of the energy derived from the reaction implies expansion of the product gases, in which case it may be considered that the reaction is conducted at approximately constant pressure. Consequently, data for both the constant volume and constant pressure process were considered desirable and are included.

METHOD OF CALCULATION

(1) Reaction at Constant Volume

A general method outlined by Hirschfelder[4] in connection with computations involving solid propellants was employed in the present instance. Initial assump-

[1] M. J. Zucrow, S.A.E. Journal **54**, 375 (1946).
[2] L. McKee, Mech. Eng. **68**, 1045 (1946).
[3] F. Bellinger *et al.*, Ind. Eng. Chem. **38**, 160, 310, 627 (1946).

[4] J. O. Hirschfelder *et al.*, "Thermodynamic properties of propellant gases," NDRC A-116, OSRD-547 (1942).

TABLE I. Calculated thermodynamic data for the stoichiometric reaction of 100 percent N_2H_4 and 100 percent H_2O_2 at constant volume.

T_e	(°K)	3335°	3360°	3400°	3440°	3500°	3565°
Δ	(g/cc)	0.04898	0.06864	0.1150	0.1947	0.3261	0.5520
P	(atmos)	715	1020	1784	3262	6122	12,585
$n_1(H_2O)$		0.729200	0.734500	0.742300	0.749200	0.759000	0.766000
$n_2(H_2)$		0.035500	0.033000	0.029100	0.025200	0.020950	0.016500
$n_3(H)$		0.002887	0.002487	0.001945	0.001542	0.001202	0.000959
$n_4(O_2)$		0.008312	0.007515	0.006056	0.004667	0.002955	0.000978
$n_5(O)$		0.001202	0.001041	0.000808	0.000651	0.000513	0.000400
$n_6(OH)$		0.024165	0.022694	0.020307	0.018109	0.016024	0.013412
$n_7(N_2)$		0.190905	0.191329	0.192086	0.192710	0.193200	0.193201
$n_8(N)$		0.000107	0.000100	0.000090	0.000090	0.000096	0.000160
$n_9(NO)$		0.007239	0.007171	0.006972	0.006929	0.007110	0.008109
$n_{10}(NH_3)$		0.000012	0.000015	0.000023	0.000037	0.000058	0.000110
$n_{11}(NH)$		0.000047	0.000048	0.000048	0.000048	0.000048	0.000053
M		19.4761	19.5227	19.5790	19.6267	19.7219	19.7611
b'	(cc/g)	0.7670	0.7647	0.7612	0.7578	0.7534	0.7490
$*-\Delta F_{18}°$		−13,371	−13,397	−13,437	−13,471	−13,505	−13,525
$*-(E_T{}^0-E_0{}^0)$		−27,802	−28,128	−28,631	−29,121	−29,906	−30,656
$*-E_0{}^0$		41,034	41,382	41,896	42,340	42,942	43,358
$*-E$ (gas imp.)		77	108	181	307	512	863

* Expressed in units of calories/mole.

tions under which this method was applied are as follows:

(a) Stoichiometric quantities of 100 percent hydrazine and 100 percent hydrogen peroxide enter into reaction at atmospheric pressure and an initial temperature of 15°C, and chemical equilibrium is attained in the chamber.

(b) The reaction product components are H_2O, H_2, H, O_2, O, OH, N_2, N, NO, NH_3, and NH; the sum of their mole fractions, $n_1 \cdots n_{11}$, is equal to one mole of propellant gas.

(c) The reaction process is adiabatic.

(d) Motion of the product gas is neglected.

Since eleven product components are being considered, it is necessary to derive eleven expressions for their mole fractions. Inasmuch as

4 (No. atoms N) = No. atoms H = 2 (No. atoms O),

and if X and Y be taken as the number of moles of hydrazine and hydrogen peroxide required for formation of one mole of propellant gas, where $Y=2X$, so that

$$X \cdot N_2H_4 + Y \cdot H_2O_2 = n_1\,(H_2O) + \cdots n_{11}\,(NH),$$

then only three expressions containing eleven unknowns result. Since $P_i = n_i P$, the equilibrium constants, K_i, for eight reactions in the combustion process can be written for a given temperature, T, in terms of pressure and mole fractions, giving a total of eleven expressions having eleven unknowns, $n_1, \cdots n_{11}$. However, P and T are functions of the quantity of reactants and the volume of the reaction chamber, and hence are additional variables which necessitate the introduction of two more independent equations, a modified van der waals equation of state

$$PV/RT = 1 + b'\Delta + 0.625b'^2\Delta^2 + 0.2869b'^3\Delta^3 + 0.1928b'^4\Delta^4,$$

TABLE II. Calculated thermodynamic data for the stoichiometric reaction of 100 percent N_2H_4 and 100 percent H_2O_2 at constant pressure.

T_e	(°K)	3000°	3010°	3020°	3020°	3010°	2960°
Δ	(g/cc)	0.05504	0.07743	0.1294	0.2205	0.3703	0.6388
P	(atmos)	715	1020	1784	3262	6122	12,585
$n_1(H_2O)$		0.766000	0.769402	0.774000	0.780000	0.785061	0.790908
$n_2(H_2)$		0.018100	0.016430	0.013780	0.010850	0.007803	0.004861
$n_3(H)$		0.000805	0.000671	0.000488	0.000330	0.000207	0.000112
$n_4(O_2)$		0.004427	0.003939	0.003085	0.002125	0.001153	0.000226
$n_5(O)$		0.000310	0.000261	0.000191	0.000129	0.000083	0.000041
$n_6(OH)$		0.011036	0.010084	0.008565	0.006913	0.005336	0.003364
$n_7(N_2)$		0.195600	0.195900	0.196500	0.196920	0.197429	0.197900
$n_8(N)$		0.000023	0.000022	0.000019	0.000016	0.000014	0.000017
$n_9(NO)$		0.003749	0.003629	0.003403	0.003129	0.002951	0.002754
$n_{10}(NH_3)$		0.000005	0.000007	0.000010	0.000014	0.000019	0.000028
$n_{11}(NH)$		0.000011	0.000011	0.000011	0.000010	0.000008	0.000004
M		19.7648	19.7949	19.8279	19.8737	19.9073	19.9517
b'	(cc/g)	0.7534	0.7519	0.7498	0.7471	0.7446	0.7420
$*-\Delta F'_{18}°$		−12,758	−12,773	−12,805	−12,823	−12,850	−12,875
$*-(H_T-H_0)$		−30,775	−30,974	−31,242	−31,518	−31,856	−32,244
$*-H_0{}^0$		43,501	43,719	44,010	44,386	44,704	45,070

* Expressed in units of calories/mole.

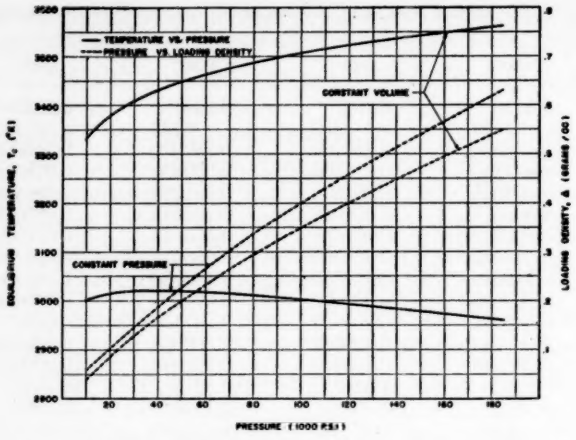

FIG. 1. Pressure-temperature-reactant density relationships for constant volume and constant pressure reaction of N_2H_4 and H_2O_2.

and the energy balance equation

$$E_T - E_0 = E_T^0 - E_0^0 + E(\text{gas imp.})$$

$$= \sum_1^{11} n_i(E_0^0)_i - X \cdot \Delta F_{15°,\,N_2H_4} - Y \cdot \Delta F_{15°,\,H_2O_2}$$

which states that the internal energy acquired in raising the product gas from 0°K to T is equal to the energies of formation of the product gas components at 0°K (constant volume) less the energies of formation of the reactants (constant volume) at 15°C. In turn, $\Delta = M/V$, where V is the specific volume (c.c./mole), and $b' = n_i \cdot b_i$, in which b_i represents the covolume of component i of the gas. These fifteen equations would yield, on simultaneous solution, the eleven mole fractions and values for P, T, Δ, and b'.

In the present instance, the equilibrium constants, K_i, are modified by replacing partial pressures (P_i) with activities. Internal energies for perfect gases, corrections to account for gas imperfection, and the energies of formation of the product components at 0°K were obtained from data[4] given by Hirschfelder. Corrected energies of formation at 15°C at constant volume of N_2H_4 (liq.) and H_2O_2 (liq.) were computed[4] using $-12{,}050$ cal/mole for the heat of formation of N_2H_4 (liq.)[5] at 25°C at constant pressure, and 45,200 cal/mole for H_2O_2 (liq.)[6] under identical conditions. Heats of vaporization (at 25°C) amounting to $-10{,}200$ cal/mole[5] and $-11{,}600$ cal/mole[6] were employed for N_2H_4 and H_2O_2, respectively.[7]

Solution of these equations is accomplished by the usual iterative process, commencing with computation of an approximate reaction temperature from a simplified energy balance expression assuming $N_2H_4 + 2H_2O_2 = N_2 + 4H_2O$. Two repetitions of the iterative process are usually sufficient to produce an accurate equilibrium temperature and final values for the various unknowns.

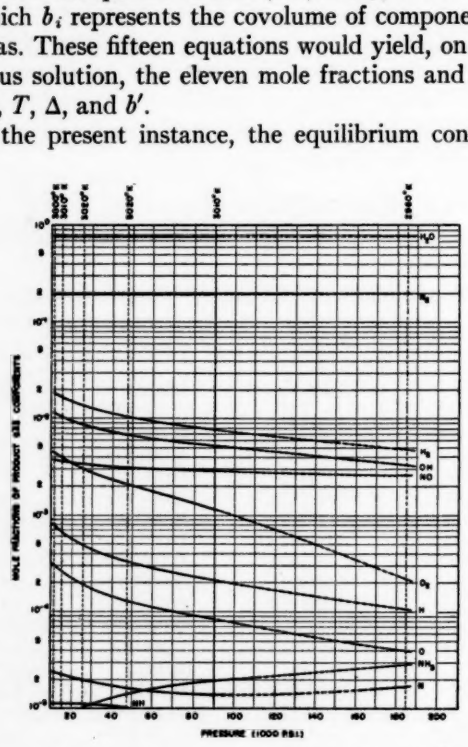

FIG. 2. Relation between mole fractions of product gas components, temperature and pressure for reaction of N_2H_4 and H_2O_2 at constant volume.

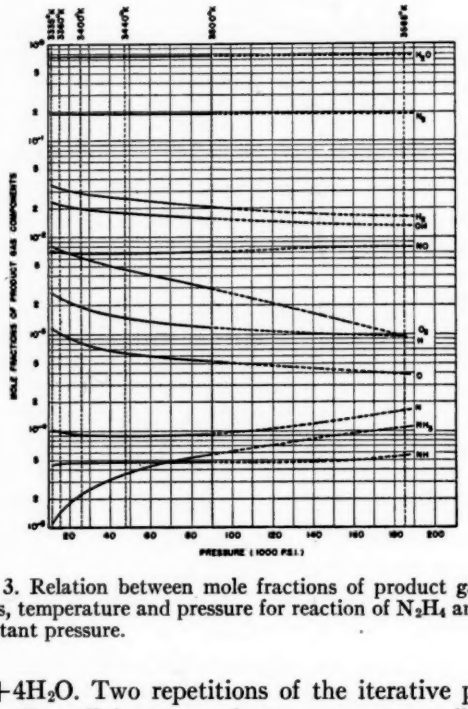

FIG. 3. Relation between mole fractions of product gas components, temperature and pressure for reaction of N_2H_4 and H_2O_2 at constant pressure.

(2) Reaction at Constant Pressure

In deriving corresponding quantities for a constant pressure reaction, the assumptions listed in (1) also apply. For simplicity, it is considered that the N_2H_4 and

[5] Hughes, Corruccini, and Gilbert, J. Am. Chem. Soc. **61**, 2639 (1939).

[6] F. R. Bichowsky and F. D. Rossini, *The Thermochemistry of the Chemical Substances* (Reinhold Publishing Corporation, New York, 1936).

[7] After completion of the present work, a value of $-10{,}700$ cal/mole for the heat of vaporization of N_2H_4 at 25°C was published (Huffman, *et al.*, J. Am. Chem. Soc. **71**, 2293 (1949). This larger value would increase all equilibrium temperatures at constant volume approximately 1 percent, if employed in the procedure outlined above.

H_2O_2 initially are contained in a combustion chamber at each of the final pressures computed for the constant volume process. Reaction is assumed to take place at these same pressures, held constant by chamber enlargement.

The procedure followed is similar to the above, except that the heats of formation of the reactants at constant pressure ($\Delta F'$) are substituted for those at constant volume, and enthalpies rather than internal energies are employed in computing the energy released. The energy balance equation thus becomes

$$H_T - H_0 = \sum_1^{11} n_i (H_T - H_0)_i$$

$$= \sum_1^{11} n_i (H_0^0)_i - X \cdot \Delta F'_{15°,\ N_2H_4} - Y \cdot \Delta F'_{15°,\ H_2O_2}$$

where $H_T - H_0$ is the enthalpy acquired (corrected for gas imperfection) in raising the product gas from 0°K to T°K, and H_0^0 is the heat of formation of the product gas at 0°K from its elements at 0°K and constant pressure, equivalent to E_0^0. The data of Corner[8] were employed for H_2O, N_2, and H_2 enthalpy corrections; other product gas components are in such small concentrations that adjustments of this type make no significant changes and can be neglected.

RESULTS AND DISCUSSION

Tables I and II contain the pertinent computed data for reaction at constant volume and constant pressure, respectively. The relationships between T_c, P and Δ for each case are expressed in graphic form in Fig. 1. It is observed that T_c undergoes only a relatively minor change with change in Δ in both instances.

The higher temperature for constant volume reaction, in the neighborhood of 3400°K as compared with 3000°K for constant pressure, is as expected in consideration of the work performed in the latter instance. An additional difference is that at constant volume, T_c increases with increasing Δ over the range examined, while at constant pressure it passes through a maximum in the neighborhood of 35,000 pounds per square inch (corresponding to a reactant density of 0.17 g/cc). Decrease of T_c at smaller pressures is a result of increasing dissociation, while at higher pressures the increasing heat contents of the imperfect gases produce a corresponding effect.

The mole fractions of the eleven components considered as composing the product gas are plotted as functions of T_c and pressure in Figs. 2 and 3. In these graphs, the dotted portions of the curves at pressures in excess of 90,000 psi indicate inaccuracy of the computations, owing to inadequate knowledge of corrections for non-ideality. Examination of the mole fraction data indicates that the amounts of O, N, NH_3, and NH are minor and ordinarily need not be included in calculations of this type; this would result in a considerable reduction in the amount of effort involved. The data are carried to the sixth decimal place in order to indicate trends for the minor constituents; actually, in view of the uncertainty of the thermodynamic data, accuracy to five places is optimistic.

Data for reactions in which the $N_2H_4 - H_2O_2$ ratio departs from stoichiometric, or in which H_2O forms a third component, are not included in this paper, although it is recognized that utilization of this bireactant combination may require consideration of such adjustment, for example, in order to reduce operating temperatures.

ACKNOWLEDGMENT

The authors wish to express their appreciation for the continued interest of Dr. C. M. Hudson, Office of Chief of Ordnance, and for the support of the Department of the Army, Ordnance Department.

[8] J. Corner, Proc. Phys. Soc. (London) **58**, 737 (1946).

The Reaction of Methylcyclopentane with Hg $6(^3P_1)$ Atoms*†

M. SCHLOCHAUER AND H. E. GUNNING
Department of Chemistry, Illinois Institute of Technology, Chicago, Illinois

(Received November 13, 1950)

The reaction of methylcyclopentane with photo-excited Hg $6(^3P_1)$ atoms was investigated in a static system at 29.35±0.01°C, over a range of initial pressures of 5–110 mm. After an initial slight pressure rise, the reaction exhibited a linear pressure decrease, the magnitude of which increased linearly with initial pressures of methylcyclopentane above 15 mm. The average rate of hydrogen formation also increased with initial pressure of methylcyclopentane and decreased with time in the course of a run. The products found were hydrogen, methylcyclopentenes, and a heavy fraction with the formula $C_{12}H_{22}$. Upon the basis of chemical and physical properties, strengthened by kinetic considerations, it was concluded that the $C_{12}H_{22}$ compound was predominantly dimethyldicyclopentyls. Quantum yields reached a maximum of 0.44 for hydrogen formation and 0.42 for methylcyclopentane consumption.

The mechanism postulated proceeds through an initial carbon-hydrogen bond split, thus:

(1) cyclo C_6H_{12}+Hg $6(^3P_1)$ →cyclo C_6H_{11}+H+Hg $6(^1S_0)$
(2) H +cyclo C_6H_{12}→H_2 +cyclo C_6H_{11}
(3) H +cyclo C_6H_{11}→cyclo C_6H_{12}
(4) H +cyclo C_6H_{11}→cyclo C_6H_{10}+H_2
(5) cyclo C_6H_{11}+cyclo C_6H_{11}→$C_{12}H_{22}$
(6) H_2 +Hg $6(^3P_1)$ →H+H+Hg $6(^1S_0)$

This mechanism yields rate expressions which confirm the trends observed in the experimental work.

INTRODUCTION

THE cycloparaffins represent a particularly interesting example of the relationship between structure and mechanism of decomposition within the broad field of the mercury-$6(^3P_1)$-photo-sensitized reactions of the hydrocarbons. Thus, Gunning and Steacie[1] have shown that cyclopropane reacts with Hg $6(^3P_1)$ atoms with primary scission of the C−C bond to form an energy-rich trimethylene biradical, which, in turn, initiates polymerization of the cyclopropane. And recently Scott and Gunning[2] have shown that the cyclopropane polymer is itself a complex mixture of high molecular weight cycloparaffins. This behavior is in sharp contrast to that of the paraffins[3–10] which appear to decompose primarily through the rupture of a C−H bond. Cyclopentane[11] and cyclohexane,[12] on the other hand, are much more paraffinic in their behavior than cyclopropane, in that decomposition is initiated primarily by the rupture of a C−H bond. Finally, recent data obtained in this laboratory suggest that cyclobutane[12] resembles cyclopentane much more closely than it does cyclopropane.

The present investigation on methylcyclopentane was undertaken for the purpose of studying a molecule which was at once both paraffinic and cycloparaffinic in nature. In addition, methylcyclopentane offers interesting possibilities for studying the specificity of Hg $6(^3P_1)$ atoms for various types of C−H linkages. This arises from the fact that of the twelve C−H bonds in methylcyclopentane, three are primary, eight are secondary, and one is tertiary. The details of our investigation follow.

EXPERIMENTAL

In order to facilitate comparison with previous work on the cycloparaffins, the decomposition of methylcyclopentane was carried out in a static system which was maintained at a temperature close to 30°C. For a general description of the reaction and analytical systems used, and the experimental technique, reference should be made to an earlier publication.[13]

The connecting tubing of the reaction system was constructed entirely of heavy walled 3-mm i.d. capillary tubing, in order to minimize the effects of random fluctuations in laboratory temperature on the pressure measurements. The cylindrical fused-quartz reaction cell was 8.5 cm long and 5 cm in diameter. It was connected to the system by means of a 14/35 standard taper joint to facilitate removal for cleaning. The taper joint was rendered vacuum-tight with Cenco "Sealstix" cement, which was found to be ideal because of its inertness to hydrocarbon vapors.

The quartz reaction cell was immersed in a metal water bath, 36 cm square and 30 cm deep. The cell was so oriented that one circular end was parallel to, and 30 mm from a fused-quartz window, 6.5 cm square,

* This work was supported by the AEC under Contract AT(11-1)-43.

† Part of a dissertation submitted by one of the authors (M.S.) in partial fulfillment of the requirements for the M.S. degree at Illinois Institute of Technology.

[1] H. E. Gunning and E. W. R. Steacie, J. Chem. Phys. **17**, 351 (1949).
[2] R. J. Scott and H. E. Gunning, J. Phys. and Colloid Chem. (to be published).
[3] Morikawa, Benedict, and Taylor, J. Chem. Phys. **5**, 212 (1937).
[4] B. de B. Darwent and E. W. R. Steacie, J. Chem. Phys. **13**, 563 (1945).
[5] B. de B. Darwent and E. W. R. Steacie, J. Chem. Phys. **16**, 381 (1948).
[6] B. de B. Darwent and E. W. R. Steacie, J. Am. Chem. Soc. **70**, 2285 (1948).
[7] B. de B. Darwent and C. A. Winkler, J. Phys. Chem. **49**, 150 (1945).
[8] A. W. Hay and C. A. Winkler, Can. J. Research **B21**, 149 (1943).
[9] E. W. R. Steacie and R. L. Cunningham, J. Chem. Phys. **8**, 800 (1940).
[10] E. W. R. Steacie and D. J. Dewar, J. Chem. Phys. **8**, 571 (1940).
[11] Allen, Kantro, and Gunning, J. Am. Chem. Soc. **72**, 3588 (1950).
[12] H. E. Gunning, unpublished work.
[13] G. A. Allen and H. E. Gunning, J. Chem. Phys. **16**, 1146 (1948).

which was set into the side of the water bath. The distilled water in the bath was maintained at 29.35±0.01°C by means of a temperature control system consisting of a 100-watt Aminco "LoLag" heater, an Aminco mercury thermoregulator, a variable speed stirrer, a copper cooling coil, and an electronic relay circuit employing a thyratron tube.

Pressure changes were followed with a Pearson type differential manometer.[14] The accuracy of the manometer was considerably enhanced by using special constant bore tubing in its fabrication. The large center tube which made connection to the reaction system was 19.07-mm i.d., while the capillary arm was 2.007-mm i.d. A one-meter cathetometer was employed for making the absolute pressure measurements. Determinations were made at the beginning and end of each run, with the manometer in operation. The water jackets around the manometer were connected in series with a copper coil in the thermostat bath. Water circulation was maintained with a small centrifugal pump. The solenoid valve of the manometer was actuated by a thyratron control circuit.

The reaction system was entirely mercury sealed by means of two U-type mercury cutoffs provided with iron-core check valves. One cutoff made connection to the main evacuation manifold, and the other led to the analytical system.

The light source consisted of a Hanovia Sc-2537 quartz mercury resonance lamp, wound in the form of a five-coil helix. It was clamped broadside to the thermostat window at a distance of 15 mm. The lamp was operated from a Sola luminous tube transformer, with a 115-volt primary and a 3000-volt 30-ma secondary. Fluctuations in intensity arising from variations in line voltage were eliminated by interposing a 125 VA Sola constant voltage transformer between the line and the primary of the lamp transformer. In order to prevent any 1849A radiation from entering the reaction cell, two Corning Vycor filters 3.5 cm square, polished to stock thickness, were placed between the quartz window of the thermostat and the source.

The methylcyclopentane used was National Bureau of Standards sample No. 208a-8S. Stated limits of impurities were 0.11±0.06 mole percent. The samples, which were obtained in ampoules provided with internal break-off tips, were sealed to the reaction system via a Warrick-Fugassi valve.[15]

The ultraviolet absorption spectrum of methylcyclopentane was studied in 1912 by Zelinsky and Rosanoff.[16] They found that alcoholic solutions of the hydrocarbon were transparent to wavelengths greater than 2390A. And in this connection MacLean, Jencks, and Acree[17] have recently shown that highly purified liquid methylcyclohexane shows 99 percent transmission at 2537A. And since this molecule bears strong structural similarities to methylcyclopentane, it would be reasonable to expect that their upper limits of absorption would be similar. It was, therefore, concluded that no direct photolysis of the methylcyclopentane vapor was possible under the conditions of our investigation.

The volume of the system was, of course, dependent on the position of the mercury level in the differential manometer. The system was, therefore, calibrated for the zero-pressure setting of the manometer, and the volume was found to be 291 ml. Since the large center tube was of known constant diameter, the actual volume for any given run could easily be calculated.

At the end of each run, liquid nitrogen was placed around a small finger trap attached to the reaction cell by means of a standard taper joint. The noncondensable gas was transferred to the gas burette in the analytical unit by means of a Toepler pump backed by a mercury diffusion pump. After its volume and pressure had been measured, the gas was circulated over copper oxide deposited on glass wool and maintained at 250°C. The residual gas from the combustion was passed through a liquid nitrogen trap to remove water vapor, and finally it was collected in the gas burette. The residual gas was recycled until its PV product became constant.

The condensable products were treated in various ways depending upon the information to be obtained from them. By surrounding the finger trap on the reaction cell with an ice-water bath, a light fraction, which included the unreacted cyclopentane, could be distilled off and condensed with liquid nitrogen into a storage trap which was attached to the main manifold. The heavy fraction, which remained behind in the finger trap, was removed for characterization at the end of each run.

The boiling point data were obtained by the standard micromethod, after Siwoloboff;[18] refractive indices were measured with an Abbe refractometer maintained at 20°C and illuminated with a sodium lamp.

The olefin content of the condensable products was obtained by titration of the sample with a dilute standardized solution of bromine in glacial acetic acid.[19]

A sample of the heavy fraction was sent to Clark Microanalytical Laboratory, Urbana, Illinois, for carbon-hydrogen analysis by combustion, a molecular weight determination by the micromethod of Rast,[20] and a terminal methyl determination.[21] A sample of the

[14] D. J. LeRoy, Ind. Eng. Chem. Anal. Ed. **17**, 652 (1945).
[15] E. Warrick and P. Fugassi, Ind. Eng. Chem. Anal. Ed. **15**, 13 (1943).
[16] N. Zelinsky and N. Rosanoff, Z. phys. Chem. Stoich. u. Verw. **78**, 629 (1912).
[17] MacLean, Jencks, and Acree, J. Research Natl. Bur. Standards **34**, 271 (1945).
[18] A. Siwoloboff, Ber. **19**, 795 (1886).
[19] S. W. Benson, Ind. Eng. Chem. Anal. Ed. **14**, 189 (1942).
[20] K. Rast, Ber. **55**, 1051, 3727 (1922).
[21] F. Pregl and J. Grant, *Quantitative Organic Microanalysis* (The Blakiston Company, Philadelphia, Pa., 1946).

TABLE I. Rates of pressure decrease *vs* initial pressure of methylcyclopentane.

Run (No.)	P_0 (mm)	Duration of run (min)	Rp (moles/min $\times 10^6$)
25	6.4	90	0.31
24	14.8	90	0.42
23	31.3	90	0.55
48	45.1	75	0.63
22	46.2	90	0.66
21	61.5	90	0.77
20	75.0	90	0.86
28	75.1	60	0.85
19	89.8	90	0.92
18	99.4	90	0.97
17	106.1	90	1.17
26	107.0	90	1.08

light fraction was sent to the Mass Spectrometry section of the National Bureau of Standards for analysis.

The intensity of 2537A radiation entering the reaction cell was measured very conveniently by using the cyclopropane reaction as an actinometer.[1]

Cyclopropane (from the Ohio Chemical and Manufacturing Company, Cleveland, Ohio) of minimum purity 99.5 percent was further purified by several trap-to-trap distillations.[1] The rates of pressure decrease were corrected for the small amount of hydrogen formed to obtain true rates of disappearance of cyclopropane. Under these conditions, the light input I, in einsteins per minute, can be calculated from the simple relation

$$I = V \cdot Rp/(8500T),$$

where V = volume of system in ml, T = the absolute temperature of the reaction, and Rp = the corrected rate of pressure decrease in mm/min.

RESULTS

The Variation of Pressure with Time

As soon as the shutter between the lamp and the cell was removed, the pressure initially increased, reaching a maximum increase of the order of 0.1 mm after 3 to 5 minutes of irradiation. The pressure then began to decrease slowly, passing through its initial value 10 to 15 minutes after the beginning of the run. The pressure decrease became linear in time after 15 to 20 minutes and remained linear throughout the entire course of the 90-minute runs. This type of behavior has been observed previously with cyclopentane[11] and more recently with cyclobutane.[12]

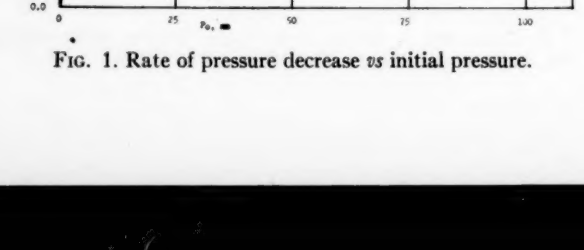

FIG. 1. Rate of pressure decrease *vs* initial pressure.

The linear rates of pressure decrease have been investigated for initial pressures of methylcyclopentane from 5 mm up to its vapor pressure at 20°C, i.e., 110 mm. These results are summarized in Table I, and the pressure rates Rp are plotted against the initial pressure P_0 in Fig. 1. It will be noted that the rates are linear in the initial pressures above approximately 15 mm. Converting pressure into moles, we obtain 4.1 $\times 10^{-4}$ min^{-1} for the value of dRp/dP_0 in the linear region.

Products Noncondensable in Liquid Nitrogen

Considerable noncondensable gas was found at the end of each run. The quantities in a 90-minute run varied from about 15 mole percent of the initial quantity of reactant, for the low pressure runs, to 3.8 percent, for the high pressure runs. Combustion established the noncondensable gas to be at least 99 percent hydrogen.

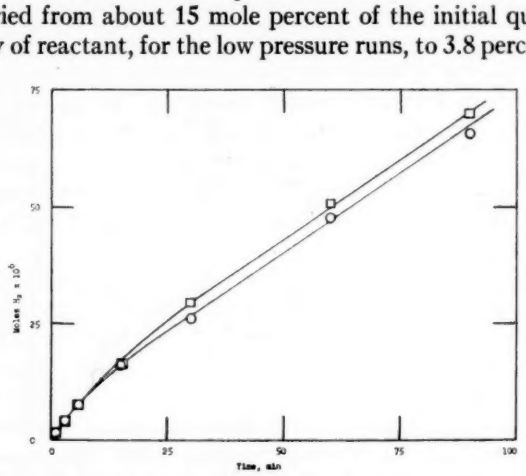

FIG. 2. Moles of hydrogen formed *vs* length of run. The upper curve is for the interrupted run 33a-f; the lower curve represents the single runs. Initial methylcyclopentane pressure = 74 1.5 mm.

In an attempt to obtain values for the initial rates of hydrogen formation, a series of runs were made at approximately identical pressures of 74±1.5 mm. The runs varied in duration from 1 minute to 90 minutes, These data are presented in the lower curve of Fig. 2. as a plot of micromoles of hydrogen *vs* duration of run. It can be seen from this graph that the rate of hydrogen formation decreases with increasing time of exposure, reaching a constant value above approximately 15 minutes. In short, both the rate of hydrogen formation and the rate of pressure decrease attain a steady state in exposure time, after approximately 15 minutes of irradiation.

It is apparent from Fig. 2 that only runs of short duration would be of value in obtaining initial rates of hydrogen formation. Consequently, 1-, 3-, 6-, and 10-minute hydrogen runs were carried out at each of four different initial pressures. The average rates of hy-

drogen formation, i.e., (moles of hydrogen formed)/(duration of run), are presented for these runs together with data for the 90-minute runs in Table II.

The data in Table II have been rounded off by making maximum allowance for the possible experimental errors in the determinations. The extrapolations of the average rates of hydrogen formation to zero time, calculated to obtain a true initial rate, are, of course, open to considerable error. We have used a logarithmic plot to obtain our values for these initial rates. We have also calculated steady-state values for the hydrogen rate. These data are presented in Table III.

It is clear from Table III that the initial rate of hydrogen formation is some two and one-half times greater than the steady-state value for the rate of hydrogen formation.

Products Condensable in Liquid Nitrogen

In the high pressure runs, tiny colorless droplets of liquid could be seen to condense out on the exposed window of the reaction cell. The amount of visible condensate decreased rapidly with decreasing initial pressure.

As a preliminary test for the presence of C_2 and C_3 hydrocarbons, the condensable products frozen down in liquid nitrogen were allowed to warm up to -78.5°C with dry ice-acetone. The vapor pressure of the mixture was measured on the McLeod Gauge. In none of the runs did the vapor pressure measured in the above fraction exceed 5×10^{-2} mm, suggesting that no appreciable quantities of C_2 and C_3 hydrocarbons were present. More convincing evidence for this statement is presented below.

Distillation of the condensable products from a trap immersed in an ice-water bath to a liquid nitrogen trap resulted in the separation of these products into a light fraction and a residue which we shall call the heavy fraction. Since the quantities of products from any given run were very small, it was necessary to combine the condensables from a number of runs in order to obtain sufficient amounts for characterization. Toward this end, the total condensables from twenty 90-minute runs, which were carried out at pressures from 5–110 mm, were combined and fractionated as described above. We shall refer to the heavy fraction from these combined runs as Fraction A.

Another sample of the heavy fraction was obtained by combining the distillation residues from fifteen 120-minute runs, made at an initial pressure of 110 mm. This sample will be referred to as Fraction B.

Both heavy fractions A and B had a terpene-like odor, reminiscent of turpentine. They both became very viscous when cooled to -78.5°C and were found to solidify in liquid nitrogen. Fraction A had a boiling point of 215–216°C at 750 mm, while Fraction B boiled at 220–222°C at the same pressure. The refractive index, n_D^{20}, for Fraction B was 1.4693.

TABLE II. Average rate of hydrogen formation as a function of initial pressure and time.

Duration of run (min)	Average rates of hydrogen formation in moles/min $\times10^6$ for initial pressures in mm Hg of: 16.5±2	44±2.5	74±1.5	107±1
1	1.1	1.3	1.6	1.4
3	0.9	1.2	1.4	1.4
6	0.90	1.00	1.28	1.31
10	0.77	1.07	—	1.16
15	—	—	1.08	—
30	—	—	0.89	—
60	—	—	0.80	—
90	0.44	0.62	0.73	0.77

A 20 mg sample of Fraction B was sent to Clark Microanalytical Laboratories, as stated above. The carbon-hydrogen analysis gave C: 86.97 percent, H: 12.90 percent (total 99.87 percent). Molecular weight values were 181 and 191, and the terminal methyl determination gave 10.80 percent by weight. The C—H values would not serve to distinguish between $C_{12}H_{22}$ and $C_{13}H_{24}$, and the molecular weight would appear to favor the latter. However, the C_{13} compound can be rejected from other considerations, which will be adduced below. Furthermore, it has been shown in this laboratory[2] that Rast's method gives high values with the higher cycloparaffins.

The terminal methyl value converts to the following methyl numbers: for molecular weights of 166, 181, and 191, the number of CH_3 groups becomes 1.2, 1.3, and 1.4, respectively. And, in this connection, it should be emphasized that this type of determination is not always stoichiometric.[22] Thus, Barthel and La Forge[22] point out that methylcyclohexene yields 0.53 methyl groups per molecule by this technique. These authors recommend that determinations be run on a compound of similar structure before drawing conclusions on an unknown. To that end, a sample of pure 2,2′-dimethyldicyclopentyl was obtained for analysis through the kindness of the Pittsburgh Research Division of the U. S. Bureau of Mines. This compound, strangely enough, is a solid, m.p. 46–47°C, while the 3-3′-dimethyldicyclopentyl is a liquid. Unfortunately, the test failed completely. For some unknown reason, the compound proved completely stable to the chromic acid mixture and distilled up into the reflux condenser where it crystallized.

TABLE III. Initial and steady-state values for the rates of hydrogen formation.

P_0 (mm)	Initial rate of hydrogen formation (moles/min $\times10^6$)	Steady-state rate of hydrogen formation (moles/min $\times10^6$)
16.5±2	1.2	0.40
44 ±2.5	1.4	0.56
74 ±1.5	1.7	0.66
107 ±1	1.7	0.72

[22] W. F. Barthel and F. B. La Forge, Ind. Eng. Chem. Anal. Ed. **16**, 434 (1944).

TABLE IV. Comparative rates of hydrogen formation for interrupted and single runs. Initial pressure = 74±1.5 mm.

Duration (min)	Interrupted run Run (No.)	Average rate of hydrogen production (moles/min ×10⁶)	Single runs	Run (No.)
3	33a	1.3	1.4	30
6	33b	1.3	1.3	32
15	33c	1.11	1.08	31
30	33d	0.98	0.87	29
60	33e	0.84	0.80	28
90	33f	0.78	0.73	20

A sample of the light fraction, which was obtained by combining the distillates from nine 2-hour runs at 110 mm pressure, proved to be 99.4 mole percent methyl cyclopentane and 0.6 percent C_6H_{10}. Dr. F. L. Mohler, Chief, Mass Spectrometry Section, National Bureau of Standards, stated in his report that the C_6H_{10} appeared to be methylcyclopentene(s) by comparison with similar compounds. However, the possibility that some of the isomeric methylenecyclopentane might be present could not be completely rejected.

The combined light fractions from ten runs of from 1 to 6 minutes' duration were combined and titrated for olefins. The average duration of these runs was 3 minutes. The titration yielded 0.17 mole percent olefins, based upon methyl cyclopentane. From these data, one can obtain a rough estimate of the initial rate of olefin formation which becomes 0.5×10^{-6} mole/min.

The Effect of Intermittent Removal of Hydrogen from the Reaction Mixture

A special run, No. 33(a-f), was made to investigate the effect of removal of hydrogen from the reaction mixture both on the average rate of hydrogen formation and on the over-all reaction rates. Irradiation of the cell was interrupted at periods of respectively 3, 6, 15, 30, 60, and 90 minutes from the start of the run. At each of these points the condensable products were frozen down, and the hydrogen was transferred to the analytical unit where its PV product was measured. The condensable products were then allowed to revaporize, and after the system had again attained equilibrium, the run was resumed.

The total quantity of hydrogen formed as a function of time for the interrupted run is plotted as the upper curve in Fig. 2. An inspection of this figure shows that the steady-state rate of hydrogen formation is the same for the single runs as for the interrupted run. The average rates of hydrogen formation for this run are compared with those for the single runs of the same duration in Table IV. The effects observed are definitely greater than the experimental error. Hence, we are led to the conclusion that the average rate of hydrogen formation is palpably increased by intermittent freezing down of the condensable products and removal of all hydrogen present. While this effect is only perceptible for irradiation periods greater than 15 minutes, the coincidence of the points for shorter periods may well be due to experimental error.

Other effects were noticed in the course of the interrupted run. Thus, it was found that the condensable products, after revaporization following hydrogen removal, returned to a lower pressure than could be explained on the basis of hydrogen extraction alone. This observation would indicate that some relatively nonvolatile component was present in the reaction mixture at a partial pressure higher than its vapor pressure. Furthermore, the over-all rates of pressure decrease, as found in the last two half-hour periods of this run, were considerably less than the pressure rates for pure reactant at the same pressure. Thus, after 30 and 60 minutes of exposure time, the pressures in the system were, respectively, 71.2 and 68.2 mm after hydrogen removal. The observed rates of pressure decrease were 0.78 and 0.62×10^{-6} mole/min, respectively. For pure methylcyclopentane, the rates of pressure decrease at these pressures would be 0.83 and 0.80×10^{-6} mole/min, respectively. The slight difference in the rates of hydrogen formation for these runs will not explain the discrepancy. Finally, it was observed for the last two 30-minute periods of the interrupted run, i.e., parts 33d–33e, and 33e–33f, that the period of induction was much less pronounced, both in magnitude of pressure rise and in duration, than in runs with pure reactant at the same initial presures.

TABLE V. Actinometric data from cyclopropane.

Initial pressure (mm)	Corrected rate of pressure decrease (moles/min ×10⁶)	Light intensity (einsteins/min ×10⁶)
98.9	0.55	4.0_5
117.4	0.56	4.1_5

LIGHT INTENSITY AND QUANTUM YIELD

The results of the actinometric runs with cyclopropane are presented in Table V. The runs were carried out at the beginning and at the end of the entire investigation in order to detect possible changes in light intensity. From Table V, we obtain an average value of 4.1×10^{-6} einsteins/min for our light intensity.

Combining our light intensity with the data of Tables I and III, we find at the highest pressure investigated, 107±1 mm, that the initial quantum yield of hydrogen formation is at a maximum at 0.42, and the corresponding maximum quantum yield for methylcyclopentane consumption is 0.44.

DISCUSSION

The Identification of the Reaction Products

As will become clear from the following discussion of the mechanism of the reaction, it must be assumed that methylcyclopentane reacts with Hg $6(^3P_1)$ atoms with the formation, primarily, of H atoms and cyclic C_6H_{11} radicals. The heavy fraction, therefore, is pre-

TABLE VI. Physical properties of known dimethyldicyclopentyls, of 1,2-dicyclopentylethane, and of the heavy fractions.

Substance	m.p. (°C)	b.p. (°C at mm)		n_D at °C		Terminal methyl number	Reference
1,2-dicyclopentylethane	—	206–207	748	1.4651	22	—	a, b
		109–110	17	1.4657	20		
2,2′-dimethyldicyclopentyl	46.5	212	760	1.4500	50	—	c, d, e
	46 –47	216.9	760	1.4463	60		
	45.5–45.7						
3,3′-dimethyldicyclopentyl	—	213–214	738	1.4755	20	—	f, g, h
		218–219	760	1.4755	18.5		
		213–215	760				
Heavy fraction A	—	215–216	750	—		—	This paper
Heavy fraction B	—	220–222	750	1.4693	20	1.2	This paper

[a] See reference 23.
[b] P. S. Pinkney and C. S. Marvel, J. Am. Chem. Soc. **59**, 2669 (1937).
[c] C. D. Nenitzescu and C. N. Ionescu, Ann. **491**, 189 (1931).
[d] V. N. Ipatieff and V. I. Komarewsky, J. Am. Chem. Soc. **56**, 1926 (1934).
[e] M. Orchin and J. Feldman, J. Am. Chem. Soc. **68**, 2737 (1946).
[f] J. Schmidt and A. Sigwart, Ber. **45**, 1779 (1912).
[g] Zelinsky, Titz, and Fatejew, J. Am. Chem. Soc. **59**, 2585 (1926).
[h] Zelinsky, Schuikin, and Fatejew, J. Gen. Chem. USSR **2**, 671 (1932).

sumably a radical recombination product, or a mixture of such products with formula $C_{12}H_{22}$ and a molecular weight of 166. Our data on the heavy fraction are consistent with the above type of product, considering the exceedingly small samples used for the characterization. The $C_{13}H_{24}$ compound may be rejected, since its presence would require that methyl radicals and, hence, methane should be present, contrary to our findings.

Primary scission of the C—H bond could conceivably lead to three main types of radicals, corresponding to the rupture of primary, secondary, and tertiary bonds. We shall denote these C_6H_{11} cyclic radicals by R_I, R_{II} and R_{III} respectively. The stable products resulting from radical recombination could then be of three main types:

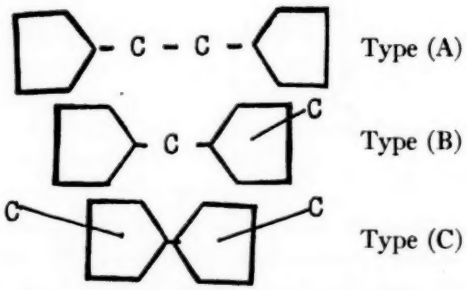

Type (A) is non-isomeric, assuming free rotation; Type (B) has three structural isomers; and Type (C) has six structural isomers. We have ignored optical isomers arising from various asymmetric centers.

Unfortunately, only three of all the possible isomers have been described in the literature. The physical properties of these isomers, together with the pertinent data on the heavy fraction, are summarized in Table VI.

In attempting to deduce the particular types of compounds in the heavy fraction, the methyl number assumes great importance. Thus, Types (A), (B), and (C) possess zero, one, and two terminal methyls, respectively. Hence, since our methyl number is 1.2, we can conclude that some compounds of Type (C) must be present. What is more, if the heavy fraction consisted entirely of Type (C) compounds, the methyl number would indicate a 60 percent yield for the terminal methyl determination, which appears to be a reasonable yield for cyclic compounds.[23] The remainder of the data on the heavy fraction are not inconsistent with the hypothesis that the fraction consists entirely of dimethyldicyclopentyls. Thus, the boiling points of the heavy fraction are within the range of the known 2,2′- and 3,3′-compounds. The solid 2,2′-compound would probably have a value of n_D^{20} of approximately 1.46, and, therefore, our heavy fraction could be composed of a mixture of the 2,2′- and 3,3′-compounds. In this connection it should be pointed out that the R_{III}–R_{III} recombination of Type (C) would be unlikely from steric considerations. Further comments on the products of the reaction will be found in the following discussion of the mechanism of the reaction.

The Mechanism of the Reaction

The observations which have been reported in this paper bear striking resemblances to the cyclopentane reaction,[11] suggesting a similar mechanism for both molecules. Summarizing, any mechanism proposed for the reaction of methylcyclopentane with Hg $6(^3P_1)$ atoms must fit in with the following observations:

(a) The pressure initially increases slightly, but begins to decrease after 3 to 5 minutes of exposure. The rate of pressure decrease becomes independent of time after 15 to 20 minutes of irradiation.

(b) The rate of pressure decrease increases with increasing initial pressure of methylcyclopentane, even in the pressure region where it may be assumed that quenching is complete. The pressure rate is a linear function of the initial pressure above about 15 mm.

(c) Hydrogen is a major product of the reaction.

(d) The average rate of hydrogen formation decreases with time of exposure.

(e) The initial rate of hydrogen formation increases

[23] Zelinsky, Michlana, and Evantowa, Ber. **66**, 1422 (1933).

with increasing reactant pressure, reaching a maximum quantum yield of 0.44 at 107±1 mm.

(f) The instantaneous rate of hydrogen formation reaches a constant value after 15–20 minutes of exposure, simultaneously with the instantaneous rate of pressure decrease.

(g) The maximum quantum yield of methylcyclopentane disappearance is 0.42 at 107±1 mm.

(h) Intermittent removal of hydrogen from the reaction mixture increases the average rate of hydrogen formation over that found for comparable single runs.

(i) Intermittent removal of hydrogen depresses the rate of pressure decrease below that observed for runs with pure reactant at the same pressure. Under these conditions the induction period is also depressed.

(j) The major hydrocarbon products of the reaction are cyclic C_6H_{10}—very probably a mixture of isomeric methylcyclopentenes, together with a bicyclic $C_{12}H_{22}$ which appears to be a mixture of dimethyldicyclopentyls.

The absence of methane, together with the large amounts of hydrogen formed, definitely rule out C−C bond rupture as a significant primary process. It is concluded, therefore, that the primary reaction is a C−H bond split. Furthermore, the C_6H_{11} radical thus formed must needs be cyclic, since the 112.2 kcal/mole of energy available from the Hg $6(^3P_1)$ atoms are not sufficient to open the ring simultaneously with splitting off a hydrogen atom.

The reaction will be discussed in terms of a sequence, similar to the one proposed for cyclopentane,[11] with the addition of a hydrogen quenching step. The mechanism is as follows:

$$\text{cyclo } C_6H_{12}+\text{Hg } 6(^3P_1)\rightarrow \text{cyclo } C_6H_{11}+\text{H}+\text{Hg } 6(^1S_0) \quad (1)$$

$$\text{H}+\text{cyclo } C_6H_{12} \rightarrow H_2+\text{cyclo } C_6H_{11} \quad (2)$$

$$\text{H}+\text{cyclo } C_6H_{11} \rightarrow C_6H_{12} \quad (3)$$

$$\text{H}+\text{cyclo } C_6H_{11} \rightarrow H_2+\text{cyclo } C_6H_{10} \quad (4)$$

$$2 \text{ cyclo } C_6H_{11} \rightarrow C_{12}H_{22} \quad (5)$$

$$H_2+\text{Hg } 6(^3P_1) \rightarrow 2\text{H}+\text{Hg } 6(^1S_0). \quad (6)$$

This mechanism accounts for all products found, namely hydrogen, $C_{12}H_{22}$, and C_6H_{10}. As we have pointed out previously, the cyclo C_6H_{11} radicals formed in steps (1) and (2) could result from the splitting of primary, secondary, or tertiary bonds. Since there are 3 primary, 1 tertiary, and 8 secondary C−H linkages, statistical considerations strongly favor a secondary C−H split. However, even if the two radical-forming steps give rise to primary, secondary, and tertiary radicals, the following considerations should apply:

Since the C−H bond energies decrease in the order primary through secondary to tertiary, the following abstraction reactions are energetically possible:

$$R_I + C \rightarrow R_{II} + C, \quad (7)$$

$$R_{II} + C \rightarrow R_{III} + C, \quad (8)$$

where C represents the methylcyclopentane substrate. However since methylcyclopentane has only one tertiary C−H bond, one would expect that R_{II} would predominate. Moreover, R_{III} radicals would be less likely to recombine, since steric factors probably inhibit the formation of the 1,1′-dimethyldicyclopentyl. For this reason, it seems more likely that any R_{III} radicals formed will be largely responsible for steps (3) and (4).

The above considerations lead us to the conclusion that R_{II} radicals will be mainly responsible for the recombination products, which will, therefore, be a mixture of 2,2′-, 3,3′-, and 2,3′-dimethyldicyclopentyls. Our data on the heavy fraction are in general agreement with these deductions.

While the assumption of steady-state concentrations of radicals does not permit the determination of the explicit kinetics predicted by the proposed mechanism, the trends indicated by the rate equations can be shown to be in agreement with the experimental data. Let $(R)=(C_6H_{11})$, I_a the intensity of the absorbed light in the complete quenching region, and K an inefficiency constant for the primary process, equal to or less than unity. We shall assume that quenching is partitioned between hydrogen and methylcyclopentane. Under these conditions, the over-all rate of pressure decrease and the rates of formation of hydrogen, C_6H_{10}, and $C_{12}H_{22}$ are then given by the following expressions:

$$-dP/dt = KI_a - k_3(H)(R) - 2k_4(H)(R) \quad (9)$$

$$dH_2/dt = KI_a - k_3(H)(R) \quad (10)$$

$$d(C_6H_{10})/dt = k_4(H)(R) \quad (11)$$

$$d(C_{12}H_{22})/dt = k_5(R)^2. \quad (12)$$

It can be easily shown that as the initial concentration of methylcyclopentane is increased, (R) increases while (H) and (H)(R) decrease. Therefore, it follows from Eq. (9) that the rate of pressure decrease increases with initial methylcyclopentane pressure, as we have found experimentally. It has not been possible to show, on the basis of the proposed mechanism, that the increase is linear.

It follows from Eq. (10) that the rate of hydrogen formation also increases with methylcyclopentane pressure, in agreement with the experimental data. Equations (11) and (12) show that the rates of olefin and dimer formation, respectively, decrease and increase with increasing initial pressures of methylcyclopentane. No experimental data are available to check these implications.

Considering now the variation of these rates with time, treating the concentration of methylcyclopentane

as a constant, an assumption which is only approximately correct, the steady-state calculations show that under these conditions

(R) decreases with time,
(H) increases with time, and
(H)(R) increases with time.

Thus, it follows from Eq. (9) that the rate of pressure decrease will decrease with time, whereas the data show it to be constant within the limits of experimental error.

Equation (10) predicts a decreasing rate of hydrogen formation with time, which is in agreement with the data presented. Equation (11) predicts an increasing rate of olefin formation with time, while Eq. (12) indicates a rate of formation for the dimer which decreases with time. No experimental data are available to check these predictions.

Inspection of Eqs. (9) and (10) will also show them to be in agreement with the experimental evidence that rates of hydrogen formation are always larger than the rates of pressure decrease. The limiting values for both are the same.

The initial pressure rise and time lag observed in each run before the pressure starts to decrease can be accounted for by the necessity of building up the gas-phase $C_{12}H_{22}$ concentration to its vapor pressure before condensation starts. Also, reaction (4) is pressure increasing, so that the over-all reaction prior to condensation of the $C_{12}H_{22}$ product will be pressure increasing. Furthermore, physical effects, such as the heat evolved by absorption of radiation by the quartz cell or by the recombinations of radicals, may play a part during this induction period.

In run 33, in which the products were frozen down and hydrogen pumped off at intervals, it may be assumed that each time irradiation was recommenced the dimer was already present in the gas mixture at its vapor pressure, so that condensation could start immediately. This may explain the fact that the induction effect for the latter parts of this run was found to be smaller and of much shorter duration than at the beginning of a normal run.

Again for run 33, the increase in average rate of hydrogen formation over that found for independent runs of identical duration and similar initial pressures is seen to result naturally from step (6) in the proposed mechanism. If hydrogen is pumped off, its mole fraction in the mixture at any moment will be less than if it were allowed to accumulate. Since it quenches Hg $6(^3P_1)$ atoms in proportion to its mole fraction in the mixture, its rate of disappearance by quenching will be less, and its apparent average rate of formation will, consequently, be higher than in runs where all the hydrogen is left in the mixture.

The kinetic expressions give no indication of the size of the inefficiency constant K. The low quantum yield of initial hydrogen formation of only 0.44, at the highest pressures used, can be explained, at least in part, by the recombination step (3) in the proposed mechanism which reduces the efficiency of the process. This step is, furthermore, necessary if the equation for the rate of hydrogen formation is to express its increase with initial pressure of methylcyclopentane.

It should be noted that the olefins accumulating in the reaction mixture will undoubtedly also compete with methylcyclopentane in the quenching reaction. Apparently, however, they do not initiate chemical reactions resulting in the formation of secondary products. Presumably, olefin quenching here results in the formation of excited molecules which are then deactivated by collision, so that its only appreciable effect would be an effective decrease in the light intensity; however, it was not found feasible to take this into consideration in the rate equations. If the rate of formation of olefin decreases with initial pressure, as indicated by Eq. (11), quenching by olefins will be less at higher pressures.

CONCLUSIONS

Methylcyclopentane bears strong resemblances in its reactions to those of the unsubstituted ring. And both, in turn, are decidedly paraffinic in their reactions to Hg $6(^3P_1)$ atoms in their tendency to rupture at the C—H bond. It is apparent from this investigation that studies on methylcyclopentane itself will not solve the problem of the presence or absence of specificity of the Hg $6(^3P_1)$ atoms for the various types of C—H bonds. It is, therefore, our intention to investigate the reactions of deuterated methylcyclopentanes with Hg $6(^3P_1)$ atoms in order to gain further insight into this fundamental problem.

The mechanism of the reaction is remarkably complex. However, it is felt that the inclusion of the hydrogen quenching step—reaction (6) above—has considerably broadened the scope of the mechanism and brought it into closer consonance with the experimental findings.

It should be emphasized in closing that the six-step mechanism discussed here for methylcyclopentane is also completely applicable to the cyclopentane reaction.

ACKNOWLEDGMENTS

The authors would like to express their appreciation to Dr. F. L. Mohler, Chief, Mass Spectrometry Section, Division of Atomic and Radiation Physics, National Bureau of Standards, for his assistance in the characterization of the reaction products. Furthermore, the authors are also indebted to the Research and Development Division of the U. S. Bureau of Mines for a sample of pure 2,2′-dimethyldicyclopentyl, prepared by Dr. M. Orchin of that laboratory.

The Growth of Uniform Colloidal Dispersions*

HOWARD REISS
Department of Chemistry, Boston University, Boston, Massachusetts
(Received November 6, 1950)

Recently, much interest has been focused upon the preparation of monodispersed colloids using the "growth by diffusion" process. Although these colloids are useful tools in experimental procedures, no well-established reason has been given to explain why the "growth by diffusion "method should produce such uniform dispersions. In this paper it is shown that an assembly of competing particles, growing by diffusion, develop the squares of their radii at equal rates. This condition provides a mechanism leading towards uniformity.

A method, based on this equal square rule, is suggested for the determination of size distributions in polydispersed systems.

I. INTRODUCTION

IN recent years, much attention has been directed toward the growth of uniform colloidal dispersions. Research in this field has been quite successful, and there is now an extensive literature on the subject.[1–14] Very uniform, so-called "monodispersed" colloids are ideally suited as tools in certain experimental procedures, and investigations which were previously impossible have now been carried out. A list of applications in these lines is given below. The starred items refer to those procedures which have already been carried out, while the unstarred items indicate procedures now in progress or projected in the future.

Uses for Monodispersed Colloids

*(1) Experimental verification of light scattering theories.[2]
*(2) Standards in light scattering work.[11,12]
*(3) Experimental verification of coagulation theories.[15]
*(4) Measurement of Avogadro's number.[16]
*(5) Experimental study of the relation between particle size and particle retention in the human lung.[7]
*(6) Measurement of diffusion coefficients in supersaturated solutions.[8,9]
(7) Experimental verification of theories on surface thermodynamics.[14]
(8) Meteorological applications. (In progress.) Unpublished work by V. K. La Mer.
*(9) Studies of reaction kinetics.[13]

The most fruitful method for preparing uniform dispersions has been the "growth by diffusion" method, employed by La Mer and his co-workers. The distribution of particle radii in these colloids is so narrow that they exhibit the strikingly beautiful scattering phenomenon which has been called the "higher order Tyndall spectrum."[2,5]

Although the "growth by diffusion" method has been given much experimental use and the colloids formed have furnished very handy tools, no truly sound exposition exists to explain why the method improves the uniformity so markedly. The purpose of this paper is to provide such an explanation.

La Mer and Wilson[7] have attempted to explain the phenomenon. These authors introduce a valid assertion (i.e., that all particles in an assembly, growing by diffusion, develop the squares of their radii at equal rates), but they do not offer any proof for this statement. Their considerations are based upon the so-called Langmuir equation, which is derived for a *single isolated* particle, growing either in the presence of an infinite diffusion field or in a region where the concentration of diffusing material remains constant at some fixed distance from the particle. In all cases, the Langmuir treatment assumes a *steady state*, and in no case is a uniformly distributed source (e.g., a chemical reaction) considered.

It is impossible to develop any conclusion concerning the manner of growth of a competitive assembly by using an equation whose derivation does not, in some way, contain the assembly in its formulation. Furthermore, the assumption of a steady state is invalid during the growth of most aerosols, and during a major part of the growth of hydrosols,[8] even when a uniformly distributed source, such as a chemical reaction, is present. Even if, in the latter case, a steady state could be assumed, the uniformly distributed source would have to appear in the formulation, and it does not in the Langmuir treatment.

* This investigation has been supported by the Geophysical Research Directorate of the Air Force Cambridge Research Laboratory under contract AF 19(122)-168.

[1] La Mer, J. Phys. and Colloid Chem. **52**, 65 (1948).
[2] La Mer and Sinclair, Chem. Revs. **44**, 245 (1949).
[3] La Mer and Barnes, J. Colloid Sci. **1**, 71, 79 (1946).
[4] La Mer and Kenyon, J. Colloid Sci. **2**, 251 (1947).
[5] Johnson and La Mer, J. Am. Chem. Soc. **69**, 1184 (1947).
[6] Barnes, Kenyon, Zaiser, and La Mer, J. Colloid Sci. **2**, 349 (1947).
[7] Wilson and La Mer, J. Ind. Hyg. and Toxicol. **30**, 265 (1948).
[8] Reiss and La Mer, J. Chem. Phys. **18**, 1 (1950).
[9] La Mer and Dinegar, J. Am. Chem. Soc. **72**, 4847 (1950).
[10] Kerker and La Mer, J. Am. Chem. Soc. **72**, 3516 (1950).
[11] Zimm, J. Chem. Phys. **16**, 1093 (1948).
[12] Dandliker, J. Am. Chem. Soc. **72**, 5110 (1950).
[13] Zaiser and La Mer, J. Colloid Sci. **3**, 571 (1948).
[14] Reiss and Wilson, J. Colloid Sci. **3**, 591 (1948).
[15] Whytlaw, Gray, and Patterson, *Smoke* (Edward Arnold and Company, London, 1932).
[16] Perrin, Compt. rend. **146**, 967 (1908); **147**, 530; **149**, 477; 549 (1909).

The Langmuir equation simply states that the isolated particle in question will grow so that the square of its radius develops linearly with time and says nothing concerning the relative rates of growth of particles in a competitive assembly. What is needed is some demonstration of the existence of a natural growth-regulating mechanism founded on well-established physical principles. This mechanism should permit nature to "apply the brakes," so to speak, to retard the growth of larger particles while hastening the development of smaller ones. We shall show that such a mechanism does exist.

II. THE GROWTH EQUATION FOR A COLLOID INITIALLY UNIFORM

Interest will be focused upon an assembly of particles growing by diffusion. In this section, let us assume that, initially, all of the particles have the same radius, which we may conveniently assume to be zero. In a later section it will be demonstrated that the distribution of sizes improves (becomes narrower) with growth, so that if the distribution is already perfect, it will have to remain so. Consequently, if all of the particles are, initially, of the same size, they will grow at the same rate, and at any time, t, the common radius can be denoted by the function of time alone,

$$x=x(t). \tag{1}$$

Since, under the above conditions, the growth of any one particle is representative of the growth of every particle, it will be sufficient to consider just one particle. In deriving the growth law, we shall appeal to a method developed by Reiss and La Mer[8] for the treatment of non-steady-state diffusion, in which one of the geometrical boundaries of the diffusion field varies with time. This method has been applied to spherically symmetric cases in which one boundary is a sphere impermeable to the diffusing species. The method is approximate, but it can be shown that an error of less than 10 percent is introduced providing that the radius, h, of the impermeable sphere is at least ten times as large as the radius, x, of the growing particle. The approximation has been justified both theoretically and experimentally.[8,9]

The main features of the method consist of

(1) The replacement of the diffusion equation (based on Fick's law[17])

$$(\partial^2 c/\partial r^2)+(2/r)(\partial c/\partial r)=(1/D)(\partial c/\partial t) \tag{2}$$

(where c is the concentration of the diffusing species, r is the distance from the center of the growing particle, and D is the coefficient of diffusion) by

$$(\partial^2 c/\partial r^2)+(2/r)(\partial c/\partial r)=0. \tag{3}$$

Notice that this expression differs from

$$(d^2 c/dr^2)+(2/r)(dc/dr)=0 \tag{4}$$

in that c is still considered to be a function of time.

[17] Longsworth, Ann. N. Y. Acad. Sci. **46**, 212 (1945).

(2) The replacement of the normal condition for an impermeable shell

$$(\partial c/\partial r)_{r=h}=0 \tag{5}$$

by the requirement that

$$c(h, t)=\bar{c}(t), \tag{6}$$

where $\bar{c}(t)$ is the space average concentration at the time, t.

Condition (6) is based upon the supposition that it is impossible, in diffusion, to maintain sharp concentration gradients anywhere except in the immediate neighborhood of a source or sink. Of course, this is intuitively reasonable, but we do not, off hand, know how far the *immediate neighborhood* of a sink extends into the diffusion field. The fact that condition (6) leads to reasonable results indicates that it is safe to say that such a neighborhood does not extend beyond ten sink diameters from the sink.

This result is very important for the treatment of competition between sinks, for it makes it possible to assume that at any instant the concentrations will be the same (no concentration gradients) at two points which are, respectively, just outside the neighborhoods of two sinks, provided that they are not inside the neighborhoods of other sinks. If the sinks are, on the average, separated by twenty sink diameters, the proportion of cases in which such points are in the neighborhood of other sinks will not be appreciable. It is important to realize that at such points the concentrations are *changing* with time and are not constant, although they change at the same rate.

In what follows, one of the things we shall show is that the concept of the impermeable shell is unnecessary, and that the same result will be obtained if it is only possible to take $c(h, t)$ for some value, h, outside of the immediate neighborhood of the sink.

If the particles are droplets of condensate, growing because the assembly is being cooled, we may conveniently write

$$c(x, t)=c_0 e^{-\gamma B t}, \tag{7}$$

where c_0 is the concentration, initially uniform in space, corresponding to the temperature, T_0, where the cooling began. γ is the cooling rate, and B is a constant, characteristic of the vapor being cooled. For the details of the origin of (7) (Eq. (9) of reference 8), see reference 8. Fick's law[17] has the form

$$\mathbf{f}=-D(\partial c/\partial r), \tag{8}$$

where $\mathbf{f}$ is the flux density of diffusing material.

On the basis of (3) integrated and combined with (8)

$$Q(t)=4\pi r^2|\mathbf{f}(r)|, \tag{9}$$

where $Q(t)$ is the flux through a spherical shell, concentric, at any value of r, with the growing particle. Q is constant with respect to r; a function of time alone.

Equation (9) can be rewritten with the aid of (8) to yield

$$(\partial c/\partial r) = -Q(t)/4\pi Dr^2, \tag{10}$$

and this can be integrated with respect to r to give

$$c(r, t) = [Q(t)/4\pi Dr] + f(t), \tag{11}$$

where $f(t)$ is some arbitrary function of time. At x and h, Eq. (11) reduces to

$$c(x, t) = [Q(t)/4\pi Dx] + f(t), \tag{12}$$

and

$$c(h, t) = [Q(t)/4\pi Dh] + f(t), \tag{13}$$

and the simultaneous solution of these yields

$$Q(t) = \frac{4\pi D}{(1/h - 1/x)}[c(h, t) - c(x, t)], \tag{14}$$

$$f(t) = c(x, t) - \frac{1}{x(1/h - 1/x)}[c(h, t) - c(x, t)]. \tag{15}$$

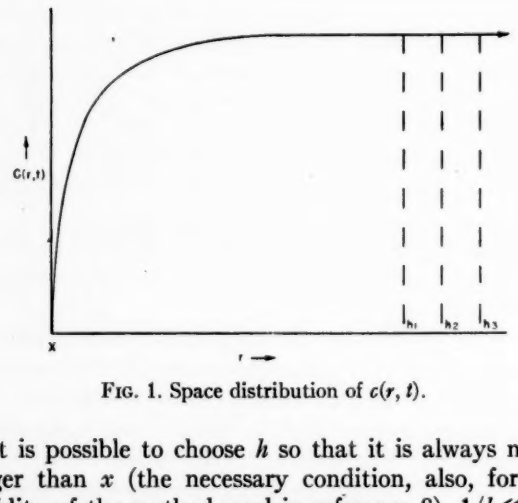

FIG. 1. Space distribution of $c(r, t)$.

If it is possible to choose h so that it is always much larger than x (the necessary condition, also, for the validity of the method used in reference 8), $1/h \ll 1/x$, and (14) and (15) can be simplified. Thus,

$$Q(t) = -4\pi Dx[c(h, t) - c(x, t)], \tag{16}$$

$$f(t) = c(h, t). \tag{17}$$

These expressions can be used in (11) for the evaluation of $c(r, t)$.

In accordance with (5),

$$c(h, t) = \bar{c}(t) = c_0 - (A\rho/w)(4/3)\pi x^3(t)n, \tag{18}$$

where A is Avogadro's number, ρ the density of the condensate, W the molecular weight of the diffusing species, and n the number density of growing particles. Because sharp concentration gradients can only be maintained in the neighborhood of sinks, a plot of $c(r, t)$ *versus* r will resemble the curve of Fig. 1. There is a steep concentration gradient in the neighborhood of the sink at x. At some distance, h, from x the curve flattens out. In fact, the concentrations at h_1, h_2, and h_3 are all substantially the same. It is immaterial whether we choose h_1, h_2, h_3, etc., as the h for our problem, since it is apparent from (16) that it is not h, but $c(h, t)$ which appears in the problem explicitly.

The rate of change of volume of the growing particle, when multiplied by the scale factor, introduced above, can be set equal to the negative flux. Thus,

$$(A\rho/w)(d/dt)(4/3)\pi x^3 = (A\rho/w)4\pi x^2(dx/dt) = -Q(t). \tag{19}$$

Substituting (18) and (7) into (15) and (16) into (19) leads to the following differential equation for x^2.

$$d(x^2)/dt = 2WDc_0/A\rho[1 - e^{-\gamma Bt}] - (8/3)\pi Dnx^3. \tag{20}$$

This equation *does not* assert that x^2 increases linearly with time. In reference 8, Eq. (58) for the rate of growth was derived on the assumption that the single particle was enclosed by an impermeable spherical shell of radius h, where

$$(4/3)\pi h^3 = 1/n. \tag{21}$$

This shell was introduced to account for the fact that the other particles in the assembly were competing for the vapor. The device of the shell was somewhat artificial, since it organized the system to the extent that the particles were considered as equidistant from each other, but it was necessary insofar as it made possible the comparison of the approximate method with an exact method. This comparison indicated that the approximation was valid when $h \gg x$. As it has been indicated, equations on the type of (58) have now been tested experimentally also.

If (20) is introduced into (19), the result is

$$d(x^2)/dt = 2WDc_0/A\rho[1 - e^{-\gamma Bt}] - 2Dx^3/h^3, \tag{22}$$

which is identical with (58) of reference 8. This result indicates that the approximate method used above is valid under the condition which we have already applied to it, namely, $h \gg x$. Indeed, the above method is really identical with the approximation which appears in reference 8, except for the fact that it does not contain the device of the impermeable shell. The existence of competing particles is signalized by the appearance of their number density, n, in (20), in place of the explicit appearance of h. There is a distinct advantage in this treatment, since the particles are in no way required to be equidistant, so that a more natural, random space distribution may be considered. In addition, the older treatment would be useless for the discussion of non-uniform colloidal dispersions, since all of the particles, regardless of their size, would have to grow by the same amount because the vapor available to each particle would be enclosed in an impermeable shell of radius, h, the same for each particle. Any opportunity for discovering a natural growth regulating mechanism would be eliminated at the start, since, in effect, its existence would have been assumed in setting up the problem.

The arbitrariness, within limits, of h has been men-

tioned previously by Langmuir[18] in his treatment of the evaporation of an assembly of particles. He arrives at the conclusion that the individual particles of the assembly are *independent* of each other. This result *should not* confuse the present issue. In the situation treated above, the particles are *not* independent. In Langmuir's case, $c(h, t)$ and $c(x, t)$ were constants, independent of time, and so a real independence for the particles was possible. A real steady state was also possible.

In closing this section it should be mentioned that in the specification of $c(x, t)$ in (7) the Kelvin effect[19] has not been considered. This is due to the fact that only particles which are so large ($x>10^{-5}$ cm) that their vapor pressures are not influenced by their radii will be treated. Even if an assembly starts to grow in a size range where the Kelvin effect is appreciable, so long as it grows into the range where it is inappreciable, the regulating mechanism to be demonstrated, below, will exert its effect, and so tend to produce a uniform dispersion. In other words, the initial distribution and the zero of time may always be taken as the distribution and time which are obtained in the system as it enters the range in which the Kelvin effect may be ignored.

Finally, the condition $h \gg x$ will be well enough satisfied if $n \leqslant 10^6$/cc, and the largest value of x which must be considered is 5×10^{-4} cm. If n is appreciably less than 10^6/cc, the largest x which can be considered may be increased beyond 5×10^{-4} cm.

III. THE GROWTH EQUATION FOR A COLLOID, INITIALLY NON-UNIFORM

At a given time during the growth of a non-uniform colloid, the radii of different particles will be different. In contrast to the situation in Sec. II, this fact can be signified by writing in place of (1)

$$x=x(a, t), \tag{23}$$

where a is the initial radius of the particle. Equation (19) must now assume the form

$$4\pi x^2(a, t)\frac{\partial x(a, t)}{\partial t}=-\frac{W}{A\rho}Q(a, t)$$

$$=\frac{4\pi DW}{A\rho}x(a, t)[c(h, t)-c(x, t)], \tag{24}$$

which can be simplified to

$$\partial[x^2(a, t)]/\partial t=(2WD/A\rho)[c(h, t)-c(x, t)]. \tag{25}$$

From the discussion in Sec. II, it is evident that $c(h, t)$ and $c(x, t)$ are functions of time alone. We are thus driven to the important conclusion that *the rate of increase of x^2 is the same for all particles independent of the initial value a^2*. Analytically,

$$x^2(a, t)=a^2+R^2(t). \tag{26}$$

Equation (26) represents the regulating mechanism which is sought. Combined with the fact that there is only a definite amount of depositable, diffusing material available, it determines how much a given process of growth will sharpen a size distribution. It *demands* that distribution *always* be sharpened by growth. This will be explained more clearly later.

Obviously,

$$x^3(a, t)=[a^2+R^2(t)]^{\frac{3}{2}}. \tag{27}$$

If, initially, the number of radii lying in the range between a and $a+da$ is $n(a)da$, then, in place of (18) for $c(h, t)$, there must appear the expression

$$c(h, t)=c_0-(4/3)\pi(A\rho/W)\int[x^3(a, t)-a^3]n(a)da, \tag{28}$$

which, with the inclusion of (27), becomes

$$c(h, t)=c_0-(4/3)\pi(A\rho/W)$$

$$\times\int[(a^2+R^2(t))^{\frac{3}{2}}-a^3]n(a)da. \tag{29}$$

It is understood that the integral covers the entire range of initial sizes. According to (29), Eq. (20) must be replaced by

$$\frac{\partial[x^2(a, t)]}{\partial t}=\frac{dR^2}{dt}=\frac{2WDc_0}{A\rho}[1-e^{-\gamma Bt}]-(8/3)\pi D$$

$$\times\int[(a^2+R^2(t))^{\frac{3}{2}}-a^3]n(a)da. \tag{30}$$

This equation *does not* assert that x^2 increases linearly with time.

If $n(a)$ is known, the integral on the right may be evaluated so that a simple function of time is left in its stead, and a differential equation for R^2 is obtained, subject to the initial condition

$$R^2(0)=0. \tag{31}$$

In comparing (20) with (58) of reference 8, it was pointed out that the technique used in their developments had been tested theoretically[8] and experimentally.[8,9] The same can be said of (30), since it was derived using the same technique. We may, therefore, hope that (30) is accurate enough to be verified experimentally whenever $n(a)$ is known. In this connection it would be of great value in the determination of $n(a)$ when it is *not known*.

This is apparent from the following considerations. In view of (26), the total increase in integrated cross section per cubic centimeter would be

$$R^2(t)\int n(a)da=nR^2(t). \tag{32}$$

The observed integrated cross section, measured by some convenient method, such as the determination of

[18] Langmuir, Final Report, Project Cirous, General Electric.
[19] Thomson, Phil. Mag. (4) 42, 448 (1881).

optical transmission, can be denoted by $\varphi^2(t)$. If $R^2(t)$ can really be computed from (30),

$$\varphi^2(t)=nR^2(t),$$

or

$$\log\varphi^2(t)=\log n+\log R^2(t). \tag{33}$$

By assuming various forms for the distribution function, $n(a)$, the integral in (30) can be evaluated, and $R^2(t)$, in turn, can be calculated. If the correct distribution has been assumed, a plot of $\log\varphi^2$ *versus* $\log R^2$ should, according to (33), be a straight line with intercept, $\log n$. This method will be most sensitive at small growths before R^2 gets so large that a^2 is negligible beside it.

It should not be concluded that the method is restricted to condensation processes. Any colloidal "growth by diffusion" process will be subject to the same reasoning. An equation, somewhat different from (30), may be obtained, but it will be an equation for R^2 containing $n(a)$. The rule concerning the equal increase of squares will still hold. For other types of equations (in connection with uniform dispersions), see references 8 and 9. Nor should it be concluded that the measurements have to be made while the colloid is growing. The process may be started and stopped, the transmission being measured when the growth is stopped. In the condensation case, this may be achieved by discontinuing the cooling process.

IV. THE REGULATING MECHANISM

Suppose, for simplicity, that the initial distribution is a block distribution so that

$$\begin{aligned} &n(a)=0, && a<5\times10^{-5}\text{ cm},\\ &n(a)=10^9\text{ cm}^{-4}, && 5\times10^{-5}\text{ cm}<a<15\times10^{-5}\text{ cm},\\ &n(a)=0, && a>15\times10^{-5}\text{ cm}. \end{aligned} \tag{34}$$

Accordingly,

$$n=\int n(a)da=10^9\int_{5\times10^{-5}}^{15\times10^{-5}}=10^5\text{ cm}^{-3}. \tag{35}$$

The average initial radius is

$$\bar a=\frac{10^9}{10^5}\int_{5\times10^{-5}}^{15\times10^{-5}}ada=10^{-4}\text{ cm}, \tag{36}$$

and the relative distribution in terms of $u=a/\bar a$ is

$$G(u)=\bar a n(\bar a u). \tag{37}$$

If the particles are water droplets, initially, in equilibrium with water vapor at 20°C, let them grow, because the assembly is cooled to 0°C. The concentrations of vapor molecules corresponding to the saturation pressures at 20°C and 0°, respectively, are[20]

$$\begin{aligned} c_{20^\circ}&=5.816\times10^{17}\text{ mole/cc},\\ c_{0^\circ}&=1.630\times10^{17}\text{ mole/cc}. \end{aligned} \tag{38}$$

[20] Lange, *Handbook of Chemistry* (1941), 4th edition, p. 1265.

The difference between these values corresponds to a volume of liquid water, available in each cubic centimeter, upon condensation, given by

$$[c_{20^\circ}-c_{0^\circ}]W/A\rho. \tag{39}$$

This volume must be distributed among the n growing particles in such a manner that R^2 is the same for each particle. Thus,

$$[c_{20^\circ}-c_{0^\circ}]W/A\rho=(4/3)\pi\int([a^2+R^2]^{\frac{3}{2}}-a^3)n(a)da. \tag{40}$$

Upon the introduction of (34), the integral can be evaluated, and the following condition on R^2 is obtained.

$$\begin{aligned} \frac{(3\times10^{-9})}{4\pi}[c_{20^\circ}-c_{0^\circ}]\frac{W}{A\rho}+\left|\frac{a^4}{4}\right|_{5\times10^{-5}}^{15\times10^{-5}}&\\ =\left|\frac{a}{8}(2a^2+5R^2)(a^2+R^2)^{\frac{1}{2}}\right.&\\ \left.+\frac{3R^4}{8}\ln[a+(a^2+R^2)^{\frac{1}{2}}]\right|_{5\times10^{-5}}^{15\times10^{-5}}.& \end{aligned} \tag{41}$$

This transcendental equation can be solved for R^2 by plotting both sides against R^2 and determining the abscissa for the point of intersection. In the present case,

$$R^2=9\times10^{-8}\text{ cm}^2, \tag{42}$$

where

$$\begin{aligned} W&=18\text{ g},\\ \rho&=1\text{ g/cc},\\ A&=6.06\times10^{23}\text{/mole}. \end{aligned} \tag{43}$$

When we have the value of R^2, it is possible to determine the new distribution function, $N(x)$, for the assembly when the process of growth is complete. Thus,

$$N(x)dx=n(a)da, \tag{44}$$

where, through (26),

$$x=(a^2+R^2)^{\frac{1}{2}} \tag{45}$$

so that

$$dx=(x^2-R^2)^{\frac{1}{2}}/(x)da. \tag{46}$$

$N(x)$ can be identified by combining (46) and (44).

$$N(x)=(x)/(x^2-R^2)^{\frac{1}{2}}n[(x^2-R^2)^{\frac{1}{2}}]. \tag{47}$$

The limits on x are obtained by substituting the limits on a (5×10^{-5} cm and 15×10^{-5} cm) into (45). These are

$$\begin{aligned} &3.35\times10^{-4}\text{ cm},\\ &3.04\times10^{-4}\text{ cm}. \end{aligned} \tag{48}$$

The average value of x, $\bar x$ is calculated as

$$\bar x=\frac{1}{10^5}\int_{3.04\times10^{-4}}^{3.35\times10^{-4}}\times N(x)dx=3.17\times10^{-4}\text{ cm}. \tag{49}$$

Comparison of $\bar{x}$ and $\bar{a}$ shows that the colloid, on the average, has undergone a three-fold radial growth.

The relative distribution has been very noticeably sharpened. The relative distribution on x, $P(u)$, is obtained by writing $N(x)$ in terms of $u=x/\bar{x}$. Thus,

$$P(u)=\bar{x}N(\bar{x}u). \tag{50}$$

In Fig. 2, both $G(u)$ and $P(u)$ have been plotted against u. It is apparent that $P(u)$ is very much sharper than $G(u)$. Furthermore, the maximum in $P(u)$ lies on the side of the small particles, which indicates that the growth of the larger particles has been retarded, while the smaller ones have overtaken them.

In closing, it should be mentioned that the distribution on the first power of the radius has been under consideration. It has been shown that in this case both the absolute and relative distributions are narrowed by growth. However, the concept of uniformity is to a large extent defined by the nature of the experimental parameters which are measured. Thus, measurements on scattered light involve the sixth or other powers of the radius. It cannot be said that (26) implies a general mechanism leading to uniform dispersions until it has been shown that it also demands that the relative distribution on any nth power of the radius is narrowed by a sufficiently large growth process. Fortunately, it is easy to show this.

Consider the limiting sizes for the initial distribution to be given by a_1 and a_2, where $a_2>a_1$. The breadth of the initial distribution on the nth power may be measured by

$$(a_2{}^n-a_1{}^n)/\bar{a}^n, \tag{51}$$

where $\bar{a}^n$ is the mean of the nth power of a. Similarly, after growth, the breadth is measured by

$$(x_2{}^n-x_1{}^n)/\bar{x}^n. \tag{52}$$

If the distribution is to be relatively narrowed by the growth process, then the ratio of (52) to (51) must be less than unity; i.e.,

$$(\bar{a}^n/\bar{x}^n)[(x_2{}^n-x_1{}^n)/(a_2{}^n-a_1{}^n)]<1. \tag{53}$$

This ratio is surely less than

$$(a_2{}^n/x_1{}^n)[(x_2{}^n-x_1{}^n)/(a_2{}^n-a_1{}^n)] \tag{54}$$

so that if it can be shown that (54) is less than unity, the distribution will have been narrowed. According to (26),

$$\begin{aligned} x_1{}^n&=(a_1{}^2+R^2)^{n/2}, \\ x_2{}^n&=(a_2{}^2+R^2)^{n/2}. \end{aligned} \tag{55}$$

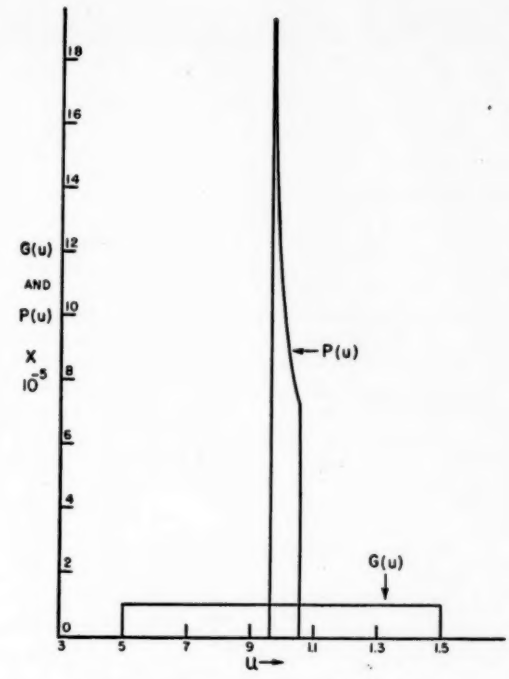

FIG. 2. $P(u)$ compared with $G(u)$.

If the growth is extensive, i.e., if $R\gg a_2$, these expressions can be expanded in terms of $(a/R)^2$ to yield

$$\begin{aligned} x_1{}^n&=1+(n/2)(a_1/R)^2, \\ x_2{}^n&=1+(n/2)(a_2/R)^2. \end{aligned} \tag{56}$$

These can be substituted into (54) to give

$$\frac{1}{[2R^2/na_2{}^2+(a_1/a_2)^2]}\frac{[1-(a_1/a_2)^2]}{[1-(a_1/a_2)^n]}<1$$

for

$$\frac{2R^2}{n}>a_2{}^2-a_1{}^2. \tag{57}$$

The criterion $2R^2/n>a_2{}^2-a_1{}^2$ does not demand that the growth be extremely large before the narrowing process begins. However, it is really not an independent condition, since its derivation hinges on the validity of the approximations (56) which in turn may require a considerable growth. In any event, it is now valid to assert that a sufficiently large growth will narrow the relative distribution on *any* nth power of the radius.

THE JOURNAL OF CHEMICAL PHYSICS VOLUME 19, NUMBER 4 APRIL, 1951

Note on Frequency Spectra of Simple Solids from Specific Heat Data

E. KATZ
Physics Department, University of Michigan, Ann Arbor, Michigan
(Received December 18, 1950)

If the specific heat $C(T)$ of a solid is given as a function of temperature from $T=0$ to ∞ with infinite accuracy, the frequency spectrum $f(\nu)$ is uniquely determined. What information about $f(\nu)$ can be derived from specific heat data of experimental accuracy? The following conclusions give the answer.

(1) Experimental specific heats determine accurately the low frequency part of the frequency spectrum but allow a latitude, wide enought to fit almost any theory, for its high frequency part.

(2) In a Debye plot (effective Debye temperature θ *versus* T) peaks and dips in the region $0<T<\theta/10$ represent dips and peaks in the low frequency part of the frequency spectrum. The correspondence is so simple that it can be interpreted at a glance. The peaks and dips are superimposed on a simple Debye spectrum and presumably have a direct physical meaning, in terms of lattice irregularities. Only their centers and total weights are obtainable, so that they act effectively as single Einstein frequencies.

(3) In the region $\theta/5<T<\infty$ all information obtainable about $f(\nu)$ consists of the first few even moments (three for specific heat errors of order one percent, five for 0.1 percent). These can be represented respectively by two or three weighted equivalent Einstein functions without direct physical meaning.

(4) The region $\theta/10<T<\theta/5$ corresponds to the high frequency part of the frequency spectrum, but hardly any information can be derived here.

INTRODUCTION

SEVERAL authors[1] have attempted to refine the Debye-Born-von Karman theory of the specific heat of solids by deriving expressions for the frequency spectrum $f(\nu)$ on the basis of more or less detailed assumptions about the elastic interactions between the atoms of the solid. The resulting specific heat*

$$C(T)=\int^{\nu_{\max}} E(h\nu/kT)f(\nu)d\nu \qquad (1)$$

is then compared with experiment. Here $E(x)=(x/2)^2/\sinh^2(x/2)$, the well-known Einstein function. The agreement between theory and experiment is reasonable but not excellent.

The present paper centers about the inverse problem, of finding $f(\nu)$ when the specific heat $C(T)$ is given from $T=0$ to ∞. This is a special case of the more general problem of finding kinetic data from thermodynamic ones, treated by Bauer[2] and by Blade and Kimball.[3] These authors have shown that the state sum $Z(T)$ of a system determines uniquely the distribution of energy levels $g(E)$. It follows from their work that $C(T)$ determines $f(\nu)$ uniquely, since $C(T)$ obviously determines $Z(T)$ and $g(E)$ determines $f(\nu)$ uniquely. A direct method for finding $f(\nu)$ from $C(T)$ was first worked out by Montroll[1] and has recently been simplified by Grayson-Smith and Stanley.[4] The results were disappointing because small uncertainties in the specific heat appear as tremendous uncertainties in the frequency spectrum. Bauer, and Blade and Kimball, reported similar large uncertainties in $g(E)$ as a result of small errors in $Z(T)$.

This state of affairs is discomforting to those who believe in the essential correctness of the theoretical frequency spectra of Blackman, Montroll, Houston, and Leighton. For, the small remaining discrepancies in the specific heat between theory and experiment may possibly mean serious errors in the frequency spectra employed by these authors.

An additional difficulty stems from the question of the constancy of the frequency spectrum with temperature. Whereas for low temperatures it is reasonable to approximate the lattice vibrations as harmonic, the anharmonicity, even when volume expansion is suppressed, must influence the result at higher temperatures. In first approximation this influence can be described as a change of the frequency spectrum with temperature, associated with a change in elastic constants. The present discussion is limited to those cases where this dependence of the frequency spectrum on temperature can be ignored. In fact, if such a dependence is present, it must be given by some other, independent source of information. It cannot be detected from specific heat data alone, since there is a one-to-one correspondence between infinitely accurate specific heat data over the entire temperature range and a—possibly fictitious—frequency spectrum satisfying Eq. (1).

Assuming a frequency spectrum which is independent of temperature, the present paper aims at revealing what details of the frequency spectrum are relevant for specific heat data of reasonable accuracy. The guiding idea throughout the present analysis is, that the Debye theory is a good first order approximation, i.e., the effective Debye temperature θ, plotted *versus* the temperature T, differs only by amounts of the order of

[1] M. Blackman, Rept. on Progress in Physics, Phys. Soc. London **8**, 11 (1941). E. W. Montroll, J. Chem. Phys. **10**, 218 (1942), and **11**, 481 (1943). W. V. Houston, Revs. Modern Phys. **20**, 161 (1948). R. B. Leighton, Revs. Modern Phys. **20**, 165 (1948).

* We abbreviate $C(T)$ for the specific heat divided by its high temperature value. The present paper deals only with the constant volume specific heat due to lattice vibrations, exclusive of the electronic contribution.

[2] S. H. Bauer, J. Chem. Phys. **6**, 403 (1938), and **7**, 1097 (1939).

[3] E. Blade and G. E. Kimball, J. Chem. Phys. **18**, 626 (1950).

[4] H. Grayson-Smith and J. P. Stanley, J. Chem. Phys. **18**, 236 (1950).

10 percent from a constant.† The deviations of θ from a constant must yield the deviations of $f(\nu)$ from a pure Debye spectrum. It appears expedient to divide the discussion into three parts referring to:

a. a low temperature range $0<T<\theta/10$,
b. a high temperature range $\theta/5<T$,
c. an intermediate range $\theta/10<T<\theta/5$.

THE LOW TEMPERATURE RANGE $0<T<\theta/10$

It will be shown that all essential details of the low frequency part of the frequency spectrum can be obtained from this range.

For sufficiently low temperatures the specific heat is $\sim T^3$, and can therefore always be represented by $p^3D(p\theta_0/T)$, where p is an arbitrary constant and θ_0 is the value of θ extrapolated to absolute zero. The physical basis for this relation is that the low frequency vibrations, which are the only ones to be excited at low temperatures, have too long wavelengths to be influenced by the individual atoms. They must then follow the theory of vibrations in an anisotropic continuous medium, which is just the Debye theory, giving $f(\nu)\sim\nu^2$ and $C\sim T^3$.

In order to describe C for somewhat higher temperatures we investigate the sum of a Debye spectrum, adapted to the very low temperature behavior of C, and several Einstein frequencies:[5]

$$C(T)=aD(p\theta_0/T)+\sum_i \beta_i E(q_i\theta_0/T). \qquad (2)$$

Here, the q_i are arbitrary constants, usually less than two, indicating the frequencies. The β_i are small, positive or negative weight factors for each frequency. In order to make things right at very high (see below) and at very low temperatures we require:

$$a+\sum_i \beta_i=1,$$
$$a=p^3.$$

Introducing the effective Debye temperature $\theta(T)$ and approximating the Debye function by

$$D(y)=4\pi^4/5y^3, \qquad (3)$$

we get for the relative deviation $\delta=(\theta-\theta_0)/\theta_0$ the following expression:

$$\delta=\frac{-5}{12\pi^4}\sum_i \frac{\beta_i}{q_i^3}\frac{x_i^5 e^{x_i}}{(e^{x_i}-1)^2}, \qquad (4)$$

where $x_i=q_i\theta_0/T$.

† The effective Debye temperature θ is commonly defined by an implicite equation of the Debye function D:

$$C(T)=D(\theta/T)\equiv 3\int_0^1 x^3E(x\theta/T)dx.$$

[5] A combination of Debye and Einstein spectra was previously introduced by Nernst (see E. Schroedinger, *Handbuch der Physik* (1926), Vol. X, p. 314). His viewpoint, however, was entirely different. His Einstein components represented optical branches for polyatomic crystals and would not occur in monatomic lattices. In the present paper this form is chosen as a way of describing mathematically any empirical $C(T)$ in a rapidly convergent series.

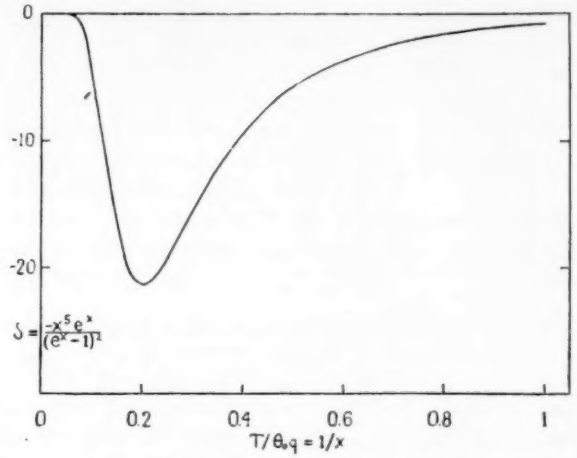

FIG. 1. The characteristic shape of the dip δ in the Debye plot for an added monochromatic frequency.

The following conclusions can be drawn from Eq. (4):

(a) δ is simply the superposition of the effects of the single frequencies.

(b) Each frequency gives rise to a dip (or, if β_i is negative, a peak) in δ as a function of T/θ_0. The dips (and peaks) all have the same basic shape, represented in Fig. 1. The shape is modified by a horizontal scaling factor depending only on q_i and a vertical scaling factor proportional to β_i/q_i^3.

(c) Each dip has a steep front at the low temperature side and a longer tail. Its minimum lies at $T_m/\theta_0=q/4.93$ or $q/5$ for all practical purposes. The depth of the minimum is $\delta_m=-0.09\beta_i/q_i^3=-7.3\ 10^{-4}\beta_i\theta_0^3/T_m^3$. The frequency causing the dip is directly proportional to T_m; in fact, $\nu=5kT_m/h$.

(d) Higher frequencies cause considerably smaller dips than lower ones with the same β-value (spectral weight), owing to the factor q^3. This fact may lead to important future applications of specific heat measurements at very low temperatures for the investigation of the (average) spacing of lattice perturbations in the range of 10 to 1000 lattice spacings, such as may be due to various types of hardening, mosaic structure, or impurities, etc. Superstructures of these types would give rise to slight irregularities in $f(\nu)$ for wavelengths of the order of their average spacing which would appear magnified in a Debye plot.

In analyzing an empirical $\theta(T)$ curve one first defines θ_0. In view of the extreme sensitivity of the curve, near absolute zero, for the slightest deviations from a regular quadratic frequency spectrum, the value of θ_0 may be slightly ambiguous. Such ambiguity is of a harmless nature, fortunately, as will be shown below. Next the deviations δ are analyzed in terms of dips (or peaks) of the shape as in Fig. 1, noting especially the location and depth (height) of each extremum. Thus, the frequency q_i and the spectral weight β_i of each line is obtained. The results have to be superimposed on a regular quadratic frequency spectrum corresponding to θ_0.

The above procedure can be applied up to $T\approx\theta_0/10$ or $\theta_0/12$, where the error in Eq. (3) becomes 3 percent or 1 percent, respectively. The complications, arising at higher temperatures, are described below in the section of the intermediate range. Inspection of experimental curves such as in Fig. 2 indicates that not many

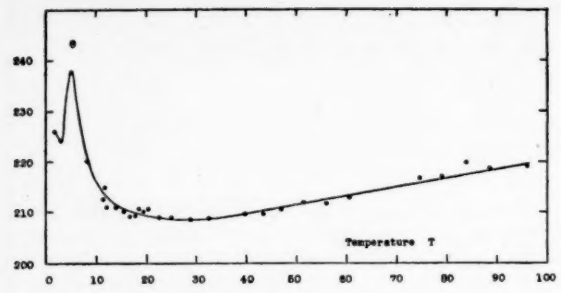

FIG. 2. Experimental specific heat for silver from literature (see R. B. Leighton, reference 1).

more than four dips or peaks can be analyzed from each curve in the low temperature range. The data will not allow, in general, drawing any conclusion concerning the shape of the corresponding peak in $f(\nu)$ but give only its average location and total weight. Hence, this represents all the significant detail obtainable in this region.

The following figures give an idea of the sensitivity of the method: at $q=0.1$ (frequency 0.1 of the fictitious maximum frequency of the quadratic spectrum with the same θ_0) and $\beta=10^{-3}$, one has $\delta_m=0.09$; for $q=0.5$ (the limit of the low T range) and $\beta=0.014$, one has $\delta_m=0.01$.

We return now the the question of what happens if θ_0 is off by a relative amount $d_0\ll 1$. It is easily shown that this changes $f(\nu)$ by adding a little bit of a quadratic Debye spectrum to it. Quantitatively, a spectrum $\varphi(\nu)d\nu=-9d_0(h/k\theta_0)^3\nu^2d\nu$ is added between $\nu=0$ and $k\theta_0/2h$. It is clear that this spectrum will never introduce spurious peaks, nor affect the recognition of local maxima or minima, and is thus rather harmless.

THE HIGH TEMPERATURE RANGE $T<\theta/5$

Assuming a frequency spectrum which is independent of temperature, the following discussion shows that the high temperature specific heat data yield at most information equivalent to the first three even moments of the frequency spectrum.

We replace the frequency spectrum by a substitute spectrum giving within the limits of error the same specific heat. The substitute spectrum[6] consists of s weighted single frequencies $\nu_1\cdots\nu_s$ with weights $\alpha_1\cdots\alpha_s$, where $\sum_j\alpha_j=1$. This introduces $2s-1$ parameters and we have

$$C(T)\approx\sum_j\alpha_jE(h\nu_j/kT). \tag{5}$$

The question is now: *How many frequencies must be used for a reasonable approximation of $C(T)$ or $\theta(T)$?* In answering this question we expand all quantities involved in inverse powers of T^2.

Suppose an empirical function $\theta(T)$ is given. One will then determine the constants p_i of the expansion:

$$[\theta(T)/\theta_\infty]^2=1+\sum_i p_i(\theta_\infty/T)^{2i}, \tag{6}$$

where θ_∞ is the constant value, approached by θ, for temperaturea above θ_∞. On account of the weak dependence of θ on T the constants p_i must be small, and would vanish for an ideal Debye spectrum. On the other hand, the Debye temperature $\theta(T)$ is defined by that value of $y=\theta/T$ which will make the Debye function $D(y)$ equal to $C(T)$:

$$C(T)=D(y)\equiv 1+\sum_{n=1}^{\infty}b_ny^{2n}, \tag{7}$$

where

$$b_n=(-)^n3(2n-1)B_n/(2n)\,!(2n+3) \tag{7a}$$

and B_n are the Bernoulli numbers (1/6; 1/30; 1/42; 1/30; 5/66; $\cdots$). This expansion converges rapidly for $y<2\pi$, the radius of convergence. Substituting Eq. (6) into Eq. (7), one obtains an expansion of C in inverse powers of T^2:

$$C(T)=1+\sum_{n=1}^{\infty}c_n(\theta_\infty/T)^{2n}, \tag{8}$$

where

$$\begin{aligned}
c_1&=-1/20\\
c_2&=(1/28-p_1)/20\\
c_3&=-(5/4536-p_1/14+p_2)/20\\
c_4&=(1/31680-5p_1/1512+(p_1^2+2p_2)/28-p_3)/20\\
&\text{etc.}
\end{aligned}$$

This has to be matched by the corresponding expansion of Eq. (5) with

$$E(x)=1+\sum_{n=1}^{\infty}a_nx^{2n}, \tag{9}$$

where

$$a_n=(-)^n(2n-1)B_n/(2n)\,!,$$

yielding

$$C(T)\approx 1+\sum_{n=1}^{\infty}a_n(h/kT)^{2n}\left(\sum_{j=1}^{s}\alpha_j\nu_j^{2n}\right). \tag{10}$$

The number of terms that can be matched obviously is $2s-1$ and the first unmatched term (number $2s$) of the difference between Eqs. (10) and (8) is a measure for the remaining error in $C(T)$. In fact, because the terms of this difference have usually alternating sign, this term sets an upper limit to the absolute error Δ in C. Moreover, the relative error δ in θ is easily seen to be

$$\delta=10\Delta T^2/\theta_\infty^2 \tag{11}$$

in the temperature range under discussion.

Case $s=1$

This case has one single frequency ν_1 and is actually the old Einstein approximation. The matching of Eqs.

[6] The qualitative merit of this substitute spectrum was previously pointed out by E. W. Montroll, Quart. App. Math. 5, 223 (1947).

(10) and (8) leads to the single condition:[7]

$$\theta_\infty^2=(5/3)(h\nu_1/k)^2\equiv(5/3)\theta_E^2, \tag{12}$$

where θ_E is the "Einstein" temperature defined by the second part of (12). When comparisons between the theories of Einstein and Debye have been made, curves of C *versus* T for equal θ_{Debye} and θ_{Einstein} have usually been given.[8] These curves seem to differ considerably, but a proper scaling factor of $(5/3)^{0.5}$ would bring out their equivalence over a substantial temperature range. In order to see how far this range extends, we consider the term $n=2$ for Eqs. (10)–(8), giving

$$\Delta\approx(\theta_D/T)^4[(-1/3500)+(p_1/20)]. \tag{13}$$

For a pure Debye spectrum $p_1=0$ and so for all temperatures down to $\theta/2$, the error in C is less than one percent and so is δ practically. This means that, from an experimental standpoint, the Debye and Einstein approximations are fully equivalent for $\theta/2<T<\infty$. For actual spectra p_1 is usually negative but rarely much more than 0.005. Consequently, all spectra are equivalent with the Einstein approximation for temperatures down to $\theta/1.5$ or $\theta/2$. And this is all the information concerning the frequency spectrum that can be derived from specific heat data in this temperature range.

Case $s=2$

In this case the specific heat is approximated by a combination of two Einstein functions $\alpha E(x_1)+(1-\alpha)E(x_2)$ with frequencies ν_1 and ν_2. The matching of Eqs. (8) and (10) gives the three equations:

$$\alpha(x_1/y_\infty)^{2n}+(1-\alpha)(x_2/y_\infty)^{2n}=c_n/a_n \quad (n=1,2,3). \tag{14}$$

Consider first the special case of a pure Debye spectrum. The solutions of Eqs. (14) are then

$$\alpha=0.5837,\quad x_1/y_\infty=0.906,\quad x_2/y_\infty=0.538.$$

In this approximation the Debye function is therefore equivalent to

$$D(y)\approx0.584E(0.906y_\infty)+0.416E(0.538y_\infty). \tag{15}$$

This seems to be the true reason why a similar formula by Nernst and Lindemann,[9]

$$C(T)\approx0.5E(y)+0.5E(0.5y), \tag{16}$$

worked quite well. From the above discussion it is seen that the reason for the validity of Eqs. (15) and (16) is *not*, that the frequency spectrum has two peaks at frequencies differing by a factor of approximately two. The perfectly smooth Debye spectrum already creates this feature and it cannot be used, therefore, as an argument in support of such two-maxima spectra as calculated by Blackman, *et al.*

In order to see over what temperature range this approximation is valid we consider the term $n=4$ for Eqs. (10)–(8), giving:

$$\delta\approx2.6\ 10^{-7}(\theta_\infty/T)^6. \tag{17}$$

Numerically, this means $\delta=0.3$ percent for $T=\theta_\infty/5$ and 1.1 percent for $T=\theta_\infty/6$. Since the radius of convergence of all these series expansions lies at $T=\theta_\infty/2\pi$, this is about as far as one can go with this type of approximation for the Debye spectrum. For a general spectrum the situation is essentially the same as will now be shown.

In the general case ($p_i\neq0$) the solutions of Eqs. (14) are, fully written out:

$$\begin{aligned}\alpha&=0.5+0.0837f\\ x_1/y_\infty&=0.906g\\ x_2/y_\infty&=0.538h\end{aligned} \tag{18}$$

with

$$f=(1-49612.5p_2)/\{1-283.5(9p_1/5+49p_2/5-315p_1^2-1944810p_2^2/8+18375p_1^3)\}^{0.5}$$

$$g^2=[1-130p_1+2720p_2+0.328(N-1)]/(1-175p_1)$$

$$h^2=[1-362p_1+7600p_2-0.915(N-1)]/(1-175p_1),$$

and N is the denominator of f and can often be approximated by $(1-280p_1)$. The expressions for f, g, h show that the value of α never deviates far from 0.5 and the ratio x_1/x_2 is always about 2, for values of $0<p_1<10^{-2}$ and $0<p_2<10^{-4}$, which more than covers the range of these variables in many trial cases.

The error term $n=4$ is given by

$$\delta\approx2.6\ 10^{-7}(\theta_\infty/T)^6(1+m), \tag{19}$$

where $m\to0$ when $p_{1\,2\,3}\to0$. The exact expression for m is too lengthy to be given here. A typical case of $p_1=-0.005$ and $p_2=2.10^{-5}$, $p_3=0$ gives $m\sim1$, which proves the contention that Eqs. (19) and (17) are practically equivalent.

Case $s=3$

This case will be of only theoretical interest unless specific heat measurements become possible with an accuracy far better than obtainable at present. Here we have to match three weighted single frequencies:

$$\alpha_1E(x_1)+\alpha_2E(x_2)+(1-\alpha_1-\alpha_2)E(x_3).$$

One now obtains five equations of a structure similar to Eq. (14). For a pure Debye spectrum this yields the following solutions:

$$\begin{aligned}\alpha_1&=0.350 & \alpha_2&=0.461 & 1-\alpha_1-\alpha_2&=0.189\\ x_1/y_\infty&=0.950 & x_2/y_\infty&=0.742 & x_3/y_\infty&=0.406.\end{aligned}$$

[7] This relation differs slightly from that given by Mott and Jones in *Properties of Metals and Alloys* (Oxford University Press, 1936), p. 8, whose factor is 16/9 instead of 5/3.

[8] See for instance F. Seitz, *Modern Theory of Solids* (McGraw-Hill Book Company, Inc., New York, 1950), p. 104 or E. Schroedinger, reference 5.

[9] Mott and Jones, reference 7, p. 8, or M. Blackman, reference 1, p. 13.

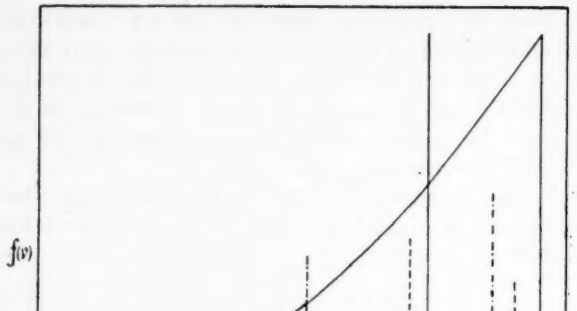

FIG. 3. High temperature analysis of Debye spectrum into 1, 2, 3 equivalent Einstein components.

The range of validity is given by the relative error δ in θ:

$$\delta \approx 0.08(\theta_\infty/10T)^{10},$$

which is less than 0.1 percent for $\theta_\infty/T=2\pi$. A similar order of magnitude may be expected for any reasonable frequency spectrum. It is unlikely that any closer approximation will ever be needed for this temperature region. The relations for the cases $s=1, 2, 3$ are graphically illustrated for the Debye spectrum in Fig. 3.

CONNECTION WITH MONTROLL'S MOMENTS

The matching of the Eqs. (8) and (10) is evidently similar to giving the first $2s-1$ moments M_k defined by

$$M_k{}^{2k}=\int_0^{\nu_{\max}} f(\nu)\nu^{2k}d\nu,$$

where $f(\nu)$ is normalized such that its integral is unity. However, the present method of representing the spectrum by single frequencies takes into account a little more than these moments only. It incorporates the fact that certain inequalities exist between moments,[10] in particular:

$$M_{k+1} \gtrless M_k \qquad (k>0)$$

and

$$M_{k+2}/M_{k+1} \gtrless (M_{k+1}/M_k)^{k/k+2}$$

or, in general:

$$M_{k+p+q}/M_{k+p} \gtrless (M_{k+p}/M_k)^{qk/p(k+p+q)} \quad k, p, q>0.$$

Knowledge of the first $2s-1$ moments yields lower bounds for all higher moments. This information is just incorporated by using the frequency spectrum consisting of s single frequencies. Among all spectra with the same first $2s-1$ moments this type gives to moments beyond the $(2s-1)$th their minimum values, consistent with the above relations. This additional information concerning the higher moments as used in the present method results in errors that are almost an order of magnitude less than would be the case if the series were simply cut off after the terms containing the known moments.

The connections between the moments and the constants p used here are

$$(hM_k/k\theta_\infty)^{2k}=c_k/a_k,$$

where the Boltzmann $k\theta_\infty$ will not be confused with the index k in all other places of the formula.

THE INTERMEDIATE RANGE $\theta/10<T<\theta/5$

In this range, it will be shown, very little information about the high frequency part of the frequency spectrum can be obtained. An approach similar to that used for low temperatures will be followed, but the dependence of D on T is no longer simply Eq. (3). One has the well-known asymptotic expansion:

$$\begin{aligned} D(y)&=4\pi^4/5y^3-\Delta(y)\\ \Delta(y)&=12y\sum_{n=1}^{\infty}e^{-ny}\{(1/4)+(1/ny)\\ &\qquad +[3/(ny)^2]+[6/(ny)^3]+[6/(ny)^4]\}\\ y&=\theta/T. \end{aligned} \tag{20}$$

In the low temperature range Δ can be neglected; in the intermediate range all terms $n>1$ may be neglected for an error of less than 1 percent. Setting $y=y_0(1+\delta)$, where $y_0=\theta_0/T$, we have to find δ as a function of T satisfying:

$$D(y)=p^3D(py_0)+\textstyle\sum_i \beta_i E(q_i y_0). \tag{21}$$

Substituting Eq. (20) into Eq. (21), expanding about y_0, and retaining only terms up to the first power in δ one finds:

$$\delta=-\frac{\sum \beta_i E(q_i y_0)+\{\Delta_0-p^3\Delta(py_0)\}}{(12\pi^4/5y_0{}^3)+\Delta_0 u_0}, \tag{22}$$

where $u=d\log\Delta/d\log y$ and the subscript zero refers to the value taken for $y=y_0$. In discussing Eq. (22) we note first that a term has been added to the numerator and the denominator, but otherwise this formula is similar to Eq. (4). Consider first the first term of the numerator together with the denominator. The value of u_0 in this range is almost exactly equal to $-y_0$. The denominator varies between $0.91(12\pi^4/5y_0{}^3)$ at $y_0=10$ and $0.31(12\pi^4/5y_0{}^3)$ at $y_0=5$. For a qualitative analysis the coefficient could be taken 0.6 throughout this range. The effect of the changing coefficient is to counteract the rapid decrease in sensitivity of δ somewhat, and to modify the shape of the dip that corresponds to a single frequency a little. Its maximum is shifted to the left, making the front steeper and the tail longer. These changes do not affect the general qualitative features of the analysis. More important are the effects arising from the added term in the numerator.

[10] H. Cramer, *Mathematical Methods in Statistics* (Princeton University Press, Princeton, 1946), p. 255.

This term, together with the denominator, represents a contribution to δ, the absolute value of which rises gradually from practically zero at $y_0=10$ to a maximum at $y_0\approx 4$, and this maximum is about $0.3\sum\beta_i$. Consequently, if $\sum\beta_i\approx 0$, then the effects of this contribution vanish; but if this sum differs markedly from zero, an effect is produced through this term which has to be compensated by adding a single frequency at this spot. However, it turns out that this gives a major contribution to $\sum\beta_i$, always in the sense of increasing its absolute value. This aggravates the second-term influence, etc. The question is now whether this procedure converges rapidly. Unfortunately, it is divergent or very slowly convergent and therefore cannot be used. In practice the only way to avoid this difficulty is to make sure that $\sum\beta_i=0$ and this can always be done by choosing θ_0 about equal to θ at $T=\theta/4$. (See the final remark in the low temperature section.)

With these precautions Eq. (22) can now be used up to $q\approx 1$. It is not practical to attempt extending the present method to greater values of q (or T). In the first place the method loses elegance and ease of comprehension. Secondly, sensitivity is lost with higher q (at $q=1$ and $\delta_m=0.01$ one has $\beta=0.04$, in other words, a dip with area of 4 percent of the total area of the frequency spectrum just escapes detection). Finally, the divergent or slowly convergent effects outlined above stop further extension of the method.

As a rule of thumb, one may say that the present approach divides the actual frequency spectrum into two parts, roughly in half on the frequency scale. The low frequency part can be obtained from specific heat data with reasonable accuracy. As one approaches the halfway mark, the method becomes rapidly insensitive; and for the high frequency part one sees very little detail. The halfway mark corresponds to a value of q somewhere between 0.5 and 1. The spectrum may, of course, extend beyond $q=1$, since the Debye limit is not necessarily the real limit.

AN EXAMPLE OF FITTING

The data of Fig. 2, copied from Leighton's paper,[1] show the Debye temperature as a function of the temperature for silver. We take $\theta_0=212°$, the value of θ near $T=\theta/4$. The graph indicates in the low temperature region:

(1) A dip in $f(\nu)$ for $q=0.04$, corresponding to a maximum in $\theta(T)$ at 1.6°. The height of this maximum is about 13° or 6 percent and so we have $\beta_1=-0.4\times 10^{-4}$.

(2) A dip in $f(\nu)$ for $q=0.12$. Taking into account the tail of the first dip, the depth of this one is 23° or $\delta_m=0.11$; and so we have $\beta_2=-2.1\times 10^{-3}$.

(3) A peak in $f(\nu)$ at $T=14°$ or $q=0.33$. The maximum depth of the corresponding dip in θ is 3.0 percent and we have $\beta_3=+0.012$.

This description fits the data, as shown in Fig. 4, to within the experimental error, over the entire range from 0 to 60°. Since $\sum\beta=0.010$, the complications of divergence can be ignored in the intermediate range.

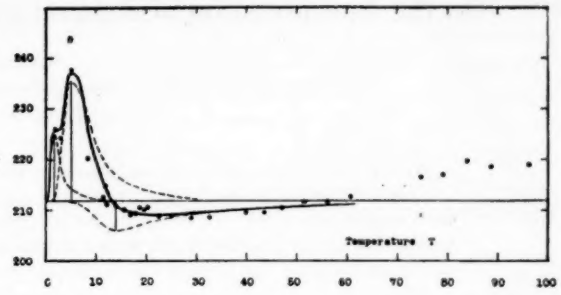

FIG. 4. Analysis of data in terms of a Debye spectrum and superimposed monochromatic frequency peaks or dips. The full drawn curve is the sum of the three dotted curves and $\theta_0=212°$.

The few points at higher temperatures are not accurate enough to warrant an analysis for the high temperature range.

CONCLUDING REMARKS

It has been shown that two main types of information about the frequency spectrum can be obtained.

From the low temperature specific heat data one obtains physically real peaks and dips of approximately monochromatic character in the low frequency part of the frequency spectrum. Their detection becomes extremely sensitive at low temperatures. Insofar as they cannot be accounted for by differences between the results of lattice theories and the Debye theory, the effects of which usually do not extend much below $\theta/10$, they may be caused by mosaic structure and other lattice imperfections. This hypothesis can, in principle, be tested by influencing the lattice structure in a known way and measuring low temperature specific heats. In the opinion of the author, these peaks and dips may be ascribed to such structure sensitive causes rather than being attributed to experimental errors in the (old) specific heat measurements, as was suggested by Casimir.[11] More detailed speculations, however, seem premature until more systematic experimental data are available.

On the other hand, from high temperature specific heats one can in practice obtain at best the first three to five even moments of the frequency spectrum and some limitations concerning higher moments. This information can best be incorporated by representing the spectrum by two or three weighted "effective" Einstein frequencies which possesses, however, no direct physical meaning but may be useful parameters for the comparison of data. All theoretical predictions concerning finer details of the high frequency part of the spectrum must escape observation.

It is a pleasure to thank Professor G. E. Uhlenbeck for helpful criticism of the manuscript.

[11] H. B. G. Casimir, oral communication at the summer symposium lectures, Ann Arbor, 1948. It was suggested that Keesom's measurements on KCl, which show a similar type of fine structure, were not accurate enough to warrant theorizing about this point. This suggestion was based on a discussion of this question between Casimir and Keesom.

THE JOURNAL OF CHEMICAL PHYSICS VOLUME 19, NUMBER 4 APRIL, 1951

On the Interpretation of Relaxation Time Measurements in Gas Mixtures*

RICHARD A. WALKER
Engineering Experiment Station and Department of Physics, Iowa State College, Ames, Iowa
(Received January 25, 1951)

Most studies of the excitation of molecular vibrations in gas mixtures have been carried out using very low concentrations of the B type "impurity" gas to excite basic gas A. It is pointed out in this paper that such studies very likely fail to detect the possible importance of triple collisions of the AAB type. Indeed, data of Eucken and Aybar on mixtures containing quite high concentrations of B molecules is felt to furnish strong evidence for the triple collision excitation of COS molecules by argon and by nitrogen molecules.

I. INTRODUCTION

THE excitation of the vibrations of gas molecules by collisions has been studied in considerable detail during the past twenty-five years.[1] Throughout the history of the experimental work in both pure and mixed gases it has been quite generally believed that double collisions are in almost all cases responsible for vibrational excitation. Very few exceptions have been reported to date. In 1934 Kneser[2] found evidence that triple collisions involving two water molecules are principally effective in exciting the vibration of an oxygen molecule. And in 1941 Buschmann and Schäfer[3] reported a small effect due to triple collisions in pure N_2O.

The gas mixtures studied have all been binary mixtures, and practically all have consisted of a B type gas, usually not capable of appreciable vibration at the temperature concerned, added in very low concentrations to an A type gas, whose vibrational excitation by B type molecules is of principal concern. In 1940, however, Eucken and Aybar[4] reported a few measurements on relatively high concentrations of nitrogen and argon in COS. As a result of these measurements they concluded that the formula which they, and others, had previously used to calculate β_{AB}, a quantity which measures the ability of B molecules to excite A molecules, is incorrect and they proposed a new formula to explain their results. It is the purpose of this paper to point out that an explanation for their results exists which does not require the abandonment of the old formula. Rather, it seems that their results may give strong evidence for the triple-collision-excitation of COS by argon and by nitrogen.

This immediately suggests the further possibility that many other cases in which triple and higher order collisions are the predominant mechanism of vibrational excitation may have been overlooked in the multitude of low concentration mixture studies made to date.

* This study was carried out under contract with the National Advisory Committee for Aeronautics, contract No. NAw-5752.

[1] See Richards, Revs. Modern Phys. **11**, 39 (1939) for orientation in this field.

[2] H. O. Kneser, Physik. Z. **35**, 983 (1934).

[3] K. F. Buschmann and K. Schäfer, Z. physik. Chem. **B50**, 73 (1941).

[4] A. Eucken and S. Aybar, Z. physik. Chem. **B46**, 195 (1940).

II. RELAXATION TIMES IN MIXTURES

Let us consider a binary gas mixture consisting of a basic gas A and an added gas B, the molecules of the latter being incapable of vibration. For simplicity let us assume that gas A possesses only one normal mode of vibration, and that the temperature is such that only the first excited state of vibration is appreciably occupied. This case is actually of wide practical applicability. Let N_1 represent the number of vibrating A molecules, N_0 the number of non-vibrating A molecules. $N_0+N_1=N$, the total number of A molecules. If A and B are not chemically reactive, N is constant.

The continuous exchange of A molecules between the 0 (nonvibrating) and 1 state of vibration is influenced by both A and B molecules. The reaction rate equation for the excitation of vibration of A molecules is

$$dN_1/dt=(F_{01}{}^{AA}+F_{01}{}^{AB})N_0-(F_{10}{}^{AA}+F_{10}{}^{AB})N_1, \quad (1)$$

where $F_{01}{}^{AA}$ specifies the number of 0→1 transitions per nonvibrating A molecule per second caused by A molecules, $F_{01}{}^{AB}$ specifies the number of 0→1 transitions per A molecule per second caused by B molecules, and $F_{10}{}^{AA}$ and $F_{10}{}^{AB}$ are the corresponding numbers of 1→0 transitions. Since $N_0+N_1=N$,

$$N_1=\text{const}_1+\text{const}_2\exp[-(F_{01}{}^{AA}+F_{10}{}^{AA}+F_{10}{}^{AB}+F_{01}{}^{AB})t]. \quad (2)$$

The *relaxation time* for the mixture is clearly given by

$$1/\bar{\beta}=(F_{01}{}^{AA}+F_{10}{}^{AA})+(F_{01}{}^{AB}+F_{10}{}^{AB}). \quad (3)$$

At equilibrium, of course, $dN_1/dt=0$. When gas B is absent $F_{01}{}^{AB}=F_{10}{}^{AB}=0$, and the relaxation time in pure gas A, β_{AA}, is given by[5]

$$\beta_{AA}=1/(f_{01}{}^{AA}+f_{10}{}^{AA}), \quad (4)$$

where f's are used to emphasize that in general the number of transitions per molecule per second depend upon the conditions of the gas under investigation.

An expression like (1) does not assume a collision

[5] The theory of Landau and Teller, Physik. Z. Sowjetunion **10**, 34 (1936), gives $\beta_{AA}=\dfrac{1}{f_{10}-f_{01}}$. This comes about through the inclusion of other possible states of vibrational excitation than the 0 and 1. However, the minus sign is not essential to the arguments of this paper, nor does Eucken and Aybar's derivation of expression (8) of this paper depend on this sign.

mechanism for exciting vibrations at all. It merely recognizes the fact that energy transfers do take place, with rates specified by F_{01} and F_{10}. When one introduces the assumption that the energy transfers are incurred by collisions, then one can say something about the functional dependence of F_{01} and F_{10} on pressure, temperature, molecular diameters and the other quantities on which collision rates in gases depend; for F_{01}, the average number of 0⟶1 transitions per A molecule per second is then certainly proportional to the average collision rate per A molecule, as is F_{10}. The collision rate per A molecule for double collisions of the type AB is proportional to ρ_B, the density of gas B. For triple collisions of the type ABB the collision rate is proportional to ρ_B^2, and so forth for higher order collisions.

In a pure gas the observed relaxation time is then inversely proportional to the density (or pressure) if double collisions are solely responsible for vibrational excitation, to the square of the density if triple collisions are solely responsible, and so forth. For all pure gases studied to date, except N_2O, the experimentally observed relaxation times have been found to vary inversely as the pressure,† indicating that the double collision mechanism is principally, if not solely, responsible for the vibrational excitation of these gases.

To indicate the difficulty with which vibrations are excited in pure gas A the usual practice is to multiply β_{AA}, the time for the departure from thermal equilibrium to be reduced to $1/e$ of its initial value, by the appropriate collision rate per molecule. The appropriate collision rate is determined from studies of the pressure dependence of the relaxation time which show what type of collisions are responsible for the energy transfers. The product of β_{AA} and the collision rate gives the number of collisions per A molecule occurring during the time β_{AA} and is referred to as the "number of collisions per molecule necessary to dissipate a vibrational quantum."

The primary interest in mixture experiments is to determine whether collisions of A molecules with B molecules are more effective in exciting the vibrations of A than collisions of A with other A molecules, as observed in studies of pure gas A. That is, it is of interest to compare β_{AA} to the relaxation time that would characterize a hypothetical mixture in which only collisions of A molecules with B molecules occur. Mixture experiments yield a relaxation time $\bar{\beta}$ which results from the simultaneous excitation of A by A and B.

$\bar{\beta}$ can be expressed in terms of β_{AA} and the relaxation time for the hypothetical gas. It is usually convenient to determine $\bar{\beta}$ experimentally in a mixture whose total pressure is one atmosphere. It is also convenient to express the relaxation time of pure gas A, β_{AA}, in terms of a pressure of one atmosphere. If γ is the fractional concentration of the added gas B, $1-\gamma$ is the fractional concentration of gas A. $F_{01}^{AA}+F_{10}^{AA}$ is the average total number of 0⟶1 and 1⟶0 transitions per A molecule per second occurring in the mixture due to AA collisions. But for a mixture at a total pressure of one atmosphere this is only $(1-\gamma)$ times the total number of transitions per A molecule per second which occur in pure gas A at a pressure of one atmosphere, providing *double* collisions *only* are effective in the pure gas A. That is,

$$F_{01}^{AA}+F_{10}^{AA}=(1-\gamma)/\beta_{AA} \tag{5}$$

where $\bar{\beta}$ in (3) and β_{AA} in (5) are for total pressures of one atmosphere.

$F_{01}^{AB}+F_{10}^{AB}$ is the average total number of 0⟶1 and 1⟶0 transitions per A molecule per second occurring in the mixture due to AB collisions. Providing that only AB *double* collisions are effective in exciting the vibrations of A molecules, the above is proportional to the density of gas B and is only γ times the total number of transitions per A molecule per second which occur in a hypothetical mixture of A and B in which only AB double collisions cause transitions, AA collisions being ineffective, and in which the partial pressure of gas B is one atmosphere. Let us define β_{AB} as the relaxation time that would characterize such a hypothetical gas. Then,

$$F_{01}^{AB}+F_{10}^{AB}=\gamma/\beta_{AB}. \tag{6}$$

Thus (3) becomes

$$1/\bar{\beta}=(1-\gamma)/\beta_{AA}+\gamma/\beta_{AB}. \tag{7}$$

Since β_{AA} is known from pure gas studies, β_{AB} can be calculated from the observed $\bar{\beta}$ for the mixture. One multiplies β_{AB} by the collision rate per A molecule with B molecules in the hypothetical gas to obtain the "number of AB collisions necessary to dissipate the vibrational energy of an A molecule." Expression (7) has been consistently used by all the investigators of mixtures, and was unchallenged until 1940 when Eucken and Aybar argued that it was apparently incorrect.

III. EXPERIMENTAL RESULTS

The values of β_{AB} calculated from observed $\bar{\beta}$-values should, of course, be independent of the concentration γ of the B gas. Using COS as the basic gas Eucken and Aybar observed the values listed in column I of Table I for mixtures with nitrogen and argon. Calculating β_{AB} from this data using expression (7) gives the values listed in column II of the table. Since values of β_{AB} thus calculated are not independent of the percentage composition of the mixture, one must conclude that expression (7) cannot be used in these experiments.

Eucken and Aybar propose the following expression,

$$1/\bar{\beta}=(1-\gamma)^2/\beta_{AA}+\gamma(1-\gamma)/\beta_{AB} \tag{8}$$

stating that expression (7) is valid only if the concen-

† This is not so, however, in the case of the rotational excitation of pure hydrogen.

TABLE I. Comparison of β_{AB} values obtained from expressions (7), (8), and (10).

	I $\bar{\beta}\times10^6$ (1 atmos)	II $\beta_{AB}\times10^6$ using (7)	III $\beta_{AB}\times10^6$ using (8)	IV $\beta_{AAB}\times10^6$ using (10)
COS+ 8.46 percent N_2 (Eucken and Aybar)	1.45 sec	0.596 sec	0.412 sec	0.545 sec
COS+50.3 percent N_2 (Eucken and Aybar)	1.31	1.08	0.407	0.538
COS+19.58 percent Ar (Eucken and Aybar)	1.82	2.88	0.969	2.31
COS+45.9 percent Ar (Eucken and Aybar)	2.42	5.16	1.04	2.79
COS ($\beta_{AA}=$)	1.67			
CO_2+ 8.6 percent He (Eucken and Nümann)	0.60	0.25	0.21	
CO_2+ 34.6 percent He (Küchler)	2.0	0.22	0.14	
CO_2 ($\beta_{AA}=$)	7.0			

tration of the basic gas A in the mixture is the same as the concentration of pure gas A when β_{AA} is measured. They present a derivation of (8) in which they compare reaction equations similar to expression (1) to find "effective" reaction rate constants $\bar{k}_{01}$ and $\bar{k}_{10}$ for the mixture, but this doesn't seem to be a legitimate procedure because the ratio C_{A1}/C_A is importantly different in the pure gas and in the mixture. Furthermore, one can integrate their reaction equation,

$$\frac{dC_{A1}}{dt}=(1-\gamma)^2\left(k_{01}{}^{AA}-k_{10}{}^{AA}\frac{C_{A1}}{C_A}\right)C^2$$

$$+\gamma(1-\gamma)\left(k_{01}{}^{AB}-k_{10}{}^{AB}\frac{C_{A1}}{C_A}\right)C^2,$$

directly to find the observed relaxation time $\bar{\beta}$, which can still be shown to be given by expression (7). Nevertheless, values of β_{AB} calculated using (8), as listed in column III in Table I, are independent of γ within probable limits of experimental error and consequently Eucken and Aybar proposed that (8) replace (7).

However, an alternative explanation seems possible. One should recall that expression (6) is valid only if AB double collisions produce the energy transfers. Suppose instead, that only triple collisions of the type AAB are responsible for the vibrational excitation of an A molecule by B molecules. The number of collisions of this type per A molecule per second is proportional to the product of the density of A and the density of B. $F_{01}{}^{AB}+F_{10}{}^{AB}$ is then only $\gamma(1-\gamma)$ times the total number of transitions per A molecule per second which occur in a hypothetical mixture of A and B in which only AAB collisions cause transitions, and in which the partial pressures of both A and B are one atmosphere. If β_{AAB} is defined as the relaxation time that would characterize this hypothetical gas,

$$F_{01}{}^{AB}+F_{10}{}^{AB}=\gamma(1-\gamma)/\beta_{AAB}. \tag{9}$$

Expression (3) then gives

$$1/\bar{\beta}=(1-\gamma)/\beta_{AA}+[\gamma(1-\gamma)]/\beta_{AAB}. \tag{10}$$

Values of β_{AAB} calculated from (10) are listed in column IV of Table I. They are also reasonably independent of γ. In terms of Kneser's results in O_2, it seems reasonable to expect that possibly both AB binary collisions and AAB triple collisions are important, in which case (10) would need to be modified to include the double collisions. However, with only two experimental measurements available for calculations on each mixture, it is impossible to verify the possible effect of double collisions here.

As a further check of Eucken and Aybar's contention that (8) is correct, there are the measurements of Eucken and Nümann[6] and Küchler[7] on mixtures of carbon dioxide and helium. Here expression (7) rather than (8) appears to fulfill the requirement of yielding a β_{AB} that is constant with changing γ within probable limits of experimental error, as seen in the table. Eucken and Aybar do not explain why (8) fails here. According to the viewpoint of this paper, CO_2—He double collisions are principally effective in exciting CO_2.

It is understandable that the effectiveness of AAB type triple collisions might very well have escaped detection in the multitude of low concentration studies, where $(1-\gamma)$ is approximately unity. In such cases, of course, (10) doesn't differ appreciably from (7).

Also, in 1940 Fricke[8] reported measurements of the absorption of sound in COS. His experimental method consisted of adding COS in fractional concentrations up to about 25 percent to nitrogen, measuring the absorption as a function of the percent of COS added. Since the vibrations of nitrogen molecules are not appreciably excited at room temperature, nitrogen does not exhibit any relaxation absorption; such absorption observed in the mixture is due to COS molecules. Extrapolation of the measured absorption to the 100 percent COS point presumably gives the absorption in pure COS. It should be noted, however, that this is strictly true only if N_2 molecules have no ability to excite the vibrations of COS molecules. The study of Eucken and Aybar shows this is definitely not the case, and consequently the value Fricke reports for the frequency of maximum absorption in pure COS is probably too high. Indeed, Eucken and Aybar report a col-

[6] Eucken and Nümann, Z. physik. Chem. **B36**, 175 (1937).
[7] Küchler, Z. physik. Chem. **B41**, 209 (1938).
[8] E. F. Fricke, J. Acoust. Soc. Am. **12**, 245 (1940).

lision number of 17,700 for pure COS, while ν_{max} reported by Fricke yields a collision number of only about 10,000.

It is felt that the absorption measurements reported by Fricke are not inconsistent with the triple collision possibility suggested in this paper.

The author is very grateful to Professor Sam Legvold for his constant guidance and many suggestions during this study. He also wishes to express thanks to Professor W. H. Pielemeier and Dr. Ralph Simon of Pennsylvania State College for the kind interest they have shown and the helpful comments they have made.

THE JOURNAL OF CHEMICAL PHYSICS VOLUME 19, NUMBER 4 APRIL, 1951

LCAO Self-Consistent Field Calculation of the Twisting Frequency and π-Electron Energy Levels of Allene*

ROBERT G. PARR AND G. RUSSELL TAYLOR†
Department of Chemistry, Carnegie Institute of Technology, Pittsburgh, Pennsylvania
(Received December 27, 1950)

The twisting frequency of allene is computed by the nonempirical method of antisymmetrized products of molecular orbitals in self-consistent field *LCAO* approximation, as applied to the four unsaturation electrons of the molecule, molecular orbitals for these electrons being taken as linear combinations of $2p$ Slater atomic orbitals. By comparison with a previous calculation by the same method on ethylene, the ratio of the twisting frequency of ethylene to the twisting frequency of allene is computed to be 1.7, sensibly independent of the effective charge in the atomic orbitals, which is the only extrageometrical parameter entering the theoretical calculations. The first ionization potential of allene is predicted to be 10.4 ev and the mean of the first allowed singlet electronic absorption band and the corresponding triplet is predicted to lie at 5.1 ev.

INTRODUCTION

THE nonempirical method of antisymmetrized products of molecular orbitals (in *LCAO* approximation) has recently been employed to compute certain electronic energy levels and vibrational force constants of ethylene,[1] benzene,[2,3] and 1,3-butadiene.[4] In these studies unsaturation (π) electrons alone were considered, the effects of the underlying single-bonded structures being represented by an effective potential. Thus, ethylene was treated as a two-electron problem, benzene as a six-electron problem, and 1,3-butadiene as a four-electron problem.

In the present work we consider another simple unsaturated organic molecule, allene, $CH_2=C=CH_2$, hoping to answer the question: Can a rational valence-theoretical explanation be given for the fact that the ratio of the most recent values for the twisting frequencies[5] of ethylene and allene, 1027 and 812 cm^{-1},[6,7] respectively, is 1.26? One might expect allene to behave on torsion much like an elastic rod twice as long as ethylene, which would give $\sqrt{2}=1.41$ as this ratio; the problem is to account for a negative deviation of 10 percent from this value.

Allene, like 1,3-butadiene, is a four-electron problem. The two problems are indeed formally identical; they differ only in numerical values for basic integrals. The earlier paper[4] may accordingly be referred to for many of the formulas and other details.

ENERGY OF THE GROUND STATE AS A FUNCTION OF TWISTING ANGLE. TWISTING FORCE CONSTANT AND TWISTING FREQUENCY

We assume the following geometry for allene:[8] carbon atoms, C_1, C_2, C_3, on the z axis; planes determined by the two CH_2 groups intersecting along the z axis at an angle of $90-2\theta$ degrees ($\theta=0$ yields the equilibrium configuration); C=C bond length 1.33A, C−H bond length 1.087A, C=C−H and H−C−H bond angles 120 degrees.

As starting orbitals for the four unsaturation electrons we take normalized Slater $2p$ atomic orbitals (χ's),[9]

* This paper is based on part of a thesis to be submitted by G. Russell Taylor in partial fulfillment of the requirements for the degree of Doctor of Science, Carnegie Institute of Technology.

† Research Corporation Fellow, 1950; Du Pont Postgraduate Fellow, 1950–1951.

[1] R. G. Parr and B. L. Crawford, Jr., J. Chem. Phys. **16**, 526 (1948).

[2] B. L. Crawford, Jr., and R. G. Parr, J. Chem. Phys. **17**, 726 (1949).

[3] Parr, Craig, and Ross, J. Chem. Phys. **18**, 1561 (1950).

[4] R. G. Parr and R. S. Mulliken, J. Chem. Phys. **18**, 1338 (1950).

[5] The twisting frequency of ethylene or allene is the frequency of that vibrational motion in which the end CH_2 groups are twisted relative to each other about the longitudinal axis of the molecule.

[6] For ethylene, see R. L. Arnett and B. L. Crawford, Jr., J. Chem. Phys. **18**, 118 (1950). The value 1027 cm^{-1} was obtained from a careful normal coordinate analysis of the infrared spectrum of a mixture of deuterated ethylenes and so may be regarded as having direct experimental confirmation.

[7] For allene, see H. W. Thompson and C. P. Harris, Trans. Faraday Soc. **40**, 295 (1944). The value 812 cm^{-1} was obtained indirectly from heat capacity data and has no direct experimental confirmation.

[8] E. H. Eyster, J. Chem. Phys. **6**, 580 (1938).

[9] The normalized Slater p orbital (for an electron) centered at a point 0 with major axis the W axis has the form (in atomic units—distances measured in units of the first Bohr radius, a_0)

$$2p_w=(Z^5/32\pi)^{\frac{1}{2}}w\exp(-Zr/2),$$

where Z is an effective charge (usually assigned a value near 3.2 for p orbitals in carbon), r is the distance (of the electron) from the point 0, and w is the W component of this distance.

TABLE I. Self-consistent ground-state molecular orbitals, orbital energies,[a] and total unsaturation electron energy, as functions of the twisting angle.[b]

$\rho=ZR$[c]	Z[c]	θ[b]	d_{12}/d_{11}[d]	d_{22}/d_{24}[d]	ϵ_1[a,e]	ϵ_2[a,e]	E_N[e]
6	2.38646	0°	1.42721	1.42721	−0.259945	−0.259945	−5.161221
		5°	1.32701	1.54086	−0.272352	−0.245254	−5.159190
		10°	1.23946	1.67850	−0.281185	−0.227721	−5.152210
8.37	3.32912	0°	1.09534	1.09534	0.040579	0.040579	−4.740287
		5°	1.06573	1.12692	0.030039	0.052507	−4.738450
		10°	1.04423	1.15317	0.021586	0.067328	−4.730383
		45°	0.86065	1.56775	0.050625	0.221976	−4.528623
10	3.97744	0°	1.05006	1.05006	0.232959	0.232959	−4.486791
		5°	1.03659	1.06416	0.224566	0.242365	−4.485311
		10°	1.02305	1.07904	0.219030	0.253005	−4.478534

[a] For definitions of the so-called "orbital energies," see reference 4.
[b] Equilibrium (CH_2 groups perpendicular) configuration: $\theta=0°$; least stable (CH_2 groups coplanar) configuration: $\theta=45°$.
[c] Z is the $2p$ atomic orbital effective charge—see reference 9—and R is the C=C distance in units of $a_0=0.5292A$, the first Bohr radius, $R=1.33/0.5292$.
[d] Equations (5) and (6) of the text give the molecular orbitals ϕ_i in terms of the coefficients d_{ip} and the symmetry orbitals σ_p. Orthonormalization conditions on the ϕ_i determine all of the d_{ip} once the ratios d_{12}/d_{11} and d_{22}/d_{24} are known.
[e] Energies are in atomic units: 1 atomic unit = 13.602 ev. The one-electron energies ϵ_i are relative to W_{2p}, the total four-electron energy E_N is relative to $4W_{2p}$, where W_{2p} is the energy of a $2p$ electron of a carbon atom in its valence state.

oriented as follows:

χ_1: centered on C_1 with major axis perpendicular to the plane determined by the C_1 methylene group;

χ_2: centered on C_2 with major axis perpendicular to the z axis and parallel to and in the same direction as χ_1 when the molecule is in its equilibrium ($\theta=0$) configuration;

χ_3: centered on C_2 and related to χ_4 as χ_2 is to χ_1;

χ_4: centered on C_3 with major axis perpendicular to the plane determined by the C_3 methylene group.

χ_2 and χ_3 remain stationary during torsional vibration; χ_1 and χ_4 rotate with their respective methylene groups, the angle between their positive axis being $90-2\theta$. From the vector property of p orbitals, the χ's may be written in terms of a set of stationary Slater orbitals:

$$\left.\begin{aligned}\chi_1&=\chi_a\cos\theta+\chi_{a_s}\sin\theta\\ \chi_2&=\chi_b\\ \chi_3&=\chi_{b_s}\\ \chi_4&=\chi_c\sin\theta+\chi_{c_s}\cos\theta\end{aligned}\right\}. \tag{1}$$

TABLE II. Integrals over stationary atomic orbitals.[a]

Integral[b]	Value[d,e] $\rho=6$[e]	$\rho=8.37$	$\rho=10$	Integral	Value $\rho=6$	$\rho=8.37$	$\rho=10$
Overlap integrals				$aa\|bb$	0.2616×Z	0.2086×Z	01806×Z
				$aa\|b_sb_s$	0.2484	0.2036	0.1774
S_{ab}	0.46800	0.25995	0.16396	$aa_s\|bb_s$	0.0066	0.0025	0.0016
S_{ac}	0.08874	0.01772	0.00534	$aa\|cc$	0.1550	0.1149	0.0970
				$aa\|c_sc_s$	0.1536	0.1145	0.0970
Penetration integrals				$aa_s\|cc_s$	0.0007	0.0002	0.00007
				$ab\|ab$	0.0751	0.0213	0.0081
$a:bb$	0.07730×Z	0.01976×Z	0.00703×Z	$ab\|a_sb_s$	0.0681	0.0189	0.0073
$a:cc$	0.00182	0.00006	0.0000046	$ab_s\|ab_s$	0.0035	0.0012	0.0004
$a:ab$	0.12000	0.04364	0.02090	$ac\|ac$	0.0022	0.00008	0.0000
$a:ac$	0.00856	0.00084	0.000174	$ac\|a_sc_s$	0.0020	0.00008	0.0000
$a:bc$	0.00625	0.000323	0.000035	$ac_s\|ac_s$	0.0001	0.0000	0.0000
$b:ac$	0.05200	0.01038	0.00313	$aa\|bc$	0 0910	0.0377	0.0202
				$aa\|b_sc_s$	0.0861	0.0363	0.0195
Coulomb-exchange integrals				$aa_s\|bc_s$	0.0025	0.0007	0.0004
				$ab\|ac$	0.0133	0.00145	0.00025
$aa\|aa$	0.3914×Z	0.3914×Z	0.3914×Z	$ab\|a_sc_s$	0.0117	0.00134	0.00024
$aa\|a_sa_s$	0.3492	0.3492	0.3492	$ab_s\|ac_s$	0.0008	0.00005	0.0000
$aa_s\|aa_s$	0.0211	0.0211	0.0211	$ab\|bc$	0.0573	0.0143	0.00485
$aa\|ab$	0.1538	0.0766	0.0448	$ab\|b_sc_s$	0.0544	0.0138	0.00477
$aa\|a_sb_s$	0.1399	0.0704	0.0415	$ab_s\|bc_s$	0.0015	0.00025	0.00004
$aa_s\|ab_s$	0.0069	0.0031	0.0016	$ac\|bb$	0.0347	0.0069	0.0020
$aa\|ac$	0.0220	0.0037	0.0010	$ac\|b_sb_s$	0.0310	0.0062	0.0018
$aa\|a_sc_s$	0.0210	0.0035	0.0010	$ac_s\|bb_s$	0.0018	0.00035	0.0001
$aa_s\|ac_s$	0.0005	0.0001	0.0000				

[a] The atomic orbitals are $2p$ Slater atomic orbitals as defined in reference 9.
[b] For definitions of integrals, see reference 4.
[c] See note c, Table I.
[d] Overlap integrals are dimensionless. The other integrals have dimensions of energy; their values are given in atomic units: 1 atomic unit = 13.602 ev
[e] Integral values were obtained from R. G. Parr and B. L. Crawford, Jr., J. Chem. Phys. 16, 1049 (1948); M. Kotani, *et al.*, Proc. Phys.-Math. Soc. 20 Extra No. 1 (1938); *ibid.* 22, Extra No. (1940); the approximation method of A. L. Sklar, J. Chem. Phys. 7, 984 (1939); or asymptotic formulas good for large values of ρ.

TABLE III. Integrals over moving atomic orbitals.[a]

Formulas for integrals[b] in terms of integrals over stationary atomic orbitals

Overlap integrals

$S_{12}=A\cdot S_{ab}$
$S_{13}=B\cdot S_{ab}$ $\quad\begin{pmatrix}A=\cos\theta^{c}\\ B=\sin\theta\end{pmatrix}$
$S_{14}=2AB\cdot S_{ac}$
$S_{23}=0$

Core integrals

$-I_{11}=(a:bb)+(a:cc)+(aa|bb)+(aa|b_sb_s)+(aa|c_sc_s)+8A^2B^2(aa_s|cc_s)$
$-I_{22}=2(a:bb)+(aa|bb)+(aa|b_sb_s)+(aa|a_sa_s)$
$-I_{12}=A[(a:ab)+(a:bc)+(aa|ab)+(aa|a_sb_s)+(aa|b_sc_s)+4B^2(aa_s|bc_s)]$
$-I_{13}=B[(a:ab)+(a:bc)+(aa|ab)+(aa|a_sb_s)+(aa|b_sc_s)+4A^2(aa_s|bc_s)]$
$-I_{14}=2AB[(a:ac)+(b:ac)+(aa|ac)+(ac|bb)+(ac|b_sb_s)]$
$-I_{23}=4AB(aa_s|bb_s)$

Coulomb-exchange integrals

$11|11=(aa|aa)$
$11|12=A(aa|ab)$
$11|13=B(aa|ab)$
$11|14=2AB(aa|ac)$
$11|22=A^2(aa|bb)+B^2(aa|b_sb_s)$
$11|23=2AB(aa_s|bb_s)$
$11|24=B(aa|b_sc_s)+4A^2B(aa_s|bc_s)$
$11|33=A^2(aa|b_sb_s)+B^2(aa|bb)$
$11|34=A(aa|b_sc_s)+4AB^2(aa_s|bc_s)$
$11|44=(aa|c_sc_s)+8A^2B^2(aa_s|cc_s)$
$12|12=A^2(ab|ab)+B^2(ab_s|ab_s)$
$12|13=AB[(ab|a_sb_s)+(ab_s|ab_s)]$
$12|14=B(ab_s|ac_s)+A^2B[(ab|ac)+(ab|a_sc_s)]$
$12|23=B(aa_s|ab_s)$
$12|24=AB[(ab|bc)+(ab_s|bc_s)]$
$12|33=A(aa|a_sb_s)$
$12|34=A^2(ab|b_sc_s)+B^2(ab_s|bc_s)$
$13|13=A^2(ab_s|ab_s)+B^2(ab|ab)$
$13|14=A(ab_s|ac_s)+AB^2[(ab|ac)+(ab|a_sc_s)]$
$13|22=B(aa|a_sb_s)$
$13|23=A(aa_s|ab_s)$
$13|24=A^2(ab_s|bc_s)+B^2(ab|b_sc_s)$
$14|14=(ac_s|ac_s)+2A^2B^2[(ac|ac)+(ac|a_sc_s)]$
$14|22=AB[(ac|bb)+(ac|b_sb_s)]$
$14|23=(ac_s|bb_s)$
$22|33=(aa|a_sa_s)$
$23|23=(aa_s|aa_s)$

[a] See the text and reference 9 for definitions of the moving atomic orbitals.
[b] For definitions of integrals, see reference 4.
[c] θ is the twisting angle, see note b, Table I.

Here χ_a, χ_b, and χ_c are parallel, and similarly χ_{a_s}, χ_{b_s}, χ_{c_s}.

Instead of forming molecular orbitals directly from the atomic orbitals χ_p, one may equivalently use any four orbitals which are independent linear combinations of the χ_p. The most convenient such orbitals are given by the formulas

$$\left.\begin{aligned}\sigma_1&=(1/N_1)(\chi_1+\chi_4)\\ \sigma_2&=(1/N_2)(\chi_2+\chi_3)\\ \sigma_3&=(1/N_3)(\chi_2-\chi_3)\\ \sigma_4&=(1/N_4)(\chi_1-\chi_4)\end{aligned}\right\}, \tag{2}$$

where the N_p are normalizing factors.[10] These may be called symmetry orbitals.

We now seek an approximate wave function for the ground state of our four-electron system of the form

$$\Psi_N=\frac{1}{(4!)^{\frac{1}{2}}}\begin{vmatrix}(\phi_1\alpha)^1(\phi_1\beta)^1(\phi_2\alpha)^1(\phi_2\beta)^1\\ (\phi_1\alpha)^2(\phi_1\beta)^2(\phi_2\alpha)^2(\phi_2\beta)^2\\ (\phi_1\alpha)^3(\phi_1\beta)^3(\phi_2\alpha)^3(\phi_2\beta)^3\\ (\phi_1\alpha)^4(\phi_1\beta)^4(\phi_2\alpha)^4(\phi_2\beta)^4\end{vmatrix}, \tag{3}$$

where superscripts number the electrons, α and β are the two possible spin functions for an electron, and the molecular orbitals ϕ_i are orthonormal linear combinations of the σ_p:

$$\phi_i=\sum_p d_{ip}\sigma_p. \tag{4}$$

The coefficients d_{ip} must be determined so as to minimize the total electronic energy, E_N, associated with Ψ_N. This requires the *LCAO* self-consistent field theory of Roothaan,[11] the application of which to the analogous four-electron problem, 1,3-butadiene, has been described in detail elsewhere.[4] The self-consistent field treatment leads to *four* orbitals of the form of Eq. (4);

[10] $N_1^2=2(1+S_{14})$, $N_2^2=N_3^2=2$, and $N_4^2=2(1-S_{14})$, where S_{14} is the "overlap" integral between χ_1 and χ_4, given by $S_{14}=2\sin\theta\cos\theta S_{ac}$, where S_{ac} is the overlap integral between χ_a and χ_c. S_{ac} is tabulated in Table II.

[11] C. C. J. Roothaan, Ph.D. thesis, University of Chicago, 1950.

TABLE IV. Twisting force constant and twisting frequency of allene. Ethylene-allene twisting frequency ratio.

	Z[a]	2.386	3.329	3.977	Experimental
Allene	k_N[b]	0.5139	0.4268	0.3374	
	l_N[b]	0.3062	0.8805	0.8065	
	ω_N[c]	730	665	591	812[e]
Ethylene	ω_N[c,d]	1180	1120	1020	1027[f]
ω_N ethylene÷ω_N allene		1.62	1.68	1.73	1.26

[a] Z is the $2p$ atomic orbital effective charge.
[b] Atomic units, see note e, Table I. For definition of k_N and l_N, see Eq. (7).
[c] Twisting frequency in cm^{-1}.
[d] This is labeled ω_1 in reference 1.
[e] See reference 6.
[f] See reference 7.

more precisely, it leads to the "ground-state orbitals"

$$\left.\begin{aligned}\phi_1&=d_{11}\sigma_1+d_{12}\sigma_2\\ \phi_2&=\qquad\qquad d_{23}\sigma_3+d_{24}\sigma_4\end{aligned}\right\} \tag{5}$$

and also to the "excited state orbitals"

$$\left.\begin{aligned}\phi_3&=d_{31}\sigma_1+d_{32}\sigma_2\\ \phi_4&=\qquad\qquad d_{43}\sigma_3+d_{44}\sigma_4\end{aligned}\right\}. \tag{6}$$

For a given value of the twisting angle θ, the procedure required for the evaluation of the coefficients d_{ip} and the energy E_N is just that used in the 1,3-butadiene problem.[4] Numerical results are given in Table I for $\theta=0°$, 5°, 10°, and 45° and several values of the effective charge Z.

The basic integrals required for the calculations are over the "stationary" atomic orbitals χ_a, χ_{as}, etc.; these are given in Table II. Table III gives formulas for integrals over the "moving" atomic orbitals χ_1, χ_2, etc., in terms of the basic set in Table II and the angle θ. For a given θ and Z, one first computes integrals over the moving atomic orbitals from the formulas in Table III, then computes integrals over the symmetry orbitals from expansion formulas for them in terms of integrals over the moving atomic orbitals, and then proceeds with the self-consistent field calculation of the d_{ip} and E_N as described in the 1,3-butadiene paper.[4]

To obtain values for the twisting force constant, we fit equations of the form

$$E_N=E_N{}^0+(1/2)k_N\theta^2+(1/24)l_N\theta^4 \tag{7}$$

to the $\theta=0°$, 5°, and 10° results in Table I. Values of k_N and l_N obtained in this way are given in Table IV, together with values for the twisting frequency itself, which is given by the formula

$$\begin{aligned}\omega_N&=(1/2\pi c)(k_N/I)^{\frac{1}{2}}\\ &=1018k_N{}^{\frac{1}{2}}\ [\omega_N \text{ in cm}^{-1},\ k_N \text{ in atomic units}],\end{aligned} \tag{8}$$

where c is the velocity of light and I is the total moment of inertia of the molecule about the C=C=C axis.

TABLE V. Excitation energies and ionization potentials of allene, $Z=3.329$.

	Symmetry	Singlets	Triplets
Ground state:	A_1	0.0 ev	...
Singly excited states:	A_1	11.1 (F)[a]	0.9 (F)
	A_2	5.1 (F)	5.0 (F)
	B_1	5.5 (F)	4.5 (F)
	B_2	8.9 (A)	1.4 (F)
Ionization potentials: $I_1=I_2=10.55$ ev[b]			

[a] (F) indicates transition from ground state forbidden; (A) indicates transition from ground state allowed.
[b] $W_{2p}=-11.10$ ev is assumed, see note e, Table I.

The importance of reminimizing the energy for each value of the angle θ should perhaps be emphasized. Molecular orbital coefficients definitely depend upon θ. If one assumes the molecular orbitals independent of θ and gives the coefficients their equilibrium ($\theta=0$) values, one obtaines 923, 698, and 601 cm^{-1} as the theoretical allene twisting frequencies for $Z=2.386$, 3.329, and 3.977.

ENERGIES OF EXCITED STATES. IONIZATION POTENTIALS

In the ground state of allene, two electrons occupy each of the molecular orbitals ϕ_1 and ϕ_2. Excitation of one or more electrons to ϕ_3 or ϕ_4 gives rise to excited electronic states. Approximate wave functions for these states must take cognizance of molecular symmetry and must be antisymmetric in the electrons, but may be built up by standard methods[12] from the one-electron orbitals ϕ_i.[13]

The only excited states we shall consider are those resulting from excitation of one electron from the ground-state configuration. Each such "singly excited" state has singlet and triplet components whose energy relative to the ground state may be expressed in terms of the basic integrals in Table II. Table V gives numerical results for $Z=3.329$.

Complete removal of an electron from a ground-state orbital ϕ_1 or ϕ_2 corresponds to a process of ionization. The energy required is given approximately by the formula[14]

$$I_1=-\epsilon_1 \quad \text{or} \quad I_2=-\epsilon_2, \tag{9}$$

where ϵ_1 and ϵ_2 are the "orbital energies" as given in Table I. Numerical values for $Z=3.329$ are given in Table V.

DISCUSSION

Comparison of the present allene results with the previous ethylene results (also displayed in Table IV)[1]

[12] E. U. Condon and G. Shortley, *Theory of Atomic Spectra* (Cambridge University Press, Cambridge, 1935).
[13] Use of orbitals obtained from the self-consistent field solution of the variational problem for the ground state is not strictly the best (from the point of view of the variational principle) procedure which one can employ—see reference 4.
[14] R. S. Mulliken, J. chim. phys. **46**, 497 (1949); **46**, 675 (1949).

yields a theoretical ethylene-allene twisting frequency ratio appreciably bigger than $\sqrt{2}$ and quite independent of Z, the only parameter which enters the calculations. The theoretical value (1.7) for this ratio should probably not be taken too seriously, but the inescapable conclusion of valence theory would seem to be that *the ethylene-allene twisting frequency ratio*[15] *should be somewhat greater than 1.41.*

To be sure, hydrogen atom repulsions and hyperconjugation have been ignored in these calculations, and these effects would favor a lower twisting frequency ratio. A rough calculation by the method of Lassettre[16] shows that hydrogen atom repulsions are essentially negligible; for $Z=3329$ they cause a decrease of only about 2 percent in the ratio. From Table I we see that in allene (for $Z=3.329$) the unsaturation electron energy is 66.4 kcal/mole less for the perpendicular ($\theta=0°$) than for the planar ($\theta=45°$) configuration; hydrogen repulsions favor the perpendicular form by only about 0.1 kcal/mole. The effect works in the opposite direction in ethylene, but is little bigger (*ca* 1.8 kcal/mole). Hyperconjugation, on the other hand, may be important, but its magnitude is difficult to estimate.

The ultraviolet spectrum of allene has not been measured. Previous experience[14] indicates that singlet-triplet splittings computed by the molecular orbital method come out too large but computed singlet-triplet centers of gravity quite good; we therefore predict that the mean value of the first allowed (B_2) singlet absorption band and the companion triplet will lie near 5.1 ev. Experience indicates computed ionization potentials somewhat high; we predict the first ionization potential of allene to be about 10.4 ev.

[15] A slight twist of the CH_2 groups in allene causes the double-bonding p orbitals χ_1 and χ_4 accompanying them to begin to interact, giving the molecule an increased stability. It is this factor, absent in ethylene, which renders allene somewhat easier to twist than an elongated ethylene molecule.

[16] E. N. Lassettre and L. B. Dean, Jr., J. Chem. Phys. **17**, 317 (1949). The method consists (essentially) of assuming a charge distribution for the covalent C—H bonds (including the protons), which is approximated by a Taylor series up to quadruple terms in order to calculate the electrostatic energy of interaction of the two methylene groups.

ACKNOWLEDGMENTS

We are grateful to J. F. Mulligan for helpful correspondence regarding asymptotic formulas for certain integrals, and to the Research Corporation for a grant in support of this work.

Letters to the Editor

THIS section will accept reports of new work, provided these are terse and contain few figures, and especially few half-tone cuts. The Editorial Board will not hold itself responsible for opinions expressed by the correspondents. Contributions to this section should not exceed 600 words in length and must reach the office of the Managing Editor not later than the 15th of the month preceding that of the issue in which the letter is to appear. No proof will be sent to the authors. The usual publication charge ($8.00 per page) will not be made and no reprints will be furnished free.

The Structure and Dipole Moment of SO_2 from Microwave Spectra*

GEORGE F. CRABLE AND WILLIAM V. SMITH
Department of Physics, Duke University, Durham, North Carolina
(Received February 12, 1951)

THE structure of SO_2 has been determined previously from measurements of rotational transitions between relatively high energy levels where centrifugal distortion may be important.[1] Measurements of the $0_{00}\rightarrow1_{11}$, $2_{02}\rightarrow2_{11}$, and the $3_{13}\rightarrow4_{04}$ transitions provided a means of determining the structure from transitions between low energy levels. The measured frequencies of these transitions with the measured and calculated frequencies of the $4_{04}\rightarrow4_{13}$, $6_{15}\rightarrow5_{24}$, and $7_{26}\rightarrow8_{17}$ transitions are given in Table I.

The $0_{00}\rightarrow1_{11}$ transition gives directly the sum of the rotational constants A_0 and C_0. Equations for the energy differences of the transitions $2_{02}\rightarrow2_{11}$ and $3_{13}\rightarrow4_{04}$ were obtained from the expressions developed by King, Hainer, and Cross for a perturbed symmetric rotor.[2] A_0, B_0, and C_0 were obtained from these three relations.

TABLE I. SO_2 rotational transition frequencies.

Transition	Frequency (Mc) Measured	Calculated
$0_{00}\rightarrow1_{11}$	69576.06 ±0.18	
$2_{02}\rightarrow2_{11}$	53529.16 ±0.16	
$3_{13}\rightarrow4_{04}$	29321.22 ±0.03	
$4_{04}\rightarrow4_{13}$	59225.00 ±0.07	59225.1
$6_{15}\rightarrow5_{24}$	23414.33 ±0.03	2343_5
$7_{26}\rightarrow8_{17}$	25392.797 ±0.014	2539_6

TABLE II. Molecular constants of $S^{32}O_2^{16}$.

A_0	2.02740 cm^{-1}	I_a^0	13.8031×10^{-40} g cm^2
B_0	0.344179 cm^{-1}	I_b^0	81.3077×10^{-40} g cm^2
C_0	0.293534 cm^{-1}	I_c^0	95.3361×10^{-40} g cm^2

$r_{s-0}=1.4321$A
$\angle$O−S−O$=119°\ 2.1'$

Constants used: $c=2.99776\times10^{10}$ cm/sec.
$h=6.62373\pm0.0011\times10^{-27}$ erg sec.
1 A.M.U. $=1.64972\times10^{-24}$ g.
$M_s32=31.9823$ A.M.U.
$M_o16=16.0000$ A.M.U.

The values of r_{s-0} and $\angle$O−S−O were calculated from I_a^0 and I_b^0. These results compare favorably with the values $r_{s-0}=1.433$A and $\angle$O−S−O$=119.5°$ obtained by Dailey, Golden, and Wilson.[1] The molecular constants of $S^{32}O_2^{16}$ are presented in Table II.

The observed stark splittings for the four transitions of lowest J are:

$$0_{00}\rightarrow1_{11}\quad \Delta\nu_{(MC)}=0.820E^2_{(\text{esu/cm})}$$
$$2_{02}\rightarrow2_{11}\quad \Delta\nu_{(MC)}=(0.341+0.0817M^2)E^2_{(\text{esu/cm})}$$
$$3_{13}\rightarrow4_{04}\quad \Delta\nu_{(MC)}=(0.322-0.0345M^2)E^2_{(\text{esu/cm})}$$
$$4_{04}\rightarrow4_{13}\quad \Delta\nu_{(MC)}=(-0.180+0.0573M^2)E^2_{(\text{esu/cm})}.$$

The dipole moment of $S^{32}O_2^{16}$ was found from the stark splitting of the $0_{00}\rightarrow1_{11}$ transition to be 1.59±0.01 Debye units, agreeing well with results of 1.611 and 1.60 Debye units found by other methods.[3,4] An effective electrode spacing for the K band stark cell was found by measuring the stark splitting of the $J=1\rightarrow2$ transition of $O^{16}C^{12}S^{32}$. The dipole moment of OCS was assumed to be 0.7085.[5] The theoretical expression for the stark line displacement was obtained by the method of Golden and Wilson.[6] Values of $\mu=1.52$ for $M=1$ and $\mu=1.56$ for $M=2$ were calculated from the $2_{02}\rightarrow2_{11}$ transition. As a consequence of large errors in the interpolations between Cross, Hainer, and King's tabulated line strengths,[7] these values of μ, as well as values calculated from the higher transitions, have a much larger error than that calculated for the $0_{00}\rightarrow1_{11}$ transition.

We wish to acknowledge helpful correspondence with Professor E. B. Wilson, Jr. on this problem.

* The research reported in this document has been made possible through support and sponsorship extended by the Geophysical Research Directorate of the Air Force Cambridge Research Laboratories under Contract No. W19-122-ac-35. It is published for technical information only and does not represent recommendations or conclusions of the sponsoring agency.
[1] Dailey, Golden, and Wilson, Jr., Phys. Rev. **72**, 871 (1947).
[2] King, Hainer, and Cross, J. Chem. Phys. **11**, 27 (1943).
[3] C. T. Zahn, Phys. Rev. **27**, 455 (1926).
[4] Smitz, Z. physik. Chem. **B35**, 60 (1936).
[5] R. G. Shulman and C. H. Townes, Phys. Rev. **77**, 500 (1950).
[6] S. Golden and E. B. Wilson, Jr., J. Chem. Phys. **16**, 669 (1948).
[7] Cross, Hainer, and King, J. Chem. Phys. **12**, 210 (1944).

On the Latent Heat of Fusion and the Hole Theory

N. R. MUKHERJEE
Department of Chemistry and Chemical Engineering, University of Washington, Seattle, Washington
(Received December 26, 1950)

IN most cases fusion is accompanied by an increase in volume, and at the fusion temperature a liquid may be distinguished from the corresponding solid state by its relatively large specific volume. Since temperature remains constant during fusion, we attribute this increase in volume to the formation of additional holes, and the total energy of their formation is equal to the latent heat of fusion.

The additional number of holes, N_h, formed during fusion is

$$N_h=V/v, \tag{1}$$

where V is the increase in volume during fusion, and v average volume of a hole.

According to Frenkel[1] the average radius, r, of a hole at room temperature is

$$r\simeq(kT/\sigma)^{\frac{1}{2}}, \tag{2}$$

where k is the Boltzmann constant, T the absolute temperature, and σ the surface tension.

On the other hand, if we consider the mechanism of the process of hole formation, it may be assumed that the average volume of a hole at the fusion temperature is equal to the volume occupied by a molecule of the substance. Actually, a hole may be of any shape. We shall, however, assume it to be of spherical shape of radius, r, the volume being equivalent to the molecular volume. This assumption will have effect on the value of surface tension, because for a micro-particle of solid or a drop of liquid it varies with the size and shape. Hill[2] indicates that for spherical drops the magnitude of the effect of drop radius on surface tension is not large at zero-order approximation. However, the values of surface tension available for macrosize are used in the calculation, making necessary correction for temperature.

The energy, $W(r)$, required to form a hole is associated with the surface formed, and

$$W(r)=4\pi r^2\sigma. \tag{3}$$

According to our assumption the latent heat of fusion, Q, is

$$Q=W(r)\cdot N_h=4\pi r^2\sigma\cdot V/v=3V\sigma/r \tag{4}$$
$$[\because v=4/3\pi r^3].$$

TABLE I.

Substance (1)	T Triple point in °K (2)	σ Surface tension in dynes/cm (3)	r_1 Radium of atom or molecule in A (4)	V Change of volume per mole during fusion, in cc (5)	Q/RT Observed (dimensionless) (6)	Q/RT Calculated by Eq. (6) (7)	Q/RT Calculated by Eq. (5) (8)	Obs Q. (Col. 6) / Calc Q. (Col. 8) (9)
Na	371	294	1.86	0.51	0.85	1.11	0.78	1.09
K	335	411 98.2	2.27	1.07	0.80	4.46 0.52	2.08 0.50	0.39 1.60
Cu	1356	1123	1.27	0.32	0.98	0.74	0.75	1.30
Ag	1233.6	812	1.44	0.49	0.92	0.80	0.81	1.13
Au	1336	1000 580	1.4	0.55	1.13	1.09 0.48	1.06 0.62	1.06 1.82
Zn	693	756	1.34	0.63	1.2	2.19	1.85	0.65
Cd	594	600	1.49	0.65	1.2	2.03	1.59	0.76
Hg	230	500 436	1.49	0.52	1.2	5.02 4.17	2.74 2.39	0.44 0.50
Al	931	550	1.43	0.75	1.11	1.05	1.12	1.00
Ga	303	358	1.22	0.63	2.19	2.49	2.20	1.00
Tl	561	400	1.99	0.55	0.7	1.02	0.81	0.86
Sn	500	518	1.4	0.46	1.65	1.49	1.23	1.34
Pb	600	440	1.74	0.66	1.05	1.28	1.00	1.05
Ne	24.6	5.6	1.12	2.19	1.6	0.73	1.61	1.00
A	83.8	13.5	1.54	3.05	1.6	0.61	1.15	1.39
H_2	14	1.91	1.24	2.82	1.01	0.44	1.12	0.90
N_2	63	11.8	1.06	2.02	1.36	0.51	1.29	1.05
O_2	54.3	20	1.4	1.64	0.97	1.13	1.55	0.63
P_4	317	52	2.16	2.4	1.00	0.5	0.66	1.51
Se_2	473	98	2.32	2.82	2.24	0.82	0.91	2.46
Br_2	266	44	2.26	8.16	4.80	1.69	2.16	2.22
CCl_4	250.4	32	2.73	3.97	1.15	0.56	0.67	1.71
CS_2	157.3	45	2.62	3.27	2.10	1.54	1.40	1.50

Hence,

$$Q/RT=3V\sigma/RTr_1, \tag{5}$$

where r_1 = radius of a molecule = r, and, from Eq. (2),

$$Q/RT=3V\sigma^{\frac{1}{3}}/RT^{\frac{1}{3}}k^{\frac{1}{3}}. \tag{6}$$

Again, the sum total of the attractive and repulsive forces, U, can be written as

$$U=-2\epsilon(r^*/r')^6+\epsilon(r^*/r')^{12}, \tag{7}$$

where r' is the distance between a pair of molecules, r^* their equilibrium distance, and ϵ a constant. Under equilibrium condition, $r^*=r'$ and $U^*=-\epsilon$. The mechanism of hole formation may be visualized as if a molecule has been pushed to a linear distance of $4r_1$ from its nearest neighbor, thereby creating a hole of radius $r(=r_1)$. Considering only the nearest neighbors, the work done in creating a hole is $W(r)\simeq p/2(U^*-U)$, where p is the number of nearest neighbor.

$$\therefore \frac{Q}{RT}=\frac{W(r)\cdot N_h}{RT}\simeq\frac{p}{2}\frac{(U^*-U)}{RT}\cdot\frac{V}{v}=\frac{3p(U^*-U)V}{8\pi RTr_1^3}. \tag{8}$$

The surface tension of fused substances is difficult to determine accurately and hence provides some source of error in the result. Moreover, in the case of potassium, $\sigma=411$ dynes/cm was reported by Meyer,[3] whereas $\sigma=98.2$ dynes/cm was obtained from the recent data of Quarterman and Primak.[4] σ of mercury has also been reported to be anomalous, and it changes with time.[5] σ of gold is given as a range 500 to 1000 dynes/cm.

TABLE II.

Substance	r^* in A	$r'=4r_1$ in A	$\epsilon\times10^{15}$ in ergs	p	Q/RT Observed (dimensionless)	Q/RT Calculated by Eq. (8)	Obs Q / Calc Q
A	3.83	4.16	16.5	12	1.6	2.52	0.64
Ne	3.08	4.48	4.89	12	1.6	4.26	0.37
H_2	3.28	4.96	4.25	6 (?)	1.01	3.25	0.30

The high experimental values of Q/RT for P_4, Se_2, S_8, Br_2, etc. (Table I) compared to the calculated values is due partly to the energy of rotation of the molecule, which has not been accounted for in the Eqs. (5) and (6). Quite arbitrarily, however, if we substitute for r_1 the radius of a single atom, the experimental and calculated values are close to each other. (See Table II.)

In conclusion it can be said that the method of calculation by Eq. (5) is applicable at least in the case of monatomic liquid substances.

The author wishes to thank Professors R. W. Moulton, P. C. Cross, and B. S. Rabinovitch, University of Washington, for their helpful criticism.

[1] J. Frenkel, *Kinetic Theory of Liquids* (Clarendon Press, Oxford, 1946), p. 179.
[2] T. L. Hill, J. Am. Chem. Soc. **72**, 3925 (1950).
[3] *International Critical Tables* **4**, 440 (1928).
[4] L. A. Quarterman and W. L. Primak, J. Am. Chem. Soc. **72**, 3035 (1950).
[5] R. S. Burdon and M. L. Oliphant, Trans. Faraday Soc. **25**, 205 (1927).

Calculation of the Molecular Diameters from Sutherland's Constant

M. EL NADI
Faculty of Science, Fouad I University, Cairo, Egypt
(Received January 2, 1951)

RECENT theoretical developments explaining the nature of the forces between molecules have produced a variety of successful applications. In this note we shall show that, applying this theory to Sutherland's molecular model, we deduce values for the molecular diameters which are consistent with those derived by different methods.

Sutherland considered the gaseous molecules as smooth rigid elastic spheres surrounded by an attractive field of force $-\mu/r^n$ and derived the following equation for the coefficient of viscosity η:

$$\eta=A\frac{T^{\frac{1}{2}}}{1+(C/T)}, \tag{1}$$

where A and C are constants. The latter is called after Sutherland

and is given by:[1]

$$C=\frac{\mu I(n)}{(n-1)\sigma^{n-1}k},\qquad(2)$$

where σ is the diameter of one molecule, k Boltzmann's constant, and $I(n)$ a function of the force index n.

Now, in 1930, F. London has shown that the molecular force arises from the polarizability of the molecules in the electrostatic field of each other, and that the index n has the value 7. Thus introducing the values:[1]

$I(7)=0.1736$, $k=1.372\times10^{-16}$ erg per deg, and $\lambda=\mu/6$, we get from (2):

$$\sigma=\left(\frac{0.1736\times10^{16}\times\lambda}{C\times1.372}\right)^{1/6}.\qquad(3)$$

Table I gives the values of σ, as calculated from (3). These are denoted by σ_c. For comparison, we have mentioned the values

TABLE I.

Gases	$\lambda\times10^{60}$ (erg·cm^6)[a]	C	Remarks on C	$\sigma_c\times10^8$ cm	$\sigma_\eta\times10^8$ cm[b]	$\sigma_b\times10^8$ cm[b]
He	1.49 1.23 1.63 1.52 1.23	80	$C=80.3$ in the temp. range[4] 15.3°→184.6°C	1.693 1.640 1.719 1.699 1.640	2.08	2.30
Ne	7.97 7.48 4.67	56	in the range 13.8→100.0°C	2.376 2.352 2.174	2.62	2.39
A	69.5 63.5 55.4	142	in the range 16.0→99.6°C	2.919 2.876 2.811	2.94	2.86
Kr	129.0 136.0 107.0	188	in the range 16.3→100°C	3.089 3.116 2.993	3.19	3.14
Xe	273.0 233.0	252	in the range 15.3→100.1°C	3.333 3.246	3.52	3.42
H_2	11.4	84.4		2.356	2.40	2.32
N_2	57.2	104.0	C constant up to 830°C	2.977	3.18	3.53
O_2	39.8	125.0	C constant up to 830°C	2.717	2.97	2.93
CO_2	152.0	254.0	C constant above 300°C	3.019	3.44	3.40
CH_4	112.0	164.0		3.086	3.28	3.23
NH_3	70.0	503.0	C constant from 20→300°C	2.368	2.64	3.05
Cl_2	321.0	330		3.273	3.69	3.30
HCl	111.0	362		2.704	2.92	3.12
HBr	185.0	357		2.947	3.18	3.28
HI	370.0	331		3.351	3.45	3.47

[a] H. Margenau, Revs. Modern Phys. 11, 32 (1939).
[b] Schuil, Phil. Mag. 28, 679 (1939). We might add that the van der waals "b" are deduced from the critical data.

of σ as calculated by the usual formulas:

$$\eta=0.499\frac{m\bar{v}}{\sqrt{2}\pi\sigma^2}\quad\text{and}\quad b=\tfrac{2}{3}N\pi\sigma^3,$$

where m is the mass of one molecule, $\bar{v}$ its average velocity, and b is the van der waal's volume coefficient. These two values of σ are denoted in the table by σ_η and σ_b, respectively.

The agreement is not good for helium, but this might be attributed to the fact that Sutherland's model was found inappropriate for the helium gas. The general agreement for the other gases is a further proof for the consistency of both London and Sutherland theories.

[1] Chapman and Cowling, *The Mathematical Theory of Non-Uniform Gases* (Cambridge University Press, London, 1939), p. 184.

Polymorphism of RbBr*

L. G. SCHULZ
Institute for the Study of Metals, University of Chicago, Chicago, Illinois
(Received January 29, 1951)

WHEN grown from solution on oriented silver films, RbBr, which normally has the NaCl type crystal structure, was found to have an abnormal CsCl type structure. This result is a consequence of the close atomic matching of the CsCl type structure with silver. When consideration is given to the effect of the change in coordination number,[1] the predicted lattice constant of the abnormal CsCl structure of RbBr is 4.06A, which is very close to 4.08A, the lattice constant of silver.

The silver films, which were prepared after the manner of Lassen and Brück[2] on heated NaCl substrates, had a pseudo-single crystal structure with a (100) crystallographic plane parallel to the surface. A layer of RbBr about 200A in average thickness was deposited from the vapor in a vacuum onto such films. As grown from the vapor, the RbBr had its normal NaCl structure with a [111] fiber orientation. When dissolved by exposure to moist air and then recrystallized by drying, the RbBr changed to the CsCl structure oriented with its crystallographic axes parallel to those of the silver film. The lattice constant of the new structure was found to be 4.08A±0.02A. Additional experimental details will be given later.

* This research was supported in part by U. S. Army Air Force Contract AF-33 (038)-6534.
[1] W. H. Zachariasen, American Crystallographic Association, Spring Meeting, 1950.
[2] H. Lassen and L. Brück, Ann. Physik. 22, 65 (1935).

Preparation of Carrier-Free Manganese 52

JOHN T. BYRNE
Department of Chemistry and Laboratory for Nuclear Science and Engineering, Massachusetts Institute of Technology, Cambridge, Massachusetts
(Received January 26, 1951)

STRICKLAND and Spicer[1] report that milligram amounts of heptavalent manganese can be distilled from sulfuric acid. The sulfuric acid concentration must be maintained at approximately 10M to obtain the optimum separation, and they suggest the addition of 40 percent nitric acid during the distillation to keep the volume of solution constant. Using their procedure, it is possible to separate tracer quantities of radioactive manganese 52 from deuteron-bombarded chromium without the addition of carrier.

A target of 2 g of chromic oxide was bombarded with 16-Mev deuterons in the M.I.T. cyclotron. It was fused with 10 g of sodium peroxide and the melt dissolved in sulfuric acid. The solution was then made 10M in sulfuric acid and 1 g of potassium meta-periodate added. A volume of 40 percent nitric acid, equal to the volume of distillate, was added continuously during the distillation so that the volume of distilling solution remained constant. The fraction distilled depends on the relative volumes of distillate and distilling solution. Using equal volumes (100 ml), a 75 percent recovery was effected. With 200 ml of distillate, over 90 percent of the manganese was distilled. A spectrophotometric analysis showed less than 1 ppm of chromium in the distillate. Identification of the manganese 52 was made by its decay (5.8-day half-life) and by an absorption curve.

The author wishes to thank Professor L. B. Rogers for his encouragement and advice.

[1] Strickland and Spicer, Ann. chim. Act. 3, 543 (1949).

Cluster Integrals and the Thiele Semi-Invariants

SYÛ ONO
Institute of Applied Science, Faculty of Engineering, Kyushu University, Fukuoka, Japan
(Received February 21, 1951)

GIBBS' equation for the grand canonical ensemble is written as

$$\exp[pV/kT]=\sum_{n=0}^{\infty}\lambda^n Q_n/n!,\qquad(1)$$

where p is the pressure, V is the volume, T is the absolute tem-

perature, k is Boltzmann's constant, and λ is the absolute activity defined by $\exp[\mu/kT]$, with μ the chemical potential. $Qn/n!$ is the partition function for a system consisting of n molecules contained in a vessel of the volume V.

$$Qn/n! = \sum_{l=1}^{\infty} g_l \exp[-E_l/kT], \tag{2}$$

in which E_l is the lth eigenvalue of the system, and g_l is the degeneracy of the state. And we assume that the pressure can be expressed as a power series in the absolute activity:

$$pV = kT \sum_{s=1}^{\infty} \lambda^s \Lambda_s/s!. \tag{3}$$

If Ω_n is regarded as the nth moment in mathematical statistics, Λ_s is the sth Thiele semi-invariant,[1] which is given by

$$\Lambda_s = s!\Sigma[\Sigma i n_i = s](-)^{\Sigma n_i - 1}(\Sigma n_i - 1)!\Pi\{(Q_i/i!)^{n_i}/n_i!\}, \tag{4}$$

where the summation goes over all sets of such integers $n_1, n_2, \cdots, n_i, \cdots$ that $\Sigma i n_i = s$.

If the classical laws of mechanics are applied to the system, Q_n may be written as

$$Q_n = (2\pi mkT/h^2)^{3n/2}\Omega_n, \tag{5}$$

where m is the mass of a molecule. The configurational partition function Ω_n is defined as

$$\Omega_n = \int\int_V \cdots \int \exp[-U_n\{n\}/kT]d\{n\}, \tag{6}$$

where $U_n\{n\}$ is the potential energy of the system composed of n molecules, and $d\{n\}$ is the configuration element of the set of n molecules. Let us define the auxiliary functions $g_s\{s\}$, similar to that first introduced by Mayer and Montroll,[2] by the equation

$$g_s\{s\} = \Sigma\{k\{n_i\}_s\}(-)^{k-1}(k-1)! \prod_{i=1}^{i=k} \exp[-U_n\{n_i\}/kT], \tag{7}$$

in which the summation goes over all unconnected sets of subsets, and the product over all k subsets. And we define the cluster integrals by

$$b_s = \frac{1}{s!V}\int\int_V \cdots \int g_s\{s\}d\{s\}. \tag{8}$$

Then it follows immediately from Eqs. (4), (5), (6), and (8) that

$$\Lambda_s = (2\pi mkT/h^2)^{3n/2} Vs!b_s. \tag{9}$$

Then Eq. (4) can be written in the form

$$pV = kT \sum_{s=1}^{\infty} b_s Z^s, \tag{10}$$

where Z is the fugacity given by

$$Z = (2\pi mkT/h^2)^{3/2}\lambda. \tag{11}$$

Equation (10) was first derived by Mayer[3] after rather complicated reasoning. If the total potential energy of the system is representable as the sum of the potentials between the pairs, $u(i, j)$, Eq. (8) may be rewritten in the usual form,

$$b_s = (1/Vs!)\int\int_V \cdots \int \sum_{s \geq i > j \geq 1} \prod f(i, j)d\{s\} \tag{12}$$

(sum over all connected products),

in which $f(i, j) = \exp[-u(i, j)/kT] - 1$.

Furthermore, from Eqs. (2) and (3) we obtain Kahn and Uhlenbeck's equation for the pressure,[4] which was derived on the basis of quantum statistics, if we write, instead of Eq. (9),

$$\Lambda_s = Vs!b_s. \tag{13}$$

Thus, the present theory may be useful to simplify and to generalize the theory of cluster integrals.

[1] H. Cramér, *Random Variables and Probability Distributions* (Cambridge University Press, London, 1937), chapter 4.
[2] J. E. Mayer and E. Montroll, J. Chem. Phys. **9**, 2 (1941).
[3] J. E. Mayer, J. Chem. Phys. **5**, 67 (1937).
[4] B. Kahn and G. E. Uhlenbeck, Physica **5**, 399 (1938).

Erratum: Intermolecular Forces in Benzene and Ammonia

[J. Chem. Phys. 18, 1442 (1950)]

VERNON MYERS
The Pennsylvania State College, State College, Pennsylvania

PROFESSOR W. O. Stockmayer has kindly pointed out to the author that dimerization does not modify the formal expression for the second virial coefficient. This does not affect any of the calculations, since a comparison was made between the theoretical and experimental virial rather than between the theoretical virial and monomer coefficient of Eq. (7).

Intensities of Bands Due to Free and Bonded Hydroxyl Groups in the 3 Micron Region

S. A. FRANCIS
Beacon Laboratories of The Texas Company, Beacon, New York
(Received January 18, 1951)

IN a recent article in this journal, Coggeshall[1] calculated theoretically the ratio of the squares of the matrix elements of dipole moment for the 3 micron stretching vibration of hydrogen-bonded and of free hydroxyl groups. The calculated value of 1.16 was found to be in good agreement with the ratio of the absorption coefficients at the spectral positions of maximum absorption for bonded and free benzyl alcohol molecules. The purpose of this note is to point out that when a more exact test of the theory is made using integrated absorption intensities rather than maximum absorption coefficients, this good agreement with the calculated value disappears.

The ratio of the squares of the matrix elements of dipole moment for bonded and for free molecules, R, is given approximately by[2]

$$R = \nu_F A_B/\nu_B A_F, \tag{1}$$

where ν_F and ν_B are the frequencies of the bands, and A_F and A_B are the corresponding integrated intensities per molecule for free and bonded molecules. Only if the two absorption bands had similar shapes (that is, if their profiles obeyed the same type of absorption law and their half-widths were the same) would a comparison of maximum absorption coefficients be equivalent to a comparison of integrated intensities of the bands. The absorption curves for benzyl alcohol in Fig. 3 of Coggeshall's article indicate that the band due to bonded hydroxyl groups is much broader than that due to free hydroxyl groups. It thus appears that the ratio of the integrated intensities and also the value of R are appreciably greater than the calculated value of 1.16.

Some data obtained in this laboratory on the integrated intensities of free and bonded n-propyl alcohol are of interest in this connection. Figure 1 shows plots of the absorption coefficient

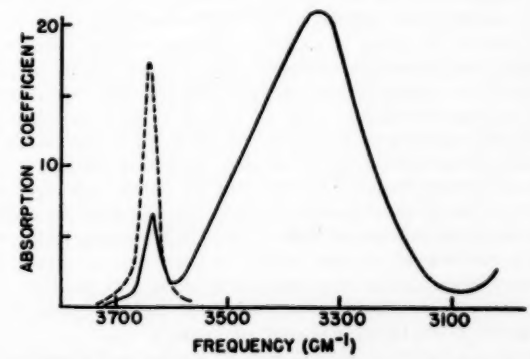

FIG. 1. Absorption curves for solutions of n-propyl alcohol in CCl_4. - - - - 0.00430 molar solution, ——— 0.502 molar solution. (Absorption coefficient in units of 10^{-20} cm²/molecule).

per molecule *versus* spectral frequency for 0.00430 and for 0.502 molar solutions of *n*-propyl alcohol in CCl_4. These data were obtained under conditions of high resolution with a grating and using a spectral slit width of 1.4 cm^{-1}. For the 0.00430 molar solution the low frequency band due to hydrogen-bonded molecules is absent, and a value of 2.28×10^{-7} cm^2/molecule sec is obtained for the integrated intensity per molecule of the band due to free molecules. The integrated intensities for the 0.502 molar solution are 18.5×10^{-7} cm^2/molecule sec for the 3100–3600 cm^{-1} band and 0.82×10^{-7} cm^2/molecule sec for the 3640 cm^{-1} band, calculated using the total concentration of alcohol molecules in the solution. This corresponds to 36 percent of the molecules existing in a free condition and, by difference, 64 percent in a bonded condition. The integrated intensity per molecule for the bonded molecules is, therefore, 28.9×10^{-7} cm^2/molecule sec and the value of R calculated from Eq. (1) is 13.8.

A similar calculation for a 1.005 molar solution showed 31 percent of the molecules existed in a free condition and gave a value of 33.2×10^{-7} for the integrated intensity per bonded molecule. This indicates that not only the number of molecules in a bonded condition but also the absorption per bonded molecule increases with increasing concentration of alcohol molecules.

It is probably not surprising that the intensity of the hydroxyl stretching band cannot be calculated satisfactorily on the basis of a theory which considers charges residing on the bonded atoms and the charges oscillating with the atoms. This picture was also found to be inadequate to explain the intensities of the ethylene and nitrous oxide bands measured by Thorndike, Wells, and Wilson.[3]

The large increase in intensity of the band due to bonded OH in alcohols compared to that for free OH is in marked contrast with the results of Lüttke and Mecke[4] for the similar bands of phenol. They found the integrated intensity per molecule of the band for pure phenol was approximately one-half as great as for a very dilute solution of phenol in CCl_4.

[1] Norman D. Coggeshall, J. Chem. Phys. **18**, 978 (1950).
[2] G. Herzberg, *Infrared and Raman Spectra* (D. Van Nostrand Company, Inc., New York, 1945), p. 261.
[3] Thorndike, Wells, and Wilson, Jr., J. Chem. Phys. **15**, 157 (1947).
[4] W. Lüttke and R. Mecke, Z. Electrochem. **53**, 241 (1949).

Surface Tension of Small Droplets as a Function of Size from Critical Supersaturation Data*

G. M. POUND
Metals Research Laboratory, Carnegie Institute of Technology, Pittsburgh, Pennsylvania
AND
V. K. LAMER
Chemistry Department, Columbia University, New York
(Received February 20, 1951)

SOME recent publications in this Journal[1,2] have dealt with the evaluation of surface tension of small droplets as a function of curvature. The present authors have suggested[3] that critical supersaturation data, i.e., critical supersaturation required for spontaneous production of stable droplets from the vapor phase, be used to measure their surface tension. This experimental approach has significance, because droplet surface tension may be expressed analytically as a function of critical supersaturation ratio, and because the size of a stable nucleus of the liquid phase is determined by its surface tension and the critical supersaturation required for its spontaneous production.[4,5] Further, the authors[3] have analyzed the data of Volmer and Flood[6] dealing with critical supersaturation of various vapors to show that no appreciable decrease in surface tension occurs with increase in particle curvature down to droplet diameters of about 20A, in apparent contradiction of the theoretical work of Tolman.[1]

However, the experimental work of Volmer and Flood was not carried to low temperatures, where appreciable decrease of stable droplet size below about 20A may be expected to occur considering the following thermodynamic relationship,[5] which is derived from the Gibbs-Thomson formula, and the fact that critical supersaturation ratio increases markedly as temperature is lowered.

$$n_k=\frac{32\pi\rho N}{3M}\left(\frac{\sigma M}{\rho RTx}\right)^3, \tag{1}$$

where n_k = number of molecules/stable liquid nucleus, ρ = density of liquid, M = molecule weight, N = Avogadro's number, σ = surface tension of droplet, x = critical supersaturation ratio, $\ln(p/p_\infty)$, R = gas constant, T = absolute temperature, p = partial pressure required for spontaneous production of droplets from vapor, and p_∞ = equilibrium vapor pressure in bulk liquid phase.

Sander and Damköhler[7] have extended the critical supersaturation measurements on water vapor to lower temperatures, i.e., down to about 200°K. The present authors believe that these data are not as reliable as the earlier data of Volmer and Flood because of certain experimental difficulties. Further, we prefer the Becker and Doering[5] expression of the phase transformation rate equation to the one employed by Sander and Damköhler. Nevertheless, we feel that their data may be sufficiently good to demonstrate, for the first time, a small decrease in surface tension as droplet size is reduced.

In our analysis of Sander and Damköhler's critical supersaturation data, we have applied the Becker and Doering treatment to compute the surface tension of stable liquid droplets and Eq. (1) to compute the droplet size. The results are summarized in Fig. 1,

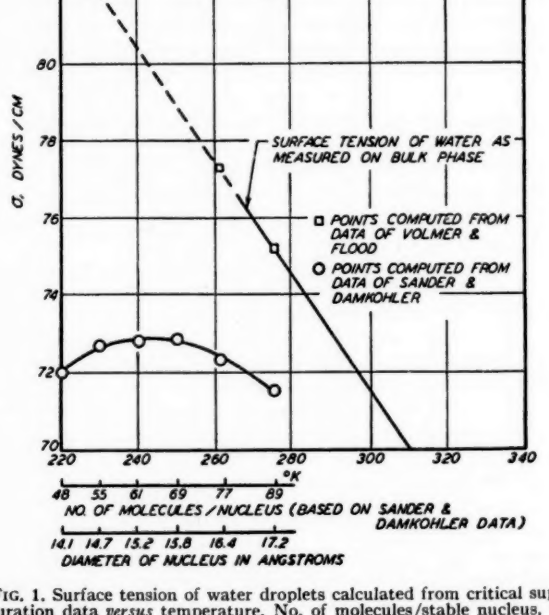
σ, DYNES / CM
82
80
78
76
74
72
70
SURFACE TENSION OF WATER AS MEASURED ON BULK PHASE
POINTS COMPUTED FROM DATA OF VOLMER & FLOOD
POINTS COMPUTED FROM DATA OF SANDER & DAMKOHLER
220 240 260 280 300 320 340
°K
48 55 61 69 77 89
NO. OF MOLECULES / NUCLEUS (BASED ON SANDER & DAMKOHLER DATA)
14.1 14.7 15.2 15.8 16.4 17.2
DIAMETER OF NUCLEUS IN ANGSTROMS

FIG. 1. Surface tension of water droplets calculated from critical supersaturation data *versus* temperature, No. of molecules/stable nucleus, and nucleus diameter.

where calculated values of surface tension are plotted *versus* number of molecules in the stable liquid nucleus, nucleus diameter, and absolute temperature. For purposes of comparison, the surface tension of water as measured on the bulk phase[8] is plotted as a function of temperature. At temperatures lower than 265°K, water of ordinary purity freezes spontaneously in the bulk phase, so that it is not possible to measure its surface tension below this temperature. Accordingly, the broken line represents an extrapolation to lower temperatures. From Fig. 1 it is seen that the difference between bulk phase surface tension and the surface tension of small droplets increases with decrease in stable droplet size. Indeed, the surface tension of the droplets appears to pass through a maximum, although the precision of the data is probably not sufficient to justify such an assertion.

It may be argued that the extrapolation of the bulk liquid

phase surface tension to low temperatures is uncertain. Accordingly, the present authors are proceeding to make critical supersaturation measurements at low temperatures on low freezing substances, e.g., ethyl alcohol, the propyl alcohols, etc. Such data, in conjunction with bulk phase surface tension measurements at low temperatures, may permit quantitative evaluation of the change in surface tension of liquid droplets due to decrease in size.

A major assumption in this approach to the problem is that the free energy of the droplet is essentially the same as that of a portion of liquid of the same volume and shape existing in a large amount of the liquid, except for the contribution due to surface tension. This assumption, together with various criticisms of the method, will be discussed in a future publication.

* The research reported in this paper has been made possible through support and sponsorship extended by the Geophysical Research Directorate of the Air Force Cambridge Research Laboratories, A.C., under Contract No. AF 19(122)-185.

[1] R. C. Tolman, J. Chem. Phys. **17**, 333 (1949).
[2] J. G. Kirkwood and F. P. Buff, J. Chem. Phys. **17**, 338 (1949).
[3] V. K. LaMer and G. M. Pound, J. Chem. Phys. **17**, 1337 (1949).
[4] M. Volmer, *Kinetik der Phasenbildung* (Edwards Bros., Ann Arbor, 1945), Chapter 4.
[5] R. Becker and W. Doering, Ann. Physik **24**, 719 (1935).
[6] M. Volmer and H. Flood, Z. physik. Chem. (A) **170**, 273 (1934).
[7] A. Sander and G. Damköhler, Naturwiss. **31**, 460 (1943).
[8] Moser, *Landolt u. Börnstein Tabellen*, IIa, p. 148.

Chemical Effects on Nuclear Induction Signals from Organic Compounds*

J. T. Arnold, S. S. Dharmatti, and M. E. Packard
Department of Physics, Stanford University, Stanford, California
(Received February 5, 1951)

THE influence of the chemical compound upon the nuclear magnetic resonance frequency of a nucleus has been previously reported. Large chemical shifts have been observed[1] for some of the heavier elements, and a line structure has been seen in complex molecules containing the observed nuclei in regions of different magnetic shielding. Small shifts have been measured between several hydrogen compounds,[2] and there has been an indication of a fine structure in some organic liquids.[3]

The development of a nuclear induction apparatus with a resolution better than 1 part in 10^7 has enabled us to measure many such chemical shifts for hydrogen in gases and in organic liquids and to measure a fine structure in the lines of a large number of organic compounds.

The apparatus includes an electromagnet operating at 7600 gauss which has 12-inch diameter pole pieces and a gap of 1.75 inches. The magnetic field is stabilized by voltage, current, and proton controlled regulators. The rf field for both the proton control and the main nuclear induction apparatus is supplied by the same crystal controlled oscillator operating at 32.4 mc. The sharp lines are achieved by a carefully shimmed magnet and a small cylindrical sample which has a diameter of 2 mm and a length of 1 cm. The magnetic field over the region of the sample is changed linearly by a pair of small coils at a sweep rate the order of 0.05 gauss per second. This slow sweep either satisfies the conditions for steady-state behavior of the signal or is slow enough so that all transient effects are over before the next peak is reached. The steady-state or near steady-state behavior of the nuclear induction signal gives line shapes which can be described by a simple solution of Bloch's nuclear induction equations.[4] The nuclear induction signal is amplified by rf and direct-coupled amplifiers, and the amplitude is plotted on an oscillograph screen as a function of the magnetic field. Figure 1 shows the fine structure in ethyl alcohol and is typical of the signals which we observe. The trace is 75 milligauss wide and is traversed in 2 seconds. A measurement of the ratios of the areas of the lines yields the ratios of the number of hydrogen atoms associated with each line. In ethyl alchol the ratios are nearly 1–2–3. In most cases it is necessary to consider the areas under the lines because the line widths are not the same for the different peaks.

Fig. 1. Oscillograph trace of the nuclear induction signal from ethyl alcohol. The total trace is 75 milligauss wide and was traversed in 2 seconds. The peaks from left to right represent OH, CH_2, CH_3.

Table I gives data for the first five primary alcohols. The peaks have been labeled on the basis of their relative areas to correspond with groups in the alcohols. The OH peak, which comes at the lowest applied field, has been taken to have unity area, and all shifts have been measured relative to its position. The listed half-line width values are measured values and include the magnet line width of about one milligauss. The third peak in the alcohols higher than ethyl contains both CH_2 and CH_3 groups which are not resolved because the natural line widths are greater than their separation.

Table I.

Name of normal alcohol	Group characteristics: Groups	Ratio of areas of lines (±10%)	Peak separation in milligauss from OH	Line widths in milligauss (±0.05)	Remarks
Methyl	OH	1		1.6	
	CH_3	2.7	13±2	1.9	
Ethyl	OH	1		2.4	
	CH_2	2.1	16±3	3.2	
	CH_3	3	37%5	2.2	
Propyl	OH	1		2.5	
	CH_2	1.8	18±4	2.5	
	CH_3CH_2	5	38±5	2.9	
Butyl	OH	1		2.5	
	CH_2	1.9	15±3	2.2	
	$CH_3(CH_2)_2$	7.1	36±5	4.2	There seem to be two peaks overlapping
Amyl	OH	1		2.2	
	CH_2	1.7	15±3	2.9	
	$CH_3(CH_2)_3$	9.2	37±5	4.2	Two peaks overlapping as in butyl

The iso- and tertiary-alcohols show a fine structure which is different from that of the primary alcohols but is compatible with the known structural formulas.

The greatest shift which we have observed in a single molecule is in the organic acids and is about 75 milligauss between the COOH and the other groups.

It seems to us that there may be certain chemical problems besides analysis, such as the study of chemical reactions and equilibria, which can be investigated by this method. We are continuing our measurements upon related series of organic liquids and upon the question of the different transverse relaxation times.

* This work was performed with the joint support of the ONR and AEC.
[1] W. G. Proctor and F. C. Yu, Phys. Rev. **77**, 717 (1950); W. C. Dickinson, Phys. Rev. **77**, 736 (1950).
[2] Gunnar Lindstrom, Phys. Rev. **78**, 817 (1950); H. A. Thomas, Phys. Rev. **80**, 901 (1950).
[3] E. L. Hahn, Phys. Rev. **80**, 580 (1950).
[4] F. Bloch, Phys. Rev. **70**, 460 (1946). B. A. Jacobsohn and R. K. Wangsness, Phys. Rev. **73**, 942 (1948).

The Infrared Spectra of HOCl and DOCl

KENNETH HEDBERG AND RICHARD M. BADGER
Gates and Crellin Laboratories of Chemistry, California Institute of Technology, Pasadena, California*
(Received February 16, 1951)

WE have recently observed the spectra of hydrogen hypochlorite and deuterium hypochlorite in the region 1–15μ as part of a general program of study of simple molecules. Since, so far as we are aware, no spectroscopic data has heretofore been reported on these substances, the preliminary results are of sufficient interest to be presented at this time.

The hypochlorites were prepared by mixing H_2O or D_2O vapor with Cl_2O gas in the absorption cell. The latter gas was prepared by the action of Cl_2 on HgO,[1] dried over $Mg(ClO_4)_2$, and fractionally distilled, a middle fraction being used for the experiments.

Low dispersion spectra were obtained with a Beckman IR-2 recording spectrophotometer (NaCl prism), and high dispersion spectra were obtained with a vacuum grating spectrometer.[2] The 42-cm absorption cell was equipped with NaCl windows cemented on with Apiezon W wax. Spectra were taken at several different partial pressures for each reactant; but, because of lack of knowledge concerning the extent of the gas phase reaction, the partial pressures of the resulting hypochlorites are not known.

Low dispersion spectrograms for HOCl and DOCl are shown in Fig. 1, and the bands observed are listed in Table I. The P branch of the band due to the ν_3 vibration (739 cm^{-1}) is in each case overlapped by a Cl_2O band. The first overtone of the O–H stretching mode ($2\nu_1$) of HOCl (Fig. 2) was studied under high dispersion and the coarse rotational structure resolved. This band is a nice example of a hybrid band of a nearly symmetrical top molecule with the top axis the least axis of inertia. Analysis of the band gave the results summarized in Table II. Only enough lines were observed to permit the determination of three values for $A''-\bar{B}''$† and four for $A'-\bar{B}'$, and unfortunately the positions of several of these lines are made uncertain by overlapping lines from the 1.4μ water band, leading to corresponding uncertainties in the rotational constant. If it is assumed that the best value for $A''-\bar{B}''$ is about 19.97 cm^{-1} (obtained by a reasonable extrapolation) and that $\bar{B}''$ is about 0.48 cm^{-1} (which may be calculated by adopting $r_{OH}=0.957$Å as in water,[3] $r_{OCl}=1.70$A as in chlorine monoxide,[4] and $\angle HOCl=90$–$120°$),‡ then $\angle HOCl$ is calculated to be about 113°.

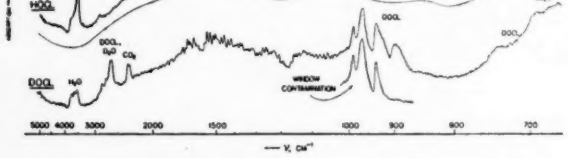

FIG. 2. The 1.42μ band ($2\nu_1$) of HOCl.

TABLE I. Observed and calculated vibrational frequencies for HOCl and DOCl, cm^{-1} (vac).

HOCl obs.	HOCl calc.	DOCl obs.	DOCl calc.	Assignments
739	742	739	733	ν_3 (O–Cl)
1242	1240	911	916	ν_2 (bend)
3626	3627	2674	2675	ν_1 (O–H)
7024	—	—	—	$2\nu_1$

TABLE II. Analysis of the 7023.9-cm^{-1} ($2\nu_1$) band of HOCl.

	⊥ Component				∥ Component	
K	^RQ, cm^{-1}	^PQ, cm^{-1}	$A''-\bar{B}''$	$A'-\bar{B}'$	^QQ, cm^{-1}	$(A'-A'')$ $-(\bar{B}'-\bar{B}'')$
0	7043.2					
1	7078.0	7003.3	19.88	18.68	7022.0	1.90
2	7108.7	6963.7	19.85	18.12	7017.6	1.58
3	7137.4	6919.2	19.73	18.18	7009.7	1.58
4	7161.6	6871.9		18.11		

The fundamental vibrational frequencies shown in Table I were used to calculate values for the potential constants in the potential function

$$2V=k_{OH}\Delta r_{OH}^2+k_{OCl}\Delta r_{OCl}^2+k_\theta r_{OH}r_{OCl}\Delta\theta^2+2g r_{OCl}\cdot\Delta r_{OCl}\Delta\theta.$$

The calculation was carried out using the $F-G$ matrix method of Wilson,[5] assuming the above values for the structural parameters of the molecule. In order to obtain reasonable values for the potential constants, it was found necessary to factor off[6] the highest frequency for each molecule. The factored frequencies gave appreciably different values for the O–H, D stretching force constant, a k_{OH} and a k_{OD} (Table III). The k_{OH} and k_{OD} values were then substituted into the equations for HOCl and DOCl, respectively, which were solved for the remaining potential constants. This technique, which provides in effect a correction for the anharmonicities associated with the OH and OD stretching vibrations, yields the two sets of values for the constants k_{OCl}, k_θ, and g shown in Table III. Each set, together with the appropriate $k_{OH,OD}$ leads to the calculated frequencies shown in Table I.

TABLE III. Potential constants for HOCl and DOCl $\times 10^{-5}$ dynes/cm.

Constant	From HOCl	From DOCl	From both HOCl, DOCl Set 1	Set 2
$k_{OH,OD}$	7.35	7.54		
k_{OCl}			3.86	4.02
k_θ			$0.84_7\cdot r_{OH}^2$	$0.84_8\cdot r_{OH}^2$
g			$0.46_4\cdot r_{OH}$	$0.60_9\cdot r_{OH}$

The frequency product ratio for HOCl and DOCl predicted by the Teller-Redlich product rule differs from the observed by about 1.8 percent:

$$\nu_1^i\nu_2^i\nu_3^i/\nu_1\nu_2\nu_3=(mM^i/m^iM)(I_z^i/I_z)^{\frac{1}{2}}=0.531,$$
$$\nu_1^i\nu_2^i\nu_3^i/\nu_1\nu_2\nu_3=0.541,$$

where the superscript i refers to DOCl. This difference almost certainly arises chiefly from the anharmonicities associated with the OH and OD stretching vibrations. By multiplying the observed frequency ratio by $(k_{OH}/k_{OD})^{\frac{1}{2}}$, a quantity which should provide a good correction for the error introduced by the use of the observed instead of the zeroth order frequencies, one obtains the value 0.534, in much better agreement with the predicted value.

We intend to continue our study of HOCl and DOCl with the hope of obtaining improved experimental data to permit a more complete rotational analysis and the determination of a more complete potential function.

We are grateful to Professor Bryce L. Crawford for helpful discussions.

* Contribution No. 1528.
† $\bar{B}=\frac{1}{3}(B+C)$.
‡ The *Pr* separation is ~30 cm^{-1}, from which the value $\bar{B}=0.53$ is calculated [S. L. Gerhard and D. M. Dennison, Phys. Rev. **43**, 197 (1933)].
[1] C. H. Secoy and G. H. Cady, J. Am. Chem. Soc. **62**, 1036 (1940).
[2] Badger, Zumwalt, and Giguére, Rev. Sci. Instr. **19**, 861 (1948).
[3] See G. Herzberg, *Infrared and Raman Spectra of Polyatomic Molecules* (D. Van Nostrand Company, New York, 1945), p. 489.
[4] J. D. Dunitz and K. Hedberg, J. Am. Chem. Soc. **72**, 3108 (1950).
[5] E. Bright Wilson, Jr., J. Chem. Phys. **7**, 1047 (1939).
[6] B. L. Crawford and S. R. Brinkley, Jr., J. Chem. Phys. **9**, 69 (1941).

The Infrared Spectra of Cl_2O and ClO_2

KENNETH HEDBERG
*Gates and Crellin Laboratories of Chemistry, California Institute of Technology, Pasadena, California**
(Received February 16, 1951)

THE infrared spectra of Cl_2O[1] and of ClO_2[2a] in the 1–18 μ-region has been obtained by Bailey and Cassie. In the course of our study of HOCl and DOCl (preceding note), we have had occasion to re-examine the infrared spectrum of each of these substances in the 1–15 μ-region. The results of our work have revealed points of interest in connection with each compound: For Cl_2O, it seems certain that the band at 1245 cm^{-1} observed by Bailey and Cassie and designated as $\nu_2+\nu_3$ in the most plausible assignment[3] of the vibration of frequencies is actually to be attributed to the ν_2 (bending) vibration of HOCl (Fig. 1). For

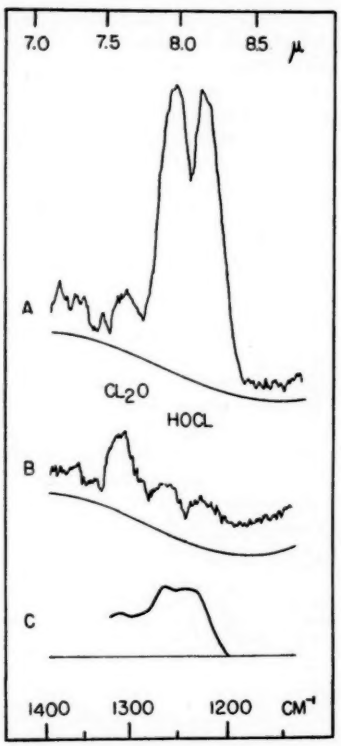

FIG. 1. Spectrum of Cl_2O and H_2O mixture. (A) $P_{Cl_2O}=410$ mm, $P_{H_2O}=15.0$ mm; (B) $P_{Cl_2O}=625$ mm, P_{H_2O} very small; (C) Representation of spectrum as observed by Bailey and Cassie (see reference 1) in this region.

ClO_2 we have observed two new bands which serve to substantiate the correctness of the early assignment.[2b]

The preparation of the Cl_2O and the apparatus used in the experiments is described in the preceding note. The ClO_2 was prepared after the description of Spinks and Taube,[4] and purification procedures similar to those employed with Cl_2O were followed.

In Fig. 1 are shown the spectrum of Cl_2O, Cl_2O+H_2O, and the curve obtained by Bailey and Cassie for Cl_2O. It is clear from the curves that the sample of Cl_2O used in these investigators' experiments was contaminated by HOCl (preceding note), probably present as a result of inadequate drying of their material. We have found that considerable care must be taken in the drying process in order to remove all water; evidence of the presence of HOCl is still seen in curve *B* even though the gas had been passed through a $Mg(ClO_4)_2$ drying tube. Since the spurious band of HOCl provided support for the location of ν_2 at ~320 cm^{-1}, the evidence for the frequency of this fundamental is somewhat weakened.

TABLE I. Vibrational frequencies for ClO_2.

Freq., cm^{-1}	Rel. intensity	Type	Assignment
3333	v.w.	—	$3\nu_3$
2954	w	—	$2\nu_1+\nu_3$
2031	m	—	$\nu_1+\nu_3$
1870	w	—	$2\nu_1$
1108	v.s.	∥	ν_3
945	s	⊥	ν_1

In Table I the bands observed for ClO_2 are shown. The new bands at 3333 cm^{-1} and 2954 cm^{-1} support the early assignment of ν_1 and ν_3. The $P-R$ branch separation in ν_1 is about 26 cm^{-1}, in rough agreement with the value 22 cm^{-1} calculated from the geometry of the molecule as determined by electron diffraction.[5]

We have calculated a number of values for the three potential constants, k, k_θ/r^2, and k_{12} for Cl_2O and ClO_2 from the dimensions and assumption of the general potential function,

$$2V=k_r[(\Delta r_1)^2+(\Delta r_2)^2]+k_\theta\Delta\theta^2+2k_{12}\Delta r_1\Delta r_2+2l(\Delta r_1+\Delta r_2)\Delta\theta,$$

using the fourth constant l/r as a parameter. A part of the results obtained is shown in Table II. The values of the bond stretching

TABLE II. Potential constants for Cl_2O and ClO_2, $\times10^{-5}$ dyne/cm.

Frequencies, cm^{-1} assign.	obs.	l/r (assumed)	k	k_θ/r^2	k_{12}
		Cl_2O			
ν_1	688	+0.0[b]*	3.7	0.8	−1.2
ν_2	(320)[a]	+4.5*	5.7	2.0	+0.8
ν_3	969	+0.1 to +1.0	3.9 to 4.9[b]	0.6[b] to 0.5	−1.0 to +0.1
		ClO_2			
ν_1	945	−1.4*	4.4	1.4	−1.6[b]
ν_2	(447)[b]	+3.5*	6.1	2.0	−0.7[b]
ν_3	1108	−1.0 to +1.0	6.1 to 7.1	0.6[b] to 0.7[b]	−0.9 to +0.1

[a] See reference 3.
[b] See reference 2b.
* Limiting values which give real solutions for the other potential constants.

constants found by assuming that the interaction constants are small ($|k_{12}|$, $|l/r|\leqslant1.00$ as shown in last line of Table II for each molecule) are in accord with the idea that the bonds in ClO_2 are essentially double bonds.[5] We feel that the values for the other constants are not very reliable because of uncertainty in the frequency of the ν_2 vibration; however, this uncertainty does not affect the magnitudes of the bond stretching constants sufficiently to invalidate the conclusion reached as to the bond character.

* Contribution No. 1529.
[1] C. R. Bailey and A. B. D. Cassie, Proc. Roy. Soc. (London) **142A**, 129 (1933).
[2a] C. R. Bailey and A. B. D. Cassie, Proc. Roy. Soc. (London) **137A**, 622 (1932).
[2b] J. B. Coon, Phys. Rev. **58**, 926 (1940).
[3] G. B. B. M. Sutherland and W. G. Penny, Proc. Roy. Soc. (London) **156A**, 678 (1936).
[4] J. W. Spinks and H. Taube, Can. J. Research **B15**, 499 (1937).
[5] J. D. Dunitz and K. Hedberg, J. Am. Chem. Soc. **72**, 3108 (1950).

Thermal Diffusion in Hydrogen-Water Vapor Mixtures

E. WHALLEY
Division of Chemistry, National Research Council, Ottawa, Canada
(Received February 15, 1951)

THERMAL diffusion in hydrogen-water vapor mixtures has been studied by Shibata and Kitagawa.[1] They have calculated the thermal diffusion ratio k_T from the slope of their

TABLE I. R_T for hydrogen-water vapor.

T_1	T_2	T_r°K/c_1	0.1	0.2	0.3	0.4	0.5	0.6	0.7	0.8	0.9
291	474	368	0.41	0.39	0.40	0.39	0.40	0.38	0.35	0.31	0.24
291	573	402	0.43	0.44	0.43	0.42	0.41	0.38	0.35	0.32	0.26
291	673	431	0.41	0.43	0.44	0.43	0.42	0.38	0.34	0.30	0.26
291	772	455	0.43	0.46	0.45	0.44	0.43	0.39	0.35	0.31	0.25
292	872	481	0.43	0.44	0.45	0.46	0.45	0.40	0.35	0.29	0.23
292	973	502	0.46	0.49	0.47	0.47	0.46	0.41	0.35	0.28	0.21
294	994	509	0.42	0.45	0.46	0.47	0.44	0.38	0.31	0.25	0.29
297	1094	532	0.58	0.59	0.56	0.53	0.48	0.43	0.37	0.31	0.24
296	1194	550	0.62	0.63	0.60	0.56	0.49	0.44	0.38	0.31	0.24
296	1294	566	0.73	0.70	0.65	0.59	0.53	0.47	0.41	0.35	0.29
		$(k_T)_{cs}$	0.0370	0.0711	0.1015	0.1272	0.1470	0.1586	0.1585	0.1408	0.0953

$\Delta c - \ln(T_2/T_1)$ curve instead of from the ratio $\Delta c/\ln(T_2/T_1)$. Their values for k_T and for R_T at $T_2 > 700$°C are quite wrong and contrary to the statement in their paper; R_T never exceeds unity. We have therefore recalculated k_T from their results.

For each temperature range k_T was calculated for all their results and plotted against the concentration. A smooth curve was drawn through the points, and the values of k_T corresponding to $c_1 = 0.1$, 0.2, 0.3, etc., to 0.9 were read off. The theoretical values of k_T, assuming that the gases behave as elastic spherical molecules with the diameters obtained from viscosity data $\sigma_1(H_2) = 1.365$,[2] $\sigma_2(H_2O) = 2.29$,[3] were calculated from the equations given by Chapman and Cowling, and gave

$$(k_T)_{cs} = c_1 c_2 \frac{2.27c_1 + 2.63c_2}{1.708c_1^2 + 6.87c_2^2 + 8.094c_1c_2}. \quad (64)$$

For each of the experimental values of k_T obtained above, the corresponding value of R_T was calculated from the equation

$$R_T = k_T/(k_T)_{cs}.$$

In assigning a temperature to the experimental value of R_T, which is measured over a considerable temperature range, the equation of Brown[4] was used.

$$T_r = (T_1T_2/\Delta T)\ln(T_2/T_1)T_1. \quad (65)$$

The value of R_T for various concentrations and values of T_r are given in Table I. The values are rounded to two significant figures, as the consistency of the results does not warrant any greater accuracy.

[1] Z. Shibata and H. Kitagawa, J. Faculty Sci., Hokkaido Imp. Univ. Sec. III, 2, 223 (1938).
[2] S. Chapman and T. G. Cowling, *Mathematical Theory of Non-Uniform Gases* (Cambridge University Press, 1939), p. 229.
[3] J. H. Jeans, *Kinetic Theory of Gases* (Cambridge University Press, 1921), third edition, p. 327.
[4] H. Brown, Phys. Rev. 58, 661 (1940).

Effect of Small Refractive Index Differences between Solution and Solvent on Light Scattering*

P. DEBYE AND W. M. CASHIN
Department of Chemistry, Cornell University, Ithaca, New York
(Received February 9, 1951)

A QUESTION has been raised[1] concerning the validity of the usual equation relating the turbidity of a polymer solution to the molecular weight of the polymer. As used—for small particles at infinite dilution—the equation states:

$$\tau = HcM,$$

where

$$H = (32\pi^3\mu_0^2/3N\lambda^4)(\mu - \mu_0/c)^2,$$

τ = excess turbidity, c = concentration in g/cc, M = molecular weight, N = Avogadro's number, λ = wavelength in cm, μ_0 = refractive index of solvent, and μ = refractive index of solution.

The reference cited above suggests that the equation is not valid when $(\mu - \mu_0/c)$, the refractive index increment, is too small. In the initial development of the equation the assumption had been made that $\mu - \mu_0$ is not too large. In principle, the difference may be as small as one chooses. Experimentally, it may be hard to work with such solutions where the turbidity increment of solution over solvent is very small.

In Table I are listed experimental results obtained on an unfractionated Dow polystyrene sample by 90° scattering with the blue Hg line ($\lambda = 4358$A). Dissymmetries (45° against 135° angle) were measured only on benzene and 2-butanone solutions and found to be near 1.2. The correction factor for the other solutions was assumed to be the same.

TABLE I. Experimental results.

Solvent	μ_0	$(\mu - \mu_0/c)^2$	M
2-butanone	1.383	5.72×10^{-2}	300000
Carbon tetrachloride	1.478	2.83×10^{-2}	320000
Benzene	1.522	1.40×10^{-2}	295000
Chlorobenzene	1.543	0.98×10^{-2}	310000

Results on bromobenzene solutions, $(\mu - \mu_0/c)^2 = 0.44 \times 10^{-2}$, are not recorded, since the molecular weight obtained is reliable only to within 30 percent. Within that error limit, however, it is the same as the values in the table.

It appears then that the only effect of low $\mu - \mu_0$ values is to decrease the reliability of the turbidity measurements with a consequently larger error limit on the molecular weight determination.

In conclusion we may point out that the equation as used is for polymer-single solvent systems only, and as such, is not applicable to the system cellulose acetate tetrachloroethane-ethylene chloride which the aforementioned authors studied.[2] Anomalous results in the GRS-toluene system could perhaps be attributed to the presence of microgel, without which GRS solutions do not often occur.

Accepting the fact that there is no flaw in the theory, it might be possible to make good use of the observed deviations in order to characterize the microgel.

* The work reported herein was done in connection with the Government Research Program on Synthetic Rubber under contract with the Office of Rubber Reserve, Reconstruction Finance Corporation.
[1] R. Rivest and M. Rinfret, J. Chem. Phys. 18, 1513 (1950).
[2] Ewart, Roe, Debye, and McCartney, J. Chem. Phys. 14, 686 (1946).

Numerical Integration as a Labor-Saving Device in the Compilation of Thermodynamic Properties of Polyatomic Molecules

ROBERT E. PENNINGTON AND KENNETH A. KOBE
Department of Chemical Engineering, University of Texas, Austin, Texas
(Received February 13, 1951)

THE summing of the Einstein function contributions of the numerous frequencies of polyatomic molecules to the various thermodynamic properties is a tedious task. Some of the labor involved may be avoided in the following manner.

(1) The total heat capacity (translational, vibrational, internal, and external rotational) is calculated as usual, say at 100° increments.

(2) The enthalpy and entropy are calculated at the ice-point, 300°K, and 1500°K (or at any desired limit).

(3) The enthalpy and entropy at 100° increments above 300°K may then be calculated by numerically integrating the functions C_p^0 and C_p^0/T, respectively. The calculated values at the upper limit serve as a very close check.

This integration is easily carried out using lagrangian integration polynomials. The five-point polynomial seems the most applicable in this case, and it may be used to represent an integral:

$$\int_{T_0+mh}^{T_0+(m+1)h} f(T)dT = h\sum_{k=0}^{k=4} F_k(m)f(T_k),$$

where $m=0, 1, 2, 3$, and T_0 is the first of five consecutive temperatures, h is the increment, and values of $F_k(m)$ are given in Table I.[1]

TABLE I. Five-point lagrangian integration coefficients.

k	$m=0$	$m=1$	$m=2$	$m=3$
0	0.34861 11111	−0.02638 88889	0.01527 77778	−0.02638 88889
1	0.89722 22222	0.48055 55556	−0.10277 77778	0.14722 22222
2	−0.36666 66666	0.63333 33333	0.63333 33333	−0.36666 66666
3	0.14722 22222	−0.10277 77778	0.48055 55556	0.89722 22222
4	−0.02638 88889	0.01527 77778	−0.02638 88889	0.34861 11111

This calculation may be carried out quite rapidly on an ordinary calculator, and an error in calculation is almost always quite obvious. This method has been applied to several molecules, and in each case discrepancies between calculated and integrated results were traced to the calculated results, where smaller errors are not always so obvious. The time required for the calculation of thermodynamic functions of a molecule can be cut in half by the use of numerical integration as suggested here.

Tables of lagrangian interpolation coefficients are available,[1,2] and values at temperatures other than the even hundreds of degrees may be easily obtained (without making difference tables) by using these.

It is regrettable that so many of the scientists who calculate thermodynamic functions start at 298.16°K (25°C) rather than at 273.16°K, the ice-point, which serves as a basic reference point for relative enthalpy. The values at 25°C can be calculated readily, using an interpolation formula.[2]

[1] *Tables of Lagrangian Interpolation Coefficients*, Mathematical Tables Project of W. P. A. (Columbia University Press, New York, 1944), p. 390.
[2] Kobe and Pennington, Petroleum Refiner **30** (1951).

On the Polarization of Rayleigh Scattering as an Aid to Determine Molecular Configuration in Liquids*

D. H. RANK
Physics Department, Pennsylvania State College, State College, Pennsylvania
(Received February 19, 1951)

IT is well known that from the analysis of the vibration spectra (Raman and infrared absorption) much information can be obtained concerning the arrangement of the atoms in the molecule. In most cases, when these vibrational analyses are coupled with calculations of the entropy, satisfactory and unique solutions of the structure problem can be obtained. It is generally accepted that the determination of the state of polarization of the Raman lines is necessary for any rigorous vibrational analysis.

The purpose of this note is to point out the utility of a much older phenomenon, namely, the polarization of the Rayleigh scattering as an aid to solving the molecular structure problem.

It is well known that certain molecules in the liquid phase form associated complexes. In many cases this association is caused by hydrogen bonding. The phenomenon of association is accompanied, in general, by the observation of a boiling point very much higher than would normally be expected for liquids of the molecular weight in question.

Bhagavantam[1] has assembled a great deal of the data in the literature on the Rayleigh scattering of liquids. Inspection of Bhagavantam's table brings to light the following empirical regularities which qualitatively would be expected theoretically.

(1) Nonassociated liquids in which the molecular form approaches spherical symmetry show a high degree of polarization of Rayleigh scattering.

(2) Liquids which definitely are associated (the associated complex must certainly approach spherical symmetry) show a high degree of polarization of Rayleigh scattering.

(3) Nonassociated liquids, the molecular form of which is linear or approximately planar, produce highly depolarized Rayleigh scattering.

It should be noted further that, in general, the interaction of the light wave with the scattering entity to a large extent ignores the very light hydrogen atoms, e.g., liquid CCl_4 yields a $\rho=0.06$, while the chloroform molecule $CHCl_3$, which is also of tetrahedral structure, gives a $\rho=0.24$.

Recently, in this laboratory, the vibrational spectra of methyl hydrazine has been under investigation by Axford, Russell, and Janz. Considering only the heavy atoms, this molecule can be considered to be approximately linear. From various properties of liquid methyl hydrazine it might be supposed that association in the liquid state is present. The author suggested, from the above reasoning, that the Rayleigh scattering would be strongly polarized if association, which is presumably due to hydrogen bonding, was present. The experimental results obtained by Axford, Russell, and Janz, which will be published elsewhere, completely confirm the above contention.

In the case of liquids where association is unlikely, the state of polarization of Rayleigh scattering can be useful in deciding between different geometrical forms when the usual methods do not give a unique answer. This phenomenon might be particularly useful in the case of some of the boranes which exist as liquids, since the approximately planar, pyramidal, or "basket" structures should yield very different values for the polarization of the Rayleigh scattering.

* This research was carried out under Contract N6onr-269, Task V of the ONR.
[1] S. Bhagavantam, *Scattering of Light and the Raman Effect* (Chemical Publishing Company, New York, 1942), p. 84.

The Use of Punched Cards in Molecular Structure Determinations. IV. Approximations to the Temperature Factor

MORTON E. JONES AND VERNER SCHOMAKER
Gates and Crellin Laboratories of Chemistry, California Institute of Technology, Pasadena, California*
(Received February 22, 1951)

THE punched-card method[1] which we use for the functions $\Sigma_i G_i \sin y_i x$ that have to be evaluated in the course of diffraction studies of the molecular structures of randomly oriented molecules requires that the coefficients G_i be constants, independent of x. However, in the expression for the intensity of diffraction, in our case,[2]

$$I(s)=\Sigma'_{i,j} Z_i Z_j r_{ij}^{-1} \exp(-a_{ij}s^2) \sin r_{ij}s, \qquad (1)$$

these coefficients often include the so-called temperature factor $\exp(-a_{ij}s^2)$, which takes into account the vibrational variation or an effective vibrational variation of the interatomic distance about its mean value r_{ij}. The quantity a_{ij} is $\frac{1}{2}\langle(\delta r_{ij}^2)_{Av}$ or, in order to make negligible the variation of some of the coefficients, an effective value $(\frac{1}{2}\langle(\delta r_{ij}^2)_{Av}-a_o)$.

Previously, this variation has ordinarily been approximated by constructing the corresponding distribution of the form $\exp\{-(r-r_{ij})^2(4a_{ij})^{-1}\}$ and approximating the required integration over the distribution by a sum of equally spaced $\sin rs$ terms having constant coefficients taken from this curve with suitable normalization. But in the absence of any readily applicable analysis of the situation, the desire for accuracy has usually led to the use of more terms than are actually necessary. Therefore, it was decided to work out to known accuracy several economized representations of this type for general application.

In order to simplify the work, the equal spacing of terms was retained. Then, in terms of appropriate reduced units, the amplitudes and spacings of terms were adjusted so that the approximation differs from the desired value by no more than a fixed maximum amount for $s \leqslant s_{\max}$, with $s_{\max}$ as large as possible. This has been done for 2, 3, 4, and 5 term representations and for maximum errors of $\pm 2\frac{1}{2}$, ± 5, and ± 10 percent of the ideal initial amplitude, and the results have been arranged in a table. For each of the twelve cases, this table gives directly the a values that can be achieved with spacings of integral hundredths of an A (somewhat unhappily, continuous variation of a is not afforded), the amplitudes of the terms of the representation, and the maximum values of a for which it is accurate, respectively, to $s=20$ and $s=30$; a simple interpolation gives the maximum a values for other values of $s_{\max}$.

Use of the table has simplified the punched-card summation of Eq. (1) by reducing by 50 percent, on the average, the number of terms used to represent temperature factors. It has also reduced to almost nothing the considerable preparatory work which was previously involved in setting up the calculations.

Copies of the table and notes on its use have been prepared and are available upon request.

* Contribution No. 1536.
[1] Shaffer, Schomaker, and Pauling, J. Chem. Phys. **14**, 659 (1946).
[2] R. Spurr and V. Schomaker, J. Am. Chem. Soc. **64**, 2693 (1942).

The Vibration-Rotation Bands of OH in the Photographic Infrared*

GEORGE A. HORNBECK AND ROBERT C. HERMAN
Applied Physics Laboratory, The Johns Hopkins University, Silver Spring, Maryland
(Received January 31, 1951)

RECENTLY, Meinel[1] has obtained in emission some of the vibration-rotation bands of the OH radical in the spectrum of the night sky. These bands lie in the region ~6800—~9000A and include the vibrational transitions (7—2), (8—3), (4—0), (9—4), (5—1), (6—2), and (7—3). Benedict, Plyler, and Humphreys[2] have found in emission from the outer cones of the oxy-acetylene and oxy-hydrogen flames numerous lines of the OH vibration-rotation bands (2—0), (3—1), and (4—2). We have recently also obtained the (4—0), (5—1), and (6—2) bands from the outer cone of the oxy-acetylene flame with a Baird 2-meter grating spectrograph at 8 A/mm using a 25μ slit and I-N plates hypersensitized according to the procedure described by Meinel.[1] Spectrograms of good contrast and density were obtained with exposure times of ~1½ hours under the conditions stated. In Fig. 1 is shown a densitometer tracing of a portion of the (4—0) and (5—1) bands. In the P-branch the spin doublets are well resolved as are the Λ-doublets for high K-values. The weaker background lines in Fig. 1 are the vibration-rotation lines of the H_2O molecule. At longer wavelengths, the H_2O lines become more intense. However, the P-branch lines in the (4—0) band, for example, are readily seen at least as far as $P(15)$. The OH bands in this spectral region can also be obtained from the outer cones of methane, ethylene, and hydrogen burning with oxygen. However, in these cases the OH lines are badly overlapped by the intense H_2O spectrum. Best results have been achieved with the oxy-acetylene flame obtained from an ordinary torch burning at stoichiometric proportions, when viewing the region of the outer cone closest to the tip of the reaction zone.

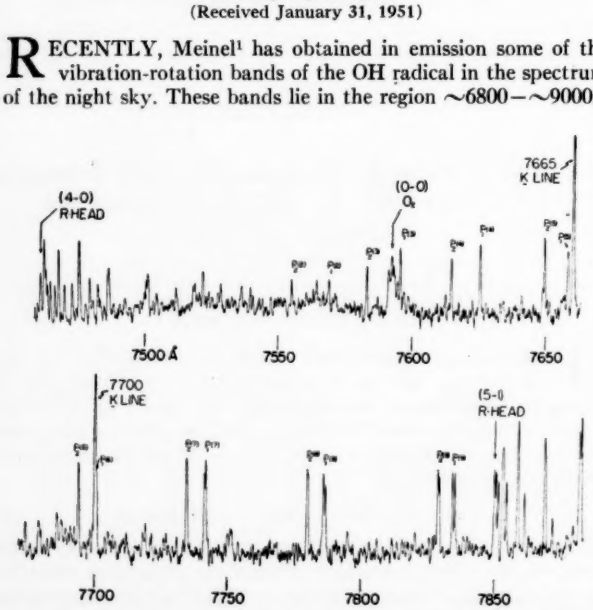

FIG. 1. Densitometer tracing of a portion of the (4—0) vibration-rotation band of OH. The R-branch heads of the (4—0) and (5—1) bands, the P lines of the (4—0) band, as well as the potassium resonance lines and the (0—0) band of the $^1\Sigma - {}^3\Sigma$ system of O_2, are indicated.

As yet, we have found no evidence in flame spectra of the vibration-rotation bands of OH reported by Meinel which originate from the higher vibration levels. Since the outer cone temperature of the oxy-acetylene flame is ~3000°K, this would lend support to Meinel's suggestion of resonance excitation of OH radicals in the night sky. As to be expected at the higher temperatures in the oxy-acetylene flame, the OH lines extend to higher K-values and the Q-branch is relatively weak as compared with Meinel's case.

Since the OH vibration-rotation bands discussed here can be obtained with high dispersion and resolution, an analysis of the bands and a determination of some of the molecular constants is in progress. We hope to report a complete account of this work in the near future.

* This work was supported by the U. S. Navy Bureau of Ordnance under Contract NOrd-7386.
[1] A. B. Meinel, Astrophys. J. **111**, 555 (1950); **112**, 120 (1950).
[2] Benedict, Plyler, and Humphreys, Bull. Am. Phys. Soc. **26**, No. 1, p. 50 (1951).

Comment on "Gas Bubbles in Solutions"

FRANK C. ROESLER
Physikalisches Institut, Technische Hochschule Graz, Graz, Austria
(Received February 20, 1951)

IN a recent issue of this Journal, Epstein and Plesset[1] have derived formulas for growth and dissolving of gas bubbles in a liquid phase. Their treatment refers to a bubble at rest and is valid if transport of the dissolved gas takes place by diffusion only.

It seems interesting to consider the opposite limiting case, in which the mechanical motions in the system more than match the diffusion; for many applications (e.g., cavitation bubbles in a strongly turbulent medium or large bubbles of great buoyancy), this case is realized.

As Epstein and Plesset, I shall treat the growth of a single bubble in an infinite volume of fluid. Let us first investigate the influence of a strong translatory motion due to buoyancy. I shall use the notation of Epstein and Plesset except for letters, the meaning of which is specially explained. For laminar flow the velocity of the bubble is proportional to the square of the radius (reference 1, l.c.)

$$v \sim R^2. \tag{1}$$

Diffusion now comes into play for transport of the gas through the boundary layer only. Outside the boundary layer adhering to the bubble the motion of the fluid outweighs it, and we take c

there to equal c_i. From a general formula for the thickness s of a laminar boundary layer,[2]

$$s\sim(\mu' l/\rho' v)^{\frac{1}{2}}; \tag{2}$$

where l is a characteristic length, which in our case we may take to be the bubble radius, we obtain

$$s\sim R^{\frac{1}{2}}. \tag{3}$$

The transport through the boundary layer per unit area and time will be given by

$$\Delta m=\kappa(c_i-c_s)/s\sim\kappa\delta R^{\frac{1}{2}}. \tag{4}$$

It follows that Eq. (8) of Epstein and Plesset will have to be replaced by

$$dm/dt\sim 4\pi R^2\kappa\delta R^{\frac{1}{2}} \tag{5}$$

or

$$dm/dt\sim 4\pi\kappa\delta R^{5/2} \tag{6}$$

and their Eq. (10) by

$$dR/dt\sim(\kappa\delta/\rho)R^{\frac{1}{2}}. \tag{7}$$

The solution is of the form

$$R=(\beta_1 t+R_0^{\frac{1}{2}})^2, \tag{8}$$

where β_1 is a constant, while in the case considered by Epstein and Plesset, one has in the first approximation

$$R=(\beta_2 t+R_0^2)^{\frac{1}{2}}. \tag{9}$$

β_2 is another constant. Of course, apart from the different power of t entering into Eqs. (8) and (9), the constant β_1 in Eq. (8) will be different from β_2 in Eq. (9).

Another case of interest is that of a strongly turbulent medium. Transport of the dissolved gas will then be effected by turbulent exchange rather than by diffusion. This, however, is only valid for dimensions large compared with any stable or growing bubble; the bubbles will be destroyed, torn apart, as soon as they reach the size of the smallest elements of turbulence. Thus, for large dimensions we can put

$$\partial c/\partial t=A\Delta c, \tag{10}$$

where A is the turbulent exchange; and for the regions immediately surrounding the bubble

$$\partial c/\partial t=\kappa\Delta c \tag{11}$$

(see reference 1, Eq. (1)). Now A is very much larger than κ, so that in the first approximation the solution of Eq. (10) will read

$$c=c_i=\text{constant} \tag{12}$$

for "large" dimensions. This suggests taking account of the situation by adopting suitable boundary conditions. Instead of the second condition in (2a) of Epstein and Plesset, we put

$$c(L,t)=c_i \tag{13}$$

for any t. L is a length equal to the mean diameter of the smallest elements of turbulence. Diffusion is responsible for the transport between $r=R$ and $r=L$. The problem may now be solved along the lines suggested by Epstein and Plesset. Of course, the approximation is rather crude. The result for $R(t)$ will, in general, again contain a higher power of t than that of Epstein and Plesset. The two solutions will, however, coincide in the limit $L\to\infty$, and one can expect their difference to be small if $L\gg R$.

In all these considerations, surface tension is neglected, as it is in the first approximation obtained by Epstein and Plesset.

[1] P. S. Epstein and M. S. Plesset, J. Chem. Phys. **18**, 1505 (1950).
[2] L. Prandtl, *Strömungslehre* (Braunschweig, 1944), p. 99.

The Infrared Spectra of Mesitylene Complexes

GEORGE C. PIMENTEL, GEORGE JURA, AND LEONARD GROTZ
Department of Chemistry and Chemical Engineering, University of California, Berkeley, California
(Received February 1, 1951)

THE interest in the Lewis acid-base reaction involving aromatic hydrocarbons with metallic ions or halogens is such that a preliminary report of our studies of the infrared absorption spectra of some of these molecules is warranted. In this letter, we wish to report our results of the investigation of the spectra of the complexes of mesitylene with iodine and magnesium laurate. The former of these two compounds was reported by Hildebrand and Benesi,[1] and the latter is to be found in earlier work of Jura and Grotz, and is now in preparation for publication. The complex with magnesium is probably similar in nature to that of silver, which has been extensively studied by Keefer and Andrews.[2]

The spectra were determined with a Model 12C Perkin-Elmer spectrograph. The cell length was 0.2 mm. The spectra of liquid mesitylene, mesitylene saturated with iodine, and a 0.02M solution of magnesium laurate in mesitylene were determined from 500 cm^{-1} to 1500 cm^{-1}.

The most striking result of this work is that mesitylene bands normally infrared inactive in the gas phase were found in the spectra of the solutions of the complexed molecules; and bands which are Raman active appear to be more intense in the infrared spectra of the complexed molecule than in that of liquid mesitylene. Further, the infrared measurements indicate a striking similarity between the two complexes. Table I summarizes the results which have been obtained on these two compounds. For purposes of comparison, we present the Raman spectrum of liquid mesitylene, and the infrared spectra of this liquid and of the two complexes. The bands which have been intensified are marked with an asterisk. The Raman data are the compilation of the results of Pitzer and Scott[3] and of Herz and Kohlrausch.[4]

TABLE I. The spectra of the iodine and magnesium laurate complexes with mesitylene.

Mesitylene			
Infrared (cm^{-1})	Raman (cm^{-1})	I_2 complex (cm^{-1})	$Mg(C_{12}H_{23}CO_2)_2$ complex (cm^{-1})
1376 (10)	1378 (7)	1375 (10)	1376 (10)
1362 ($\frac{1}{2}$)	1373 (3)	1362 ($\frac{1}{2}$)	1362 (1)*
1341 ($\frac{1}{2}$)		1341 (1)*	1341 (1)*
1319 (1)		1319 (2)*	1319 (1)
1298 ($\frac{1}{2}$)	1300 (7)	1298 (3)*	1298 (1)*
1266 (1)	1255	1266 (2)*	1266 (1)
		1214 ($\frac{1}{2}$)*	1217 (3)*
1191 (1)	1200	1191 (2)*	1191 (1)
1166 (3)	1160 (3)	1166 (3)	1166 (3)
		1143 (1)*	1143 (1)*
1094 ($\frac{1}{2}$)		1094 (1)*	1110 (1)*
1037 (10)	1036 (3)	1037 (10)	
1017 ($\frac{1}{2}$)		1017 ($\frac{1}{2}$)	
1000 ($\frac{1}{2}$)	998 (10)	1000 ($\frac{1}{2}$)	
929 (4)	930 ($\frac{1}{2}$)	929 (4)	
	879 ($\frac{1}{2}$)	888 (1)*	
882 (4)		882 (4)	
840 (10)	847, 836 ($\frac{1}{2}$)	840 (10)	840 (10)
806 ($\frac{1}{2}$)		806 ($\frac{1}{2}$)	806 ($\frac{1}{2}$)
786 ($\frac{1}{2}$)		795 ($\frac{1}{2}$)	
769 (1)		768 (1)	768 (1)
		759 (3)*	
			719 (2)
			704 (1)
686 (10)		686 (10)	686 (10)
648 (3)		648 (3)	648 (?)
577 (3)	575 (10)	577 (3)	577 (?)
516 (8)	515 (8)	516 (8)	516 (8)

In the laurate spectrum, comparison was made with the spectra of lauric acid, stearic acid, and sodium stearate. The changes in the mesitylene spectrum could not be attributed to either the acid or salt. These spectra were obtained from Dr. K. Freeman of the Division of Medical Physics.

It is evident that there is a breakdown of the selection rules. This is most readily seen from the bands at 1217 and 1214. Pitzer and Scott[3] predict a band at 1220, but in gaseous mesitylene it is forbidden in both the Raman and infrared. It is probable that the bands in the complexes at 1217 and 1214 are this forbidden transition. The most probable explanation for the breakdown of the selection rules is a reduction in the symmetry of the molecule. If the assignment of Pitzer and Scott is correct, the symmetry must be lower than C_{3v}. The decreased symmetry is explicable only if the complexing molecule is not located on the three-fold axis of rotation, i.e., the center of the molecule. This result is in

accord with the crystallographic determination of the structure of the silver-mesitylene complex studied by Rundle and Goring.[5]

We have obtained similar results when hexamethyl benzene is substituted for the mesitylene.

[1] H. A. Benesi and J. H. Hildebrand, J. Am. Chem. Soc. **71**, 2703 (1949).
[2] L. J. Andrews and R. M. Keefer, J. Am. Chem. Soc. **72**, 3113 (1950).
[3] K. S. Pitzer and D. W. Scott, J. Am. Chem. Soc. **65**, 803 (1943).
[4] E. Herz and K. W. F. Kohlrausch, Monatsch. **74**, 175 (1942).
[5] R. E. Rundle and J. H. Goring, J. Am. Chem. Soc. **72**, 5337 (1950).

Influence of Irradiation on the Low Frequency Electrodeless Discharge in Chlorine

W. L. HARRIES AND A. VON ENGEL
The Clarendon Laboratory, Oxford, England
(Received February 7, 1951)

WHEN a low frequency electrodeless discharge is established in an ozonizer filled with a halogen at 1–600 mm Hg, it has been found by Joshi and others[1–3] that the rms value of the discharge current decreases on irradiating the gas with an incandescent lamp. So far, no satisfactory explanation of the mechanism has been developed.

The current and applied voltage in such a discharge in flat-ended hard glass vessels of 6 cm diameter and 1–3 cm length (p of order 10 mm Hg) were investigated with a double-beam cathode-ray oscillograph. The current was found to consist of between one and fifty distinct pulses per half-cycle, the number increasing with the voltage. We were able to show that each pulse requires a large number of electron avalanches, which develop between opposite small areas of the inner glass surfaces. One such area may discharge within a half-cycle in several pulses.

On irradiation with a 40-watt bulb at 1/2 m distance, a reduction in pulse heights occurred. At higher voltages this reduction became less, except for the first pulse of a group in each half-cycle. We confirmed[1–3] that light of $\lambda \leqslant 4800$A caused the reduction, corresponding to the dissociation energy of Cl_2, and we base our explanation for the reduction in pulse heights on the presence of Cl atoms attaching electrons, and thus reducing effectively the secondary emission from the glass.

However, the pulses did not change on irradiating only the center of the discharge. On irradiating one wall only the pulses were reduced every other half-cycle, namely those pulses whose electron avalanches started from that wall. Calculations showed that any Cl atoms formed near the center of the vessel would not recombine before reaching the walls. Hence, the gas at the walls is the controlling factor.[4]

There is little doubt that gas molecules and atoms form adsorbed layers on glass walls. The atoms will adhere by Langmuir adsorption,[5] sharing an electron with an alkali atom in the glass. The molecules are held mainly by van der waals forces; so there will be a sparsely distributed population of atoms on the glass, with molecules on adjacent sites, and on top of the whole, several layers of molecules.[6] This phase is akin to a liquid, and when irradiated it produces a high concentration of atoms.

The secondary electrons from the wall that start the later avalanches of a pulse can become attached to these Cl atoms. The probability of attachment to Cl_2 is negligible.[6] In the wall layer, the conditions for attachment are favorable because the velocity of the electrons is low, and attachment is only likely in a "many-body" collision. Then the affinity energy (3.5 ev) can either dissociate the molecule forming the third-body, or be converted into kinetic energy. Without a "third-body," the excess energy can only be emitted as a quantum, which is rare. The loss of secondary electrons reduces the effective multiplication and hence the pulse height. At higher temperatures[1,7] adsorbed wall layers would be destroyed, accounting for the results of other workers.

It was found that the pulse heights were reduced by the preceding pulse, provided the pulses occurred within 10^{-4} sec of each other. This reduction is suggested to be due to metastable atoms (8 ev above ground level) and resonance radiation handed on from atom to atom, dissociating molecules in the wall layers. At higher voltages, where the pulses occurred closer together, this effect predominated, which explains the small reduction in pulse heights with irradiation. A full discussion of these investigations will appear elsewhere.

[1] S. S. Joshi and G. S. Deshmukh, Nature **147**, 806 (1941).
[2] S. S. Joshi and P. G. Deo, Nature **151**, 561 (1943).
[3] P. G. Deo, Proc. Indian Acad. Sci. **A19**, 117 (1944).
[4] R. Parshad and S. J. Karim, J. Chem. Phys. **17**, 667 (1949).
[5] A. R. Miller, "The Adsorption of Gases on Solids," C.U.P. (1949).
[6] L. B. Loeb, *Fundamental Processes of Electrical Discharge in Gases* (John Wiley and Sons, Inc., New York, 1939).
[7] K. S. Visvanathan and K. Kuppuswamy, Indian J. Phys. **24**, 13 (1950).

Lewis Acids and Bases and Molecular Complexes*

R. S. MULLIKEN
Physics Department, University of Chicago, Chicago, Illinois
(Received February 2, 1951)

GENERALIZATION of previous ideas[1] gives a simple quantum-mechanical theory of molecular complexes. Let A be a Lewis acid (electron acceptor) and B a base (electron donor). Typically, A may be a neutral molecule or a positive atom-ion, B a neutral molecule or negative atom-ion. For example, A may be I_2 or Ag^+, B may be benzene or I^-.

Most often, A and B have even-electron diamagnetic structures.[2] Then A and B, and therefore the complex $A \cdot B$, have totally symmetrical singlet wave functions. These can be written[3] as

$$\psi = a\psi_0 + b\psi_1 + \cdots. \quad (1)$$

Here ψ_0 is usually a *no-bond* function $\psi(A, B)$, and ψ_1 a *dative* function $\psi(A^- - B^+)$ with covalent bond between A^- and B^+ (weak in loose complexes, strong in molecules such as $R_3N \cdot BX_3$). Equation (1) also fits simple molecules like HCl or NaCl, taking A as H^+ or Na^+ and B as Cl^-; but now ψ_0 involves ionic bonding and ψ_1 only covalent bonding (A^- and B^+ are atoms).[2]

Complementary to ψ of Eq. (1), the complex (in addition to states with A or B alone excited) has a characteristic excited electronic state

$$\psi_E = a'\psi_1 - b'\psi_0 + \cdots. \quad (2)$$

An *intense* absorption band $\psi_N \rightarrow \psi_E$ is predicted, even for a loose complex. Essentially, this probably often accounts for the colors observed when molecular complexes are formed. These $N \rightarrow E$ spectra may be called (in general, *intermolecular*) *charge-transfer spectra*. They constitute a generalization of the familiar intense *interatomic* charge-transfer ($N \rightarrow V$) spectra of molecules.

Equation (1) involves resonance energy of approximate amount

$$RE \approx W_{01}^2/(W_1 - W_0). \quad (3)$$

Here W_0, W_1 are the energies of pure ψ_0, ψ_1; W_{01} is a matrix element. Study of Eq. (3) shows that low ionization energy of B or high electron affinity of A favor large RE. So do small action radii at contact. Besides further factors similarly governing base or Lewis-acid strength and attributable to A and B separately, Eq. (3) reveals factors depending on the specific interaction of a particular A and B.

The "*charge-transfer forces*" corresponding to Eq. (3), although more specific and valence-like, to some extent resemble London's dispersion forces (for example, often a loose complex $A \cdot B$ should attract an additional A or B molecule almost additively), and apparently must share with the latter in accounting for van der waals attractions. Charge-transfer forces, however, should have strong orientational properties, of possible importance in determining how molecules pack in crystals or liquids. This is because resonance requires that ψ_1 and ψ_0 have the same group-theoretical symmetry. Thus, in $Ag^+ \cdot$benzene, $\psi_1(Ag - Bz^+)$ violates this requirement if the silver atom is either on the benzene six-fold axis or in the ring plane.[4] An intermediate location is thus indicated. This prediction is supported by experimental evidence.

The theory predicts plausible paths for reactions proceeding through initial molecular complex formation. It gives insight also into possible stages through which a very weak Lewis acid like HCl may be transformed into a functioning proton acid by a basic ionizing solvent such as water or ammonia.

A detailed paper is nearly completed.

* This work was assisted by the ONR under Task Order IX of Contract N6ori-20 with the University of Chicago.

[1] Especially of Weiss, Brackmann; also Pauling, Dewar. See Mulliken, J. Am. Chem. Soc. **72**, 600 (1950). The present work was outlined at the September, 1950 American Chemical Society meeting.

[2] With appropriate changes in ψ_0 and ψ_1, Eq. (1) applies also when A and/or B are odd-electron systems (examples, I as A, I_2 as B; Cl as A, H as B).

[3] Equation (1) can be improved by additional terms. If A and B (or A^- and B^+) are identical, or are nearly alike in acid and base properties, these terms are *indispensable*.

[4] This is because the Bz^+ wave function has nodal planes through both locations, while the Ag function has none.

The Space Group of the σ-FeCr Crystal Structure*

B. Gunnar Bergman and David P. Shoemaker
Gates and Crellin Laboratories of Chemistry, California Institute of Technology, Pasadena, California†
(Received February 14, 1951)

THE general arrangement of atoms (without regard to kind) in a sigma-phase was first described in a recent communication by the present authors[1] on σ-FeCr (46.5 at. percent Cr). The tetragonal cell ($a_0=8.799$A, $c_0=4.546$A) contains thirty atoms which, in terms of space group $D_{4h}^{14}-P4/mnm$, have the following approximate positions:[2] atoms A in $2(a)$; B in $4(f)$, $x=2/5$; C in $8(i)$, $x=7/15$, $y=2/15$; D in $8(i)$, $x=11/15$, $y=1/15$; E in $8(j)$, $x=11/60$, $z=1/4$. It was not possible at that time to rule out small distortions leading to either of the two other space groups compatible with the observed D_{4h} Laue symmetry and the $(0kl)$ n-glide extinctions, namely, C_{4v}^4-P4nm and D_{2d}^8-P4n2.

We have recently obtained for σ-FeCr, by Weissenberg photography, quantitative intensity data for nearly all planes reflecting within the copper limit, including planes with l as high as five. With molybdenum radiation we have also obtained $(2kl)$ data with l as high as twelve. Throughout these data we found that for given h and k the intensities, corrected for normal decline, are, within experimental error, the same for all planes with l odd, the same for all with $l=4n$, and the same for all with $l=4n+2$. The accidental extinctions show no exceptions to this regularity. This requires that all atoms be confined to parallel planes normal to **c** and $c_0/4$ apart. The holohedral σ-FeCr structure described above conforms to this requirement. This structure can be distorted to give one or the other of the two hemihedral space groups, without introducing z displacements, only by staggering the vertical rows of atoms E, which in the holohedral structure are straight. That a structure with such staggering could retain the required perfect layering seems highly improbable from packing considerations.

Essentially the same structure as ours, but with space group C_{4v}^4, has been reported independently for β-uranium by Tucker,[3] who claimed to have ruled out D_{4h}^{14}. Recently Dickins, Douglas, and Taylor[4] have reported that σ-CoCr has essentially the β-uranium structure reported by Tucker. We have concluded from inspection of Tucker's β-uranium data that, if allowance is made for the effects of absorption of copper radiation in uranium, the presence of the above regularity in the true β-uranium intensities cannot be ruled out. It appears to us very likely that σ-CoCr and the other sigma-alloys have the same holohedral structure that we have found for σ-FeCr, and that β-uranium also has this holohedral structure rather than the hemihedral structure reported by Tucker.

We are grateful to C. W. Tucker, Jr., of the Knolls Atomic Power Laboratory, Schenectady, and to G. J. Dickins, A. M. B. Douglas, and W. H. Taylor of the Cavendish Laboratory, Cambridge, for making their results available to us prior to publication. We thank Professor Linus Pauling for helpful discussions, and Mrs. Nan Arp for computational assistance.

* Work done in part under a contract with the ONR and in part under a program sponsored by the Carbide and Carbon Chemicals Corporation.
† Contribution No. 1532.

[1] D. P. Shoemaker and B. G. Bergman, J. Am. Chem. Soc. **72**, 5793 (1950).

[2] *Internationale Tabellen zur Bestimmung von Kristallstrukturen* (Gebrüder Borntraeger, Berlin, 1935), Band I, p. 221.

[3] C. W. Tucker, Jr., *Science* **112**, 448 (1950); also (private communication, 1950), "An approximate crystal structure for the beta-phase of uranium", Document AECD-2957, Knolls Atomic Power Laboratory, Schenectady, 1950.

[4] Dickins, Douglas, and Taylor, *Nature* and *J. Iron Steel Inst.* (London), both to be published; private communication.

The Measurement of Chemical Equilibria by Means of the Critical Flow Orifice*

Henry Wise and David Altman
Jet Propulsion Laboratory, California Institute of Technology, Pasadena, California
(Received February 12, 1951)

FOR the case of isentropic flow of a perfect gas through a properly shaped nozzle, the rate of mass discharge of gas $\dot{m}$ through the orifice under the conditions of sonic velocity in the throat[1] is given by

$$\dot{m}=A_t P_2 \Gamma_{(\gamma)}/(RT_2/\bar{M})^{\frac{1}{2}}, \quad (1)$$

where $\Gamma_{(\gamma)}$ represents

$$\Gamma_{(\gamma)}=(\gamma)^{\frac{1}{2}}(2/\gamma+1)^{(\gamma+1)/2(\gamma-1)}; \quad (2)$$

and where A_t is the effective throat area; P_2 and T_2 are the pressure and temperature of the gas upstream from the nozzle; R is the gas constant; $\bar{M}$ is the average molecular weight of the gas; and γ is the ratio of the specific heat at constant pressure and constant volume of the gas at T_2.

It is apparent from Eq. (1) that the critical flow orifice lends itself to a dynamic procedure for the study of equilibrium processes and reaction kinetics, since the flow rate of gas is a function also of the average molecular weight of the gas at the entrance to the nozzle. Thus, the equilibrium constant may be evaluated by this method for a homogeneous system in the gas phase and for a heterogeneous reaction involving a gas phase as long as the overall chemical reaction results in a mole change between the gaseous products and reactants. If one considers a chemical equilibrium in a system composed of a mixture of molecules of various kinds and represented by $-\nu_a\cdot A-\nu_b B-\cdots=\nu_g G+\nu_h H+\cdots$, one obtains for the equilibrium constant, in terms of pressures, $K_p=\Pi_i P_i^{\nu_i}=\Pi_i (N_i P)^{\nu_i}$, where P is the total pressure in the system, and N_i, P_i, and ν_i refer, respectively, to the mole fraction, partial pressure, and the number of molecules of kind i (as represented by the chemical equation).

The mass-flow rate of gas through the critical orifice for such a mixture of gases is found to be

$$\dot{m}=[A_t P_2/(RT_2)^{\frac{1}{2}}](\Sigma_i N_i M_i)^{\frac{1}{2}}\Gamma_{(\gamma)}, \quad (3)$$

from which the average molecular weight of the gas may be evaluated. If the mass-flow rate of a perfect gas through the critical orifice is determined at a temperature T_1 different from the temperature T_2 at which the equilibrium is being measured, the following expression is obtained:

$$(\Sigma_i N_i M_i)^{\frac{1}{2}}\Gamma_{(\gamma)}=(M'')^{\frac{1}{2}}\Gamma_{(\gamma)}=(M_1 V/A_t T_1)(T_2/R)^{\frac{1}{2}}d\ln p/dt, \quad (4)$$

where M_1 is the average molecular weight of the gas at temperature T_1, and V is the volume of the system.

In an experimental investigation of this procedure, the vapor-phase equilibrium between N_2O_4 and NO_2 has been measured at two temperatures. The apparatus, made of Pyrex glass, consisted of a storage flask at temperature T_1 connected to a cylindrical tube (22 mm i.d.) which housed the critical flow orifice (throat area $\sim 4\times10^{-4}$ cm^2). The temperature in this portion of the

system T_2 was controlled by means of an electrically heated furnace which surrounded the glass tube. The mass-flow rate of gas through the orifice was determined from the rate of pressure change in the storage vessel as read on a manometer. With the aid of a Hyvac pump the pressure on the downstream side of the orifice was maintained well below that given by the critical pressure ratio $P_{\text{exit}}/P_2=[(\gamma+1)/2]^{\gamma/(1-\gamma)}$. The effective throat area of the orifice was measured empirically. A relatively small variation in effective throat area due to the formation of a boundary layer was noted.[2] This subject will be discussed in greater detail in a subsequent paper.

The results of the equilibrium measurements for the system $N_2O_4=2NO_2$ are shown in Fig. 1. These empirical data expressed

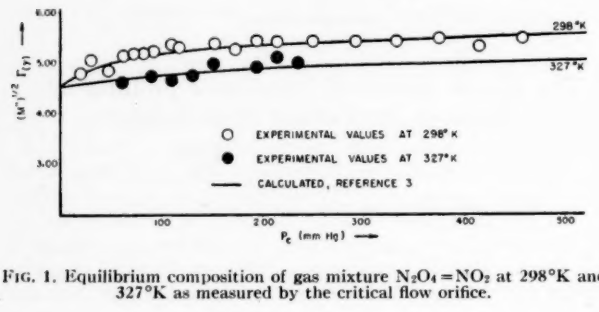

FIG. 1. Equilibrium composition of gas mixture $N_2O_4=NO_2$ at 298°K and 327°K as measured by the critical flow orifice.

as the product of square root of the molecular weight $(M'')^{\frac{1}{2}}$ and the gamma-function for the gas mixture $\Gamma_{(\gamma)}$ are compared with the calculated values based on the equilibrium constants reported by Giauque and Kemp.[3] The specific heat data for $NO_2(g)$ were taken from tables;[4] those for $N_2O_4(g)$ were calculated from the vibrational frequencies of the gas.[5] As a first approximation the ideal gas law was applied to the experimental gas mixture. The corrections due to gas imperfections will be developed in detail in a future publication. It is also to be noted that the effect of heat-capacity lag during the flow process through the orifice will cause only a small error in the results, since the gamma-function Eq. (2) is not very sensitive to variations from this source.

The experimental method described offers several advantages over the conventional static and dynamic procedures employed in the measurement of chemical equilibria. Particularly the critical flow method eliminates the need for direct measurement of the equilibrium composition of the gas phase in the high temperature region. Its application to the study of chemical equilibria and reaction kinetics in homogeneous and heterogeneous systems will be reported in subsequent publications.

* This paper presents the results of one phase of research carried out at the Jet Propulsion Laboratory under U. S. Army Ordnance Department Contract No. DA-04-495-ORD-18.

[1] Seifert, Mills, and Summerfield, Am. J. Phys. **15**, 1 (1947).

[2] W. F. Durand, *Aerodynamic Theory* (Durand Reprinting Committee, California Institute of Technology, Pasadena, 1943), Vol. III, p. 89.

[3] W. F. Giauque and J. D. Kemp, J. Chem. Phys. **6**, 40 (1938).

[4] *The NBS-NACA Tables of Thermal Properties of Gases* (National Bureau of Standards, 1950), Sec. 15.10.

[5] D. M. Yost and H. Russell, Jr., *Systematic Inorganic Chemistry* (Prentice-Hall, Inc., New York, 1947), p. 29.

On the Theory of the High Polymer Solution

HIROSHI ICHIMURA
Tokyo Institute of Technology, Oh-Okayama, Tokyo, Japan
(Received February 12, 1951)

IN the present typical theories on the high polymer solution, insufficient consideration has been given concerning the interaction between the solvent and the polymer segments. In Zimm's theory this situation has its origin in McMillan-Mayer's general theory. Here we give a formulation which may probably clarify how this interaction should be taken in consideration, especially in the case of dilute solution of flexible linear high polymers.

The configurational partition function for the system of N_1 solvent molecules and p polymer molecules of n segments in the volume V and at $T°$K may be written as

$$Z(N_1, p)=\frac{1}{N_1!p!}\int\cdots\int_V e^{-\beta U(w,R)}\,dw_1\cdots dwN_1 dR_1\cdots dR_p, \quad (1)$$
$$(\beta=1/kT)$$

where $w_1\cdots wN_1$ are the coordinates of the solvents and $R_1\cdots R_p$ represent the groups of the coordinates of the segments of the polymers.

$U(w, R)$ is the total potential energy of the system. If we assume the two-body force for the interaction, it may be written as

$$U(w,R)=\tfrac{1}{2}\sum_{i\,(\neq)}\sum_{j} u(i,j)+\sum_{i}\sum_{\lambda}\sum_{a} u(i,\lambda_a)$$
$$+\tfrac{1}{2}\sum_{\lambda}\sum_{a\,(\neq)\,b} u(\lambda_a,\lambda_b)+\tfrac{1}{2}\sum_{\lambda\,(\neq)\,\mu}\sum_{a}\sum_{b} u(\lambda_a,\mu_b), \quad (2)$$

where i, j, indicates the solvents, λ, μ indicate the polymers and λ_a means the ath segment of the λth polymer. After an approximate and model-like reasoning which conforms with the liquid-like aggregate, we obtain the following factor as the result of the integration over the N_1 solvent coordinates:

$$\{(V-pn\delta_s-(\Sigma\omega_\lambda-\tfrac{1}{2}\Sigma_\mu\omega_{\lambda\mu}))e^{\beta\epsilon_1}$$
$$+(\sum_\lambda\omega_\lambda-\tfrac{1}{2}\sum_{\lambda\,(\neq)\,\mu}\omega_{\lambda\mu})e^{\beta\epsilon_{12}}\}^{N_1}; \quad (3)$$

here we have set $V=N_1\delta_1+pn\delta_s$ (δ_1 is the volume of a solvent molecule and δ_s is that of a segment); ω_λ is the volume of the effective range of influence of the segments of the λth polymer (we assume the short-range, well-type potentials between particles), this is a function of the form of the polymer molecule, i.e., the function of the coordinates of its segments; $\omega_{\lambda\mu}$ for the part of ω_λ which is occupied by the segments of the μth polymer; and ϵ_1 and ϵ_{12} for the values of u_i,

$$u_i=\tfrac{1}{2}\sum_{j(\neq i)} u(i,j)+\sum_{\lambda}\sum_{a} u(i,\lambda_a),$$

when the ith solvent lies in the volumes indicated in the bracket factors, respectively.

Using the approximation $(1+x)^{N_1}\doteqdot e^{N_1 x}$ ($x\ll 1$), we obtain

$$Z(N_1,p)=\frac{1}{N_1!p!}(N_1\delta_1)^{N_1}e^{\beta N_1\epsilon_1}$$
$$\times\int\cdots\int e^{N_1 x}\exp\Big[-\frac{\beta}{2}\Big(\sum_\lambda\sum_{a\neq b}\sum u(\lambda_a,\lambda_b)$$
$$+\sum_{\lambda\neq\mu}\sum_{a}\sum_{b} u(\lambda_a,\mu_b)\Big]dR_1\cdots dR_p, \quad (4)$$
$$x=\frac{1}{N_1\delta_1}\Big(J\omega_\lambda-\frac{J}{2}\sum_{\lambda\neq\mu}\omega_{\lambda\mu}\Big),$$
$$J=(e^{\beta(\epsilon_{12}-\epsilon_1)}-1).$$

If we put

$$e^{J\omega_{\lambda\mu}-\beta u(\lambda,\mu)}=1-f(\lambda,\mu),$$

and use the Ursellian expansion for the product, we get finally

$$Z(N_1,p)\doteqdot\frac{1}{N_1!p!}(N_1\delta_1)^{N_1}e^{\beta N_1\epsilon_1}V^p C^p\Big\{1-\frac{p(p-1)}{2}\frac{B}{VC^2}\Big\}, \quad (5)$$

where we have set

$$\int\exp\Big[J\omega_\lambda-\frac{\beta}{2}\sum_{a\neq b}\sum u(\lambda_a,\lambda_b)\Big]dR_\lambda=V\cdot C$$

$$\iint\exp\Big[\Big\{J\omega_\lambda-\frac{\beta}{2}\sum_{a\neq b}\sum u(\lambda_a,\lambda_b)\Big\}$$
$$+\Big\{J\omega_\mu-\frac{\beta}{2}\sum_{a\neq b}\sum u(\mu_a,\mu_b)\Big\}\Big]f(\lambda,\mu)dR_\lambda dR_\mu=V\cdot B. \quad (6)$$

From this $Z(N_1, p)$ we can construct the partial molar free energy of mixing for the solvent $\Delta\bar{F}_1$ and by $\pi=-\Delta\bar{F}_1/\bar{V}_1$ ($\bar{V}_1$ is the molar volume of the solvent) we get for the osmotic pressure π,

$$\pi=(RT/\bar{V}_1)\{(v_2/n\sigma)+\tfrac{1}{2}v_2^2B/(n\sigma)^2\delta_1C^2\},$$
$$v_2=pn\delta_s/(N_1\delta_1+pn\delta_s),\quad \sigma=\delta_s/\delta_1. \quad (7)$$

By Eqs. (6) and (7), it may be seen how the interaction between the solvents and the polymer enters in the formula through the function ω_λ, which will be very complicated. In case of zero heat of mixing ($\epsilon_{12}=\epsilon_1$) or in case of the constant ω_λ, which will be the case with the rigid polymer molecule, ω_λ may disappear from the formula, and our result will become essentially identical with Zimm's result. Without very rough approximations, it will be very difficult to evaluate the integrals C and B. The details of our theory will be published elsewhere.

High Temperature Specific Heat of AgBr

R. W. Christy and A. W. Lawson
Institute for the Study of Metals, University of Chicago, Chicago, Illinois
(Received February 9, 1951)

DESPITE various doubts[1,2] expressed in the past concerning the mechanism of conductivity in AgBr, the preponderance of evidence now favors the Frenkel mechanism of transport by interstitial Ag^+ ions. Recently, a detailed analysis by Teltow[3] of the conductivity of doped AgBr samples has led to a considerably

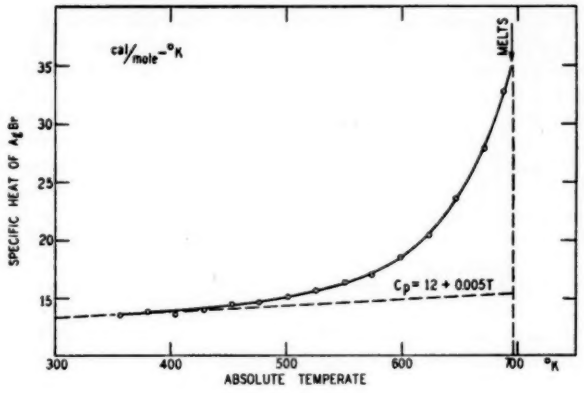

FIG. 1.

higher estimate of the heat of activation for the formation of interstitial ions than hitherto supposed. In this connection, we believe it is of interest to report some measurements of the specific heat of AgBr.

Figure 1 shows the dependence of the specific heat on temperature. This curve is the average of four runs made with the apparatus described by Smith.[4] This apparatus is essentially a device for obtaining comparative heating rates of various samples using identical power inputs. The reference sample in our case was copper. The results obtained are accurate to ±3 percent.

The rapid rise in specific heat found in AgBr is presumably associated with the energy absorbed in the creation of lattice defects. If an assumption be made as to the normal behavior of the specific heat in a perfect lattice, the data present an estimate of (a) the heat of activation for the formation of defects and (b) the number of such defects at any temperature.

For the normal behavior of the AgBr lattice, we assume

$$c_p=12+\alpha T \tag{1}$$

in cal/mole−°K, where T is the absolute temperature. For α we choose a value of 0.005 cal/mole corresponding to $c_p=13.5$ cal/mole−°K at $T=300$°K. Subtracting Eq. (1) from the data in Fig. 1, we derive values for the excess specific heat Δc_p. Now, if the mole fraction of defects n/N is governed by a law of the type

$$n/N=C\exp(-\Delta H/2RT), \tag{2}$$

where C is a constant, ΔH is the heat of activation, and R is the gas constant, then the excess specific heat per mole should be given by

$$T^2\Delta c_p=[C(\Delta H)^2/2R]\exp(-\Delta H/RT). \tag{3}$$

Figure 2 shows a plot of $T^2\Delta c_p$ *versus* $1/T$. The slope of this curve determines ΔH which turns out to be 29,400 cal/mole, in excellent agreement with the value of 29,200 cal/mole estimated by Teltow. This agreement is largely fortuitous, since it is quite sensitive to the choice of the parameter α. However, it is interesting to note that with a reasonable choice of α, our data are consistent with Teltow's result.

If we now assume Teltow's value for ΔH, we may make an estimate for n/N at any temperature, for Eq. (3) may be combined with Eq. (2) to yield

$$n/N=2RT^2\Delta c_p/(\Delta H)^2. \tag{4}$$

At $T=420$°C, just below the melting point, we find n/N to be 3.7 percent. Since at this temperature Δc_p is almost 20 cal/mole−°K, it is difficult to see how the choice of α can affect the result by more than about 10 percent. The value of $n/N=3.7$ percent is to be compared with that of 1.4 percent calculated from Teltow's Eq. (23). If we use the older estimates of $\Delta H=20{,}000$ cal/mole, our calculated value for n/N is ~7 percent. In view of the difficulties associated with obtaining an accurate value of C in Eq. (2) from conductivity data, we believe our estimate of n/N may be preferable to Teltow's.

The integrated value of the excess enthalpy at 420°C is 1070 cal/mole. The corresponding excess entropy is 1.9 cal/mole−°K and accounts for a large fraction of the discrepancy between the

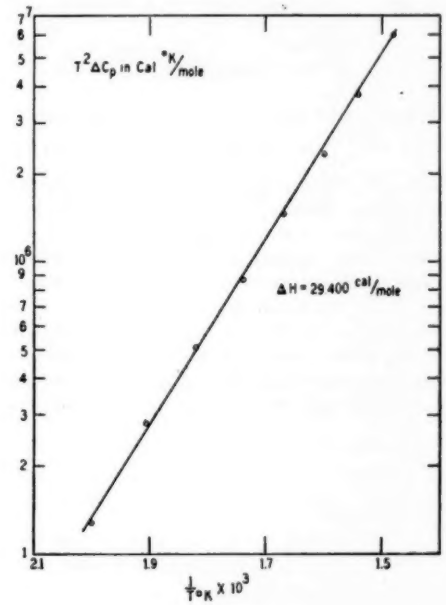

FIG. 2.

entropies[5] of fusion of AgBr and AgCl, namely, 3.4 and 6.0 cal/mole−°K, respectively. Since the density of defects in AgCl is considerably smaller than in AgBr, the excess enthalpy in the former will be about 0.3 cal/mole−°K.

Recently, one of us[2] made a similar analysis of thermal expansion data on AgBr. At that time, we were unaware of Teltow's results. As a result, by assuming that the coefficient of thermal expansion of the normal lattice was the same at higher temperatures as at 300°K, we were led to an estimate of ΔH nearer the old value of 20,000 cal/mole. This assumption is probably not justified, and if the expansion of the normal lattice increases with T, our estimate of the abnormal expansion is high and the estimate of ΔH is low. Consequently, the expansion data are probably more consistent with the Frenkel mechanism than previously supposed.

[1] J. W. Mitchell, Phil. Mag. **40**, 667 (1949).
[2] A. W. Lawson, Phys. Rev. **78**, 185 (1950).
[3] J. Teltow, Ann. Physik **5**, 63 (1949).
[4] C. S. Smith, Am. Inst. Mining Engrs. Technical Publication No. 1100.
[5] Goodwin and Kalmus, Phys. Rev. **28**, 1 (1909).

Out-of-Plane Hydrogen Vibrations in Triborine Triamine

ROBERT A. SPURR AND SHIH-CHUAN CHANG
Department of Chemistry, University of Maryland, College Park, Maryland
(Received February 8, 1951)

CRAWFORD and Edsall[1] have investigated the infrared and Raman spectra of triborine triamine. The discrepancy between the calculated and observed frequencies of the out-of-plane hydrogen vibrations was attributed to the interactions between hydrogen bonds attached in the meta positions. Bell[2] has suggested the use of a simple potential function for the out-of-plane vibrations in triborine triamine, which he has applied successfully to benzene. We have carried out the calculations and have obtained satisfactory agreement with the observed frequencies, as is shown in Table I.

TABLE I.

Observed frequency[1] cm^{-1}	Calculated frequency[1] cm^{-1}	% Deviation	Calculated frequency cm^{-1} (this research)	% Deviation (this research)
1098	1278	16.4	1117	1.7
622	756	21.6	661	6.3
415	403	2.9	437	5.3
1070	1086	1.5	1054	1.5
798	790	1.0	753	5.6
288	283	1.7	270	6.3
		Mean 7.5		Mean 4.5

The potential function assumed has the following form:

$$2V=\Sigma h_B r^2\lambda^2+\Sigma h_N s^2\mu^2+\Sigma k'(\phi_R+\phi_H)^2,$$

where h_B is the bending force constant for the B—H bond, r is the internuclear distance, and λ is the angle which the bond makes with the plane of the ring. The symbols h_N, s, and μ denote the corresponding quantities for the N—H bond. The constant k' expresses a resistance to twisting of the B—N bond. The quantities ϕ_R and ϕ_H represent the twist of the B—N bond due to ring distortion and hydrogen bending, respectively.[3] This potential function differs from that assumed by Crawford and Edsall[1] by the introduction of ϕ_H. The fairly satisfactory agreement obtained by this potential function renders unnecessary the assumption of interactions between hydrogen bonds attached in the meta positions.

The force constants were fitted to the three A'' frequencies and also to the three E'' frequencies. For the calculation of the frequencies in Table I, average values of the constants were used. These are given in Table II, together with the constants corresponding to k' for benzene and ethylene.

TABLE II. Force constants for triborine triamine, benzene, and ethylene.

Type of constant	Value
B—H bending, h_B	1.83×10^{4} dyne/cm
N—H bending, h_N	3.71×10^{4} dyne/cm
B—N twisting, k'	0.39×10^{-12} dyne-cm
benzene C—C twisting[2]	0.77×10^{-12} dyne-cm
ethylene C—C twisting[2]	1.7×10^{-12} dyne-cm

The value of the twisting force constant obtained by Crawford and Edsall[1] without introduction of ϕ_H in the potential function corresponds to 1.6×10^{-12} dyne-cm for k'. The value given here of 0.39×10^{-12} dyne-cm is more reasonable, since one would expect the ring bonds in triborine triamine to have less resistance to twisting than those in benzene and ethylene.

If it is assumed that k' varies linearly with double-bond character for different bonds, the double-bond character of the B—N bond in triborine triamine is $39/77\times1/2$ or 28 percent, taking that of benzene as 50 percent. This assumption can be tested by calculating the double-bond character of benzene by the use of the ethylene twisting constant. The value obtained is 45 percent. The double-bond character of a bond can also be estimated by the empirical formula of Pauling.[4] The B—N distance in triborine triamine has been measured in two investigations[5,6] by electron diffraction as 1.47 ± 0.07A and 1.44 ± 0.02A. These values inserted in the formula give 27 percent and 40 percent, respectively, for the double-bond character of the B—N bond, in rough agreement with the value given above.

Thanks are due to the Computing Division of the Ballistics Research Laboratory, Aberdeen Proving Ground, Maryland, for checking our calculations.

[1] B. L. Crawford and J. T. Edsall, J. Chem. Phys. **7**, 223 (1939).
[2] R. P. Bell, Trans. Faraday Soc. **41**, 293 (1945).
[3] Bell, Thompson, and Vago, Proc. Roy. Soc. (London) **A192**, 498 (1948).
[4] L. Pauling, *Nature of the Chemical Bond* (Cornell University Press, Ithaca, New York, 1940), p. 175.
[5] A. Stock and R. Wierl, Z. anorg. u. allgem. Chem. **203**, 228 (1931).
[6] S. H. Bauer, J. Am. Chem. Soc. **60**, 524 (1938).

Notice

A Symposium on Molecular Structure and Spectroscopy will be held at the Department of Physics, The Ohio State University, from June 11 through June 16, 1951. There will be discussions of the interpretation of molecular spectroscopic data as well as of methods of obtaining such data. In addition, there will be sessions devoted to those phases of spectroscopy of current interest. A dormitory will be available for those who wish to reside on the campus during the meeting. For further information or for a copy of the program when it becomes available, write to Professor Harald H. Nielsen, Department of Physics, The Ohio State University, Columbus 10, Ohio.

The Symposium will be sponsored this year jointly by the Graduate School and the Department of Physics and Astronomy of The Ohio State University and by the Division of Chemical Physics of the American Physical Society. Members of the Division who wish to contribute ten-minute papers should send abstracts not exceeding 200 words in length (in duplicate) to Professor Nielsen before April 27.